Three dimensional study to quantify the relationship between facial hard and soft tissue movement as a result of orthognathic surgery.

Anas Mohammed Yousif Almukhtar

B.D.S., M.Sc. Orthodontics

Submitted in fulfilment of the requirement for the degree of Doctor of Philosophy

To

Glasgow Dental School, College of Medical, Veterinary and Life Sciences

May 2016

I dedicate this work to the people of Iraq, my beloved home.

I know how much you are suffering

I feel for you.

Summary

Introduction

Prediction of soft tissue changes following orthognathic surgery has been frequently attempted in the past decades. It has gradually progressed from the classic “cut and paste” of photographs to the computer assisted 2D surgical prediction planning; and finally, comprehensive 3D surgical planning was introduced to help surgeons and patients to decide on the magnitude and direction of surgical movements as well as the type of surgery to be considered for the correction of facial dysmorphology.

A wealth of experience was gained and numerous published literature is available which has augmented the knowledge of facial soft tissue behaviour and helped to improve the ability to closely simulate facial changes following orthognathic surgery. This was particularly noticed following the introduction of the three dimensional imaging into the medical research and clinical applications.

Several approaches have been considered to mathematically predict soft tissue changes in three dimensions, following orthognathic surgery. The most common are the Finite element model and Mass tensor Model. These were developed into software packages which are currently used in clinical practice. In general, these methods produce an acceptable level of prediction accuracy of soft tissue changes following orthognathic surgery. Studies, however, have shown a limited prediction accuracy at specific regions of the face, in particular the areas around the lips.

Aims

The aim of this project is to conduct a comprehensive assessment of hard and soft tissue changes following orthognathic surgery and introduce a new method for prediction of facial soft tissue changes.

Methodology

The study was carried out on the pre- and post-operative CBCT images of 100 patients who received their orthognathic surgery treatment at Glasgow dental hospital and school, Glasgow, UK. Three groups of patients were included in the analysis; patients who underwent Le Fort I maxillary advancement surgery; bilateral sagittal split mandibular advancement surgery or bimaxillary advancement surgery. A generic facial mesh was used to standardise the information obtained from individual patient's facial image and Principal component analysis (PCA) was applied to interpolate the correlations between the skeletal surgical displacement and the resultant soft tissue changes. The identified relationship between hard tissue and soft tissue was then applied on a new set of preoperative 3D facial images and the predicted results were compared to the actual surgical changes measured from their post-operative 3D facial images.

A set of validation studies was conducted. To include:

- *Comparison between voxel based registration and surface registration to analyse changes following orthognathic surgery*. The results showed there was no statistically significant difference between the two methods. Voxel based registration, however, showed more reliability as it preserved the link between the soft tissue and skeletal structures of the face during the image registration process. Accordingly, voxel based registration was the method of choice for superimposition of the pre- and post-operative images. The result of this study was published in a peer refereed scientific journal.

- *Direct DICOM slice landmarking; a novel technique to quantify the direction and magnitude of skeletal surgical movements*. This method represents a new approach to quantify maxillary and mandibular surgical displacement in three dimensions. The technique includes measuring the distance of corresponding landmarks digitized directly on DICOM image slices in relation to three dimensional reference planes. The accuracy of the measurements was assessed against a set of "gold standard"

measurements extracted from simulated model surgery. The results confirmed the accuracy of the method within 0.34mm. Therefore, the method was applied in this study. The results of this validation were published in a peer refereed scientific journal.

- *The use of a generic mesh to assess soft tissue changes using stereophotogrammetry*. The generic facial mesh played a major role in the soft tissue dense correspondence analysis. The conformed generic mesh represented the geometrical information of the individual's facial mesh on which it was conformed (elastically deformed). Therefore, the accuracy of generic mesh conformation is essential to guarantee an accurate replica of the individual facial characteristics. The results showed an acceptable overall mean error of the conformation of generic mesh 1 mm. The results of this study were accepted for publication in peer refereed scientific journal.

Skeletal tissue analysis was performed using the validated "Direct DICOM slices landmarking method" while soft tissue analysis was performed using Dense correspondence analysis. The analysis of soft tissue was novel and produced a comprehensive description of facial changes in response to orthognathic surgery. The results were accepted for publication in a peer refereed scientific journal.

The main soft tissue changes associated with Le Fort I were advancement at the midface region combined with widening of the paranasal, upper lip and nostrils. Minor changes were noticed at the tip of the nose and oral commissures.

The main soft tissue changes associated with mandibular advancement surgery were advancement and downward displacement of the chin and lower lip regions, limited widening of the lower lip and slight reversion of the lower lip vermilion combined with minimal backward displacement of the upper lip were recorded. Minimal changes were observed on the oral commissures.

The main soft tissue changes associated with bimaxillary advancement surgery were generalized advancement of the middle and lower thirds of the face combined with widening of the paranasal, upper lip and nostrils regions.

In Le Fort I cases, the correlation between the changes of the facial soft tissue and the skeletal surgical movements was assessed using PCA. A statistical method known as 'Leave one out cross validation' was applied on the 30 cases which had Le Fort I osteotomy surgical procedure to effectively utilize the data for the prediction algorithm. The prediction accuracy of soft tissue changes showed a mean error ranging between (0.0006mm±0.582) at the nose region to (-0.0316mm±2.1996) at the various facial regions.

Contents

List of Tables

List of Figures

Acknowledgements

"***My Lord, indeed I am, for whatever good You would send down to me, in need" (Al_Qasas,28).*** Thanks to Allah, the almighty, for giving me the willingness and strength to complete this work.

I wish to express my most sincere gratitude and appreciation to my principal supervisor Professor A. Ayoub for his guidance, patience and encouragement throughout the development of the project. One simply could not wish for a better or friendlier supervisor.

My deepest gratitude also goes to my co-supervisors Professor B Khambay, not only for his bright ideas, which influenced the project's methodology in many aspects, but also for his persistent demand for perfection which led to the quality of this project; Dr. X Ju, for his remarkable software development skills without which this project would never see the light; and last but not the least, Professor J McDonald whose never-failing sympathy and support helped me passing the darkest parts in my study path.

I would like to express my appreciation to the Glasgow Dental School administration especially the Dean, Prof J Bagg, who offered his unlimited support when I was desperately in need. A word of thanks is also spoken to our brilliant secretary, Liz, for managing administrative issues with a high precision.

My sincere gratitude and appreciation are to my financial sponsors, the higher committee for education and development in Iraq (HCED), for their dedication to improve the quality of higher education for a better future.

Many thanks for all those who contributed to the success of my study; Mr Benington, our brilliant orthodontics consultant and Carol, our lively dental nurse, who provided all the clinical supervision and technical support.

The only way to overcome the pain and the agony of the PhD was sharing it with sincere friends. Especially mentioning Mohammed, Ali, Jamie and Faith. The warmth of their caring and support kept me contained and focused on my goals.

My parents watched me from a distance while I worked towards my degree, sacrificed their comfort to let me find mine and hid this from me so I wouldn't feel any regret. Without their love, affection and encouragement this work would not have been possible.

No words can express my thanks and appreciation for my wife. The success in this project was totally attributed to her endless love and support. Thanks for every late night I returned home and every early morning I left, thanks for bearing my ridiculousness at every furious outburst, thanks for maintaining our family while I was busy in my agonizing study. Your sacrifices are well known and very well appreciated. My children Mustafa and Maryam are the joy of my life. They only have ever known me as a student. Despite only seeing them at the weekends and sometimes not, they have never complained. Good news for them, "you have your father back".

There are many more people I could thank, but time, space, and modesty compel me to stop here.

Thank you

Anas

Author's Declaration

I declare that, except where explicit reference is made to the contribution of others, that this thesis is the result of my own work and has not been submitted for any other degree at the University of Glasgow or any other institution.

Signature

Printed name: Anas Almukhtar

October 2015

List of Abbreviations

Abbreviations	Full name
3D	Three dimensions
DICOM	Digital Imaging Communications in Medicine
BSSO	Bilateral Sagittal Split Osteotomy
VBR	Voxel based registration
SBR	Surface Based Registration
SD	Standard deviation
SE	Standard Error
FEM	Finite Element Model
MSM	Mass Spring Model
MTM	Mass Tensor Model
PCA	Principal Component Analysis
ICP	Iterative Closest Point
PA	Procrustes Analysis
PPA	Partial Procrustes Analysis
IC	Interclass Correlation
Sig	Significance level
CBCT	Cone Beam Computerized Tomography
CT	Computerized Tomography
MRI	Magnetic Resonance Imaging
HU	Hounsfield Unit
IF*	Incisive Foramen

***Abbreviations for landmarks are defined in their relevant chapters.**

1 Review of literature

Contents

Introduction

The innovation in three dimensional (3D) imaging technologies allowed the capture of a patient's face for a comprehensive diagnosis and treatment planning. These technologies succeeded in producing what is known today as the "Virtual patient", a new term introduced to the medical field which describes the creation of a digital copy of the patient's body on a computer screen where various diagnostic and virtual surgeries can be performed. Orthognathic surgical analysis and planning benefited from the availability of 3D imagining technology which promises improvement in the diagnosis and treatment planning as well as enriching the information obtained for facial anthropometry studies.

1.1 3D image capture

In general, the available 3D data of the face are either surface images captured by imaging facilities that do not penetrate through the facial skin such as Stereophotogrammetry and laser scanners, or volumetric images captured by imaging facilities that penetrate through human tissue such as CT scans , MRI and 3D ultrasound probing.

1.1.1 Acquisition of 3D Surface data:

Systems for surface data acquisition are capable of capturing the external surface of the face and do not record internal or skeletal structures. These include 3D photography and 3D laser scanners which have a variety of clinical applications including evaluation of orthognathic surgery outcome, evaluation of the changes following cleft lip repair, study of growth pattern, the variation of facial features among various populations and creating a mean face for the population.

1.1.1.1 Three dimensional (3D) photography

Four main photographic techniques were introduced to capture the 3D morphology of human face; Three-dimensional Facial Morphometry (3DFM); Contour photography; Moire's topography; and Stereophotogrammetry. Of these

four methods, Stereophotogrammetry has been the most successful in producing an accurate and reasonably practical method of facial 3D imaging.

1.1.1.2 Three-dimensional Facial Morphometry (3DFM)

Moorrees and Lebert, 1962 introduced the computerized mesh diagram analysis(1). Their idea was to capture the face using a pair of normal lateral and frontal photographs. A matrix of intersecting lines was then plotted on the photograph on which a set of landmarks were digitized. Based on the deformation of this matrix due to the shift from the frontal to the lateral photograph, the vectors for each landmark were obtained which provided the three dimensional orientation of each of them. The basic purpose of this approach was not to capture the face in 3D but only for the analysis of the three dimensional position of each landmark (Moorrees *et al.*, 1976(2).

Ferrario *et al.*, 1998 (3) introduced a computerized mesh diagram analysis and studied its application in soft tissue facial morphometry; the aim of their study was to create norms from the vector distortion matrix and to compare the difference in facial features between male and female.

1.1.1.3 3D Contour photography

E. J. Lovesey 1974 (4) introduced this method for facial anthropometric measurements. The technique was simple; a special continuous pattern of black and white lines or squares was projected on patients face. Frontal and lateral 2D photographs are captured and the changes of the contours of the pattern's lines were studied. Areas of rapid change of contour like the eyes and nose represented a major problem for this technique. Measurement of facial features was subjective and not accurate enough for a robust facial anthropometric analysis.

1.1.1.4 Moire's topography

The method is based on the projection of lines (fringes) on the face at the time of image capture; the distortion of the line on the facial features is detected by

the software which is designed to quantify fringes distortion and to create a three dimensional image. The technique however is sensitive to facial positioning especially in the evaluation of the differences between pre-surgical and post-surgical images, the change in head position would affect the pattern of lines distortion on the face. Another limitation of this method is the potential error in recording rough surfaces.

Motoyoshi *et al.,* 1992 (5) introduced one of the earliest methods of capturing the human face in 3D for objective anthropometric analysis using a cathode-ray tube (CRT) technique. Their technique was based on Moire's photography and the subject was photographed while projecting about 800 points of light onto the face using a projector and a set of three cameras (central, right and left sides).

The three photographs obtained were then transmitted to a computer as pictorial image data by an image scanner. The 2D image from each camera was recognized by the computer as a network of projected points. The 3d coordinates of each point was derived from their position into the captured set of photographs taken from the front and from each of the cameras at 45 ° angles, (figure 1).

The precision of the method was tested by imaging a facial plaster cast. The three-dimensional coordinates of the anatomical points were compared with those generated from an electromagnetic digitizer. The mean of errors and the standard deviation were less than 0.08 ± 0.23 mm in all dimensions (5).

1.1.1.5 3D Static Stereophotogrammetry

Stereophotogrammetry refers to the special photography technique where at least two cameras are configured as a stereo-pair to recover the depth of the 3D object by interpolating the third dimension of each point on the 3D object surface being imaged. The degree of disparity between the two dimensional location of the corresponding points on both images generates the third dimension. Stereophotogrammetry is based on the triangulation effect, (figure

2). An imaginary triangle represents the two cameras and the object to be imaged. The distance between the two cameras is fixed while the distance of each camera to the point on the object to be imaged varies according to their distance from the captured point; this difference is described as the degree of disparity. The (X_1,Y_1) and (X_2,Y_2) coordinates of the captured point within the right and left cameras images produce the z coordinate of that point using a mathematical formula, Equation (1).

Equation 1: Stereophotogrammetry disparity equation. Where the denominator $x_2 - x_1$ is known as the stereo disparity, d is the distance between the two cameras and f is the focal length of the camera lens, (6) Please refer to figure (2).

$$z = \frac{df}{x_2 - x_1}$$

In cases where two pairs of cameras were used to capture the face, two 3D images are produced, one for the right half of the face and the other for the left side of the face. A software programme is used to link the two stereo-images to produce the full 3D image of the face. This method has been clinically validated for its level of accuracy (7). The algorithms used to match the images from the paired sources evolved through different stages of development. Burke and Beard 1967 in Cambridge, UK (8) were the first to describe the concept of stereo 3D imaging of the face for medical purpose. Their method was not based on triangulation effect but on image stereoscopy (anaglyph photography). Two cameras were used adjacent to each other. The patient was lying in a supine position and the cameras hanging over the head. Alternative red and blue layers of transparent sheets were applied, these were placed in the front of the right and left camera respectively, (figure 3). By careful superimposition of the right and left image the viewer detected the depth of the image. The method does not produce 3D coordinates, so may not be ideal for facial analysis. However this system was adopted for multimedia and gaming industry.

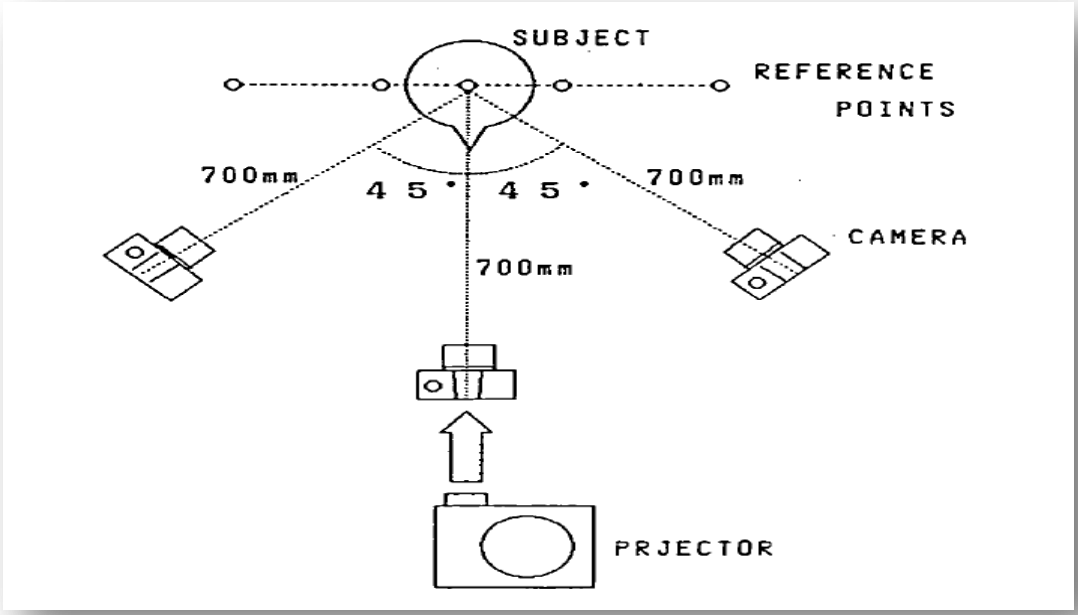

Figure 1: Moire's photography: Diagram showing the technique of using three cameras at 45º angle from each other combined with the fringes projector.

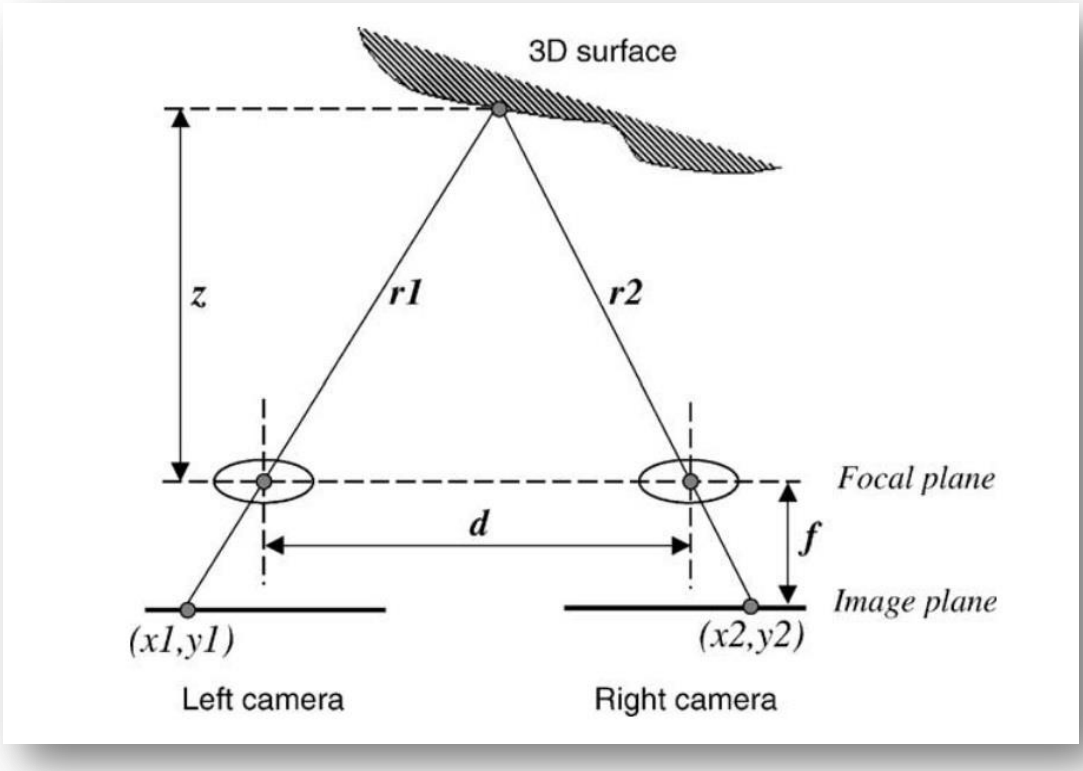

Figure 2: Diagram showing the basics of stereophotogrammetry (triangulation effect). The depth of each pixel could be calculated from the known distance between the two cameras *d;* the cameras focal length *f;* the 2D coordinates of the pixel (*x* and *y)* utilising the disparity between captures (from each camera) in Equation (1). Image quoted from (6).

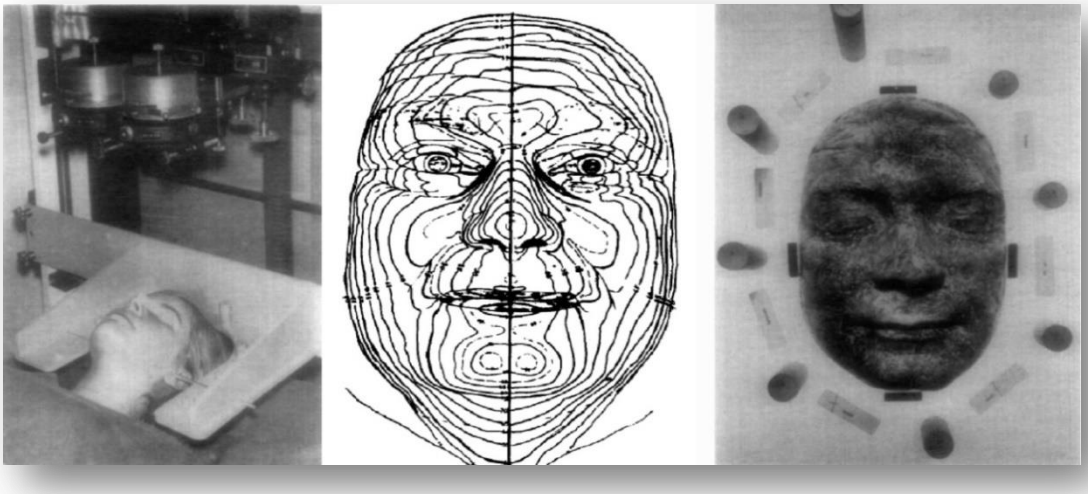

Figure 3: Anaglyph photography: The use of two colour filters to produce visual depth perception. Burke and Beard 1967 (8)

In general, there are two types for stereophotogrammetry: active and passive stereophotogrammetry, and a combination of the two known as hybrid. Active stereophotogrammetry, (figure 4), is based on utilization of a structured light to produce the 3D image. Specific pattern projects onto the patient's face while two (or more) cameras are used to capture the information provided by the deformation of the pattern on the patients face from different viewpoints. Monochrome cameras are used for easier detection of the deformation pattern. The addition of a coloured camera will facilitate the capture of the facial texture.

The 3D surface model is generated by applying the triangulation principle extracted from the stereo images; this is accomplished by calculating the third dimensional coordinate of each 2D point (pixel) visible in both camera images. The purpose of the projected textured pattern on the object to be captured is to simplify the automatic detection of corresponding points to interpolate the third dimension.

On the other hand, passive stereophotogrammetry, (figure 5), does not depend on pattern projection on the surface to generate the 3D image. The process of finding correspondences between images is more complex and high-quality cameras are necessary to capture surface details and to provide sufficient texture information to act as natural patterns to build the 3D image. Skin pores,

freckles and scars would act as a distinctive pattern to help find the correspondences and generate the 3rd dimension of the captured image. The lighting conditions must be carefully controlled as strong ambient light may result in glare thus diminishing the surface details (9). Hybrid stereophotogrammetry combines the advantages of both active and passive to achieve a better quality of the produced 3D imaging.

Ras *et al.,* 1996 (10) introduced the active stereophotogrammetry concept for facial analysis using two stereo coupled cameras at 50 cm distance from each other and a flash spot fitted between the cameras to project a dotted pattern on the face.

Hajeer *et al.,* 2003 (11) used stereophotogrammetry imaging to test the reliability of the stereophotogrammetry-based 3D imaging system (C3D) and to determine the effect of orthognathic surgery on the 3D soft-tissue morphology. The imaging setup consisted of one colour digital camera to capture the natural appearance of the face; two monochrome digital cameras serving as a 'stereo-pair' for building the 3D model; one white light flash synchronised to operate with the colour camera and one speckle texture projection synchronised to operate with the monochrome cameras, (figure 6).

The use of the monochrome cameras helps to reduce the image noise and facilitate 3D model build-up whereas the speckle texture projection pattern provide the necessary information for the software to build 3D facial images. System accuracy was validated and an error of less than 0.3 mm ± 0.13 mm in all dimensions was reported.

In order to obtain accurate 3D images, calibration of the software is necessary, ideally before each session of imaging, however one calibration at the start of the day may be sufficient to ensure a satisfactory consistency throughout that day. Calibration is the digital refinement for the software to detect the amount of disparity of a set of points on a flat surface captured, at least four times, from different angles.

Despite the use of various techniques to facilitate 3D image production, the main challenge in stereophotogrammetry is to establish which pixels from the left and right images correspond to the same point in 3D space. A common approach is to apply maps of the stereo disparities based on the correspondences provided by each image, and from this map, the surface of the object is built on the basis of triangulation.

The most common stereophotogrammetry systems are the 3dMD and Di3D. Although they are both based on stereo imaging, the algorithm and imaging techniques are different in various aspects. Di3D employ passive stereophotogrammetry, which generates 3D surface images solely on the basis of natural patterns, such as skin pores, freckles, scars and so forth. Therefore, the 3D reconstruction depends on the integrity of the pixels and requires high-resolution cameras.

3dMD combines active and passive stereophotogrammetry triangulation strategies into its systems called 'hybrid' stereophotogrammetry. The cameras are based on industrial vision standards containing sensors of higher quality and consistency than (SLR) cameras.

Tzou *et al.*, 2014 (9) compared the clinical applicability of five 3D imaging systems. DI3D and 3dMD were the stereophotogrammetry imaging systems involved in this study. The two systems were similar in many aspects. However a few differences were seen regarding the speed of processing and type of capturing technique, (figure 7).

Di3D was superior to 3dMD in its simplicity of the system as it uses high resolution cameras and flash lights normally used for photography with no need for the industrial sensors used by 3dMD.

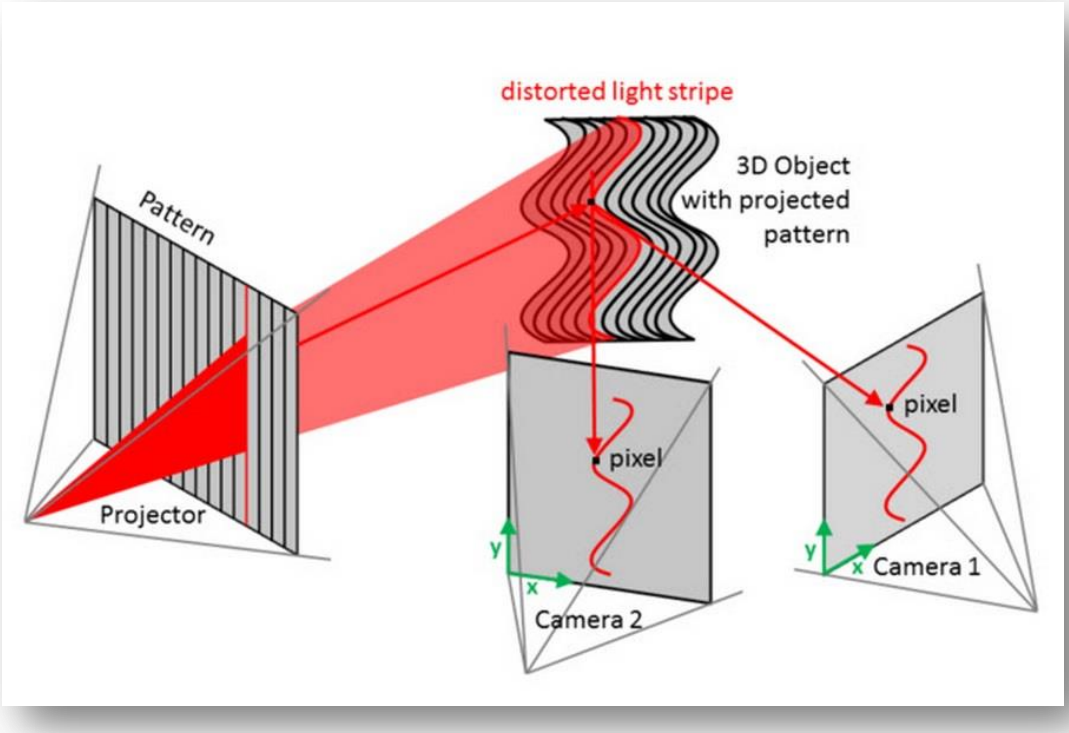

Figure 4: Active stereophotogrammetry. A diagram showing how the projected pattern helped in the identification of the corresponding pixels in order to build the disparity map (9)**.**

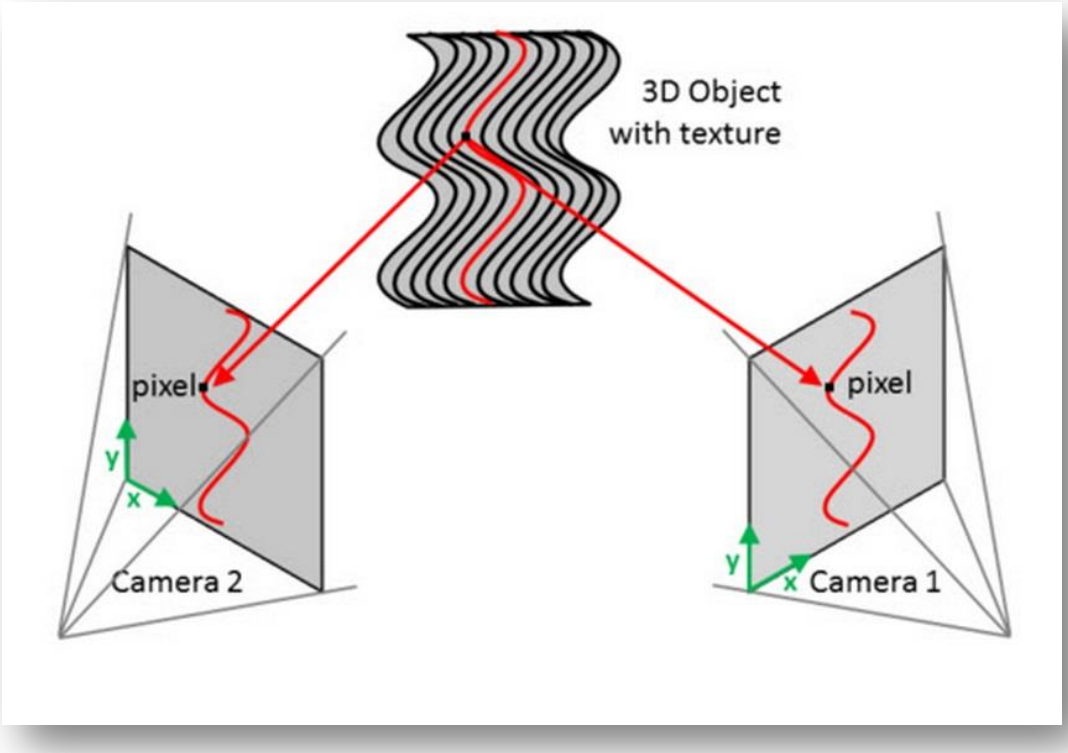

Figure 5: Passive stereophotogrammetry. A diagram showing how the high resolution cameras helped in the identification of the corresponding pixels in order to build the disparity map (9)**.**

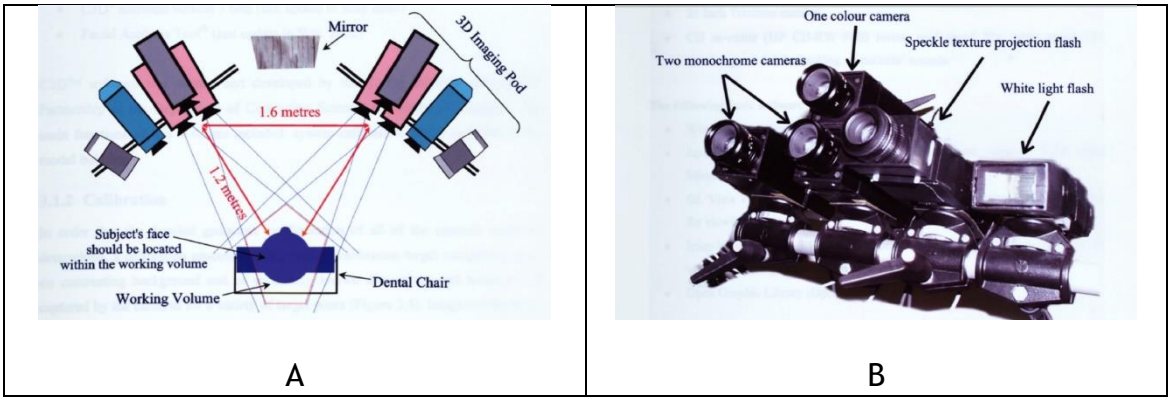

Figure 6: D3D system for active stereophotogrammetry. A diagram (left side) shows the cameras panel in relation to the patient (A), an image (right side) showing the D3D system (B). Hajeer *et al.*, 2006 (11)

On the other hand, 3dMD provide a relatively wider capture angle and higher processing speed. Despite these differences, the two systems were comparable in the accuracy and quality of captured texture images. According to the author, 3dMD was the better system (9).

Khambay *et al.*, 2008 (12) carried out an experimental study to assess the accuracy of Di3D system image capture as well as the errors associated with 3D image landmarking used for facial anthropometry. Operator error was measured by repeatedly locating landmarks on the three-dimensional image. Reproducibility error of the images was calculated by capturing three-dimensional images of the facial casts on two separate occasions; the Euclidean distance between the two matched sets of coordinates was then calculated. The Di3D system error was assessed by calculating the three-dimensional global positions of landmarks on the three-dimensional images and comparing them with those obtained by a coordinate measurement machine CMM (gold standard).

The results showed that the operator error in placement of landmarks on the three-dimensional model was 0.07 mm, range 0.02–0.11 mm. The reproducibility of the Di3D capture was 0.13 mm, range 0.11–0.14 mm. The mean distance between the CMM and Di3D landmarks, which constitutes the Di3D system error, was an average of 0.21 mm, range 0.14–0.32 mm.

Table 1 Comparison of 3D surface-imaging systems.

Company/ products	3dMDface	3dMDhead	3dMDtrio	3dMDtorso	3dMDbody	Axisthree XS-200	Axisthree XS-400	Canfield VECTRA H1	Canfield VECTRA M3	Canfield VECTRA XT	Canfield VECTRA CR 3D	Crisalix 3D MAMMO simulator	Crisalix 3D FACE simulator	DI3D™
Hardware	2 modular units of 6 medical grade, machine vision cameras, industrial-grade flash system synchronized in a single capture with a PC-controller desktop or PC-controller laptop for portability	5 modular units of 15 medical grade, machine vision cameras, industrial-grade flash system synchronized in a single capture with a PC-controller desktop	3 modular units of 9 medical grade, machine vision cameras, industrial-grade flash system synchronized in a single capture with a PC-controller desktop	4 modular units of 12 machine vision cameras and an industrial-grade flash system synchronized in a single capture with a PC-controller desktop	from 4 to 22 modular units of 12 to 66 machine vision cameras and an industrial-grade flash system synchronized in a single capture with PC-controller desktop (s)	3 imaging heads with projectors and lenses PC with Intel i3 processor	4 imaging heads, chassis unit with micro controller, actuation control, automatic Range Finder laptop	1 pod with on-board modular, intelligent flash unit	3 pods, floor stand 36 MP color texture, on-board, intelligent flash units PC + 23" monitor	3 pods, floor stand with motorized lift to adjust for patient height, 36mp color texture, on-board, intelligent flash units PC + 23" monitor	2 or more pods, floor stand system scalable and customizable PC + 23" monitor or laptop	none from Crisalix; user needs a pc/laptop and a standard consumer camera (digital camera, webcam, smartphone, etc.)	standard 3D system uses 4 Canon EOS 550D 18 MP, two head studio flash kit for illumination, optional: laptop with pre-installed software	✓
Realization	combined active and passive (hybrid)stereo photogrammetry					structured light		passive stereo photogrammetry				3D reconstruction from 2D image analysis	passive stereo photogrammetry	
Coverage	190-degree face and neck capture (ear-to-ear)	Full 360-degree capture of the head, face, and neck	Dual purpose 190-degree face, neck, and décolletage capture and torso capture for augmentation including under the breast	190-degree face neck, , and décolletage capture and torso capture for fuller figured reduction and reconstruction including under the breast	360-degree capture of body from head to toe with multiple anatomical options depending on application	~ 180-degree face capture	~180-degree face/torso capture	capturing volume (mm): 220x130x70 (H--W---D) typical application: 100-degree of left, right or front face	capturing volume (mm): 400x300x250 (H--W---D) typical application: face, neck and décolletage	capturing volume (mm): 600x550x350 (H--W---D) typical application: face, breast, torso, body	depends on number and placement of pods	~180° frontal and top-down views	~180-degrees face capture	✓
Capture Speed	~1.5 ms at highest resolution	~1.5 ms at highest resolution	~1.5 ms at highest resolution	~1.5 ms at highest resolution	~1.5 ms at highest resolution	<= 2 seconds	2 <= seconds	8 ms	3,5 ms	3,5 ms	2 ms	depends on camera of user	length of a flash ~1 ms	✓
Processing Speed	<8 seconds	<15 seconds	<10 seconds	<12 seconds	<60 seconds	depends on PC of customer	face: < 1 min torso: < 30 sec.	~20 seconds	~120 seconds	~80 seconds	~120 seconds	<= 5 min	60 seconds	✓
File Size	depends on configuration, 4MB - 26MB	depends on configuration, 15MB - 95MB	depends on configuration, 11MB - 65MB	depends on configuration, 12MB - 70MB	depends on configuration, 5MB - 100MB	3 MB	3 MB	8 MB	8 MB	8 MB	depends on configuration	there are no files (web service)	50 – 60 MB	✓
Geometry representation	a continuous point cloud available as a textured mesh and dense textured point model					a continuous point cloud -> later converted to a mesh		mesh				mesh	a continuous point cloud -> converted to mesh later	✓
Error in Geometry	< 0.2mm	< 0.2mm	< 0.2mm	< 0.3mm	< 0.2mm to 1mm	< 0.5mm	< 0.5mm	> 0.1mm (x,y,z)	> 0.1mm (x,y,z)	> 0.1mm (x,y,z)	> 0.1mm (x,y,z)	2-5 mm	<= 0.2 mm (32,33)	✓
Onsite Installation	✓	✓	✓	✓	✓	✓	✓	✓	✓	✓	✓	no need (web service)	✓	✓
Portable	✓	✓	✓	✓	✓	✓	no	✓	✓	no	✓	✓	✓	✓
Calibration time	20 seconds	90 seconds	30 seconds	45 seconds	90 seconds	< 5 minutes	< 5 minutes	no calibration	< 3 minutes	no calibration	< 2 minutes	no calibration	5 minutes	✓
Sample density	62 vertices / cm^2	62 vertices / cm^2	62 vertices / cm^2	55 vertices / cm^2	8-62 vertices / cm^2 depending on configuration	each head samples 0.5 million points	3 samples/mm^2	1.2 mm geometry resolution (polygon edge length)	1.2 mm geometry resolution (polygon edge length)	1.2 mm geometry resolution (polygon edge length)	1.2 mm geometry resolution (polygon edge length)	not specified	20 samples/mm^2 to 30 samples/mm^2	✓
approx. Price (June 2013)	Each system is custom-configured and upgraded from standard modules to meet the customer's specific imaging workflow requirements. Prices start at 21.000 EUR.					13.000 EUR	27.000 EUR	9.000 EUR	26.000 EUR	37.000 EUR	depends on setup	1590 – 5490 EUR per year	25.000 EUR	✓

Figure 7: Comparison between different 3D imaging systems. DI3D system (right side) and 3dMD (left side) showed the highest performance level. (9)

1.1.1.6 3D motion stereophotogrammetry (4D)

3D motion capture systems have been used for objective measurements of facial dynamics since early in the 21st century. Various systems have been introduced for body motion detection and analysis (13–16). The method is based on two main principles, the direct (markers based) motion detection (13) and indirect (marker free) motion detection systems (15,16). Marker based systems rely on the positions of special markers placed on specific areas to track the motion. More than one pair of cameras is required to capture the infrared signals from active emission markers or passive reflective markers attached. Vicon™, C3D system ™, Microsoft Kinect™ and Motion Analysis ™ are common brands for markers based motion detection systems. These systems are capable of accurate tracking of the captured information (13). However, the placement of the markers on patient's faces adds to the complexity of the procedure (14).

On the other hand, indirect 3D motion detection (marker-free systems) is based on a non-contact motion analysis using video recordings. An infrared projector is used to project an infrared dots pattern on the subject's face, while he/she animates (15,16).

Currently, the two commercially available marker-free 3D motion analysis systems are the 4D capture system (Di4D ™ Dimensional imaging, Glasgow, UK) and 3dMDface™ Dynamic system (3dMD, Atlanta, GA).

Di4D capture system is based on passive stereophotogrammetry which depends on surface texture to build the 3D facial model. An indirect motion detection system utilized a pair of mono chrome video recording cameras and a single coloured video recording camera. The mono chrome cameras were used to enhance the accuracy of the capture and to avoid noise from the coloured texture information while a normal white light was used for the video capture where each of the cameras simultaneously captures 60 frames per second. Landmarks are digitized on the first frame of the captured image and the software automatically tracks individually placed landmarks throughout the sequence of the captured frame during performing facial expressions. The

accuracy of the landmarks tracking has been validated by AL-Anezi *et al.*, 2013 (17) and clinically applied in various orofacial dynamics studies (18,19).

3dMD system, on the other hand, is based on active stereophotogrammetry using random infrared speckle projection. The latest version uses two pods with three cameras each (two grey scale and one coloured cameras) with infrared speckle projector in addition to normal white light. The system is capable of capturing still images and a video at up to 60 frames per second. The infrared projection helps increase the accuracy of triangulation and the output image is a continuous point cloud that theoretically eliminates the error associated with stereo image stitching (20). However, this may impact on the accuracy of the automatic tracking of facial landmarks throughout the captured frames of facial expressions.

1.1.1.7 3D laser facial scan

The development of laser scanning techniques provides a sophisticated method for capturing the orofacial region in three dimensions. It has been used for evaluation of surgical outcomes and stability of the results (21,22). High resolution facial imaging could be achieved using laser scanning; up to 20,000 coordinates could be generated on the facial surface. 3D laser scanning has been validated for its accuracy and reproducibility (23,24). The results showed an error of less than 0.56 mm in all scans.

Traditional laser scanning has the shortcomings of slow capture of the face, it takes 8- 10 seconds to scan the face, so any change in the patient's head position or facial expression during scanning will distort the scanned image; the patient's eyes should be closed during scanning for protection; soft-tissue surface texture is not captured, which results in difficulties in identification of some landmarks which are dependent on surface colour (11). Recent advancements such as using white-light laser approaches (surface texture colour), using eye-safe laser scanning which allows a safer scan and reduction of scanning time have enhanced the popularity of this approach. Laser scanning of the face has been considered in numerous studies including the quantification of facial symmetry

(25,26), evaluation of gender related facial dimorphism (27), study of facial morphology among different populations (28), evaluation of growth changes in facial morphology (29) and assessment of surgical outcome (30,31).

1.1.1.8 Electromagnetic 3D digitizer

This is not an imaging tool but a method to produce a set of 3D coordinates of selected landmarks on a 3D object which is accomplished by using a flexible arm to carefully digitize the positions of landmarks directly on patients' faces (32,33). The advantages of this method are that it is non-invasive and landmark identification is usually assisted by palpation of the underlying bony structures, such as gonial angle, for better accuracy (32,34). The outcome is a set of 3D landmark coordinates that can be used for further analysis.

1.1.2 Acquisition of 3D volumetric data

These are the imaging tools that can penetrate through the surface to capture internal structures in addition to the surface image. Traditionally facial cephalometric radiography was the main tool to evaluate facial skeletal structures. At the late quadrant of the past century, the introduction of 3D radiography such as computerized tomography (CT) and Cone Beam Computerized Tomography scan (CBCT) led the revolutionary change of the assessment of facial morphology, and later on the development of Magnetic Resonance Imaging (MRI) and 3D Ultrasonography took place to augment the amount of information provided for the whole body, and in particular, for the craniofacial region.

1.1.2.1 Computed tomography (CT)

Computed tomography (CT) is a highly specialized method of tomography and provides anatomical image slices through the body. This was developed in 1972 by Sir Godfrey Hounsfield and Allan McLeod Cormack and was manufactured by EMI (35). CT utilizes the variation of the attenuation of the x-Ray beam traversing various body tissues to map an image of grey scale which represents the shape and position of internal body structures. CT depends on multiple

sensors which are placed opposite to the x-ray beam source on a rotating gantry where both rotate around the body of the patient at the area to be scanned. Data from the sensors are transmitted to the computer to be processed into multiple axial 2D slices building the three dimensional image structures for the scanned volume (35).

In order to interpret the output data from CT an image matrix should be created. This matrix is composed of a sequence of numbers arranged in columns and rows, each square of the matrix is referred to as a picture element, and when arranged in a matrix these elements are called pixels. The pixels are arranged into a slice composing a single two dimensional slice image, and when combining multiple slices, the thickness of the slice creates an additional volume element or voxel, and each voxel has a CT number or Hounsfield Unit (HU). A HU is the number that is allocated to each individual voxel within the image and is displayed on the monitor as a level of brightness. HU value is dependent on the relative comparison of an x-ray attenuation coefficient of the tissue that is present within the voxel compared to an equal volume of water. Water is used as the reference material as it has a uniform density and is abundant within the human body; It is assigned a HU value of zero. Molecular structures that have more density than water are assigned with a positive HU value and structures that have less density are assigned with a negative HU value. The range of values varies from -1000 for air to +4000 for metals, (35).

Computed tomography has been widely used in the field of dentistry providing cross-sectional implant imaging (36), for evaluating a pathology in the maxillofacial region (37), in planning for craniofacial reconstruction (38), and for predictive surgical planning (39,40). CT allows the user to access the internal structures of bone and teeth in a virtual environment. When displayed in a 3D format it can provide valuable information as the images provide clear information about the recorded anatomical structure in a variety of directions as well as cross-sections (41–43).

1.1.2.2 Cone beam computed tomography (CBCT)

Cone beam computed tomography (CBCT) is relatively recent introduction and has similar features to that of CT. CBCT was specifically designed for use in the maxillofacial region for the visualisation of hard tissue and has gained broad acceptance in dentistry in the last 5 years (37). CBCT differs from conventional CT in many aspects:

1. While the x-ray source in CT is generated from a high output rotating anode, CBCT can use a relatively low energy fixed anode tube comparable to dental panoramic x-ray machines.

2. CT scanners image patients in a series of axial plane slices that can be either stacked or form a continuous spiral motion, while CBCT captures the image in one 360° rotation. The maxillofacial region can be captured as a single image or the field to be imaged can be specified to capture a limited regional area of interest (38).

The CBCT scanner includes a rotating gantry to which an x-ray source or projector and detector are attached opposite to each other around patient's head. The x-ray beam projects as a cone-shaped beam through the centre of the area of interest and the image is recorded on a flat panel detector on the opposing side. The gantry rotates once around the region of interest projecting and capturing 150 to 600 sequential planer projection images of the field of view. The projection images pass through a complex algorithm where the x-ray beam attenuation is calculated for each volume unit (voxel). This procedure is normally completed within 10-30 seconds (44). The developed image files are in a DICOM format (Digital Imaging and Communications in Medicine); this is the universal format for 3D images in the medical field.

The dose of radiation is significantly reduced compared to the conventional CT and it is approximately equal to a full mouth periapical series (45). This depends on the setting and the model of CBCT device being used which ranges from 29 Sv to 477 Sv compared with the conventional CT output of 2000 Sv (44).

Some CBCT scanners enable facial capture while the patient is seated in an upright position. This is particularly beneficial when the image is used for orthognathic surgery planning.

CBCT has some other minor advantages compared to normal CT, these include a significant reduction in artefacts created by patient movement as the images are captured in one single rotation of the device (44); CBCT devices are significantly smaller and less expensive than conventional CT (46); and the isotropic resolution is relatively high ranging from 0.076 mm – 0.4 mm which makes the CBCT accurate enough to be used in craniofacial imaging. On the other hand the contrast resolution which can display soft tissue information is clearer in conventional CT scans compared to that of CBCT (37).

When imaging patients using CBCT, any intra-oral metallic objects (e.g. restorations, jewellery, implants and orthodontic appliances) create streak artefacts (43,47). This is to some extent a common problem shared with the CT and CBCT scanners alike. A few published research papers have proposed solutions for this problem (42,43). However, none of them were satisfactory enough to be considered clinically.

1.1.2.3 Magnetic resonance imaging (MRI)

Magnetic resonance imaging (MRI) was first introduced in July 1977 (48). The principles of MRI differ greatly from CT, CBCT and conventional radiography as no ionizing radiation (x-rays) is required to generate the MRI image (49,50). MRI is generated from electromagnetic energy produced by a powerful magnet. By generation of a powerful magnetic field the hydrogen atoms within the body are aligned. Radio waves are then transmitted to alter this alignment resulting in the hydrogen emitting a weak radio signal which is amplified by the scanner (51). MRI is currently regarded as the gold standard for the imaging of soft tissue, but it is of limited value for the imaging of hard tissues (48). MRI has equal resolution but much greater soft tissue contrast than CT scanning; this allowes a better visualisation of the soft tissues (50).

A few drawbacks with MRI scanners have been reported: it is relatively time consuming; equipment is expensive; it is noisy and some patients fee claustrophobic while in the gantry tube during image capture (50); MRI is contraindicated in patients who have a considerable amount of implanted metallic devices (48), metallic dental restorations, and orthodontic brackets as these materials can produce image distortion (52,53). In addition to that, MRI does not provide the natural photographic appearance of the texture of the facial surface(52).

1.1.2.4 Ultrasonography

Ultrasonography is an imaging technique that captures the reflection of transmitted pulses of ultra sound. These pulses are emitted from a probe in a direct connection to a patient's skin, and a special conductive gel is needed to improve the contact between the ultrasound probe and the skin. When the ultra sound wave crosses the junction between two tissues with different densities part of the wave is reflected back and detected as an echo by the probe (54). The depth of tissue is calculated from the duration of time for the echo to be detected. Three dimensional images are created by acquiring multiple cross sectional 2D images.

3D ultrasonography is a relatively new 3D imaging technique and has many advantages such as the relatively low cost of the equipment and the absence of ionizing radiation exposure. Modern development of high resolution ultrasonic imaging saw the introduction of the Colour Doppler Ultrasonography (CDUS) (55) and Power Doppler Ultrasonography (56) with their promising ability of differential diagnoses of malignant tumours.

Ultrasonography in maxillofacial surgery is limited for diagnoses of temporomandibular disorders (57,58). The use of ultrasonography as an imaging technique for maxillofacial surgical planning is still at an experimental stage, and there are major problems associated with data acquisition, reduction and storage (59).

The procedure is time consuming and requires a compliant patient as well as a highly skilled operator (60). Ultrasonography is not able to visualise bone abnormalities (49). Due to the need for direct skin contact, probe touching and depression of the patients skin may cause distortions of their spatial positions (60).

1.2 3D image processing

1.2.1 3D modelling and 3D image visualisation

3D modelling in the medical field has an increasing importance in diagnosis, simulation, and treatment planning. Most of the 3D models used in various medical applications are rendered from 3D images acquired using one of the multi-range scanners, most commonly CT and MRI. CT scanning detects the x-ray beam attenuation coefficient and creates a multi-slice volume image which contains the information about the internal body structure within the scanned volume in the form of grey scale gradient. Internal structures of close intensities such as muscles, nerves and blood vessels are not well differentiated using this method. However, skeletal tissue surface and soft tissue surface are easily identified and segmented from the image data. MRI detects the Hydrogen nuclei resonance in the magnetic field and internal structures such as nerves and blood vessels are clearly identifiable. However, skeletal structures are not well represented due to low water content (48).

The 3D image volume is divided into isotropic cubes which are trapped between image slices, and each of them is called a “voxel”. The size of the voxel is governed by image resolution which is represented as the number of the slices generated from the scanned volume. Each voxel has 8 vertices at the corners (four on each successive slice). Voxels are provided with a grey scale intensity level which represents the anatomical structure captured in that volume. Three dimensional (3D) models segmented from these types of images are usually rendered in 3D polygonal mesh form. Therefore, it has the capability of representing details of biological objects’ surface topography in addition to the selective mesh density option which allows rendering high density polygonal meshes at areas with detailed anatomical surface features, such as areas around

the eyes and nose in human face while choosing lower density at regions where less detail is needed, such as the cheeks areas. This will lower data size and improve processing time while high density is preserved where needed (61).

Several algorithms have been proposed for building-up a polygonal surface mesh from a scanned image. Commonly used 3D model construction algorithms are slice based surface contour detection (62) ray casting (63) and the marching cube algorithm, which is the most commonly used algorithm in the medical field and was first introduced by Lorensen and Cline in 1987 (61).

1.2.1.1 Marching cube algorithm

In 1987, Lorensen and Cline (61) proposed an innovative method of building a 3D model from volumetric images such as CT and MRI. The process involved detecting the anatomical structure surface from the grey scale intensity of the voxels in a volumetric image and rendering it as a 3D polygonal surface mesh through the following two steps; First, locating the surface corresponding to a user-specified HU value and creating triangles representing the intersection of the surface boundary with the voxel sides. Then, to ensure a quality image of the surface, the algorithm calculates the normals to the surface at each vertex of all the triangles.

Marching cubes uses a divide-and-conquer approach to locate the surface in a logical cube (voxel) created from eight pixels, (figure 8); four from two adjacent slices joined to the corresponding four from adjacent slice. The algorithm determines how the surface intersects this cube; creates a triangle then moves (or marches) to the next cube. The algorithm tests each voxels against the assigned HU value, if the data value at that voxels exceeds (or equals) the value of the surface we are constructing then these voxels are inside (or on) the surface. Voxels with values below the selected HU value are outside the surface (61).

1.2.2 3D image superimposition:

In orthognathic surgery, image superimposition is mainly aimed at comparing the change of jaw bones for surgical outcome assessment or growth monitoring. Therefore, superimposition has to be on a stable area that hasn't been significantly changed by the variables being assessed. Classic 2D analysis relies on the anterior cranial base and forehead and so does the 3D superimposition. These areas are at a significant distance from the area of surgical change and reasonably stable during growth (64). In General, three main types of 3D image superimposition were commonly applied by most of the reviewed literature. These were *landmarks based registration*; *surface based registration* and *volume (voxel) based registration*.

1.2.2.1 Landmark based registration

General Procrustes Analysis (GPA) involves translation, rotation and scaling to match two 3D objects by superimposition. In orthognathic surgery assessment, scaling is avoided to preserve the geometry of the structures being studied, therefore, Partial Procrustes Analysis (PPA) is preferred which includes object translation and rotation only. The procedure involve identifying corresponding landmarks on two related images followed by translation and rotation of one of the images bringing the corresponding landmarks into the best fit relying on their centroid match (65). The centroid is the geometric centre of the shape to be analysed. This method is also referred to as manual registration since the landmarks are manually identified. This method is easy to apply but the potential error is associated with the manual landmarking.

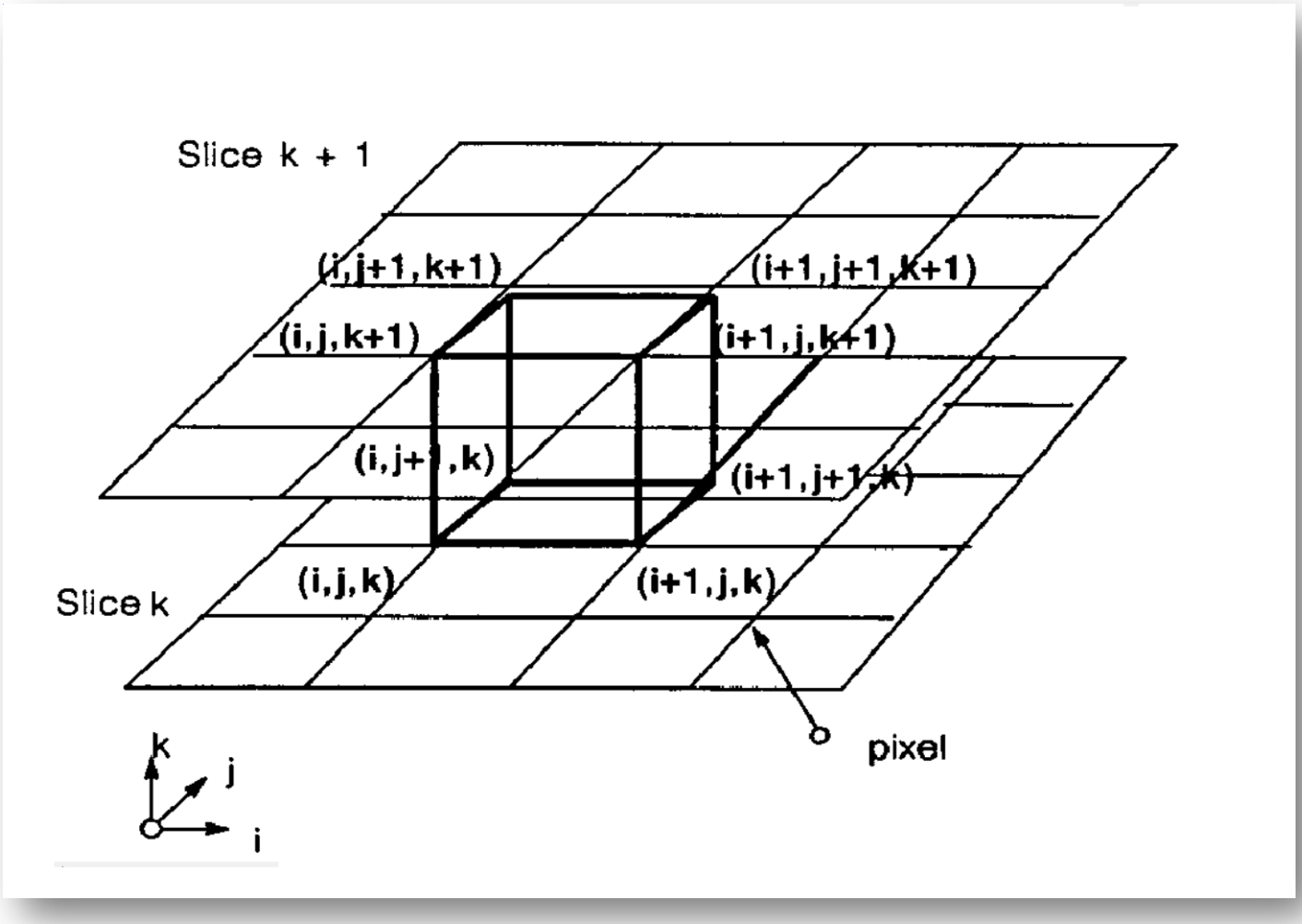

Figure 8: Marching cube algorithm. Diagram presented by Lorensen W, Cline H, 1987 showing the basics of marching cube algorithm. For each voxel, a cube is formed by locating 8 vertices, four on each adjacent slice.

1.2.2.2 Surface based Registration

From its name, this method relies on surface topography matching between the two images. The procedure is entirely automated but often preceded by a free hand registration or landmark based registration to provide a better starting point for the automated process and thus shorten the time required and increase its accuracy. The method's main objective is to bring the corresponding vertices of the two superimposed surfaces as close as possible to each other in the region of interest. The algorithm utilised for this is called *Iterative closest point* (ICP) which involves an iteration of moving (translation and rotation) followed by calculation of the mean square root distance between the two meshes measured from each vertex to the closest correspondence on the opposite mesh (66). The iteration continues until this measurement reaches its minimum value to maximise the superimposition of the two surfaces.

1.2.2.3 Voxel based registration

The method has been widely used for various medical applications and research purposes including diagnoses, treatment planning and assessment of a variety of cases utilizing CT, CBCT, MRI, and 3-D power Doppler ultrasound.

Voxel based registration algorithm utilizes the grey scale intensity difference of the superimposed DICOM images voxels to approximate the overlapping DICOM image to the best fit maximizing mutual information based on the grey scale density calculated between the two images voxel by voxel (67).

This method utilizes relatively complex algorithms for voxel based registration compared to those used for surface based registration and thus, it requires extra time to execute and more powerful computer processors are required to handle the image registration process. In addition, the higher cost of the software packages capable of voxel based registration might reach up to 10 times the cost of software packages required for surface based registration.

Researchers who used voxel based registration have claimed more accuracy in registration (68,69). However, a recently published article of our work, Almukhtar *et al.*, 2014 (70), showed that there was no statistically significant difference between the two methods.

1.2.2.4 Vestibular registration

Vestibular orientation (VO) is a technique developed initially to serve the needs of comparative anatomy and ontogeny. The lateral semi-circular canal (LSCC) is used to define the horizontal plane. Following the orientation of the skull to the horizontal plane, vertical and median planes were derived to serve as a reference planes for superimposition of sequential images to observe the effect of growth or surgery on various parts of the skull. A limited number of published articles have been found for this approach (71).

1.3 3D image analysis

1.3.1 Skeletal analysis

Radiographic imaging including lateral and frontal cephalometric radiography provides the traditional images for the analysis of the facial skeleton. Their marked short comings have been pinpointed in numerous scientific publications (72–74). The method is associated with errors in the projection, errors in landmark location and mechanical errors in tracing. Even though 3D cephalometry was not practically applicable until recently, Baumrind and Frantz 1971 stated "*The conclusion appears inescapable that the total amount of information contained in head films is not sufficiently large to make clinically meaningful predictions even if we were able to assess all the contained parameters perfectly by the use of stereo-head films or by the integration of information from lateral and frontal films (as in Broadbent's method)*" (73). Adams *et al.*, (2004) (75) compared the lateral cephalometric measurements against the direct physical measurements which were considered the gold standard. The measurements obtained from a single cephalometric radiograph were significantly different (75). Van Vlijmen *et al.*, 2010 (76) showed that

measurements obtained from 2D cephalograms were significantly different from those obtained from a CBCT image.

The Golden ratios of 'Leonardo da Vinci' in the fifteenth century and the Books of Proportions by Dürer in the beginning of the seventeenth century are the best example of the historical description of the standard measurements of the human face.

One of the first cephalometric analyses was introduced by Downs 1956 to quantify facial morphology. Downs polygon was an effective method of cephalometric analysis which included three measurements; the facial angle (N-Pog) to Frankfort plane; angle AB to the facial plane and the angle of facial convexity (N-A to A-Pog). The analysis focused on the skeletal and dental components, facial soft tissues were not considered (77,78).

Steiner introduced his analysis of the skeletal, dental and soft tissues separately (79). He was the first to consider the anterior cranial base (Sella to Nasion) as the line of reference to evaluate the position of the jaw bones (79) instead of the Frankfort Horizontal line suggested by Downs (77). According to this analysis, the lips, in well-balanced faces, should touch a line extending from the soft tissue contour of the chin to the middle of an "S" formed by the lower border of the nose. This line is referred to as the S-line (80). Steiner's S-line is still used in orthodontics and orthognathic research in addition to Steiner's skeletal and dental measurements (81).

Burstone was the first to define a set of landmarks on the soft-tissue profile (82). The nasolabial angle and facial contour angle are two of many soft-tissue measurements that he proposed in this analysis.

Vertical relationship was first emphasized by Sassouni (83). He introduced the terms "skeletal open bite" and "skeletal deep bite" depending upon the

divergence or convergence of the four horizontal anatomic planes of his analysis. However, the analysis is not routinely applied for the dentofacial diagnosis (84).

Evaluation of the facial width, facial height and facial contour were dependent on the facial angle, the XY axis and the facial plane according to Ricketts in 1961(85). Facial contour was measured as the angle between the facial plane (N-Pog) and A-Pog. The aesthetic line (E-line) is one of the common measurements to assess the balance of the facial profile (86,87). The E-line extends from soft-tissue pogonion to pronasale (tip of the nose).

Other analyses including Burstone's method (82), Di Paolo's quadrilateral analysis (88), Bergman's analysis, and Butow analysis (89) were introduced for cephalometric analysis of the craniofacial morphology.

Many measurements have been applied clinically to assess soft-tissue facial changes. The most common ones are the vertical facial proportions, facial asymmetry measurements, upper anterior teeth exposure at rest, dental exposure on smiling, middle to lower facial third ratio, upper lip to lower lip height ratio, nose width and length, nasolabial angle, upper lip prominence, lower lip prominence, inter-labial gap, labiomental fold, zero-meridian, chin prominence, chin-neck angle, soft-tissue angle of facial convexity, E-line of Ricketts, S-line of Steiner, Z angle of Merrifield, and Holdaway's soft-tissue measurements (22,24,25,26).

Various reference planes recorded the position of anatomical structures including the Sella-Nasion plane (SN), the Frankfort horizontal (FH), the mandibular plane and the maxillary plane.

Despite the short comings associated with 2D cephalometry, these analyses are still routinely applied for diagnoses and treatment planning in orthodontics and orthognathic surgery.

1.3.1.1 3D Cephalometric analysis

The development of CT and the dramatic decrease in radiation dose with the CBCT brought three-dimensional analysis of the head and face to the scene and made it possible to expand the knowledge of the craniofacial structures into the third dimension. Errors associated with conventional 2D cephalometry could be eliminated with the advent of 3D cephalometry (90).

The First attempt to apply cephalometric analysis on 3D models of the skull was established by Robert W. Fuhrmann 2002 (91). His aim was to copy a traditional 2D cephalometric analysis onto a 3D surface model of the skull segmented from a CT scan image. His approach was not successful due to the lack of clear 3D definition of anatomical landmarks. However it opened the doors for progressive research in that field. In 2006 a simultaneous publication by Gwen R. Swennen 2006 (90,92) and Raphael Olszewski 2006 (93) introduced two new 3D cephalometric analyses. The main difference from the traditional 2D Cephalometry was that the anatomical landmarks were digitized on the 3D surface model of the skull and soft tissue. This subsequently led to the need for paired digitization of the bilateral landmarks including *Orbitale, condylon, gonion,* and *porion*. 3D Planes were introduced including the Frankfort Plane which connects two *orbitale* and a mid-point between right and left *porion*, the mandibular plane which connects *menton* and two *gonion* landmarks, the maxillary plane which connects the anterior and posterior nasal spines, Mid-sagittal plane which connects *Nasion* and *sella* points, and is oriented perpendicular to the horizontal plane and the vertical (coronal) plane which is established perpendicular to both planes at the position of the sella. Transforming a line into a plane facilitated the assessment of anatomical structures in the third dimension.

In his article, Gwen R. Swennen validated the accuracy and reproducibility of his analysis by measuring inter and intra examiner errors associated with the identification of the landmarks (36 Landmarks), linear distances (78 measurements) and angular measurements (164 angles) on 26 CT scan images.

The results showed low inter and intra examiner errors with high correlation coefficient (90).

3D-ARCO analysis on the other hand was introduced by Olszewski in the same year (93). In this the 2D Delaire's cephalometric analysis was transformed into 3D to evaluate craniofacial deformities. The philosophy of this analysis is that a reference plane must not rely on landmarks located on the analysed anatomical structure. In asymmetry cases, for example, the sagittal plane that depends on external facial landmarks is not acceptable. The author proposed a sagittal reference plane (orbito-maxillary-sagittal plane) based on landmarks found on the foramina associated with trigeminal and optic cranial nerves. In this article, 13 CT scan images were utilised for validation of the analysis and a low inter and intra examiner error were observed.

The published data show that the error associated with 3D-ARCO analysis was significantly lower than that with Swennen analysis, especially when linear measurements were compared (94).

Recently, Lee *et al.*, 2014 (95) readopted Delaire's measurements for 3D analysis. Their concept was similar to the 3D-ARCO analysis except that the landmarks were placed on the slices of the DICOM image instead of the 3D surface model which was claimed in previous studies to be more accurate and reproducible (96).

Several studies have reported the accuracy of 3D cephalometric analysis (97-100); Others have compared between 2D and 3D analysis (75,76,94,101); further studies have looked at the improvement of the accuracy in landmarking the slices of the DICOM images (95,100,102,103). Two systematic reviews have been published recently (104,105), they concluded that there is still limited research to support the validity of the 3D cephalometric analysis. The large variation of approaches and measurements made it difficult to extract an objective comparison, and future approaches should provide a more standardised method of conduction.

The change in the Cephalometric analysis from 2D to 3D and the variation in the concept of the measurements between the two approaches highlighted the need to establish new norms among populations of different ethnicity. Few attempts have been made in this field. Most recently the norms in a South Korean population based on 3D architectural and structural cephalometric analysis have been published (95). Gender difference was the most prominent characteristic among the population where adult males were found to have higher ramus length, width, and total facial length.

1.3.1.2 3D surface analyses using colour coded distance map

The 3D colour coded distance map has been applied to analyse the 3D changes in the facial skeleton after orthognathic surgery (69,106–108). This tool provides a measurement of the relative distance between two 3D surface meshes by measuring the distance of each vertex from one mesh to the closest point on the compared mesh. The measurements are then verified by changing the vertices' colour in a scale ranging from blue which is the maximum –ve measurement to red which is the maximum +ve measurement. It is also possible to consider numerical values by calculating generalized mean and standard deviation, maximum and minimum measurements. This method is more commonly associated with soft tissue analysis. Thus, a thorough description has been provided in the following sections related to soft tissue analysis.

Carvalho *et al.*, 2010 applied a colour coded distance map to each anatomical component of the mandible and the maximum value represented the main displacement of that anatomical part (108).

Their method gives the opportunity to use the total surface area to analyse the skeletal movement and provide a single measurement for comparison. This point may or may not be at the site of anatomical landmarks.

1.3.1.3 Changes in centroid position

Cevidanes *et al.,* 2005(109) evaluated the 3D displacement of atomically defined areas of the mandible affected by orthognathic surgery by measuring the absolute displacement between its centroids (the centroid is the geometric centre of a 3D object).

This method simplified the analyses of the 3D movement of a structure by measuring the displacement of a single point (centroid) since its displacement depends on the movement of all the vertices of the 3D object.

The short coming of this method lies in that it measures the absolute translation of the 3D object, the rotation movements will not be recorded if it did not alter the position of the centroid. The position of the centroid is highly sensitive to the object's geometry so that any alteration of the morphology of the anatomical structure as a result of surgery (removal of the anterior nasal spine or positioning of the fixation plate) may change the position of the centroid, this will lead to inaccuracy in measuring surgical movements.

1.3.1.4 Volumetric measurements

The 3D modelling technology offers the ability to virtually measure the volume of the 3D object. Maal *et al.,* 2012 (110) analysed the displacement of jaw bones after orthognathic surgery by superimposing the preoperative and postoperative to measure the differences in volume. Although this method gives us an idea about the increase in volume of the jaws after surgery, it does not identify the new position of the anatomical structure after the surgery.

1.3.1.5 3D Vector analyses

Recently, Park *et al.,* 2013 (111) introduced a new method for assessment of the asymmetry of mandibular anatomy by analysing the vectors of mandibular functional units. The magnitude and directional difference of these vectors were measured to identify the contribution of each part of the mandible to the total

mandibular asymmetry. This method is highly informative and provides valuable information about the origin of mandibular asymmetry. However it is specific for asymmetry cases in addition to the associated landmarking error.

1.3.2 Soft tissue analysis

Direct facial anthropometric measurement is theoretically ideal for the analysis of facial morphology. However, this requires special skills for the examiners and has a considerable range of errors compared to 2D or 3D indirect measurements (33). Among indirect measurement methods, photogrammetry seems to be more frequently used. However, to be of an acceptable accuracy, it requires a standardized clinical photographic technique (112–115). Common extra-oral photographs used for facial assessment are full-face with relaxed lips, full-face with smile, 45-degree oblique and profile images (116).

During the late 20th century, standardized photographic techniques have been developed and were adopted by several investigators for facial anthropometry (112,113,117,118). In comparison with direct anthropometry, standardized indirect anthropometry allowed the measurements to be carried out on a still photo rather than on a relatively moving surface of the face, and the negative impact of the compressibility of the skin is eliminated (119–121). The measurements can be repeated without recalling the patient and the data can be permanently stored for future comparative examinations. However, the basic concept of photogrammetric analysis is to measure the shortest distance between two landmarks projected on a 2D image (flat plane), this may be different from the actual geodesic distance between the two points. Two dimensional photographs may also obscure some anatomical structures which limits the comprehensiveness of measuring facial characteristics. A compromised accuracy of land marking was also reported (117).

The introduction of the 3D (x, y and z) Cartesian coordinate system by *René Descartes* in the 15th century allowed the spatial orientation of physical objects to be measured in a digital framework. Various 3D capturing techniques were

introduced (Section 1.1.1). These are capable of providing three dimensional information (point cloud data) that allow volumetric surface and curve analyses to be carried out in addition to the classical linear and angular measurements.

In orthognathic surgery, various methods were applied to quantify facial dysmorphology and measure the changes following surgical correction. The methods ranged in their complexity from simple linear and angular measurements up to the more complex statistical models including curve analysis and PCA. More than 200 published scientific articles were reviewed in this chapter, in about 50% of these studies analysis of the facial soft tissue was the main objective. Table 1 shows the methods applied in the published data to study the impact of orthognathic surgery on the covering soft tissue.

1.3.2.1 Landmarks based analysis

Landmarks based analysis is the most common method for the evaluation of soft tissue morphology. However, the method is limited to the analysis of the changes at a set of particular points which does not describe the complex nature of the facial morphology. Measuring the shape changes at the surface between the selected points is not considered in this method. Unlike the hard tissue, this argument seems to be more appealing here since the soft tissue surface is not a solid structure and the response of a surface area to the changes in the underlying skeletal changes is too complex to analyse at a certain set of anatomical landmarks. The limited number of reproducible points of the facial soft tissue restricts the value of the landmarks based analysis.

Farkas *et al.*, 1980 (112) suggested 16 facial landmarks that are still used these days as the gold standard for facial soft tissue analysis (table 2).

Hwang *et al.*, 2012 (122) studied facial asymmetry on 60 stereophotogrammetry images using Farkas' landmarks. The orthogonal distance of each landmark to a common three dimensional reference planes were measured. The results showed that facial asymmetry was more obvious in the lower third of the face, ch, Ala

and Me landmarks showed the highest asymmetry scores. Similar studies considered more facial landmarks (123–127). G Sforza *et al.*, 2007 (128) digitized 50 landmarks to evaluate the changes following the surgical correction of skeletal class III jaw deformity in 7 cases. The surgical results were compared with the facial appearance of 87 healthy females as a control group. The results showed that facial deformities were significantly improved after orthognathic surgery.

In addition to the standard set of anatomical landmarks mathematically generated ones were also utilized for facial analysis. These were identified by the intersection of two or more lines passing between anatomical features or at a specific distance and direction from an adjacent landmark.

These extra landmarks allow a more comprehensive analysis of the facial morphology. Terajima *et al.*, 2008 (129), Kim *et al.*, 2011 (130) and Park *et al.*, 2013 (131) applied a grid of intersecting lines comprised of 10 horizontal equally distributed lines at 4.5 mm distance and 27 vertical lines equally distributed at 5mm distance from each other. The grid was orientated vertically and the top first line passes through the right and left "orbitale" landmarks. The preoperative and post-operative CBCT images were superimposed, and 270 points of intersections between the vertical and horizontal lines were dropped on the soft and hard tissue for analysis. Hoefert *et al.*, 2010 (65) used a set of mathematically generated landmarks for image superimposition and analysis such as the mid-point from (go) to (me) and mid-point from (ex) to (ch) (8,9) (figure 9).

Table 1: Types and percentage of published methods of soft tissue analysis 2000-2015

Rank	Type of analysis	Percentage
1	Landmarks based Linear and angular analysis	50%
2	Colour coded distance map	28.7%
3	Absolute surface distance	11.95%
4	Vector analysis	8.75%
5	Volumetric measurements	5%
6	Principal component analysis	3.75%
7	Dense correspondence analysis	2.5%
8	Curve analysis	1.25%
9	Centroid and GPA	1.25%
10	Statistical landmarks plotting	1.25%

Table 2: Definitions and abbreviations of facial soft tissue landmarks by Farkas 1980(67)

Landmarks	Abbr.	Definition
Glabella	Gla	Most prominent midline point between eyebrows
Nasion	Na	Deepest point of nasal bridge
Pronasale	Prn	Most protruded point of the apex nasi
Subnasale	Sn	Midpoint of angle at columella base
Labial superius	Ls	Midpoint of the upper vermilion line
Stomion	Sto	Midpoint of the mouth orifice
Labial inferius	Li	Midpoint of the lower vermilion line
Menton	Me	Most inferior point on chin
Exocanthion*	Exc	Outer commissure of the eye fissure
Endocanthion*	End	Inner commissure of the eye fissure
Alar curvature*	Ala	Most lateral point on alar contour
Cheilion*	Ch	Point located at lateral labial commissure

*** Paired (right and left) landmarks.**

The spatial information of soft tissue landmarks was either digitized directly on patients face using an electromagnetic digitizer in some studies (34,128,132,133) or virtually by digitizing landmarks on a 3D image viewed on a computer screen(129,134–137). Infra-red (IR) sensors were also utilized to detect the 3D position of IR emitting landmarks fixed on the patient's face (138,139).

The accuracy of landmarking is variable according to the technique used for imaging as well as the method of digitization. Fourie *et al.,* 2011 (140) evaluated the accuracy of landmarking of three different imaging systems (laser scanner, CBCT and stereophotogrammetry). Twenty-one linear measurements were developed based on 15 landmarks placed on the three images, and these were compared to those obtained from direct anthropometric measurements. The difference in the mean absolute distances between the three measurements was less than 0.89mm. However the study did not compare the absolute digitization error at individual landmarks. Plooij *et al.,* 2009 (141) evaluated the reproducibility and reliability of 3D landmarking of stereophotogrammetry images. 49 soft tissue landmarks were digitised twice by 2 observers. The images were loaded into specialized software (Maxilim) where the orthogonal distance of each landmark to 3D reference planes was recorded. Paired sample t-test and correlation coefficient evaluated the reproducibility and the reliability of the digitisation. The results showed no significant differences between the inter- and intra- observer measurements with a high correlation coefficient.

Othman *et al.,* 2013 (142) evaluated the reproducibility of facial soft tissue landmarks on a stereophotogrammetry image which showed no statistically significant difference between the repeated readings.

Gwilliam *et al.,* 2006 (143) digitised 24 soft tissue landmarks on six 3D facial scans. Thirty orthodontists of varying experience were asked to landmark the facial scans to establish inter-operator reproducibility. The results showed that only 50% of the landmarks were associated with less than 1 mm error when re-digitised by the same observer. Whereas only 8% of the landmarks showed less than 1mm of error in reproducibility when digitised by different observers.

Similar results were obtained by Toma *et al.*, 2009 (144). 21 landmarks were placed on 30 laser scanned facial images by two observers. This was repeated after two weeks. Bland-Altman plot was used to assess the reliability of each landmark and only 50% of the landmarks showed less than 1mm error and less than 0.5 mm error was observed in 35% only.

The results of the validation studies led to the conclusion that despite the high level of precision in digitising landmarks the accuracy level of 0.5 mm was only achievable in few of the landmarks.

Lower landmarking error was observed by Khambay *et al.*, 2008 (12). A reproducibility study was carried out to assess operator errors of landmark digitization on high resolution stereophotogrammetry images captured by the DI3D system. Operator error was measured by repeatedly locating landmarks on the three-dimensional image. The results showed that the operator error in placement of landmarks on the three-dimensional model was 0.07 mm, range 0.02 mm – 0.11 mm.

1.3.2.1.1 Linear and angular measurements

Around 50% of the reviewed published papers used this approach. Changes in facial soft tissue after surgery have been assessed using two main methods: Measuring the linear and angular distance between landmarks; and their 3D orthogonal distances against common 3D reference planes (134,136,143–147). Some of these were part of a 3D soft tissue cephalometric analysis. The measurements were made on the pre- and post-operative images separately and the results were compared to find the differences. In a minor fraction of these studies the assessments were made by measuring the net distances between corresponding landmarks on both images, and in this case an additional step of image superimposition was needed. Facial heights, A-P position of soft tissue A, B Prn, Sn, and soft tissue Pog were the common linear and angular measurements in addition to facial asymmetry measurements.

Chen *et al.,* 2012 (148) utilized linear measurements between corresponding landmarks to investigate profile changes after surgical treatment of mandibular prognathism. Thirty patients (20 females and 10 males) underwent vertical ramus osteotomy. Preoperative and postoperative cephalograms were analysed; landmarks were identified and compared. The mean setback of the pogonion (Pog) was 11.7 mm. The setback ratios of labrale inferius (Li) / incision inferius (Ii), labiomental sulcus (Si) / point B, and soft tissue pogonion (Pog) / pogonion (Pog) were 0.98, 0.99, and 0.95, respectively. There were no sex related changes in soft tissue.

Ubaya *et al.,* 2012 (147) carried out a study involving linear and angular measurements on 3D stereophotogrammetry images of 40 patients following orthognathic surgery and compared them to a control group of 112. The study aim was to evaluate the 3D naso-maxillary complex soft tissue morphology following Le Fort I maxillary advancement. The results showed that facial morphology post-surgery was similar to the reference group, except the nasal base width which was wider by 2.3 mm in males and 2.6 mm in females. In the orthognathic group, the females had a smaller nasolabial angle by 9.78° than the reference group.

1.3.2.1.2 Vector analysis

This approach was considered by about 8.75% of the reviewed articles (149–151). Vectors analysis considers the magnitude and direction of the linear displacement of corresponding landmarks. This is particularly beneficial to study the mechanism of oro-facial changes in 3D or 4D. This method can produce valuable information when combined with a more comprehensive type of analysis including dense correspondence analysis which measures the changes of every vertex on the mesh of the surface of the face (152).

1.3.2.1.3 Thin plate spline (TPS)

This approach was considered in 1.25% of the reviewed literature (153). TPS was first introduced by F L Bookstein (154). It measures the bending deformation of

the geometry of a particular shape guided by a group of corresponding landmarks. A mathematic algorithm then smooths these deformations by minimizing the localized bending energy of the shape produced by the original change.

Bugaighis *et al.,* 2010 (153) examined the facial soft tissue of 4 categories of cleft lip and /palate children (40 with a unilateral cleft lip and palate (UCLP), 23 with a unilateral cleft lip and alveolus (UCLA), 19 with a bilateral cleft lip and palate (BCLP), and 21 with an isolated cleft palate (ICP)). Patients' faces were captured using stereophotogrammetry and compared to 80 age and gender matching control group. After applying thin plate spline algorithm to measure the differences of the facial morphology among the study groups, the transformation matrix quantified the change in the mean distance of the facial landmarks from their centroids. The principal component analysis was applied to identify the morphological difference among the cleft groups.

1.3.2.1.4 Principal component analysis (PCA)

PCA is a statistical multivariate correlation analysis aimed at simplifying large data analysis by limiting the number of variations of shape differences to those with a significant contribution to the total variability. This approach does not only simplify the analysis but also emphasizes the level of importance of each associated aspect of variations by analysing the distribution of its effect around the mean. The Eigenvalues associated with variation vector for each variable are measured. The "eigenvalue" and "eigenvector" are the determinants of the transformation matrix of that shape deformation. In other words, shape deformation has both magnitude and direction which could be calculated by analysing its transformation matrix. When PCA is applied to analyse variation among populations or to quantify facial shape deformation as a result of orthognathic surgery, the input from each case may show an individual variation in its deviation from the mean shape deformation. Face length, width, alar base width may act as contributing factors to the total variability. The percentage of the variability associated with each factor can be calculated, their direction can be illustrated in the 3D dot plot. The factor that contributes to the highest

percentage of variability is considered the first principal component (PC1) and has its unique direction and magnitude. The next contributing factor with the next higher percentage is (PC2) and its direction of variation is orthogonal to the first component. The calculation of the subsequent smaller Principal components continues until a total percentage of variability <80% is reached which is considered satisfactory to measure the level of variability between shapes. In most cases 5-8 principal components describe about 80% of the level of variability of shapes.

Difference in facial forms as a result of growth, gender, and ethnic variations has been assessed using PCA (155–157). The effect of orthognathic surgery was analysed by assessing in the same manner.

Toma *et al.,* 2012 (157) applied principal component analysis to analyse facial variation among 4747 British school children. Their aim was to identify key components of variation in a sample of 15.5 years old children. Laser scanned images were obtained and 21 reproducible facial landmarks were identified and their coordinates were recorded. The images were superimposed using Procrustes analysis (PA) and principal component analysis was applied to each landmark cluster which consisted of 21 landmarks for the whole sample. 14 principal components were identified which in total constituted for 82% of the variations. The first, second and third principal component represented 46% of the variations which were the facial width, facial length and nose projection respectively. The impact of gender differences in facial shapes was minimal. Principal component analysis is a useful tool in describing the pattern of variation in large study populations where other analyses are short of description or labour intensive. However, the method provides descriptive rather than quantitative analysis.

1.3.2.1.5 Statistical landmarks plotting

Sforza *et al.,* 2010 (133) applied this approach as an adjunctive method which helped in describing the effect of associated asymmetry in faces on the level of attractiveness from childhood to early adulthood. The coordinates of 50 facial

landmarks were digitised for 148 male and 232 females (and in 669 controls consisting of 397 male and 272 female) using an electromagnetic digitizer. The landmarks were plotted on a Radar chart (web chart) where each of the mean landmarks were digitized on a radial line originated from the centre (zero). The mean of asymmetry measured at each landmark determined the position of this landmark on its radial line, (figure 10). A continuous line is then connected between the landmarks of each category in a circular fashion around the centre. Superimposing different categories on the same plot described clearly the variation among different categories. The results showed that asymmetry in attractive children was less than that in normal control group. This was not the case with adults where a considerable amount of asymmetry was found in attractive subjects especially I the male sample.

1.3.2.2 Surface based (landmarks free) analysis

The inclusion of the entire facial surface mesh in the analysis overcomes the major limitations of the landmarks based analysis. The analysis of surface mesh includes colour coded map, volumetric analysis, absolute surface distance, dense correspondence analysis and curves analysis. Despite the comprehensive nature of these analyses most of them are more descriptive in nature unless they are combined with refinements by landmark selection. Colour coded map ,as an example, will give an excellent visual description of the facial surface change after orthognathic surgery. However, it will only be objective enough when combined with landmarking either to measure the surface distance at a specific anatomical landmark area or to separate a desired surface patch (158,159).

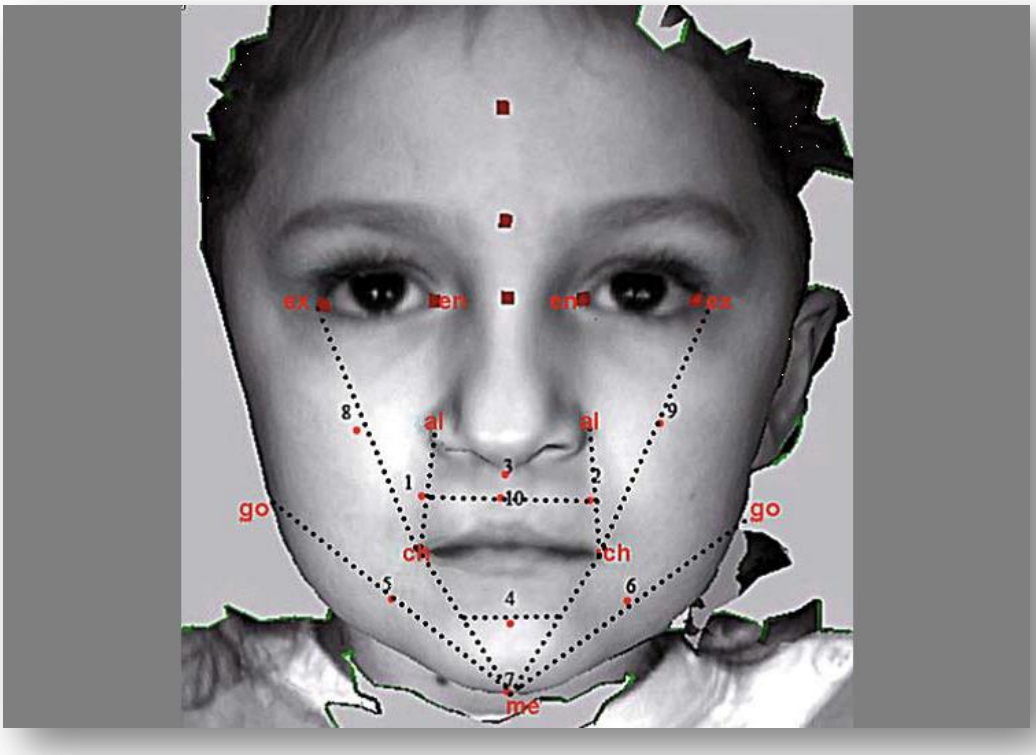

Figure 9: Mathematically generated landmarks applied by Hoefert *et al.*, 2010 (65)

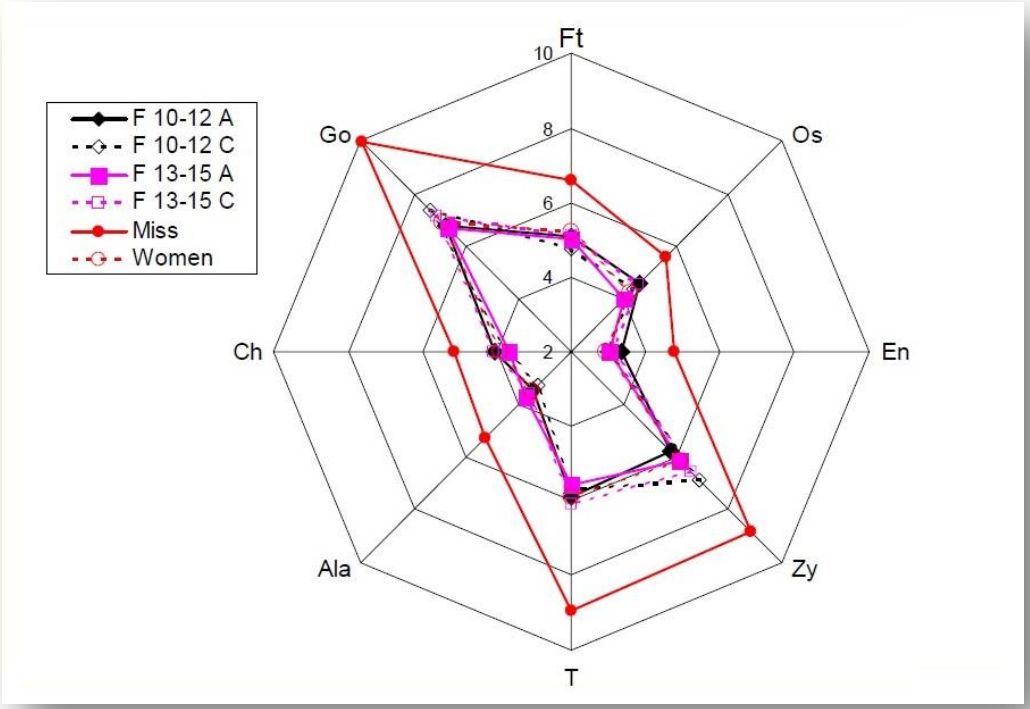

Figure 10: Landmark plotting applied to evaluate facial asymmetry by Sforza *et al.*, 2010 (133)

1.3.2.2.1 Colour coded map

This approach was the second in terms of the percentage of published articles reviewed in this section (28,160–166). Around 29% of the reviewed literature applied the colour coded distance map (163).

The entire facial surface is involved in the analysis; it produces visually displayed, easily interpreted findings for clinicians and researchers, the method provides both generalized surface measurements as well as localized patches on the area of interest.

To apply this method, the two facial image meshes to be compared should be superimposed to allow direct measurements between them. Its mathematical algorithm considers every vertex from one of the meshes (Mesh A) as a landmark and seeks for the closest point on (Mesh B) to be considered as a correspondent point for distance measurements. The results are comprehensive information which can be utilized in describing general and local facial changes after surgery. Three main outcomes are expected when adopting this method; Generalised colour coded distance map which can be displayed in a range of colours describing the distance between the two tested surface meshes, (figure 11). The shell displacement expressed as a spectral colour range in which, specific colour is allocated to each vertex according to its distance from the corresponding point (closest point) on the adjacent mesh surface. Considering the geometric centre of the two superimposed meshes as a directional reference point, the vertices of the outer mesh are highlighted in red while the vertices of the inner mesh are highlighted in blue. The higher the distance between the meshes in the direction away from the geometric centre (the outer mesh) the more the shift of the colour towards the red side of the spectrum and it has the positive sign. On the other hand the higher the distance between the two meshes in the direction towards the geometric centre of the object (the inner mesh) the more the shift of the colour toward the blue side of the spectrum and it has the negative sign. Consequently, the midpoint of the spectrum which is the green colour is allocated to the vertices with zero distance on both meshes. Variable regions on the face will take variable colour according to the magnitude

and direction of their geometrical differences which results in a descriptive colour map. To explain the concept in more details, an example of orthognathic surgery results of a patient with Class II malocclusion is shown in, (figure 11). The combined (superimposed) images (A), the Post-operative (B) and Pre-operative (C) images are shown. The combined images view shows only the positive part of the spectrum (green –red) when viewed from the outside of the 3D facial image where it will show the negative part of the spectrum (green-blue) when viewed from inside of the 3D facial image. The Post-operative view showed generally green areas at the areas of forehead and part of the midrace where no effect of surgery were evident while the lower face showed a marked shift towards the red colour which indicates a positive (forward) displacement of the soft tissue as a result of mandibular advancement as part of the treatment. The maximum positive and maximum negative values can be manually adjusted to emphasize minor changes.

Kau *et al.,* 2006 (163) introduced a slight modification to this method. Instead of using the spectral colour scale ranging in the positive and negative direction around the zero point, threshold points were determined which represented the level of clinical significance. This was named "tolerance value". Vertices with lower distance measurements were displayed in black colour whereas those with higher distance measurements were displayed in white colour. This allowed the colour coded map to be interpreted in a more objective way. The method was applied to evaluate surgical results, gender and age differences as well as variation among populations (29,160,167).

The colour coded map gives a visual description of the extent and location of the surface change. However its accuracy can be criticised by the fact that it relies on the geometric proximity of adjacent surface shells to create the correspondence rather than the real anatomical one. This limitation is clearly evident when asymmetric faces are evaluated.

Another modification is the patch displacement analysis (158,168), the mean and standard deviation of the distances between a group of interconnected

vertices (surface patch) in Mesh (A) and their corresponding nearest points on Mesh (B). It is possible to provide the mean and standard deviation for the whole face mesh. However the localization of the measurements to the region of interest provides a localized and more precise estimation of the resultant deviations. The precision in selecting patch boundaries which is based on identifying anatomical landmarking is the preferred approach in this analysis.

The mean and standard deviation of the distance between the two meshes in addition to the maximum and minimum measured distances are the numerical values which were considered in most of the studies (158,169). These measurements described the differences between the meshes especially when localized surface patches are being examined. However the lack of anatomical correspondence and the need for standardized accurate landmarking are among the limitations of the method.

1.3.2.2.2 Absolute surface distance

This type of analysis has been considered in about 11% of the reviewed articles (29,66,160,170–173). It has also been used along with other types of analysis mainly with colour coded map (158,169). The mean distance between the two adjacent facial meshes is calculated by measuring the distance from each vertex on one mesh to the nearest point on the other. The method is dependent on the accuracy of the superimposition of the images which should precede the distance analysis.

In general, analyses carried out using this method fall into one of the following four categories with marginal difference in calculated mean distance, (figure 12). The four types as stated by Miller *et al.*, 2007 (174) are:

- Normals: In this type the distance from each vertex on mesh (A) is measured to the nearest point on Mesh (B) which lie on a line perpendicular to that vertex regardless of the presence of closer points.

- Radial: The distance is measured between the two meshes along radial lines originated from the geometric centre (centroid) of the mesh (A) regardless of the presence of closer points.

- Closest point: This type measures the net distance from every vertex on mesh (A) to the closest point on mesh (B).

- Correspondence with sensitivity to movement (CSM): This type follows the geometrical similarity in identifying the correspondences between the two surfaces.

Despite the type of the analysis, this method calculates the absolute distance between the two meshes and produces the mean, standard deviation, minimum and maximum values. For a more specific analysis, this method can be applied on a local patch on the surface (66,70). In that case accurate landmarking is essential to standardise the dimensions of the selected patch.

1.3.2.2.3 Dense correspondence analysis

This method was applied for the analysis of shape change in about 2.5 % of the published articles on the topic (152,175,176). Although it is considered as a landmark free analysis, it could also be considered as a comprehensive landmark based analysis since it treats every vertex on the 3D surface as an individual corresponding landmark. It was introduced to overcome the lack of anatomical correspondence associated with the previous methods. This was achieved by providing a reproducible index of all vertices on the assessed images. This index provides the guide to create an actual anatomical correspondence between the compared images. The method combines the advantages of the comprehensiveness of the landmark free surface analysis and the objective precision of landmarks based analysis.

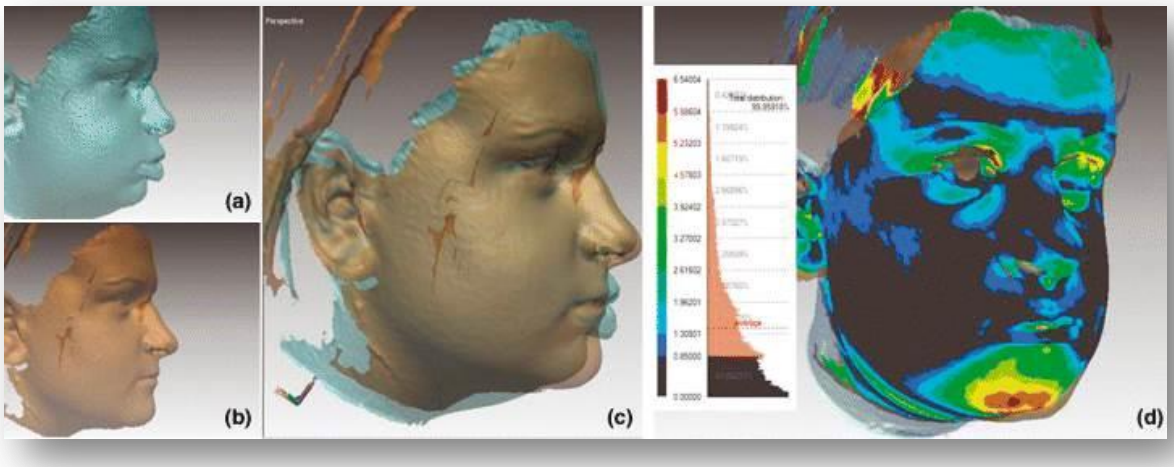

Figure 11: Colour coded map. Pre-operative (a), post-operative (b), and superimposed (c), and colour distance map (d). Kau *et al*., 2006 (263)

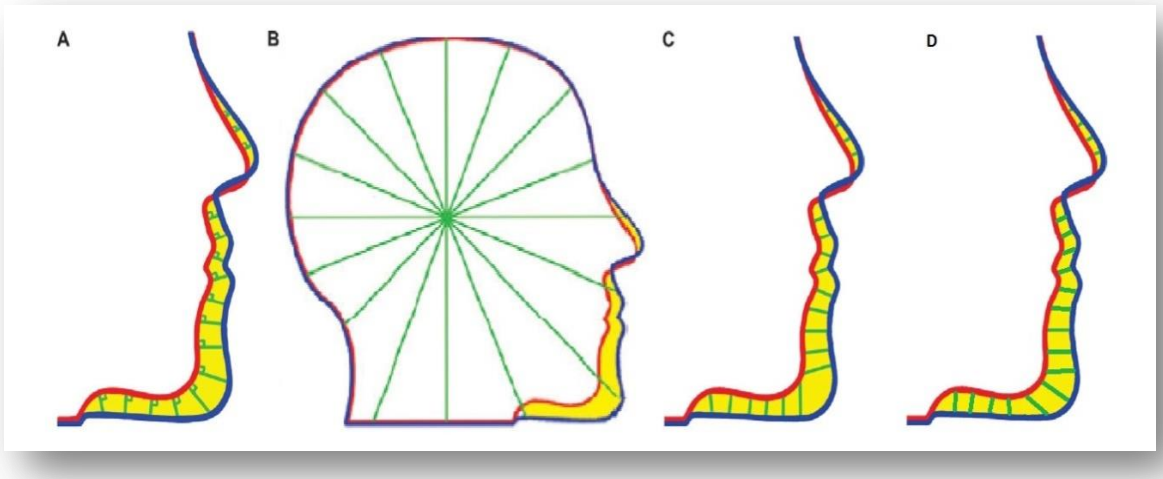

Figure 12: Types of absolute distance measurements: Normal surface distance A, radial surface distance B, Closest point surface distance C and corresponding points surface distance D. Ryckman *et al.,* 2010 (134)

The analysis is rather complicated and involves multiple stages:

a) *Construction of Generic mesh.*

The facial soft tissue surface is captured by a three dimensional acquisition devise e.g. stereophotogrammetry or laser scanner. Depending on the resolution of the scan the mesh may comprise thousands of points. Conventional landmark analysis based on anatomical structures involves a small number of these points which reduces the utilisation of the captured data. Ideally each point on the surface mesh should be a landmark; however, the manual identification of thousands of points (landmarks) would be impossible. The application of generic surface overcomes this problem and allows a more comprehensive assessment of the captured data.

A generic facial model is a simplified polygonal mesh representing the morphometric information of an average face with known 3D co-ordinates of each point of the mesh in addition to a reproducible polygonal index. The mesh is generic so it can be adapted universally to any face for the purpose of morphometric analyses. Generic meshes are a key tool in studies that deal with graphical representation of surface morphology to analyse the areas of difference and similarity.

The generic mesh model can be generated using virtual 3D modelling software. It can also be an average facial model based on the facial topography of the study population (167).

The topography of the generic mesh should include the common features of the study population and should not have extreme or unique characteristics out of the normal range, for that reason, an average face could be always chosen from the study group to guarantee accurate future analyses.

According to Kau and Richmond 2010 (177), four methods can be used to extract the average face. These include; straight forward point-wise averaging in the z-dimension(A-P); averaging in the radial direction of the average facial cylinder; averaging in the radial direction of the average face sphere; averaging in the locally normal direction to a template shell.

The first three methods, extract the average face using statistical algorithms that measure the relative distance to a plane, a vertical central line and a facial central point. The fourth method depends on the extraction of the average face by superimposing the entire study sample to a template shell produced by one of the previous averaging methods using the generalised procrustes algorithm followed by ICP.

To create the generic mesh model, most of the biological morphometric studies advocate the average polygonal 3D mesh over other modelling meshes. The choice is justified as the polygonal mesh has the capability to accurately represent a biological shape especially in detailed features areas, folds and edges combined with the possibility to produce uniform polygons of relatively equal sizes throughout the mesh. These characteristics facilitate creating a polygonal index necessary for a uniform assessment of different anatomical areas on the facial mesh (178).

b) Conformation

Conformation is the adaptation of the generic mesh to the facial surface mesh in a process known as “elastic deformation”. The generic mesh is warped onto the underlying facial morphology. This conformation process can be achieved through a two-step algorithm: In the first step (GPA) generalized Procrustes algorithm (179) is applied followed by thin-plate spline (TPS) warping (154). This brings the landmarks of both the facial surface and the generic mesh into exact alignment and produces a smooth transformation for the other parts of the mesh by minimizing the bending energy for the close adaptation of the surfaces.

The second step accomplishes fine local adaptation of the generic mesh to facial morphology by deforming each vertex of the generic mesh into the location of the closest vertex on the target mesh surface guided by surface topography. This algorithm results in cloning of the target face mesh and creating a simplified, uniform and indexed polygonal mesh which carries the same facial features of the original mesh.

c) Superimposition

In orthognathic surgery, dense correspondence analysis was used to analyse localized change on the facial soft tissue as a result of orthognathic surgery. In order to emphasize these changes, the analysed meshes (pre surgical and post-surgical) should be superimposed on stable areas unaffected by surgery. The most common method of superimposition is the surface based registration, (Section 1.2.2).

d) Dense correspondence analysis

The generic mesh is an indexed mesh; each vertex of the mesh has its analogues vertex on any other mesh with the same index. This characteristic provides a real dense anatomical correspondence for a comprehensive analysis of the whole facial surface with a high level of precision.

Dense correspondence analysis was applied to a variety of facial anthropometric analysis. In their study, Claes *et al.*, 2001 (175) applied this method to investigate growth pattern of normal and syndromic patients. In this case, the scale of the colour index is different. Although it involves the full colour spectrum (blue to red), the blue colour refers to (zero) whereas the red colour refers to the maximum value of differences between the corresponding vertices of the dense surface mesh. A similar study was carried out by Al-Hiyali *et al.*, 2015 (180). Their analysis involved motion 3D imaging (4D) to investigate the impact of orthognathic surgery for correction of asymmetry on facial animation, (figure 13).

Principal component analysis can also be applied for the comprehensive evaluation of the surface change. Curve analysis as described by Higgins 2014 (181) can be applied on the uniform structure of the indexed generic mesh to optimize curve correspondence. The method depends on multiple steps involving various procedures for image superimposition and conformation. Each of these steps has its associated margin of errors.

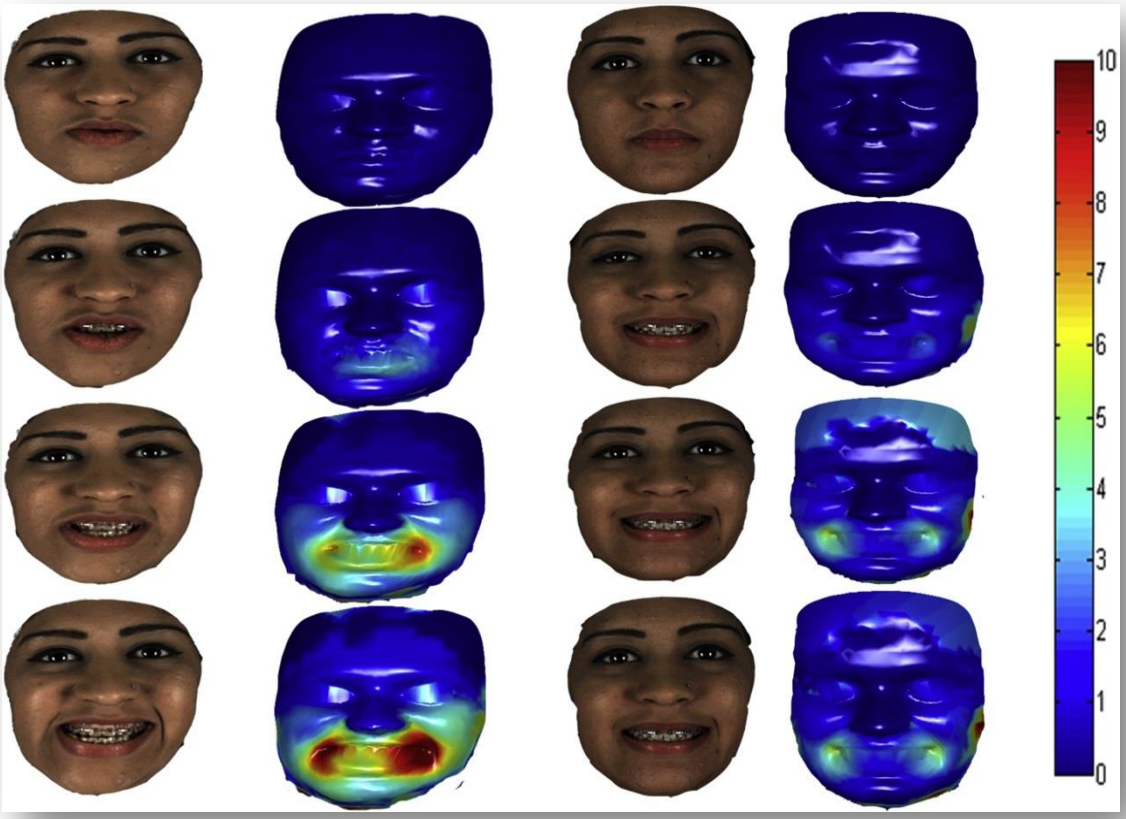

Figure 13: Dense correspondence surface analysis. Note the minimum value on the colour scale is ZERO. Al Hiyale *et al*., 2015 (180).

1.3.2.2.4 Volumetric analysis

The method was applied in 5% of the reviewed articles on the soft tissue analysis following orthognathic surgery (155,159,182,183). The analysis provides information about the change in the volume of the whole face or at specific regions (33,184). The method is considered an adjunctive to other analyses. Chau *et al.,* 2008 (182) applied angular and linear measurements in addition to the colour coded map to detect changes in volume around the nose region.

1.3.2.2.5 Curve analysis

This approach has been recently developed and applied in 2.5 % of the reviewed literature (123,181,185).

Similar to dense correspondence, 3D curve analysis is a comprehensive landmarks based analysis to describe surface morphology. Human facial features including cheeks, lips, nose and chin are represented by smooth recognizable curves that describe the morphological characteristics. These curves are detectable, reproducible and comparable (181). Curve analysis is a promising research tool to describe and quantify the change in facial form after jaw corrective surgery.

Higgins 2009 (181) demonstrates the application of curve analysis to evaluate the effect of surgical correction of cleft lip and palate and Principal Component Analysis was applied to describe the characteristics of facial morphology. Two methods of curve detection were applied. The first was named "*planner based curve identification*". Curves were identified by the creation of a plane that passes through the face, the points along the surface – plane interface represents the curve to be analysed. Some geometrically complex areas around the nostrils and lips regions may require a combination of more than one plane to accurately identify the desired curve. This method was criticized for its failure to produce satisfactory curves in all areas of interest in addition to the complexity of the computational process for curves identification (181).

The second curve identification method was "*surface curvature based curve identification*". This type utilised surface topography for curve detection minimizing the need for landmarking to only two at the ends of the curve. It is well known that facial soft tissue surface composed of a variety of surface topography features as peak, pit, saddle, ridge and valley. It is therefore logical to use surface characteristics for curve detection. The "ridge" was the ideal geometric feature to detect facial curvatures. 3D curve analysis is a promising tool, however, the accuracy of the method has not been fully evaluated.

1.3.3 Hard-Soft tissue correlations and prediction of surgical results

A review of the scientific literature from the mid-20th century until present days showed the growing interest in understanding the behaviour of the facial soft tissue following surgical repositioning of the underlying jaw bones. A common aim among researchers has been to find an approach to accurately predict the soft tissue outcome following orthognathic surgery.

Until recently, studies have been limited to the use of two-dimensional (2D) cephalometric radiography to analyse the relationship between soft and hard tissue. The main approach was dependent on linear or angular measurements to track the post-operative positional changes of certain anatomical hard and soft tissue landmarks and to extract a mathematical ratio between their movements (186–188).

The introduction of digital cephalometry resulted in an improvement in the accuracy of landmark location and measurements (189). However, the inherent inaccuracies of imaging and analysing a three-dimensional structure in 2D still remained (190). It is worth noting that the measured change of landmark position reflects the behaviour of the soft tissue at this particular point and do not indicate changes in the surrounding region. This is critical due to the multi-factorial flexible behaviour of the soft tissue. Adjacent points to the digitised landmark on the face may react entirely differently to the same underlying hard tissue surgical movement.

In the beginning of the 21st century, positive steps were taken following the introduction of 3D modelling into the medical diagnostic field in attempt to understand the correlation between the skeletal and soft tissues. The advancement of CT Scanning and MRI technology provides the accurate recording of 3D topography of the facial hard and soft tissues and allows a comprehensive analysis of the recorded morphology.

The first part of this section aimed at reviewing previous studies on the correlations of soft and hard tissue movement following orthognathic surgery using both 2D and 3D imaging modalities.

1.3.3.1 Two Dimensional correlations and ratios

1.3.3.1.1 Maxillary osteotomies

The effects of Le Fort I advancement on the naso-labial soft tissue complex have been thoroughly investigated (130,187,191–208).

In general, four points on the soft tissue profile were the basis for the linear and angular measurements to quantify the relationship between soft and hard tissue movements following maxillary osteotomy. These points were the nasal tip (Prn), the deepest point at the naso-labial angle (Sn), the vermilion border of the upper lip (Ls) and the vermilion border of the lower lip (Li). These were correlated to the skeletal movements of the following points; the anterior nasal spine (ANS), the anterior maxilla (A point), the crest of the upper alveolar bone (Par) and upper incisor edge (UI) respectively (187,191).

In response to maxillary advancement, several studies reported that the upper lip at the vermilion border moved anteriorly by a mean ratio of 0.7:1 (209) (192). However, larger ratios approaching 0.9:1 have been found (201,210). On the other hand, smaller ratios have been also reported (211). A possible explanation for this variation in the soft tissue response to maxillary surgery was caused by the associated soft tissue alteration including the V-Y closure of the mucosal surface of the upper lip and cinching of the alar base which is routinely carried out to avoid flaring. These may result in an increased thickness of the soft tissue at the naso-labial region (201). In other studies maxillary advancement was combined with a variable amount of surgical impaction which will alter soft tissue response to surgery (210), while the small test sample (8 patents including 2 cleft lip cases) may be the cause for the smaller ratios (209).

Based on the previous literature findings, the movement of the upper lip is highly variable and dependant on several factors including soft tissue thickness (196,210), the direction and amount of tooth movement and the initial position of the upper lip (212,213), Patents gender (214) and ethnic group (215) .

The thicker the lips the lower the soft to hard tissue movement ratio as the soft tissue bulk tends to absorb the skeletal movement and reduces the detected changes (196). Another parameter which may influence soft tissue response to Le Fort I maxillary advancement is the presence or absence of a gap between anterior maxilla and the upper lip. In most cases of maxillary deficiency this space exists which may reduce the ratio of soft tissue movement following maxillary advancement since the initial movement of the hard tissue will be within the existing space before it contacts the mucosal surface of the upper lip.

The effect of skeletal maxillary advancement may extend to other soft tissue structures including the nose and lower lip (192,209). However, these effects are variable and studies have reported the difficulty in analysing the correlation between the hard and soft tissues at these regions (210).

In general, maxillary advancement surgery moved the tip of the nose and subnasale anteriorly with a ratio ranging from 0.2:1 to 0.7:1 (216). Few studies have shown the effect of maxillary advancement on the position of the lower lip, the ratio was found to be ranging between 0.2:1 to 0.57:1 (192,209).

The effect of maxillary advancement is not limited to the forward movement of the overlying soft tissues. Several studies detected an upward vertical shift of the naso-maxillary complex and shortening of the upper lip. However the results were variable with a large range of the standard deviation (210). On the other hand, Carlotti *et al.*,1986 (201) showed that there is no change in the upper lip length. A possible explanation may be the surgical procedure for this group of patients included a V-Y closure which was used to maintain lip length.

The effect of skeletal maxillary advancement on the upper lip of cleft lip patients has been investigated (217). Soft tissue responses to maxillary advancement in patients with cleft palate were compared to non-cleft patients with deficient maxilla. The sample of 50 patients was divided equally into two groups; cleft lip and non-cleft with deficient maxilla. Both groups were treated with a Le Fort I maxillary advancement with no vertical change. The results showed that the cleft lip group expressed as higher ratios of soft to hard tissue movements compared to non-cleft patients in both the horizontal plane 0.66:1, 0.54:1 and in vertical plane 0.53:1, 0.23:1 respectively. This may have been due to the scar tissue formation in the upper lip following primary lip repair and the difference in the magnitude of maxillary advancement which was not standardized in this study.

In a more recent study Louis *et al.,* 2001(187) investigated the effects of maxillary advancement for treatment of class III patients with sleep apnoea. The vermilion border of the upper lip was advanced 0.8 and moved superiorly 0.16, subnasale point at the naso-labial angle was advanced 0.39 and moved superiorly 0.16 and the nasal tip was advanced 0.16 and moved superiorly 0.16 per unit of maxillary advancement measured at the upper incisal edge. The results of the study were different from those reported in previous findings. The upper incisal edge was the only hard tissue reference point to represent the complex skeletal movements which was a major limitation of the study.

1.3.3.1.2 Mandibular Osteotomy

There are numerous studies investigating the response of the soft tissue to mandibular osteotomies since the mid-20th century (218,219). In the early articles, changes in the lip and chin soft tissue, following skeletal correction of mandibular position were based on profile cephalometric measurements. Similar findings were reported, for each 1mm posterior movement of the bony chin, the soft tissue chin moved 1 mm in the same direction while the lower lip moved 0.6 mm. In other words, the ratio of soft to hard tissue movement after mandibular setback and advancement surgery was estimated to be 1:1 at the chin region whereas the ratio was 1:2 for mandibular advancement, 1:1 for mandibular

setback at the lower lip region. More recent studies have also supported the same ratios (148,186,220,221).

Several factors influenced the soft tissue behaviour in response to mandibular movements, these include, the thicker the lips the lower the soft to hard tissue movement ratio as the soft tissue bulk tends to absorb the skeletal movement and reduces the ratio; females in general tend to show higher ratios than males; a nonlinear correlation has been found between the amount of skeletal movement and the extracted ratios as higher ratios were observed with the increased magnitude of skeletal movements (214,220,221).

The effects of mandibular setback on the soft tissue profile as a whole rather than just the lower lip and chin has been reported (222). The study found that not only changes in lower lip and chin region occurred as a result of mandibular surgery but all the facial profile is affected including the upper lip and naso-labial region. The main effect of mandibular setback surgery on the soft tissue profile is an increase in facial convexity, deepening of the mentolabial fold, lengthening of the upper lip and an increase in naso-labial angle. It was also noted that changes in the soft tissue profile following small mandibular setbacks were less predictable compared to large setbacks and females demonstrated greater soft tissue movement in response to skeletal repositioning compared to males, this was statistically significant for the upper lip and chin ($p<0.05$). Lastly changes in facial aesthetics following orthognathic surgery were highly dependent on skeletal stability of the surgical procedure (222).

Interestingly two recent systematic reviews have been published by Joss *et al.*, 2010 on the effects of soft tissue profile following mandibular surgery for mandibular setbacks (186) and mandibular advancement (223). The review concluded that the current evidence-based analysis of soft tissue changes following orthognathic surgery is poor. This is mostly due to inherent problems of the retrospective nature of the published data, poor study designs and lack of standardized outcome measurements. However the review did report the ratio of soft to hard tissue movement was around 1:1 in chin area especially for the

mentolabial fold, whilst there was greater variability with the lower lip which ranged from 1:1 for mandibular setbacks and 1:2 in mandibular advancements and to a less extent in the upper lip region.

No published studies were found stating A-P, lateral or vertical ratios in 3D. This was probably as a result of the better understanding of the 3D nature of the facial changes following orthognathic surgery which made it completely irrelevant to describe surface change with a single numerical ratio.

1.4 Prediction of soft tissue changes following orthognathic surgery.

At the start, computer aided surgery with the ability to predict soft tissue changes were confined to profile view only. Common software packages were CASSOS and Dolphin. These two software packages were based on interpolating the published 2D ratios to create continuous profile contour changes. Jones *et al.*, 2007 (224) validated the accuracy of the profile prediction using CASSOS software. Their findings stated that the prediction was within acceptable accuracy with a higher range of error around the lips regions especially in the vertical dimension.

In order to achieve a successful three dimensional prediction of the facial soft tissue changes following orthognathic surgery a well-developed mathematical model is required that can mimic the actual deformation behaviour of the facial soft tissues as a result of skeletal displacement. These are known as approximation models (225).

Various models have been proposed for this function (225–227). These include: *Geometrical analysis models; Finite Element Model; Mass Spring Model* and *Mass Tensor Model*.

1.4.1 Geometrical analysis models

In these models the displacements of soft tissue vertices were estimated in relation to the movements of its corresponding hard tissue vertices (228,229).

Xia *et al.*, 2000 (229) introduced a soft tissue simulation model built on a purely geometrical analysis. The introduced algorithm was based on transferring the skeletal movement to the soft tissue. The procedure utilized the available 2D hard-soft tissue ratios and applied them to different regions on the face. According to their method, two algorithms were adopted: *Surface Normal-based Model Deformation Algorithm* and *Ray Projection-based Model Deformation Algorithm*. The first was based on the directions of the normal (perpendicular) at each vertex to allocate hard-soft tissue correspondence. This was applied to the chin area (from labiodental fold and down). A variation from this algorithm was based on an imaginary ray passing through the hard tissue to the soft tissue in a radial fashion. This was applied to the upper two thirds of the face (labiomental fold and up). This type of simulation provides a low computation time combined with a photorealistic representation of facial tissue changes. Recent well known software packages such as Dolphin 3D uses an algorithm not so far from this type for prediction planning. However not enough publications validating the accuracy of the prediction planning were found.

1.4.2 Finite Element Model

The finite element model (FEM) was first introduced to help engineers to understand the reaction of different materials to various external forces such as the reaction of a bridge to applied loads from crossing vehicles. The principal idea was to divide a continuum into smaller elements known as finite elements to simplify their analysis such as converting a circle into a hexagon (6 elements) or a pentagon (8 elements) or more elements until a satisfactory level of simplification was reached in balance with preservation of the geometrical or physical properties of the tested material. In 3D surgical simulation, the reaction of the face as a continuum was simplified by the polygonal mesh construction where each vertex represent an element across which force action and reactions

were individually analysed based on a fixed coefficient related to the type of the tissues involved (230). FEM was one of the first deformation models that has been extensively applied to orthognathic surgery prediction planning (228,231).

Keeve *et al.*, 1998 (230) introduced and explained his idea of using FEM in 3D planning. In their approach they used a grid of six node prisms. The prism elements are defined by their corner nodes, as shown in figure (14). In their displacement-based finite-element model, given displacements are specified for certain nodes on the bone surface. These displacements cause stress which in turn creates internal strain forces. To bring these forces into equilibrium, a system of differential equations was developed delivering the displacements of the unconstrained nodes of the soft tissue surface (230).

FEM has been shown to give a reasonably accurate simulation of tissues affected by maxillofacial surgery (230). However, The high computational power and memory consumption were the main short coming (227,232).

1.4.3 Mass Spring Model (MSM)

An alternative deformation model termed Mass Spring Model (MSM) has been developed to reduce the processing labour (233,234). The basic idea is to connect each element (usually one triangle) on the skeletal surface with a corresponding element on the soft tissue surface using either ray projection or closest point algorithm. This connection is represented by a spring at equilibrium state in the pre-operative model. Moving the skeletal tissue will compress or decompress the spring producing stress that will be transferred to the soft tissue surface as the spring trying to rebound to equilibrium state. The amount of soft tissue displacement depends on the stiffness of the spring and its relation to adjacent elements. As the facial soft tissue is composed of layers of different anatomical structures including muscles, facia, and fat pad, mass-spring algorithm has the ability to incorporate more than one spring with variable stiffness for each tissue type which increases its accuracy in soft tissue simulation, (figure 15). This approach has a considerable advantage over the

finite element analysis. Most importantly is its ability to combine a large number of 'elements', which results in a better modelling accuracy in addition to its faster simulation time. However, MSM lacks the biomechanical foundation (227). An example of surgery planning software that is based on this algorithm is "3dMD vultus".

1.4.4 Mass Tensor Model

MTM defined by Cevidanes *et al.*, 2011 (225) as "a mixture of the easy architecture of the MSM and the biomechanical relevance of FEM".

Cotin *et al.*, (1999) (235) explored the possibility of a hybrid model that combined both the FEM and MSM in an attempt to overcome the disadvantage of the mass spring model lacking the biological foundation, which was later termed the Mass Tensor Model (235). This deformation model provided the architectural simplicity of the mass spring model augmented with the biomechanical relevance of the finite element model. The processing time was greatly reduced (227) which allowed a real time simulation using a standard PC for routine clinical practice. An example of surgery planning software that is based on this algorithm is "Maxilim" (236).

Schendel *et al.*, 2013 reported a high accuracy of 3dMD Vultus prediction of the post-operative soft tissue changes. An average difference of 0.27 mm between the simulated and the actual soft tissue meshes was reported, the highest difference was 0.6mm at the mental fold (237). However the methodology of this study is questionable, the analysis included areas of the face that are not affected by surgery, and these were considered in the calculations of the mean changes of soft tissue following surgery. Anatomical regions were assessed by measuring distances at corresponding landmarks which limits the comprehensiveness of the analysis.

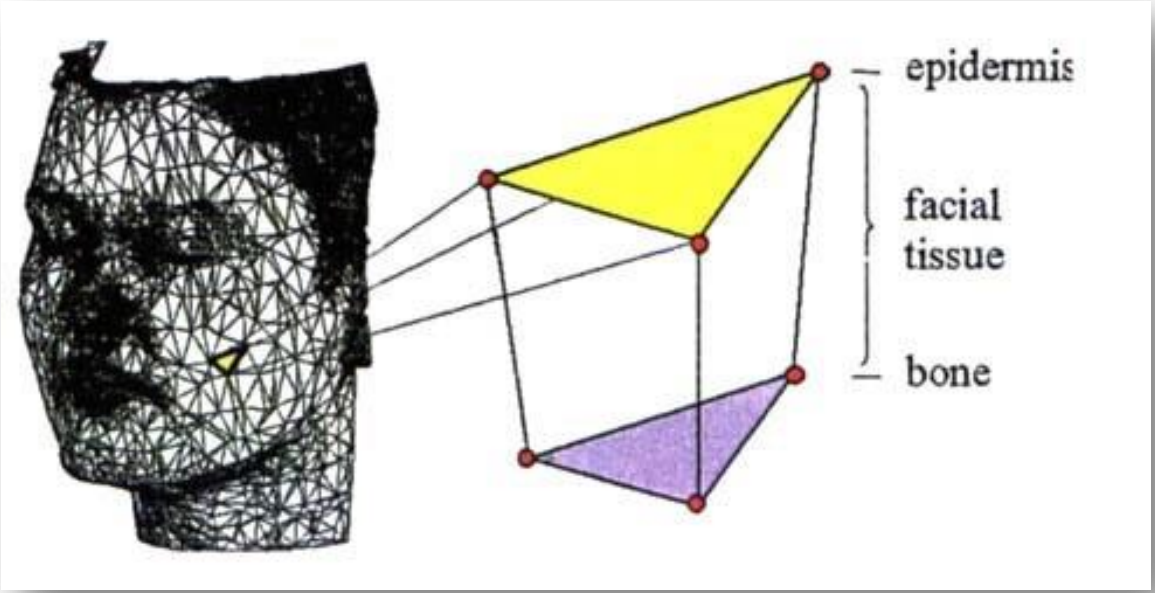

Figure 14: Basic element of the finite element model. Note that the prism could not be divided into layers. Keeve *et al.*,1998 (230)

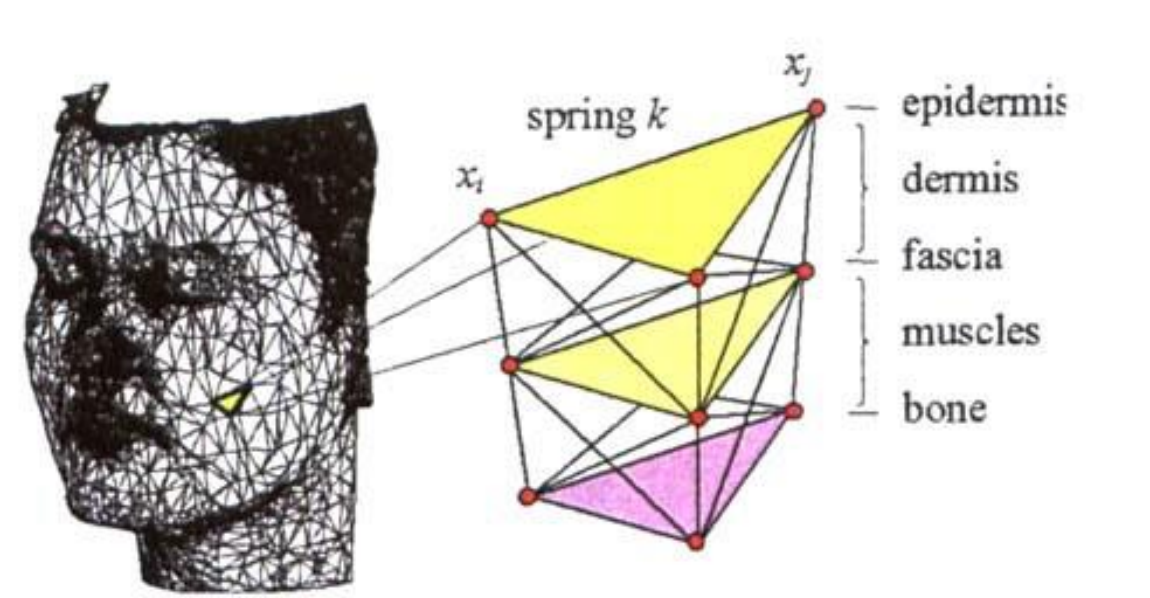

Figure 15: Basic elements of the mass-spring model. Note that the prism could be divided into layers. Keeve *et al.*,1998 (230)

1.4.5 Comparison of the different deformation models

Molleman *et al.*, 2007 (227) compared the finite element model, Mass spring model, and mass tensor model for accuracy and clinical versatility. The results showed a superior outcome achieved with the mass tensor model in orthognathic planning prediction accuracy. In general, mass tensor model and finite element model predictions demonstrated the highest accuracy, but the mass tensor model achieved the shortest processing time (227).

1.5 Aims

To introduce a new method for prediction of soft tissue changes following orthognathic surgery.

1.6 Specific objectives

The following are the aims objectives and the hypotheses to be tested.

1. To identify the most reliable approach of 3D image superimposition with the highest level of accuracy and to develop an informative method for the 3D measurement of surgical skeletal movement following orthognathic surgery.

2. To validate the accuracy of the conformation of the generic facial mesh and to apply the "anatomical dense correspondence analysis" for facial anthropometry.

3. To provide a statistical algorithm for prediction of soft tissue changes in response to orthognathic surgery.

Hypotheses to be tested:

1. The conformation of the generic mesh followed by the application of the dense correspondence analysis is valid for the assessment of facial morphology.

2. The prediction algorithm is valid with a satisfactory level of accuracy.

3. The newly developed measurement for surgical movement is accurate and reproducible.

2 Methodology

Contents

Introduction

This study relies on the use of two different imaging modalities. The first is volumetric conebeam CT imaging technology that simultaneously captures both the skeletal and soft tissue data of an individual. The second is stereophotogrammetry which captures only surface data.

Using appropriate software it is possible to separate or segment the skeletal and soft tissues captured within the 3D volume of the CBCT scan whilst still maintaining their relative positions to one another in 3D space. It is also possible to convert the volumetric data into surface data, thus producing a common file format for CBCT and stereophotogrammetry.

To avoid repetition the materials and methods section has been subdivided into the following sections.

Section A

Describe the recruitment of the main research sample.

Section B

Describe two experiments to validate the measurement of hard tissue changes as a result of surgery.

- Comparison between voxel based registration and surface registration to analyse changes following orthognathic surgery.

- Direct DICOM slice landmarking, a novel technique to quantify the direction and magnitude of hard tissue surgical change.

Section C

Describe a series of experiments to assess soft tissue changes. These include:

1. The use of a generic mesh to assess soft tissue change using stereophotogrammetry.

2. The application of dense correspondence technique on the soft tissue surface data of the CBCT scan to achieve the following:

a) Construct an average face.

b) To quantify the direction and magnitude of soft tissue change following surgery.

Section D

Describe skeletal and soft tissue measurements and quantification of the relationship between the soft tissue changes and the hard tissue changes as a result of surgery; in effect combining the above sections.

2.1 Section A: Main research sample recruitment

In this section, details concerning the recruitment of the study sample used in the main project will be described.

2.1.1 Sample

This is a retrospective study based on the conebeam CT DICOM images of orthognathic surgery patients who had been treated at the University of Glasgow Dental Hospital and School and the Southern General Hospital. Ethical approval to access and use the data was obtained from the West of Scotland Research Ethics Service (Reference 12/WS/0133). Patients were selected from the database at the Dental School and cross-referenced with the Southern General Hospital theatre list from 2008-2014. All patients were of Caucasian decent and had been diagnosed with a dentofacial deformity that required correction by orthognathic surgery. All the patients were treated by the same surgeon.

Preoperative and postoperative CBCT scans were taken for routine pre-surgical workup prior to orthognathic surgery. The preoperative CBCT scans were acquired within one month of surgery and the postoperative scans were obtained at a minimum 6 months after surgery using the same CBCT machine (i-CAT Classic, Imaging Sciences, Hatfield, UK). The protocol for CBCT image capture is discussed in details elsewhere (Section 2.1.2).

2.1.1.1 Inclusion criteria

Patient related

- Patients were Caucasian ethnic background.
- Patients 17 years of age or above with no further anticipated growth.
- Patients underwent orthognathic surgery treatment, Table (3).
- No history of previous operations involving facial soft tissue.
- No history of previously treated dentofacial deformity including cleft lip and palate.

Conebeam CT related

- All patients had pre and post-operative CBCT scans. The pre-operative image must have been taken no more than one month pre-operatively and the post-operative images within 6 to 12 months after surgery.
- All conebeam CT scans were extended field of view (EFOV) (22 cm) scans.

Surgery related

- Only patients who were treated with single piece Le Fort I and BSSO osteotomies ± genioplasty were included.

2.1.1.2 Exclusion criteria

- Defective images caused for various reasons. More than 20% of the original collected sample was excluded due to this reason, (figure 16).
- Failed to meet the specific inclusion criteria detailed above.
- Patients treated with segmental osteotomies.

A total of 137 pre- and post-operative images were located. Only 100 images were included according to the research sample inclusion criteria. Image defects were the main reason for exclusion. Table (3) details the classification of malocclusion and the surgical procedures undertaken.

2.1.2 CBCT scanning protocol

Standardised pre-operative and post-operative conebeam CT (CBCT) images were taken for all patients using a Classic iCAT (i-CAT Classic, Imaging Sciences, Hatfield, UK) 0.4mm voxel, 22cm Extended Field of View (EFOV) option. An experienced radiographer in the Radiology Department at the Glasgow Dental Hospital and School under took all the scans.

Prior to CBCT scanning the chin support on the iCAT scanner was removed and replaced with a forehead band to avoid any chin soft tissue distortion. The patients were positioned sitting upright with their back supported by the built-in

chair. Using the laser patient orientation system incorporated in the iCAT scanner the patients were positioned with their Frankfort plane and inter-pupillary parallel to the horizontal line together with the vertical line in the mid-sagittal facial line. The patient's head was then secured to the headrest with a securing band placed as high as possible on the forehead, (figure 17). Patients were instructed to relax with lips in repose by saying "Mississippi", licking their lips and saying "N" and gently putting their teeth together (Zacharrsion, 1998).

Patients who were overclosing, mainly due to vertical maxillary deficiency, had had an intra-occlusal wax wafer constructed by the Clinician responsible for their care prior to the scan; this was used during the scan and subsequent planning. The patients were asked to remain still during the CBCT scan. The images were saved in DICOM format and exported for later use.

2.1.2.1 DICOM Image anonymization

DICOM images incorporated patient indefinable information. This information was not necessary for the current research and the data was anonymized. Two online free software packages were used for this purpose "VTK DICOM anonymiser" and "DICOM files renamer". These two software packages were capable of anonymising the images by removing any tagged information in addition to renaming each slice with the case CHI number of the patient and a unique patient code. An encrypted EXCEL worksheet (Microsoft®, Redmond, CA) was created containing patients names and their corresponding CHI numbers and codes. This was kept for future need of retrieving information regarding individual patients.

Table 3: Surgical jaw correction movements.

Surgical procedure	A-P corrections combinations	Number of cases
Le Fort I	Maxillary advancement	33
Le Fort I + Genioplasty	Maxillary advancement	19
BSSO	Mandibular advancement	12
	Mandibular setback	2
BSSO + Genioplasty	Mandibular advancement	5
	Mandibular setback	1
Combined (Bimaxillary)	Maxillary and Mandibular advancement	11
	Maxillary advancement and Mandibular setback	7
Combined + Genioplasty	Maxillary and Mandibular advancement	7
	Maxillary advancement and Mandibular setback	3
Total		100

Table 4: Image pairs configurations

Patient	Registration method	tissue specific image pair
Patient X	VBR	Soft tissue (pre- and registered post-operative)
		Hard tissue (pre- and registered post-operative)
	SBR	Soft tissue (pre- and registered post-operative)
		Hard tissue (pre- and registered post-operative)
Total		8 models

Figure 16: CBCT image defect. A step at the face was formed due to patient movement during the CBCT.

Figure 17: CBCT image capture showing the patient sitting upright. The chin rest was removed and the head strap was used instead.

2.2 Section B: Validation of the hard tissue changes as a result of surgery

In order to measure the changes as a result of orthognathic surgery the pre- and post-operatives images need to be firstly superimposed on structures which have remained stable and not changed as a result of surgery. It is common practice to use the anterior cranial base in two-dimensional cephalometry (209,222) and in 3D imaging (168,238). Other structures such as the zygomatic regions have also been proposed (69) as an alternative. Following superimposition the changes in landmarks, representative of the structure being assessed, are calculated and used as a measurement of the outcome for skeletal movement.

In this section, two experiments will be described; the first to objectively assess two 3D image registration methods. The second to validate a novel technique that measures the three dimensional skeletal displacement of the maxilla and mandible.

2.2.1 Comparison between voxel based registration and surface registration to analyse changes following orthognathic surgery

2.2.1.1 Introduction

The two types of image registration are rigid registration methods and were discussed earlier (Section 1.2.2). In summary, surface based registration (SBR) was the initial method described for 3D image superimposition (10,11). The principle involves approximating two surfaces using either Partial Procrustes Analysis PPA or iterative closest point (ICP) or both of them. Voxel based registration (VBR) on the other hand utilizes the grey scale difference of the voxels to align the two DICOM images to the best superimposition achieving the least total grey scale density difference between the two images. Voxel-based registration is useful were it is difficult to detect distinct surface topography features or when the whole body of the registered structure needs to superimpose regardless of the type of tissues involved.

Studies reporting the use of voxel based registration have claimed high accuracy in registration (16-18). However, to date, no research has been published comparing the accuracy of voxel based and surface based registration methods. The choice between voxel based registration and surface based registration was vital for this PhD project. The availability of the image resources for both types of registration provided a unique opportunity to experiment each of them and to choose the type of image registration suitable for the project.

2.2.1.2 Aim

The objective of this study was to determine if there was a statistically significant difference in the accuracy of image superimposition between two registration methods i.e. surface based and voxel based.

2.2.1.3 Methods

2.2.1.3.1 Sample

The study sample composed of the pre- and post-operative CBCT images of 31 of orthognathic surgery patients. These images were randomly selected from the total 100 previously described (Section 2.1.1). All the patients had had orthognathic treatment to correct their facial deformity. The preoperative CBCT scans were acquired within one month of surgery and the postoperative scans were obtained at a minimum 6 months after surgery.

2.2.1.3.2 Voxel based registration

The principals of voxel based registration were explored in details (Section 1.2.2.3). In summary, voxel based registration (VBR) is a specialised method of DICOM images superimposition. The associated algorithm utilises the grey scale intensity of the voxels composing the DICOM image to produce the best match between two overlapping images through an automated iterative move and measure sequence. The number of iterations, the percentage of voxels involved and the region of interest were manually selected, (figure 18).

The pre- and post-treatment DICOM images for each patient were imported into Maxilim software (Medicim-Medical Image Computing, Belgium). Using the voxel based registration add-on module provided by the manufacture a region of interest including the anterior cranial base and part of the forehead, was selected on the pre-treatment and post-treatment images. This region would be used for image registration; the number of iterations was set to 30 to ensure maximum alignment. The registration process took approximately 20 minutes to complete and the registered DICOM images were saved in their new positions for further analysis.

Following registration of the pre- and post-operative volumetric DICOM images for each patient, the soft and hard tissue 3D surface models were segmented using Maxilim software. Details of the segmentation process are previously provided (Section 1.2.1). The segmented hard and soft tissue models were exported as (.stl) files and saved for the next step of the analysis.

2.2.1.3.3 Surface based registration

The principals of surface based registration were discussed in details in Section (1.2.2.2). In summary, the method is a generalized 3D image registration technique used for superimposition of two 3D surface mesh models. The method has been extensively used for engineering, medical, security and military applications, (239,240). In this study, the automated Iterative Closest Point (ICP) algorithm was used in addition to a preliminary manual landmark based registration (PPA) as a preparatory step. The (ICP) algorithm searches' for a match of the topographic features of the overlapping surface meshes where the square root distance of the involved vertices with the adjacent mesh are minimised. This is achieved in an iterative move and search fashion.

The soft and hard tissue models of the unregistered pre- and post-operative DICOM images were segmented using Maxilim software and were exported as STL files. These models were then loaded into VRMesh software (Virtual Grid, Seattle City, U.S.A) and arranged in two groups: *pre-operative group* (soft and hard tissue models) and *post-operative group* (soft and hard tissue modes). An

additional group was created and named *template* which was an exact copy of the pre-operative group. Soft and hard tissue models in the template group were cropped to the region of interest only (stable region unaffected by the surgery) to act as the bases for the surface registration procedure. The cranial base extended to involve the frontal bone, and the forehead extended to involve the eyes were the regions of interest for the hard and soft tissue models respectively, (figure 19). Since the templates were created from a copy of the pre-operative models, they were in the same 3D position as the full pre-operative model. Following this, manual registration (PPA) was carried out as a preliminary step to approximate the models. All the registration steps involved rigid registration with no scaling. For manual registration three landmarks were on the hard tissue template; left and right zygomatico-frontal sutures and nasion. The corresponding landmarks were placed on the post-operative model. The same procedure was performed for the soft tissue template and the post-operative image using left and right exocanthian and nasion. This procedure approximated the two images and provided a closer starting position for the next automated step. The post-operative models (source) were always superimposed by rotation and translation on to the template (target).

To further improve the alignment of the post-operative image to the template the (ICP) function within VRMesh was used. The iterations were set at 500 and 50% of the vertices in the region were involved in the ICP registration process. The full procedure took an average 17 minutes for each case including template construction. The template was then deleted and the original pre-operative image re-imported. As the template was based on the pre-operative image and it did not move during alignment, as it was the target image, the post-operative images were aligned on target regions of the pre-operative image. Both the registered pre- and post-operative (soft and hard tissue) models were exported and saved for further analysis.

A

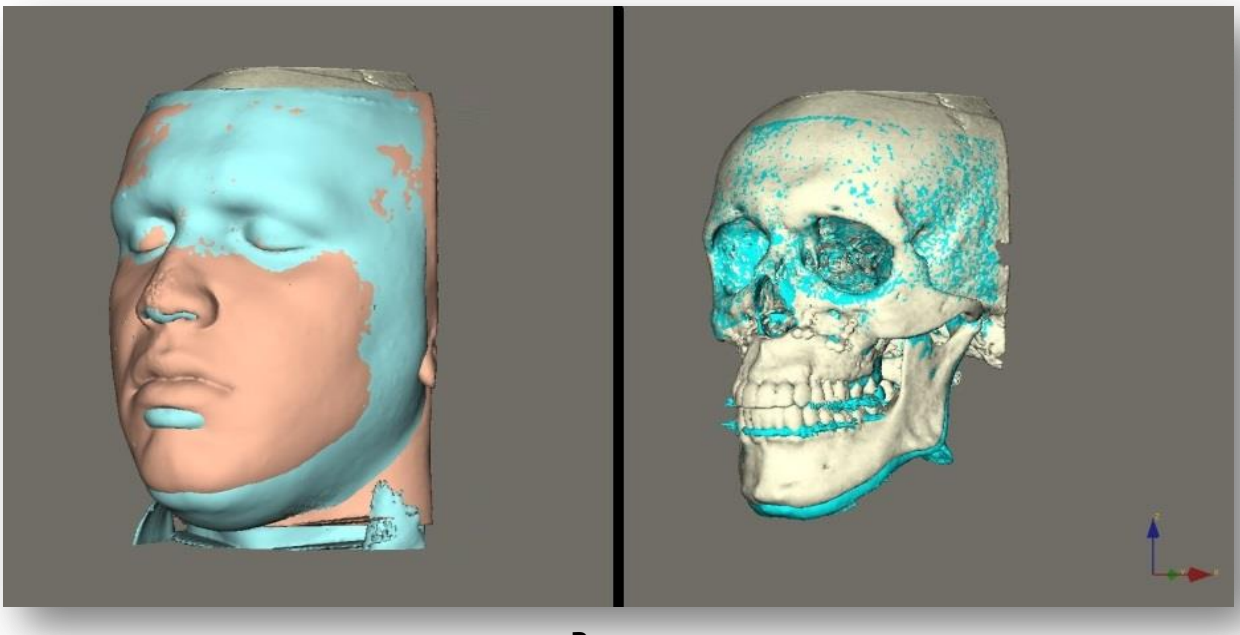

B

Figure 18: Voxel based registration. Selecting the volume of interest (A); the registered images (B), soft (left) and hard (right).

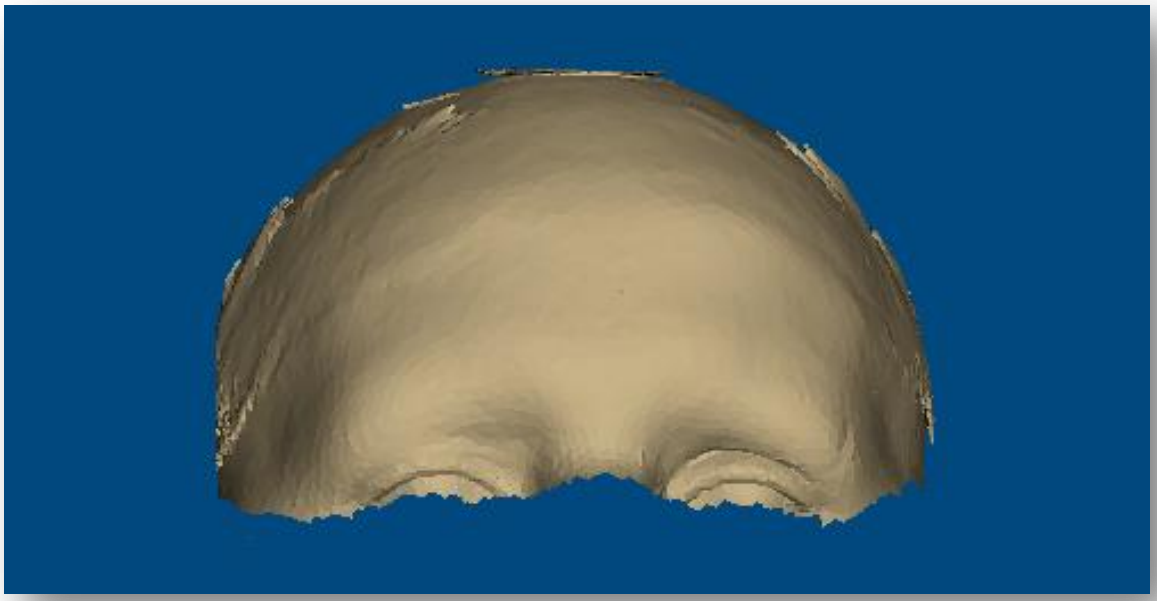

A

B

Figure 19: The registration template. Soft tissue (A) and Hard tissue (B) .

2.2.1.3.4 Analysis of registration accuracy

A standardised region for analyses was chosen for all the image pairs on the forehead and anterior cranial base using VRMesh software, (figure 20). The inferior boundary of the region was determined by a horizontal plane passing through right and left outer canthi; the superior boundary was denoted by a horizontal plane parallel to the inferior limit and located 20 mm above glabella; the posterior boundaries were limited by a coronal plane passing through sella. To insure standardisation of the region, the eight models for each patient were loaded in the same group prior to boundary selection and the same set of planes were used to croup all the models in the group.

These 8 models include two pairs for each registration method: VBR pre- and registered post-operative (soft and hard tissue models) and SBR pre- and registered post-operative (soft and hard tissue models). Isolation of the region was performed for all the loaded images simultaneously using the same cutter planes and as stated earlier above. At the end of the process, the eight models were exported and saved as VRML files for further analysis.

To perform the analysis, the images were loaded into in-house developed software. The software measured the nearest distance between two points on two adjacent meshes and produced the mean, standard deviation, maximum and minimum distances between them. The images were loaded pair wise (pre- and post-operative) as shown in table (4).

The results (mean, standard deviation, maximum and minimum distance) were exported as an EXCEL file (Microsoft®, Redmond, CA). Only 90% of the vertices were included in the analysis. This insures exclusion of the outliers due to erroneous data, which may have been attached to the isolated regions.

In addition to these measurements, the software provided a visual output of the distance measurements using a colour coded map and the distribution of the

measurements around the mean. These were saved as jpeg image files for visual observation only, (figure 21).

2.2.1.3.5 Statistical analysis

A paired Student *t*-test was used to determine if there was any statistical difference between SBR and VBR for pre- and post-operative images for both soft and hard tissues selected regions ($p<0.05$). An ANOVA and post-hoc Duncan test was used to detect any significant difference between each method of superimposition and tissue type i.e. hard or soft tissue. A Pearson correlation coefficient was used to test the correlation between superimpositions for the four groups (SBR hard, SBR soft, VBR hard and VBR soft). A one sample *t*-test was used to test if the absolute mean difference between the post-operative soft tissue 3D models aligned by each registration method was greater than 0.5 mm.

2.2.1.4 Results

Figure 22 shows the descriptive analysis of the four superimpositions groups. The four superimpositions were ranked from the lowest to the highest absolute mean distances between corresponding 3D meshes. Voxel based registration and surface based registration of the hard tissues showed the same values in the absolute mean distances between the models, 0.05 mm ± 0.21mm and 0.05 mm ± 0.26mm respectively. For soft tissue superimposition the absolute mean distances between the meshes were larger on the voxel based registration than that on surface based registration, 0.29 mm ± 0.33mm and 0.23 mm ± 0.56mm respectively.

For both hard and soft tissue the paired Students *t*-test showed no statistically significant difference between the two superimposition methods, (table 5).

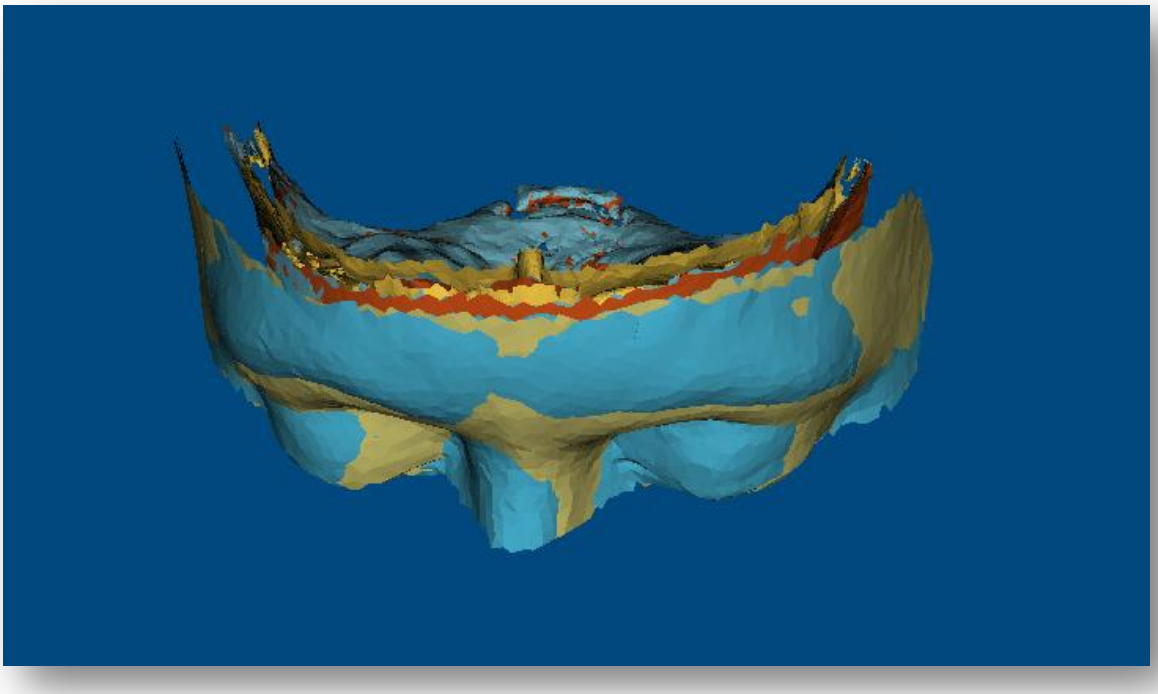

Figure 20: Standard region for analysis. Note that the soft and hard tissue of the two images were loaded and cropped at the same time.

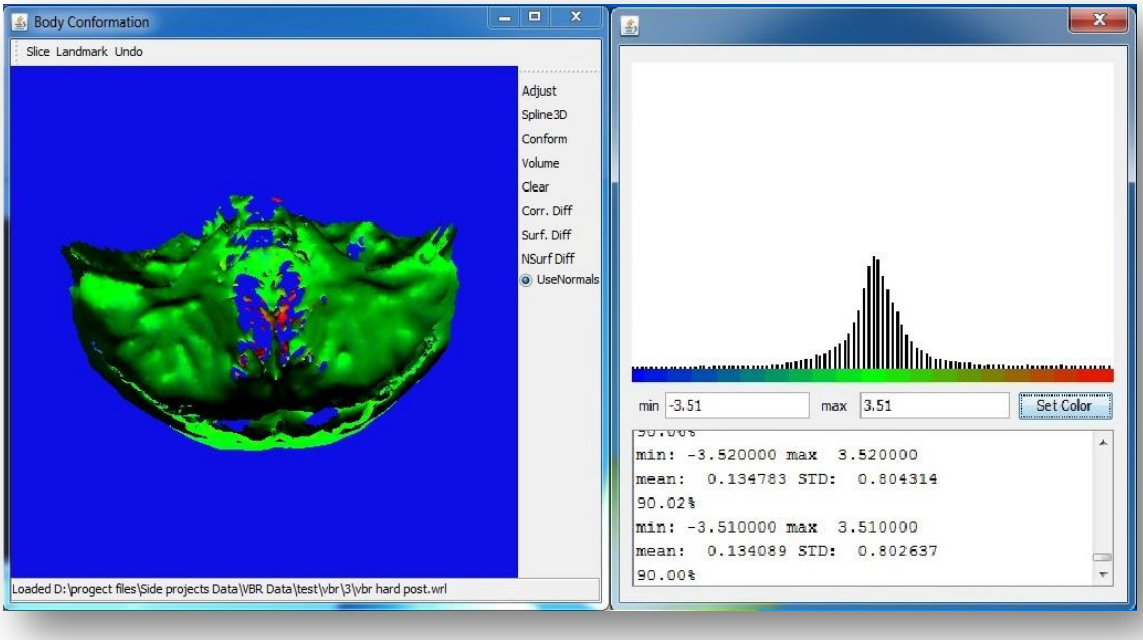

Figure 21: output colour map -registration accuracy

A one way ANOVA and post hoc Duncan test were used to investigate the statistical significance of the differences between any pair of the four groups (SBR hard, SBR soft, VBR hard and VBR soft). The result of ANOVA test showed a statistically significant difference between the four groups. The post hoc Duncan test showed that the type of tissue i.e. hard or soft tissue influenced the accuracy of superimposition using either surface based or voxel based registration methods. A statistically significant difference was found between superimposition of the soft and hard tissue models within the same method. The difference between the VBR hard and VBR soft superimpositions was statistically significant ($p<0.001$); the absolute mean difference was 0.23 mm, (table 6). However, the difference between SBR hard and SBR soft was not statistically significant ($p=0.712$).

Statistical correlation between different groups was analysed using a Pearson correlation test, (table 7). VBR hard and SBR hard superimpositions showed a strong positive correlation ($r = 0.886$). VBR soft and SBR soft showed a weak positive correlation ($r = 0.126$). This implies that the superimposition of the hard tissue did not show variability between the two methods whereas the soft tissue superimposition showed high variability.

Table 5: Paired sample t-test to compare methods accuracy for each tissue type.

		Lower	Upper	Mean	SD	SE	Sig. (2-tailed)
Pair 1	SBRhard - VBRhard	-.01	-.06	-.01	.02	.01	.39
Pair 2	SBRsoft - VBRsoft	-.18	.05	.28	.05	0.54	.24

Table 6: Paired sample t-test to compare the accuracy between different tissue types.

		Lower	Upper	Mean	SD	SE	Sig. (2-tailed)
Pair 1	sbrHard - sbrSoft	-0.42	0.29	-0.06	0.96	0.17	0.712
Pair 2	vbrHard - vbrSoft	-0.31	-0.16	-0.23	0.21	0.04	0.000

Table 7: Pearson correlation analyses showing 'correlation coefficient' and 'significance' between different tissue types and methods.

		SBRhard	VBRhard	SBRsoft	VBRsoft
SBRhard	Pearson Correlation	1	0.886**	0.190	0.102
	Sig. (2-tailed)	X	0.000	0.343	0.613
	N	27	27	27	27
VBRhard	Pearson Correlation	0.886**	1	0.126	0.182
	Sig. (2-tailed)	0.000	X	0.532	0.363
	N	27	27	27	27
SBRsoft	Pearson Correlation	0.190	0.126	1	0.126
	Sig. (2-tailed)	0.343	0.532	X	0.532
	N	27	27	27	27
VBRsoft	Pearson Correlation	0.102	0.182	0.126	1
	Sig. (2-tailed)	0.613	0.363	0.532	X
	N	27	27	27	27

**. Correlation is significant at the 0.01 level (2-tailed).

The one sample t-test showed the absolute mean difference between the pre- and post-operative soft tissue position when VBR was used to align soft tissue images or SBR was used was not statistical greater than 0.5mm ($p = 0.73$). The clinical significance was determined to be 0.5mm from a previous study (20).

2.2.1.5 Discussions

This study aimed to evaluate the accuracy of voxel based registration compared to surface based registration method and to determine if the difference between them is statistically significant. Accordingly, the research method was based on 31 pairs of preoperative and postoperative CBCT scans of patients treated by orthognathic surgery. The study investigated the accuracy of both methods in registering the postoperative image to the corresponding preoperative images.

Despite the fact that both methods of registration use the information provided by a CBCT generated DICOM image, voxel based registration deals with the raw information of the DICOM image by comparing the grey scale intensity of the voxels composing the corresponding DICOM images; on the other hand, surface based registration requires an extra step involving 3D model rendering to generate a three dimensional surface mesh model, on which the surface based registration is performed. This additional step may introduce a possible source of error since the algorithm used for segmenting the 3D model depends on Hounsfield value (HU value) of DICOM images of the CBCT. The form and dimension of the 3D surface model is dependent on the HU value (19) which in turn may be affected by image quality and tissue density. In addition, this extra step increases processing time and implies the need for multiple software packages for 3D model rendering which is unnecessary in the case of voxel based registration.

Another parameter worth considering when comparing the two methods is the amount of information utilised for the registration purpose. Surface based registration uses the 3D information provided by surface mesh topography of the 3D model. Whereas voxel based registration uses the grey scale values of all the

voxels embedded in and around the anatomical structure and is not dependent upon surface features. In other words, surface based registration deals with the "shell" covering the 3D structure while the voxel based registration deals with all the contents of the volume selected which may theoretically increase the accuracy of the method. However the use of such information implies the need for a more efficient computers and a longer processing time (16).

Despite the fact that both methods use the ICP algorithm for superimposition, which involves repetitive translation-rotation movement and measurements between the two 3D objects to reach the best matching superposition, the two approaches are considerably different. Surface based registration applies an estimation of the optimal translation and rotation between the three dimensional shapes by minimizing the mean square distance between the surfaces. The distance is measured between a specified percentage of the points randomly selected on one 3D mesh and the corresponding 3D surface mesh. Unlike voxel based registration in which the estimation of the optimal translation and rotation between the 3D volumes is determined by the mean square difference in the grey scale intensity between a specified percentage of voxels randomly selected on one image volume and the overlapped voxels in the corresponding one.

Loss of the sharpness of a 3D image during capture may be a source of error due to confusion in the estimation of the grey scale level of the voxels and therefore registration. However, the degree of DICOM image sharpness has a similar effect on the surface based registration but indirectly and may not be detected due to the automatic surface smoothing of the image. The accuracy of 3D model segmentation from DICOM image is affected by the quality of the DICOM image. In other words, the algorithm will have to decide where to place the boundaries of the hard tissue when building a skull model from a DICOM image with loss of sharpness and the resultant 3D model will represent the estimated dimensions rather than the original.

Four of the samples used in this study were considered as outliers with values reaching up to 6 times the general attitude of the sample and introducing errors by significantly changing the mean values of all of the superimposition groups. They were excluded from the study sample for this reason, (figure 23).

In all cases, surface based registration demonstrated a higher variability in superimposition as indicated by the larger standard deviation, (figure 22). This may be due to the SBR algorithm relying on well-defined surface features for registration which are present on the hard tissue but are not a prominent feature of the relatively homogenous surface of the soft tissue forehead. With respect to VBR registration, the distribution of the voxel's grey scale intensity was thought to be the reason for a lower variation in the superimposition process, which was reflected as a lower standard deviation.

Further investigation using Pearson correlation coefficient test was carried out to observe the correlation between different registration methods within each pre- and post-operative data set. A strong positive correlation ($r = 0.886$) was found between the hard VBR and SBR of the hard tissue models There were weak positive correlations among all other groups of the study. This result highlighted two important observations; firstly, surface based registration for hard tissue was as accurate and consistent as the voxel based registration. A possible explanation may be the high level of feature specific information available on the hard tissue surface which improves the performance of surface based registration. The relatively smooth surface of the soft tissue model reduces the accuracy of the registration and increases the variability of the results. On the other hand, voxel based registration relies on the grey scale intensity of the DICOM image voxels rather than the soft and hard tissue model surface features topography which makes it more consistent in both regions.

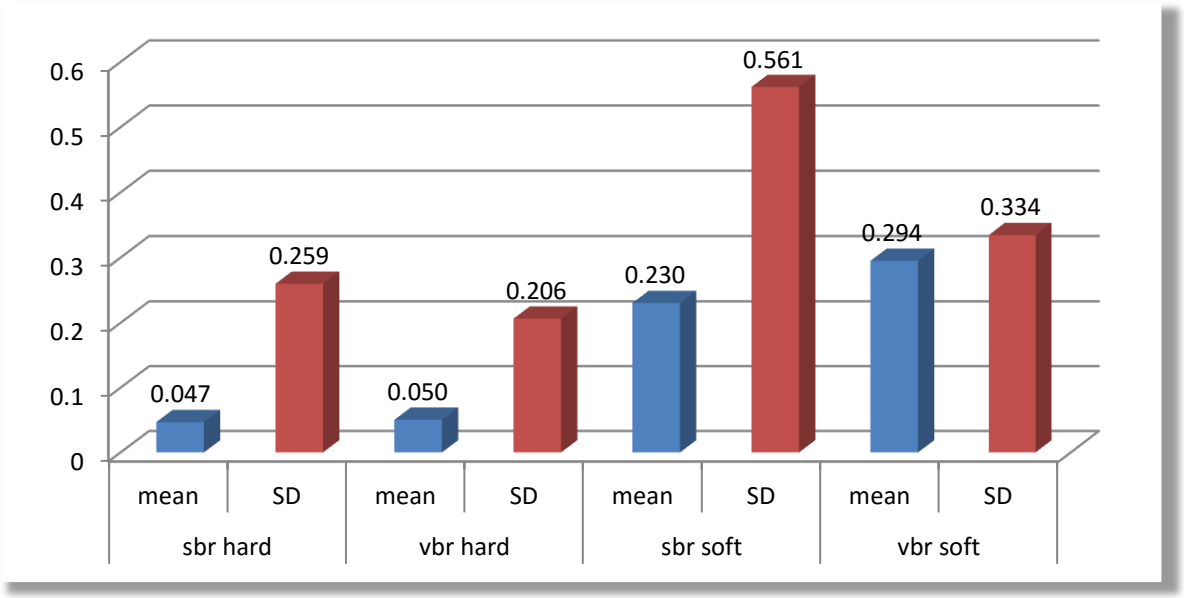

Figure 22: Comparison of the accuracy of the two 3D image registration methods. Note that the standard deviation is higher at surface based registration of the soft tissue models.

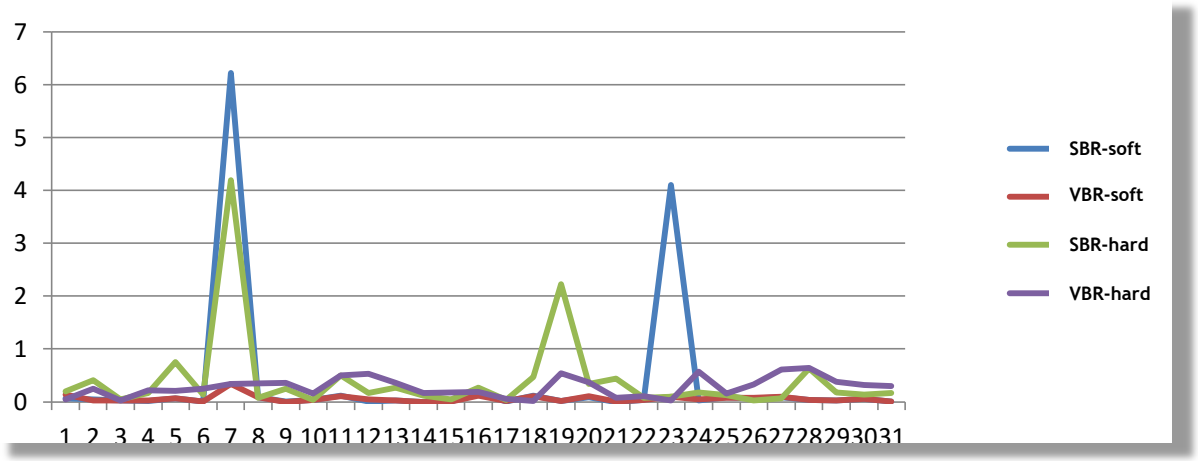

Figure 23: Excluded cases. Graphic representation of the error values showing the reason to exclude some of the study sample.

The other finding was the weak positive correlation between the soft and hard tissue models registration using voxel based registration (r = 0.126). Unlike surface based registration, the voxel based registration algorithm translates and rotates all the tissues captured in the DICOM image simultaneously. Hence, a strong correlation would be expected between the soft and hard tissue models alignment measurements. This result may be explained by the effect of variation of facial expression during the preoperative and postoperative image capture and the possibility of soft tissue thickness change as a result of weight changes in the time interval between the two scans. The fact that the voxel based registration algorithm relies on the grey scale intensity of the entire image may result in excluding these small differences in soft tissue contour as outliers during the registration process. This finding suggests that voxel based registration produces a more accurate representation of soft tissue changes as a result of surgery over surface based registration. Surface based registration of the soft tissue aligns the pre and post-operative images irrespective of the underlying hard tissue and therefore will “force” the two surfaces as close as possible; whilst VBR may be restrained by the underlying hard tissue since it is involved in the registration process. The differences between the two methods of registration are unlikely to have any clinical significance.(20)

2.2.1.6 Conclusions

No statistically significant differences were detected between the voxel based and surface based registration methods. However, voxel based registration showed more consistency in representation of the actual soft and hard tissue positions as indicated by lower mean standard deviation. Soft tissue surface based registration does not take into account changes in tissue thickness.

2.2.2 Direct DICOM slice landmarking, a novel technique to quantify the direction and magnitude of hard tissue surgical change.

2.2.2.1 Introduction

Numerous studies have reported on the three-dimensional changes of the skeletal hard tissue following orthognathic surgery, (Section 1.3.1). Previous methods used include 3D surface landmarking (137), colour coded distance maps (241) and volumetric changes (159). Each of these methods has deficiencies that limit their clinical application. For instance, changes in landmark position indicate the change of one point rather than a complete 3 dimensional structure, which can move with six degrees of freedom and volume changes, are not indicative of positional changes.

To address these shortcomings this study was designed to assess the accuracy and reproducibility of a novel method, based on landmarking DICOM image slices, to quantify the three-dimensional positional change of the maxilla and the mandible following orthognathic surgery.

To assess the accuracy of landmarking, true physical measurements were established by simulating 16 orthognathic surgery osteotomies on a plastic skull. This part of the project was carried out in collaboration with the University of Hong Kong. Measurements were directly recorded from a plastic skull for each simulated jaw movement and were considered the "gold standard" for comparison with the proposed internal 3D landmarking method.

2.2.2.2 Methods

2.2.2.2.1 Sample

Simulated surgical procedures involving Le Fort I osteotomies and bilateral sagittal split osteotomies were carried out on a plastic skull. Sixteen different combinations of vertical and antero-posterior (A-P) movements were performed, (table 8). The spatial coordinates of three landmarks on the maxilla and five landmarks on the mandible were recorded and the A-P and vertical

displacements at each of these landmarks were calculated. In total 108 (68 for maxilla and 40 for mandible) measurements were produced.

This was a collaborative study established with the University of Hong Kong, China. Thus, the method was carried out in two main parts: orthognathic surgery simulation and physical measurements (The University of Hong Kong) and digital image measurements (Glasgow University).

Table 8: Combinations of simulated surgery movements

	Anterior-Posterior (AP) (mm)	Vertical downgraft (mm)
Mandible	2, 4, 8 and 10	0
Maxilla	0, 3, 6 and 9	2
	0, 3, 6 and 9	4
	0, 3, 6 and 9	8

2.2.2.2.2 The physical measurements (Gold standard measurements)

2.2.2.2.2.1 3D surgical simulation setup

A specific device was constructed for the purpose of simulation of the surgical osteotomies and displacements. The device composed of a plastic skull which was secured to a universally adjustable camera mount fixed to a 20mm thick acrylic base. The level of the acrylic base could be adjusted to make sure it was horizontal using a spirit level. This arrangement allowed the skull to be rotated left and right, tilted up and down and tipped side to side, (figure 24).

An adjustable stage was secured to the acrylic block immediately below the occlusal plane of the maxilla. A height adjustable platform was fabricated relying on spacers of known height to adjust the vertical position of the maxilla. The adjustable stage constrained movement of the maxilla in the sagittal direction only, whilst the adjustable platform controlled vertical movement only by removing or adding “spacers” of known thickness. This ensured the maxilla could only be moved in two directions with no or minimal rotation.

2.2.2.2.2.2 Physical measurements

Using the 3D surgical simulation setup described above, a "locating mask" was produce that allowed re-location of the maxilla back to the skull following separation. A line was drawn representing the future Le Fort I osteotomy cut. Two holes were drilled on the right and left sides above and below the osteotomy cut. Four 3 mm stainless steel screws were used to secure the locating mask to the skull base. The locating mask was removed and the maxilla was detached from the skull by carrying out a Le Fort I osteotomy. Three 5 mm diameter spherical plaster markers were secured using sticky wax to the maxilla at the right greater palatine (GPR), left greater palatine (GPL) and the incisive foramina (IF). Using the locating mask the maxilla was secured to the skull using sticky wax; after which the locating mask was removed.

To assess mandibular changes, a bilateral sagittal split osteotomy (BSSO) was performed on the plastic mandible and reassembled using two 3mm stainless steel screws per side. As in the maxilla, 5 plaster sphere markers were placed on the mandible using sticky wax; left and right lingual foramen (LL and RL), left and right mental foramen (LM and RM) and genial tubercle (Ling).

A standard Dentatus face bow (Dentatus International AB, Sweden) was fitted to the skull; securing the acoustic meatus with laboratory putty and resting the orbital pointer in the right orbit. A circular spirit level was placed on the anterior region of the face bow which allowed orientation of the skull into a true horizontal position based on the Frankfort plane and parallel to the acrylic base. The skull was secured in this position.

The 3D surgical simulation setup with face bow in place was positioned in the cone beam CT (CBCT) scanner (iCAT, Imaging Science, Hatfield) so it was horizontal based on the spirit levels. The face bow was removed immediately prior to the 22 cm Extended Field Of View (EFOV) scan at 0.4mm voxel resolution being performed. This baseline scan horizontally orientated the skull within the 3D scan volume and was saved as a DICOM file.

2.2.2.2.2.3 Simulated maxillary and mandibular movements

As the skull needed to be removed from the acrylic base to carry out the simulated surgical movements six pre-marked reference points were used to make sure it was correctly re-positioned on the acrylic base. The six pre-marked points were nasion, landmarks on the right and left zygomatic buttresses, landmarks on the maxillary left and right molar region and an additional one between the central incisors. The landmarks on the molars and in between the incisors were also used to measure the simulated maxillary movements. Sagittal measurements were taken using a Vernier caliper mounted perpendicular to the acrylic base. Vertical measurements were recorded using a vertical height caliper (Chesterman, Sheffield, UK).

Following removal of the mandible, re-attachment, correct re-alignment of the skull and base line measurements, the maxilla was secured to the adjustable platform using sticky wax; and released from the base of the skull. Using the adjustable stage and platform the maxilla was moved to the desired position, re-secured to the base of the skull with sticky wax and then released from the adjustable platform. Duplicate measurements of the positions of the reference points before and after simulated maxillary movement were taken five times by the same operator. Cone beam CT scans using the EFOV option and 0.4mm voxel resolution were taken at 0, 3, 6 and 9 mm maxillary advancement; together with a 2, 4 and 8 mm “downgraft” for each 3mm increment of maxillary advancement. In total, 12 different positions of the maxilla were recorded and each scan saved as a DICOM file.

For simulated mandibular movements the mandible was re-attached to the skull and the lower border of the mandible secured to the adjustable platform. Following removal of the screws the anterior segment of the mandible was

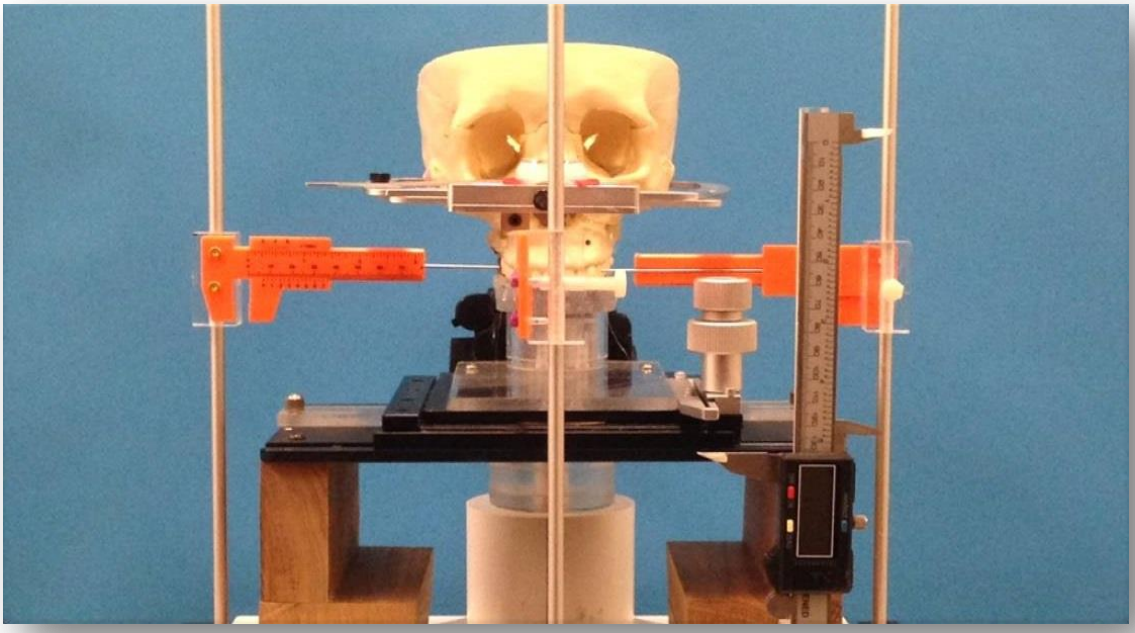

A

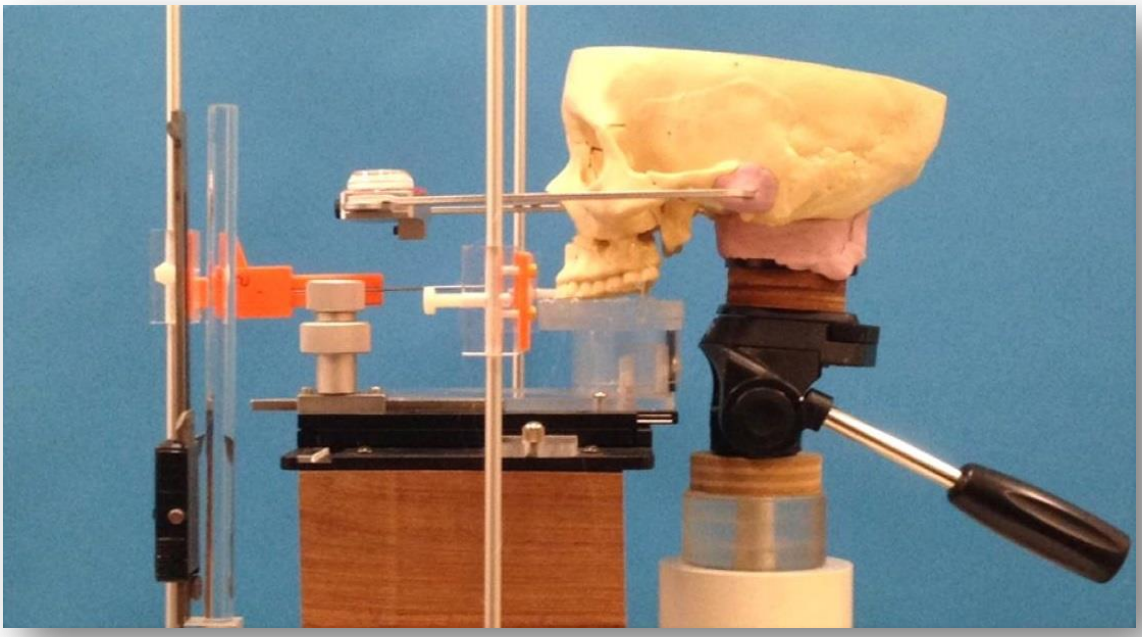

B

Figure 24: 3D Surgery simulation and measurement setup: Lateral view (A), frontal view (B)

translated forward and re-secured with sticky wax to the maxilla. Cone beam CT scans following the previous protocol were taken at 4, 6, 8 and 10mm mandibular advancements.

To accurately determine maxillary and mandibular movement all DICOM image was converted to a surface mesh using MeVisLab (MeVis Medical Solutions Ltd., Germany) with surface value of 600 and resolution 1 and saved in STL format. The original baseline skull STL file was loaded into VRMesh and all the remaining STL files were aligned to this baseline skull using the anterior cranial base as a common area of superimposition. Each image was re-saved in its new aligned 3D position. Using Minimagics (Materialise, Belgium) it was possible to import any two registered STL files, create a profile of both images and then measure the sagittal and vertical distances between the two profiles at any point. This was performed for all maxillary and mandibular movements.

2.2.2.2.3 Digital measurements

Measurements were made using OnDemand3D software (Cybermed, Seoul, South Korea). The landmarking procedure involved three steps: pre- and post-operative DICOM image superimposition; 3D image orientation and creation of reference planes (x, y and z planes) and lastly a modified 3D cephalometric analysis of the orthogonal measurements of 8 landmarks placed on the DICOM image slices. These steps were followed by calculation of the actual three-dimensional movement of each landmark due to changes in jaw position.

2.2.2.2.3.1 DICOM image superimposition

The pre- and post-operative CBCT scanned DICOM images were imported into OnDemand3D software. Superimposition of the two images was accomplished using voxel-based registration. This involved two steps: manual alignment of the two images followed by automatic registration. The registration process was a series of iterative movements aimed at achieving the “best fit” based on the grey scale intensity between the two overlapping images, voxel by voxel(69). The region of interest for superimposition was the anterior cranial base as this was a stable and unaffected by surgery (242).

2.2.2.2.3.2 Creation of reference planes

Following superimposition of the pre-and post-operative DICOM images a common reference plane could be constructed. Three reference planes were created, an axial plane based on left and right porion and right orbitale), a sagittal plane based on nasion and sella points and oriented perpendicular to the horizontal plane, and lastly, a coronal plane was created perpendicular to both the previous planes at the sella point. The x, y and z co-ordinates of any landmark placed on any of the DICOM slices could then be extracted orthogonally with reference to these three planes, (figure 25).

2.2.2.2.3.3 Orthogonal measurements

In total 8 landmarks, 3 in the maxilla and 5 in the mandible were placed. The positions of these landmarks were designed to assess the three dimensional orientation and movements of maxilla and mandible. Each landmark was placed at the centre of the spherical plaster ball placed on the skull prior to scanning as described above. To facilitate onscreen landmark placement, the centre of each sphere was identified by simultaneously viewing the sphere on the DICOM slices in the three dimensions (sagittal, axial and coronal), (figure 26).

Orthogonal measurements of each landmark on the pre-operative slice images to the common reference planes were recorded and the x, y and z coordinates of the 8 landmarks were exported to Microsoft EXCEL (Microsoft®, Redmond, CA) for further analyses. The same procedure was repeated for the post-operative slice images of each of the simulated movement.

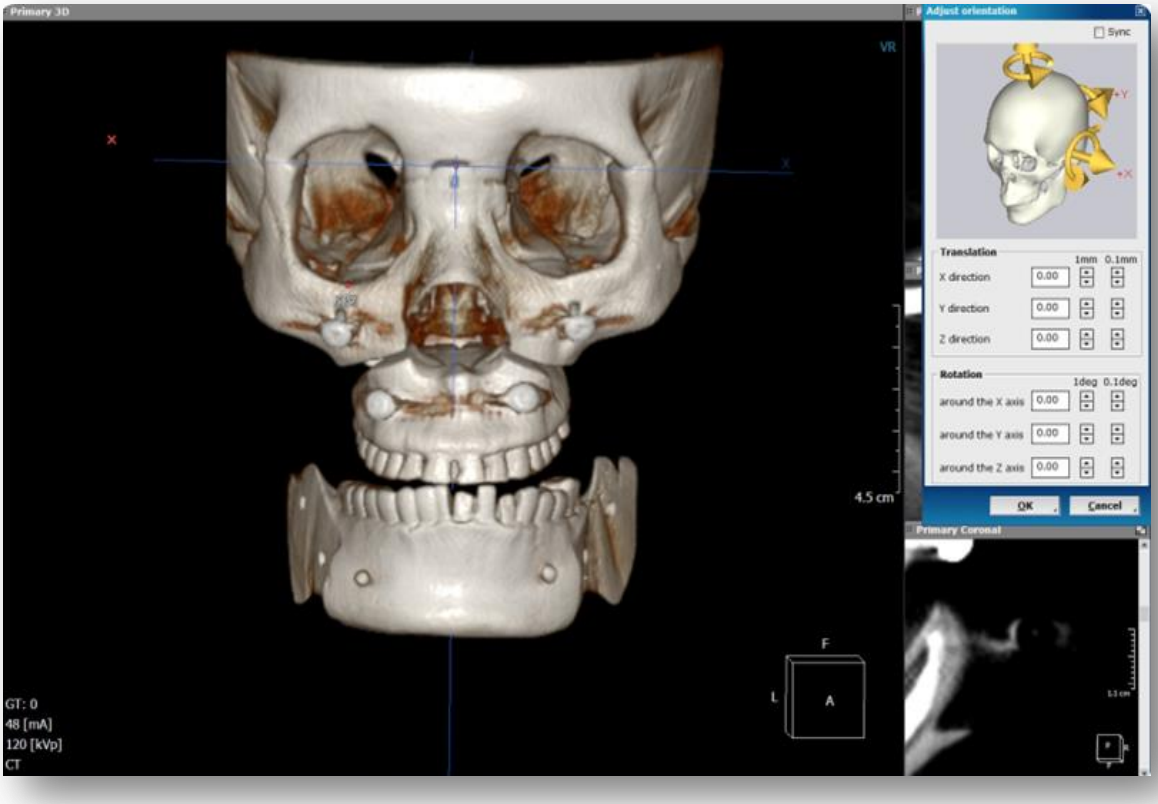

Figure 25: Reference planes (Ondemand3D software). Fine tuning of the reference planes is possible through changing the three dimensional position using the panel on the right side.

2.2.2.2.4 Error study

The inter and intra-operator reliability of landmark digitisation was assessed by the same operator re-digitising the same points two weeks apart and a second independent operator digitising the landmarks. Inter- and intra-examiner landmarking errors were evaluated by analysing the differences between the repeated readings using a one sample Students *t*-test and Interclass Correlation Coefficient (ICC) (SPSS Version 22, IBM). Inter- and intra-examiner Euclidean landmarking distances errors were calculated using the formula below, equation (2).

Equation 2: 3D Pythagoras equation where D is the Euclidean distance and x, y and z are the linear measurements in the three respective dimensions

$$D = \sqrt{(\Delta x)^2 + (\Delta y)^2 + (\Delta z)^2}$$

2.2.2.2.5 Clinical application test

The landmarking method was carried out on 5 randomly selected cases. Landmarks were successfully placed on the DICOM slices at the same anatomical locations used in this validation project and displacement measurements were calculated. The same procedure repeated two weeks later and measurements were compared using paired Students sample *t*-test.

2.2.2.2.6 Statistical analysis

The absolute distance between the pre- and post-operative positions of each landmark in x, y and z dimensions from the DICOM data were compared to the measurements obtained from the simulated orthognathic surgeries using a one sample *t*-test, Interclass Correlation Coefficient (ICC) test and Bland-Altman plot.

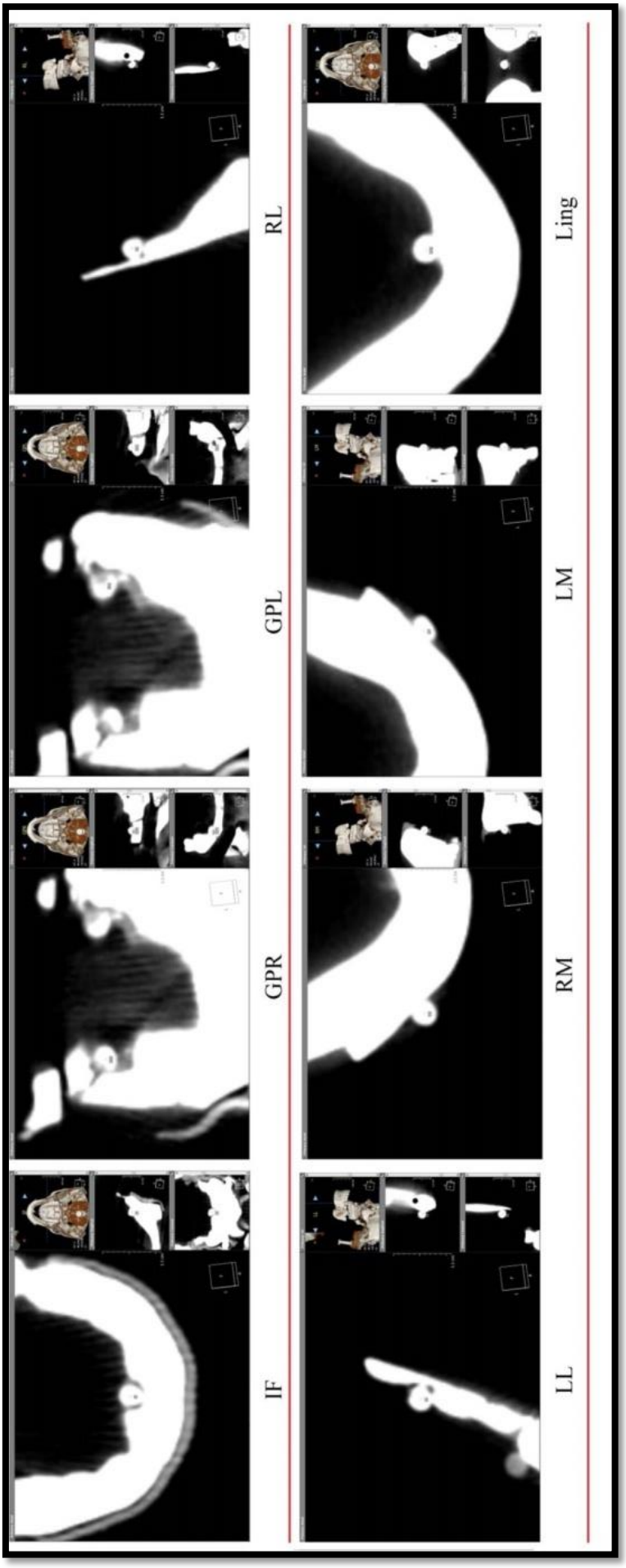

Figure 26: Landmarks digitization. The full set of landmarks was individually digitized at the centre of the indicator. The presence of the 3D viewer on the right hand side enhanced the accuracy of landmarking. Starting from the top left Incisive foramen (IF), Grater palatine Right (GPR) Greater palatine (Left), Lingual foramen Right (LR), Lingual foramen Left (LL), Mental foramen Right (RM), Mental foramen Left (LM),and Genial tubercle (Ling).

2.2.2.3 Results

2.2.2.3.1 ***Inter- and intra-examiner's landmarking error***

The magnitude of the intra-examiner and inter-examiner landmarking errors are shown in table (9). The mean landmarking distance errors were 0.35 ± 0.17 mm and 0.30 ± 0.15 mm for inter- and intra-examiner tests respectively. There was a highly significant correlation between the repeated readings for intra- and inter-examiner error test in all three dimensions, (table 10). A one sample *t*-test for repeated readings showed no significant difference ($p>0.05$) in all dimensions (x, y and z), (table 11).

2.2.2.3.2 ***Accuracy of DICOM slice landmarking compared to the gold standard measurements***

There was a significant correlation between the two measurements in both the y and z dimensions ($r = 0.999$, $p = 0.0001$), ($r = 0{,}998$, $p = 0.0001$) respectively, whereas in the x dimension there was no significant correlation ($r = 0.000$, $p=0.500$), (table 12).

A one sample *t*-test showed that there was no statistically significant difference for the y and z dimensions, (table 13). The x dimension, however, showed a significant difference.

The mean difference between the two absolute measurements was 0.34 ± 0.20 mm, 0.22 ± 0.16 mm, 0.18 ± 0.13 mm in the y, z and x dimensions respectively. Figures (27 and 28) show Bland-Altman plots for the sagittal and vertical data.

The results in table (14) show a high reproducibility of the measurements on clinical cases. The same landmarks were digitised on the superimposed pre- and postoperative DICOM images. Paired sample t-test showed a low significance values ($p = 0.3$) in x, y and z dimensions.

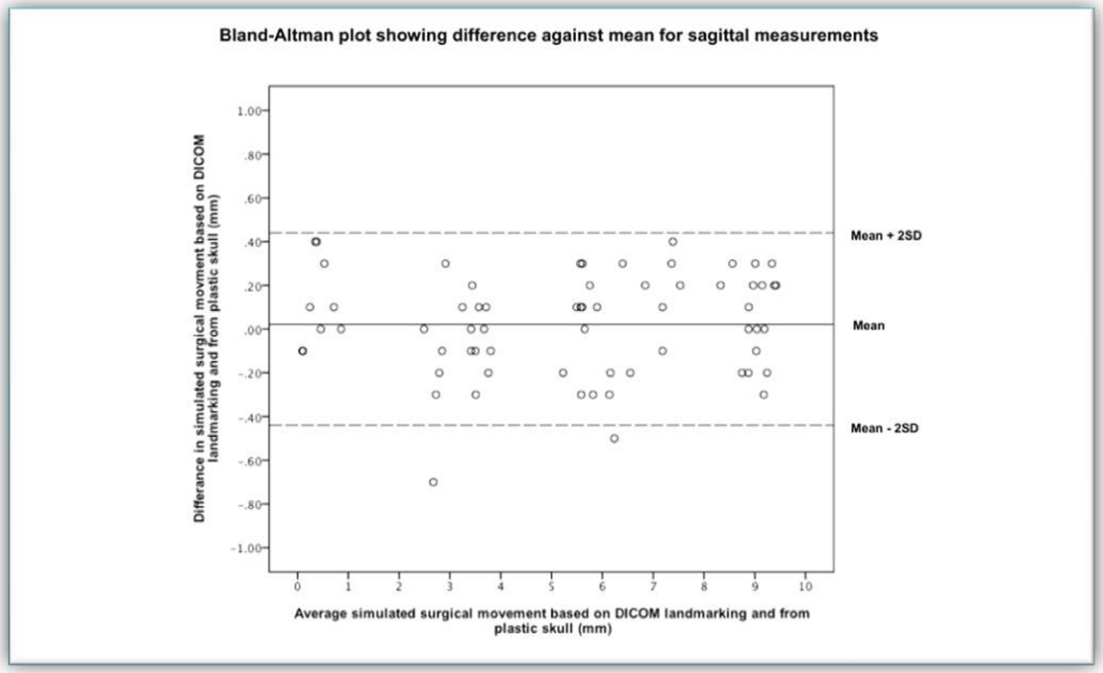

Figure 27: Bland Altman Plot for sagittal measurements. Note the uniform distribution around the mean.

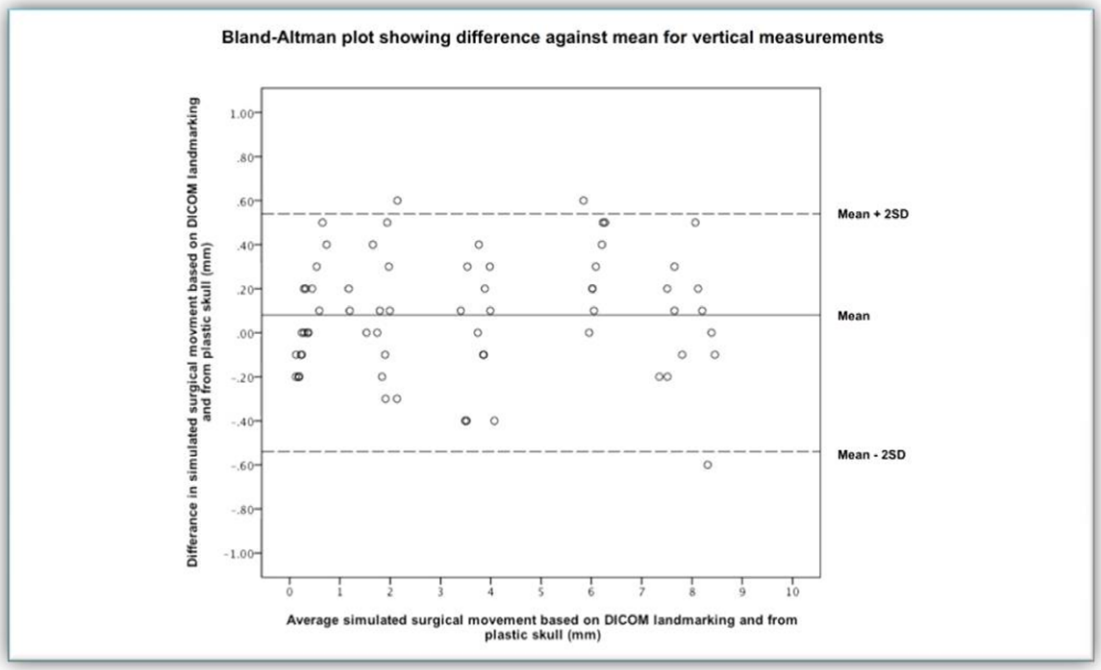

Figure 28: Bland Altman vertical measurements. Note the uniform distribution around the mean.

Table 9: The intra and inter examiner landmarking errors (Euclidian distances) between the repeated readings at each landmark.

Inter-examiner			Intra-examiner		
Landmark	Mean distance (mm)	SD	Landmark	Mean distance (mm)	SD
IF	0.22	0.15	IF	0.21	0.07
GPR	0.29	0.15	GPR	0.13	0.07
GPL	0.38	0.12	GPL	0.25	0.10
LL	0.36	0.19	LL	0.60	0.49
RL	0.39	0.22	RL	0.28	0.08
RM	0.37	0.13	RM	0.25	0.15
LM	0.38	0.30	LM	0.40	0.17
Ling	0.42	0.17	Ling	0.25	0.07

Table 10: Interclass correlation and the inter- and intra-examiner errors (three dimensional distance) between the repeated readings.

	Coordinates	Mean (mm)	SD	SE	Interclass correlation	
					r-value	p-value
Inter-examiner	x	0.02	0.2	0.03	0.638	0.003
	y	0.01	0.17	0.03	0.907	0.001
	z	-0.09	0.7	0.12	0.991	0.001
Intra-examiner	x	-0.04	0.76	0.13	0.999	0.001
	y	0.14	0.32	0.06	0.999	0.001
	z	0.14	0.32	0.06	1.000	0.001

Table 11: The inter and intra examiner errors in the three dimensions (one sample t-test)

		Intra examiner error			Inter examiner error		
Landmarks	**Coordinate**	**Mean**	**SD**	**p-value**	**Mean**	**SD**	**p-value**
IF	x	0.08	1.02	0.88	0.12	0.22	0.34
	y	0.53	0.99	0.37	0.13	0.17	0.23
	z	-0.13	0.18	0.23	0.16	0.22	0.24
GPR	x	-0.08	1.06	0.89	0.01	0.36	0.95
	y	0.62	1.05	0.32	-0.19	0.22	0.18
	z	-0.15	0.55	0.61	0.23	0.16	0.06
GPL	x	-0.15	1.17	0.82	0.10	0.31	0.57
	y	0.44	1.01	0.45	0.02	0.23	0.86
	z	-0.23	0.4	0.33	0.16	0.25	0.28
RL	x	0.26	0.44	0.32	0.08	0.19	0.48
	y	0.34	0.87	0.49	-0.11	0.17	0.27
	z	-0.21	0.25	0.19	0.24	0.32	0.23
LL	x	0.10	0.48	0.70	0.06	0.28	0.68
	y	-0.03	0.59	0.91	-0.04	0.3	0.79
	z	-0.11	0.17	0.28	0.11	0.18	0.32
RM	x	0.00	0.33	1.00	0.01	0.17	0.91
	y	-0.08	0.73	0.85	-0.08	0.34	0.66
	z	-0.05	0.42	0.82	-0.01	0.38	0.96
LM	x	0.72	0.86	0.19	0.16	0.32	0.39
	y	-0.09	0.48	0.72	-0.11	0.28	0.48
	z	-0.15	0.46	0.55	0.17	0.28	0.31
LING	x	-0.25	0.55	0.43	-0.04	0.32	0.83
	y	0.06	0.92	0.91	0.07	0.39	0.76
	z	-0.14	0.31	0.42	-0.09	0.21	0.44

Table 12: The differences between the two methods of measurements (Inter class correlation).

Coordinate	Mean (mm)	SD	SE	Interclass correlation	
				r-value	p-value
X	0.34	0.21	0.03	0.000	0.500
Y	0.08	0.27	0.03	0.998	0.001
Z	0.02	0.22	0.03	0.999	0.000

Table 13: The differences between the two methods of measurements (one sample t-test)

Landmark	Coordinate	Mean (mm)	SD	p-value
IF	x	0.35	0.21	0.02
	y	-0.01	0.26	0.99
	z	0.06	0.27	0.44
GPR	x	0.33	0.20	0.01
	y	-0.15	0.32	0.09
	z	-0.07	0.24	0.27
GPL	x	0.32	0.25	0.02
	y	-0.15	0.27	0.05
	z	0.05	0.19	0.28
RL	x	0.43	0.20	0.54
	y	-0.25	0.29	0.19
	z	-0.09	0.15	0.34
LL	x	0.29	0.20	0.13
	y	-0.18	0.12	0.06
	z	-0.18	0.11	0.05
RM	x	0.32	0.17	0.12
	y	0.04	0.12	0.59
	z	-0.08	0.13	0.37
LM	x	0.35	0.16	0.16
	y	0.05	0.21	0.70
	z	-0.07	0.25	0.64
LING	x	0.36	0.19	0.22
	y	0.11	0.13	0.20
	z	-0.11	0.22	0.40

Table 14: Results of the pilot study of a repeated measurements on clinical cases (Paired sample t-test).

Co-ordinate	Mean (mm)	SD	SE	95% Confidence Interval		p-value
				Lower (mm)	Upper (mm)	
x	-0.27	0.77	0.25	-0.87	0.32	0.31
y	-0.18	0.62	0.20	-0.66	0.29	0.39
z	0.31	0.91	0.30	-0.38	1.01	0.33

2.2.2.4 Discussion

The primary objective of this project was to introduce and validate a new method of radiographic measurements to assess the maxillo-mandibular changes following orthognathic surgery. Each of the currently available methods has its own deficiency which impacts negatively on the validity of the measurements. The proposed method attempts to overcome the problems associated with the current approaches of 3D surface model segmentation using DICOM image slices. It promises a reliable and a reproducible 3D landmarking to measure surgical changes.

Lack of anatomical correspondence is a major problem associated with the colour coded error map method that is frequently used for radiographic superimposition (243). However, the method is commonly used to evaluate facial soft tissue changes following surgery. It overcomes the difficulty of the limited number of landmarks available for soft tissue analysis. The anisotropic deformation of the soft tissues of the face in response to the surgical movement of the underlying jaw bones is difficult to measure. This is not the case when measuring bony movements of the facial skeleton. As a result of surgery, the maxilla moves as a unified unit, rigid body transformation. The addition of rotational movements such as differential impaction or central midline can produce variation in the amount of linear translation of various regions within the structure. However, this affects the whole skeletal structure as a unit since the geometric integrity is preserved.

Placement of landmarks on a CBCT scan slice is an advanced technique that can provide accurate and detailed information about the internal skeletal structures. The reliability and reproducibility of “slice” landmarking was recently validated (96). However, the validity of this method to assess skeletal changes following orthognathic surgery has not been tested yet.

Three points in 3D space are enough to create and orient a plane. The coordinates of these three points will be changed as a result of the translation of the plane in 3D space. Rotation of the plane around axes which passes through

two of the three points would change the coordinates of the third point, whereas the rotation around any point other than these three points would change the coordinates of the three points. This explains how three points could be used to monitor the position of its related anatomical structure in 3D space. If this plane forms part of a larger solid 3D object then these three points could be used to assess the exact translation and rotation movements of that solid object in 3D space.

This concept was adopted in the proposed approach to assess the skeletal displacement of the maxilla and the mandible as a result of orthognathic surgery for correction of dento-facial deformities. Three anatomical landmarks are therefore required to be marked on each hard tissue structure to accurately measure its displacement in 3 planes of space. To overcome the problems associated with surface remodelling, three landmarks within the maxilla and five landmarks within the mandible were identified directly on the DICOM image slices. Landmark positions on the maxilla and mandible were selected for their favourable geometric position, clear anatomical definitions and high reproducibility.

Simulating the surgical movement on a plastic skull allowed the maxilla and mandible to be separated and translated into different positions anteriorly and vertically with minimal lateral or rotational movements. It was not possible to measure rotational and lateral movements directly on the plastic skull using the current experimental setup; therefore the movement in the x dimension was considered to be close to zero throughout the calculations. However the small inadvertent lateral or rotational changes in the x dimension led to the expression of a significant p-value and low correlation when compared to the physical movement in the x dimension. Differences in measurements in the y and z dimensions were not statistically significant with a mean difference of 0.22 ± 0.16 mm and 0.18 ± 0.13 mm respectively. A one sample *t*-test was used to test for difference from the reference measurement set, the 95% confidence interval was narrow ranging from -0.03 to 0.15 mm for the y and z dimensions, with an upper limit of 0.15 mm confirming the clinical insignificance. The high

reproducibility of the method on clinical cases validates its applicability in clinical research environment.

The proposed method proved reliable in measuring surgical changes of the jaw bones which was demonstrated by the high correlation coefficient between the physical and digital measurements. The method lends itself to uncomplicated landmarking, the inter-examiner and intra-examiner variability were non-significant.

2.2.2.5 Conclusions

Internal landmarking of DICOM image slices is a reliable, reproducible and informative method for assessment of the 3D skeletal changes following orthognathic surgery.

2.3 Section C: Validation of basic methods of soft tissue Analysis

In this part, one experiment was carried out to validate the accuracy of Generic mesh conformation which constitutes the bases of soft tissue analysis method. Details about stereophotogrammetry system used and a brief details 3D model conformation (elastic deformation) were also explained.

2.3.1 The use of a generic mesh to assess soft tissue changes using stereophotogrammetry.

2.3.1.1 Introduction

The use of generic meshes for analysing biological geometry has previously been reported (152,175). The use of "correspondence analysis", based on generic meshes, has been suggested as a solution for the lack of accurate anatomical correspondence between the pre- and post-operative images associated with the current surface analysis methods (243).

The advantage of using a generic mesh is that there are a known number of vertices each with known co-ordinates and the triangles formed by these vertices are indexed or ordered. Most importantly following conformation this index is maintained and preserved. Conformation (elastic deformation) is a process to elastically deform the generic mesh to the pre- and post-operative patient's images. This process will then produce two meshes with the same number of vertices and triangles in the same order in the file structure, where each vertex represents a corresponding point on both pre- and post-operative conformed meshes. The accuracy of the conformation will determine the accuracy of the final correspondences. Even though the conformation process is semi-automated, it relies on an initial manual landmarking process used to match certain corresponding anatomical features and constitutes the bases for the automated process. In addition different conformation algorithms built into various software packages may also affect the final correspondences.

The in-house conformation software developed by the research group at the University of Glasgow provides a wide range of 3D imaging tools including: 3D image conformation (elastic deformation), inter-surface distance measurements, 3D landmarking and colour coded distance map generation.

For each subject six facial expressions were captured using 3D stereophotogrammetry. One facial expression image, rest position, was chosen and used as the "generic mesh". The rest position generic mesh was then conformed to the remaining five images and this was repeated for each subject. Following conformation of the rest position "generic mesh", to each of the facial expressions, the 19 landmarks pre-located on the generic mesh which were not used during conformation should "slide" into their respective positions to match each of the corresponding landmarks on each of the five facial expressions if the algorithm was functioning correctly. The distance between the actual landmarks on the non-conformed expression mesh and the landmarks on the conformed generic mesh, for the same facial expression, gives an accuracy of the conformation process. The closer to zero, the more valid and accurate is the process of conformation.

2.3.1.2 Aim

The aim of this section is to determine the accuracy of the conformation process based on 34 pre-marked facial landmarks, 15 of which are used during the conformation process and the remainder as measures of conformation accuracy.

2.3.1.3 Materials and methods

2.3.1.3.1 Stereophotogrammetry capture protocol

All three-dimensional facial images were captured using the Di3D imaging system (Dimensional Imaging, Hillington, Glasgow). The system was based on passive stereophotogrammetry and produced fully textured 3D images from ear to ear. The imaging system used two pairs of high-resolution digital cameras (Canon EOS 1000D-EOS Digital SLR, Canon, Japan) together with external flashes (Esprit

digital 1000DX, Bowens, England, UK) to create a stereo 3D image based on the principle of triangulation. Please refer to Section (1.1.1.5), (figure 29).

The Di3D system had separate image capturing software (Di3DCapture) and post-processing viewing, manipulation and analysis software (Di3DView), both running on a high performance PC (Dell OptiPlex 960) and Windows 7 (Microsoft). Di3D Capture is the user interface control panel of the Di3D system which enabled the user to capture, build and save the stereophotogrammetry images; in addition to system calibration. The "live preview" function allowed the correct positioning of the subject prior to capture, (figure 30).

Di3DView software allowed image manipulation including translation, rotation and magnification. A variety of tools were built into the software, some of which included image landmarking and 3D co-ordinate extraction, image superimposition, Euclidian surface distance measurements and asymmetry score calculations. In this study, the software was mainly used for image viewing, manipulation and assessing the quality of each image prior to saving, (figure 31).

2.3.1.3.2 System Calibration

The Di3D system was calibrated prior to the image capture sessions using the manufactures instructions. This process was semi-automatic and involved capturing several images of the calibration target in different orientations and using the "calibration" function within Di3D Capture software to complete the process, (figure 32). This process provided the intrinsic parameters for the camera configuration relying on the known spacing between the centres of the circles on the calibration target. The calibration software extracted the co-ordinates of the circles on the image and from this information the software could determine the relative positions of all four cameras without any further operator intervention.

Figure 29: Di3D Stereophotogrammetry system

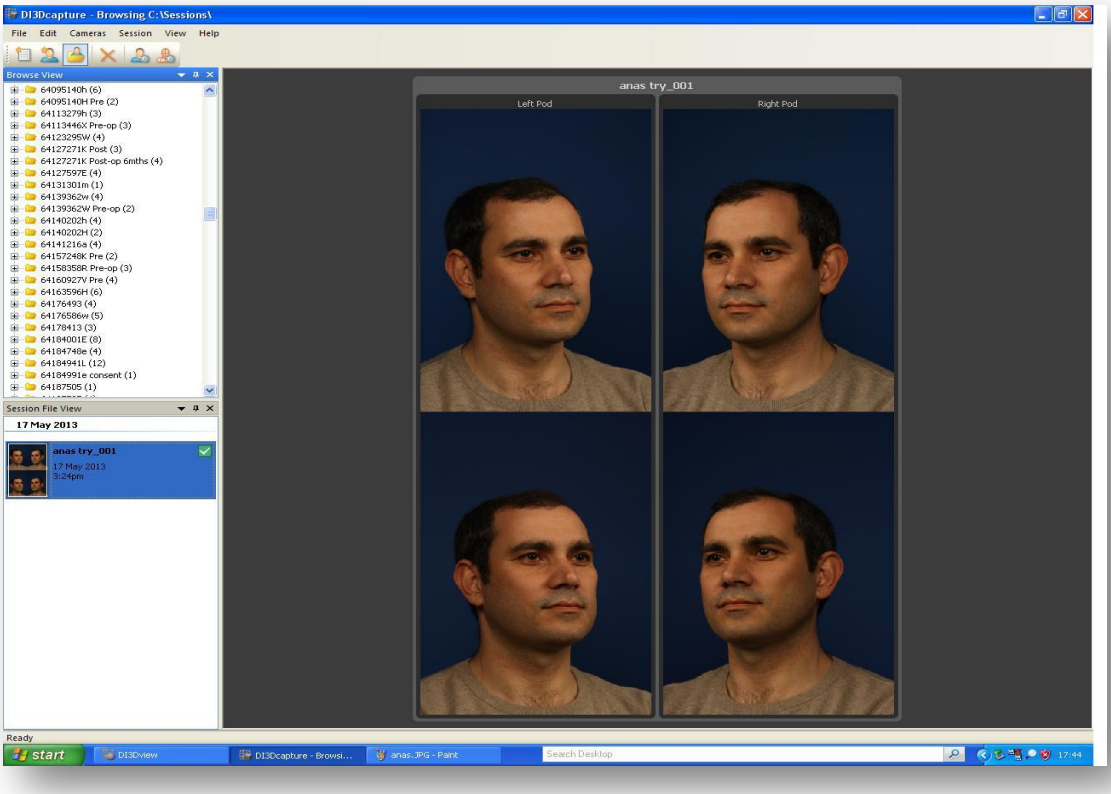

Figure 30: Di3D Capture software main panel

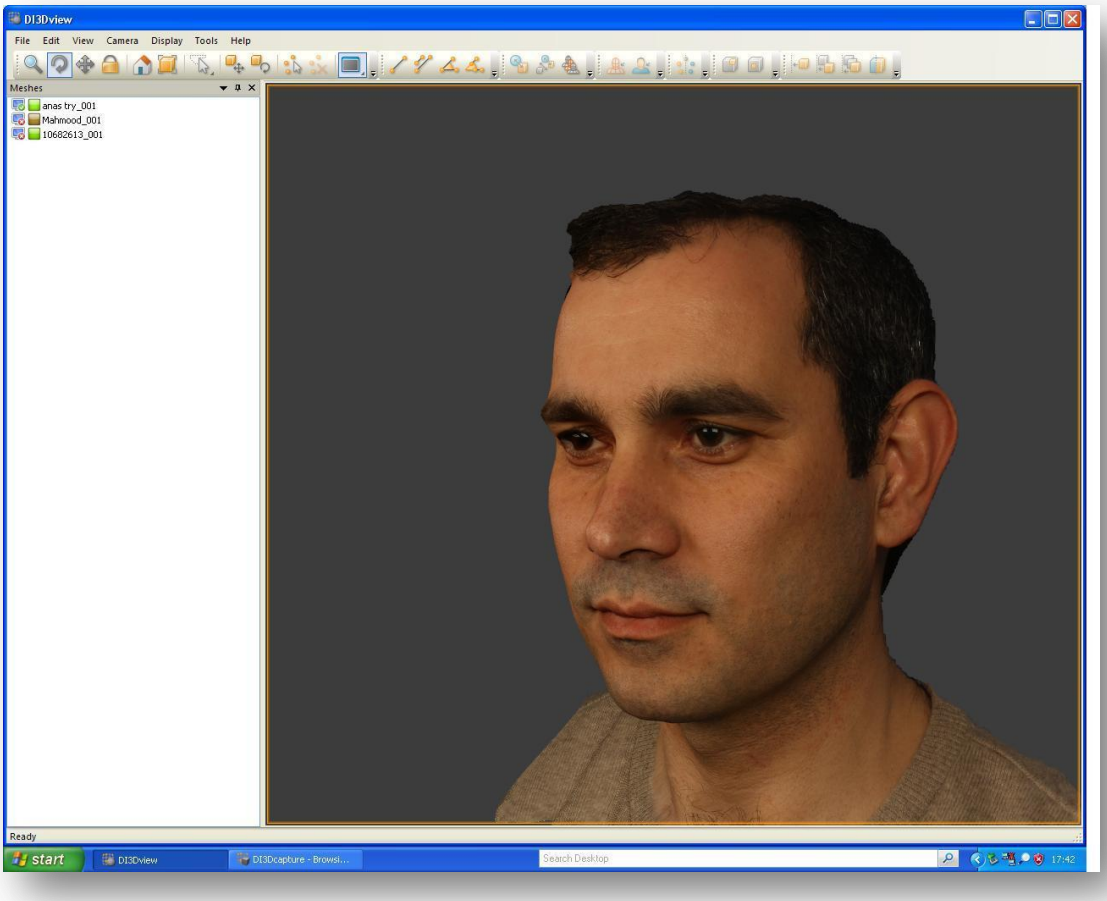

Figure 31: Di3D View software main panel

A B

Figure 32: Di3D system calibration board: calibration board (A); Calibration board in position during the calibration procedure

2.3.1.3.3 Image capture protocol

For all captures, patients were seated on a chair directly in front of the Di3D imaging system. Using the "live preview" screen provided by Di3D-Capture software, the patient was positioned correctly relative to all four cameras. To standardise the images each subject was asked to:

- Remove spectacles and jewellery,
- Keep all hair completely off the face and neck using a head cap, (Nurses cap Barrie, MOLNLYCKE, UK.)
- Remain still during image capture,
- Say "Mississippi", then told to swallow once and say "N" (guidelines to obtaining rest position natural facial expression as proposed by Zachrisson, 1998).
- Following capture each image was automatically built into a 3D model. The images were then exported in Wavefront (.obj) format for future analysis.

2.3.1.3.4 Sample

Ten individuals (6 male and 4 female) were chosen at random and consented to take part in the study. Volunteers were healthy adults with no history of facial deformity or previous surgery in the facial region. Males were clean-shaven to avoid image distortion.

2.3.1.3.5 Subject imaging

Prior to 3D facial image capture thirty-four 2mm diameter self-adhesive black non-reflective markers (Diamante, Apparel accessories Ltd, Guangdong, China) were placed on each subjects face using an application tool (Pick-it-up vacuum tool, Bead smith, China). The position of the markers were selected around the eyes, nose, mouth and cheeks in addition to the peripheries of the face i.e. the tragus, gonial angle and chin areas, (Figure 33) and (table 15).

a) The participants were then asked to rehearse six facial expressions to ensure that the markers were secure. The six expressions are shown in figure (34). There were:
b) maximum smile,
c) cheek puff,
d) lip purse,
e) mandibular displacement to the right (simulating facial asymmetry),
f) forward mandibular displacement and
g) Repose or rest position.

The images were captured using the Di3D stereophotogrammetry system and protocol previously described (Section 2.3.1.3.3). In addition subjects were asked to keep their lips closed through all captures. This would prevent distortion of the image by exposure of the teeth. Two images were captured for each facial expression and the best image was chosen. Images were individually built and viewed using Di3D view software and saved as Wavefront (.obj) file for further analysis.

Table 15: Definitions of landmarks for validation of the accuracy of 3D image conformation.

	Abbr.	Landmarks	Definition
1	EBR	Eyebrows-R	The point just above the eyebrows at a vertical line from the pupil.
2	Gla	Glabella	Most prominent midline point between eyebrows
3	EBL	Eyebrows-L	The point just above the eyebrows at a vertical line from the pupil.
4	Exc-R	Exocanthion-R	Outer commissure of the eye fissure
5	End-R	Endocanthion-R	Inner commissure of the eye fissure
6	Na	Nasion	Mid-point on the nasal bridge.
7	Exc-L	Exocanthion-L	Outer commissure of the eye fissure
8	End-L	Endocanthion-L	Inner commissure of the eye fissure
9	Sbtr-R	Subtragion-R	The most anterior inferior point of the anterior inferior attachment of the ear helix, just above the ear lob
10	Sbtr-R1/3*	Sutragion-R (1/3)	One third the distance from Sbtr-R to Ala-R
11	Sbtr-R2/3*	Subtragion-R (2/3)	Two third the distance from Sbtr-R to Ala-R
12	Ala-R	Alar curvature-R	Most lateral point on alar contour
13	Ab-R	Alar base-R	the junction between the right nostril and upper lip
14	Prn	Pronasale	Most protruded point of the apex nasi (tip of the nose)
15	Ab-L	Alar base-L	the junction between the right nostril and upper lip
16	Ala-L	Alar curvature-L	Most lateral point on alar contour
17	Sbtr-L1/3*	Subtragion-L (1/3)	One third the distance from Sbtr-L to Ala-L
18	Sbtr-L2/3*	Subtragion-L (2/3)	One third the distance from Sbtr-L to Ala-L
19	Sbtr-L	Subtragion-L	The most anterior inferior point of the anterior inferior attachment of the ear helix, just above the ear lob
20	Go-R	Gonion-R	The most lateral point of the cheeks close to mandibular angle.
21	GoR-1/3*	Gonion-R 1/3	One third the distance from Go-R to Ch-R
22	GoR-2/3*	Gonion-R 2/3	The third the distance from Go-R to Ch-R
23	Ch-R	Cheilion-L	Point located at lateral labial commissure
24	FL-R	Philtrum crest-R	The tip of the right philtral ridge at the upper lip vermilion border
25	Ls	Labiali superius	Midpoint of the upper vermilion line
26	FL-L	Philtrum crest-L	The tip of the right philtral ridge at the upper lip vermilion border
27	Ch-L	Cheilion-L	Point located at lateral labial commissure
28	Go-L2/3*	Gonion-L 1/3	One third the distance from Go-L to Ch-L
29	Go-L1/3*	Gonion-L 2/3	The third the distance from Go-L to Ch-L
30	Go-L	Gonion-L	The most lateral point of the cheeks close to mandibular angle.
31	Li+3*	Labiali inferius	Mid-point on the lower vermilion line 3mm higher than Li
32	Li	Labiali inferius	Mid-point of the lower vermilion line
33	Pog+3*	Pogonion+3	Midline point 3mm higher than pogonion
34	Pog	Pogonion	Most prominent midline point of the chin

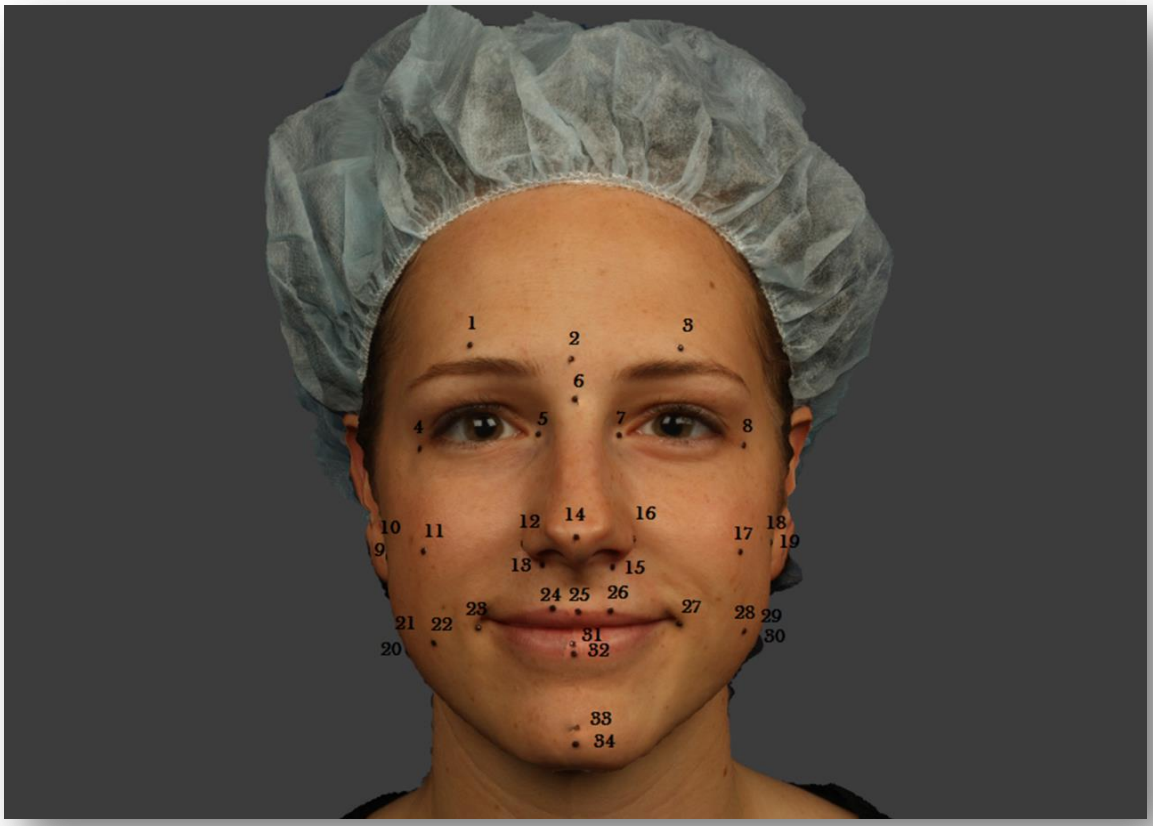

Figure 33: Full set of landmarks indicators placed on participant's face

Figure 34: The six facial expressions. The relax expression (top left) was conformed, as a generic mesh, to the other five facial expressions. The positional change of the markers on the (relax expression) facial image following conformation were tracked and compared with the positions of those on the target images.

2.3.1.3.6 Pre-analysis image processing

Two steps were necessary to pre-process each image before it could be analysed following capture, these were: *image conversion and conformation*. The first step was accomplished using 3DSMAX software. The second step and final analysis were carried out using the in-house developed conformation software.

2.3.1.3.6.1 *Image Conversion*

The conformation software required all the captured images to be converted from Wavefront (.obj) to VRML (.wrl) files. The texture information, dimensional units and the orientation of the image were maintained during the conversion process using 3DSMax software.

2.3.1.3.6.2 Image Conformation

The procedure has been previously described (Section 1.3.2.2.3.b). In summary, the conformation software provides a dual display panel, the generic mesh image (repose facial image) was imported and shown in one panel whilst the captured face (in this case the smile facial expression) was imported and shown in the second viewing panel, (figure 25).

The conformation process involved two steps that were executed in the following sequence; *initial conformation* (semi-manual) and *final conformation* (fully automated).

2.3.1.3.6.2.1 Initial conformation

The images were magnified to allow landmarks to be placed at the centres of the markers. Fifteen landmarks were digitised on the generic image (landmark 4 to 9, 13, 14, 15, 19, 23, 25, 27, 31 and 33), please refer to table (15), and the same corresponding landmarks were placed on the captured facial expression image (smile). The sequence of landmark placement in both images was identical for the process of conformation.

Figure 35: The conformation software showing the main panel with two 3D images loaded; the target image (left side) and the generic mesh (right side).

The initial conformation elastically deformed the 15 landmarks on the generic mesh (relax image) to align on the corresponding 15 landmarks on the smile expression image. The remainder of the repose mesh was automatically partially deformed through minimizing the "bending energy" to produce an approximate fit of the two mesh surfaces.

2.3.1.3.6.2.2 Final conformation

This process fully deformed the generic mesh not only in shape but also in position. At this point the generic mesh resembled the facial expression mesh in both shape and position in 3D space. The conformed image was exported as a VRML (.wrl) file and saved for further analyses. This process was used to conform the (relax) facial mesh to each of the remaining 5 facial expressions

meshes i.e. cheek puff, lip purse, smile, asymmetric mandibular movement and mandibular protrusion. For each subject, the outcomes were five conformed meshes in addition to the five corresponding original facial images; in total 50 conformations were produced.

2.3.1.3.7 Accuracy measurements

For each subject the conformed mesh was compared to original mesh for each facial expression i.e. conformed maximum smile to original maximum smile and so forth, using two methods of analyses. Ideally when the two meshes are loaded in viewing software both the meshes should be identical in shape and position. The first analysis method was based on the absolute Euclidian distances between the points of the two meshes as well as visual distance colour maps. However these measurements rely on the distances between closest-points rather than corresponding points. To overcome this, a second method of analysis, based on corresponding landmarks was undertaken i.e. the adhesive markers.

2.3.1.3.7.1 Surface Euclidian distances

For each subject the conformed mesh and the original mesh for each facial expression in turn were imported into the conformation software. The mean Euclidian distance between the two meshes was measured according to the normal surface distance, (Section 1.3.2.2.3). The mean, standard deviation, minimum, maximum and the percentage of the surface points and their distribution around the mean distance were calculated. In addition, a distance colour map was generated for visual illustration. The data from each measurement was saved in an EXCEL file for further analysis.

To determine the accuracy of the conformation, the Euclidian distances between all the points on the conformed mesh and the original facial expression mesh for all facial expressions were calculated. The mean Euclidian distances was calculated then grouped together with all conformations measurements to calculate the overall mean Euclidian distances between the two meshes. This was accomplished using Microsoft EXCEL.

2.3.1.3.7.2 Corresponding landmarks

The second method of analysis was based on corresponding landmarks. In total 34 markers were placed on the face prior to image capture, 15 were used during the conformation process whilst the remaining 19 were used for the analysis. For each subject the conformed mesh and the original mesh for each facial expression in turn were imported into the conformation software and landmarked. The x, y and z coordinates of each of the 19 landmarks were generated and exported as a plain text (.txt) file. For each expression, two text files were created, one from the conformed mesh and the other from the original mesh. The sequence of landmarking was the same for both, the original and the conformed images, this allowed easy identification of landmarks and their correspondence for analysis. The files were saved for future analysis.

The Euclidean distance between each corresponding landmark was calculated using the 3D Pythagoras equation (2). Descriptive statistical analyses and paired sample t-test were applied to analyse the data.

2.3.1.3.8 Landmarking error

Ten randomly selected images, one from each case, were landmarked twice with two weeks interval by the same operator (AAM). The Euclidean distances between the repeated digitisation of the same landmark were calculated.

2.3.1.4 Results

2.3.1.4.1 Landmarking error study

The mean Euclidean distance and standard deviation for landmarking errors for each of the 34 landmarks is shown in table (16). The overall mean error for all the landmarks was 0.25 mm ± 0.10 mm. The overall mean error for all the landmarks was 0.23 mm ± 0.11 mm. Landmarks 6 and 8 had the lowest error 0.11 mm ± 0.06 mm and 0.11 mm ± 0.10 mm respectively whilst landmark 30 had the largest error 0.57 mm ± 0.64 mm.

2.3.1.4.2 Conformation accuracy

2.3.1.4.2.1 Mean absolute distance between meshes

Table (17) shows the absolute mean distances between the conformed mesh and the original "generic" mesh. The largest distance was 0.06 mm which was observed in subject 3 across all facial expressions.

2.3.1.4.2.2 Corresponding landmarks distances

The 15 landmarks which were used for the initial stage of image conformation were excluded. The data from the remaining 19 landmarks were used to assess the accuracy of the conformation process.

Table (18) shows the Euclidean distances between the 19 corresponding landmarks on the conformed mesh and original mesh for all facial expressions. The absolute mean distances between the corresponding landmarks ranged from 0.81mm to a maximum error of the conformation process of 1.85 mm for landmarks 26 and 20 respectively. The overall mean Euclidean distance error of the conformation process was 1.21 mm ± 0.28 mm.

The effect of each facial expression on the accuracy of the conformation was also investigated. Table (19) shows the mean Euclidean distance between the corresponding landmarks on the generic and conformed facial meshes. The five facial expressions were ranked in an ascending order according to the accuracy of the conformation process starting by the lateral mandible shift, lip purse, forward mandible shift, cheek puff and smile. The lowest mean Euclidean distance between corresponding landmarks due to the potential errors of the conformation process of the facial mesh was associated with the lateral mandible shift expression which was 1.06 mm ± 0.33 mm. The largest mean Euclidean distance between corresponding landmarks due to inaccuracy of the conformation process of facial surface meshes was 1.46 mm ± 0.51 mm which was associated with maximum smile.

2.3.1.5 Discussion

Establishing an accurate conformation process (elastic deformation) of the generic facial mesh to resemble the detailed anatomy of the face is essential for a valid application of dense correspondence analysis to evaluate morphological changes.

Previous studies on image conformation and elastic deformation have evaluated the accuracy of the process using the mean surface distance measurement (231,244). The deficiency in this approach lies in the fact that the distances were between the closest points of the two surface meshes, generic mesh and conformed mesh, not the actual correspondences. It is quite possible for the meshes to slide over each other during the conformation process, measuring the closest distance between two meshes would not detect this source of errors. Assessment of the accuracy of the conformation process based on specific landmarks also carries the risk of over estimating the accuracy of the conformation process since the rest of the mesh vertices are not considered in this type of analysis. Therefore, the measurements of the 90^{th} percentile of the vertices of the two meshes were considered in this study. This is essential for the application of dense surface correspondence analysis to evaluate facial changes due to surgery, pathology or growth.

Table 16: Mean Euclidean distance and standard deviation for landmarking errors for each of the 34 landmarks.

Landmark number	Case number										Mean (mm)	SD (mm)
	1	2	3	4	5	6	7	8	9	10		
1	0.1	0.53	0.09	0.08	0.40	0.21	0.17	0.15	0.13	0.09	0.21	0.16
2	0.28	0.21	0.03	0.19	0.15	0.21	0.09	0.13	0.33	0.06	0.18	0.09
3	0.18	0.19	0.09	0.16	0.21	0.06	0.19	0.10	0.2	0.16	0.15	0.06
4	0.03	0.36	0.07	0.12	0.20	0.23	0.16	0.06	0.12	0.05	0.15	0.1
5	0.13	0.10	0.12	0.10	0.09	0.07	0.13	0.08	0.39	0.07	0.13	0.1
6	0.09	0.08	0.10	0.21	0.04	0.10	0.07	0.20	0.06	0.11	0.11	0.06
7	0.12	0.12	0.27	0.14	0.40	0.15	0.29	0.02	0.24	0.04	0.2	0.11
8	0.05	0.34	0.19	0.04	0.08	0.14	0.03	0.12	0.03	0.08	0.11	0.1
9	0.08	0.12	0.08	0.19	0.13	0.16	0.12	0.14	0.48	0.28	0.17	0.12
10	0.13	0.10	0.09	0.15	0.09	0.41	0.21	0.12	0.17	0.15	0.16	0.1
11	0.16	0.33	0.14	0.49	0.17	0.19	0.11	0.11	0.23	0.27	0.21	0.12
12	0.52	0.34	0.03	0.12	0.16	0.44	0.06	0.13	0.10	0.17	0.21	0.18
13	0.08	0.14	0.20	0.18	0.20	0.33	0.16	0.15	0.15	0.63	0.18	0.07
14	0.23	0.29	0.10	0.13	0.08	0.33	0.11	0.12	0.16	0.26	0.17	0.09
15	0.23	0.37	0.34	0.16	0.12	0.16	0.08	0.23	0.20	0.30	0.21	0.09
16	0.15	0.48	0.09	0.10	0.18	0.09	0.29	0.18	0.14	0.20	0.19	0.13
17	0.04	0.22	0.09	0.34	0.17	0.36	0.04	0.12	0.10	0.10	0.16	0.12

Continue

Landmark number	Case number										Mean (mm)	SD (mm)
	1	2	3	4	5	6	7	8	9	10		
18	0.17	0.42	0.12	0.28	0.90	0.60	0.14	0.05	0.24	0.11	0.32	0.28
19	0.21	0.34	0.28	0.20	0.18	0.17	0.25	0.35	0.94	0.52	0.32	0.24
20	0.26	0.16	0.10	0.22	0.11	0.15	0.30	0.12	0.08	0.22	0.17	0.08
21	0.1	0.28	0.12	0.20	0.23	0.19	0.07	0.07	0.08	0.23	0.15	0.08
22	0.18	0.46	0.07	0.25	0.14	0.28	0.18	0.15	0.29	0.16	0.22	0.11
23	0.14	0.15	0.28	0.08	0.03	0.13	0.24	0.14	0.23	0.07	0.16	0.08
24	0.23	0.12	0.12	0.12	0.16	0.43	0.24	0.18	0.41	0.14	0.22	0.12
25	0.16	0.19	0.30	0.74	0.85	0.32	0.20	0.24	0.05	0.01	0.34	0.27
26	0.04	0.32	0.33	0.17	0.05	0.24	0.10	0.09	0.17	0.14	0.17	0.11
27	0.17	0.29	0.07	0.13	0.20	0.38	0.14	0.14	0.18	0.18	0.19	0.09
28	0.35	0.26	0.04	0.66	0.21	0.30	0.23	0.05	0.22	0.15	0.26	0.18
29	0.29	0.40	0.19	0.29	0.22	0.34	0.25	0.19	0.22	0.29	0.27	0.07
30	0.28	2.06	0.34	1.20	0.16	0.18	0.32	0.25	0.37	0.15	0.57	0.64
31	0.23	0.38	0.42	0.47	0.24	0.75	0.07	0.16	0.50	0.33	0.36	0.21
32	0.19	0.85	0.12	1.28	0.41	0.16	0.28	0.32	0.34	0.40	0.44	0.38
33	0.18	0.31	0.47	0.50	0.41	1.21	0.21	0.29	0.41	0.32	0.44	0.31
34	0.24	0.37	0.39	0.43	0.53	0.30	0.22	0.24	0.25	0.39	0.33	0.11
Overall mean	**0.19**	**0.37**	**0.19**	**0.34**	**0.24**	**0.32**	**0.17**	**0.16**	**0.25**	**0.23**	0.23	0.11

Table 17: Mean surface distance in millimetres

	Lateral mandible shift			Cheek puff			Forward mandible shift			Smile			Lip purse		
Cases	Abs Mean	Mean	SD	Abs Mean	Mean	SD	Abs Mean	Mean	SD	Abs Mean	Mean	SD	Abs Mean	Mean	SD
1	0.04	0.01	0.84	0.04	0.01	0.07	0.04	0.01	0.06	0.04	0.01	0.07	0.04	0.01	0.09
2	0.00	0.00	0.03	0.00	0.00	0.07	0.00	0.00	0.02	0.00	0.00	0.02	0.00	0.00	0.03
3	0.05	0.01	0.10	0.06	0.01	0.10	0.06	0.01	0.10	0.06	0.01	0.10	0.06	0.01	0.11
4	0.00	0.00	0.03	0.00	0.00	0.01	0.00	0.01	0.01	0.00	0.00	0.01	0.00	0.00	0.02
5	0.02	0.00	0.03	0.02	0.00	0.01	0.02	0.03	0.03	0.02	0.00	0.06	0.02	0.00	0.04
6	0.02	0.00	0.02	0.02	0.00	0.01	0.02	0.00	0.01	0.02	0.00	0.01	0.02	0.00	0.01
7	0.02	0.00	0.04	0.02	0.00	0.03	0.02	0.04	0.03	0.02	0.00	0.03	0.02	0.00	0.03
8	0.00	0.00	0.01	0.00	0.00	0.02	0.00	0.01	0.01	0.00	0.00	0.01	0.00	0.00	0.03
9	0.02	0.00	0.17	0.02	0.01	0.12	0.00	0.02	0.05	0.00	0.00	0.02	0.00	0.00	0.05
10	0.00	0.00	0.02	0.00	0.01	0.01	0.00	0.00	0.01	0.00	0.00	0.01	0.00	0.00	0.01

Table 18: The mean Euclidean distances (mm) of the 19 corresponding landmarks between the conformed and original mesh for all facial expressions.

Landmark Number	CASE 1	CASE 2	CASE 3	CASE 4	CASE 5	CASE 6	CASE 7	CASE 8	CASE 9	CASE 10	Mean (mm)	SD (mm)
	Mean	Mean	Mean	Mean	Mean	Mean	Mean	Mean	Mean	Mean		
1	1.48	1.81	0.89	1.33	1.47	0.88	0.74	1.20	1.29	1.58	1.38	0.68
2	0.60	1.16	0.41	1.07	0.80	0.31	0.44	0.53	1.31	1.05	0.83	0.65
3	0.94	1.80	0.86	1.08	1.64	1.22	0.84	1.13	1.26	1.17	1.29	0.74
10	1.03	1.40	1.32	1.46	0.69	1.86	1.82	0.88	1.03	0.52	1.30	0.98
11	0.89	1.71	1.35	1.56	1.22	1.52	1.54	0.73	1.03	0.56	1.31	0.83
12	1.96	1.75	1.04	1.08	1.32	0.49	1.41	1.12	0.91	0.59	1.21	0.88
16	1.39	1.33	1.16	1.09	1.28	1.08	0.28	1.09	0.81	1.18	1.14	0.75
17	1.15	1.74	0.90	1.43	1.66	1.55	0.89	0.65	0.69	1.16	1.28	0.86
18	1.12	1.43	1.04	1.01	1.48	1.09	1.79	0.60	0.85	1.01	1.24	0.74
20	1.17	1.72	1.53	1.41	1.27	2.06	3.12	2.26	1.88	0.93	1.85	1.36
21	1.35	1.37	1.33	1.44	0.52	1.92	2.48	0.83	1.47	0.98	1.49	0.86
22	1.00	1.48	1.33	0.91	0.91	0.49	0.37	0.31	0.27	0.52	0.83	0.72
24	1.11	1.08	0.86	0.85	0.90	0.88	0.77	0.73	0.54	0.41	0.82	0.58
26	0.94	1.21	0.75	0.62	0.92	0.62	0.73	0.65	0.36	0.56	0.81	0.49
28	0.71	1.06	0.12	0.91	1.02	1.35	2.36	1.44	0.21	1.32	1.10	1.10
29	1.43	1.34	0.78	1.31	1.52	1.17	2.43	1.65	1.14	1.38	1.53	1.02
30	1.34	1.43	1.13	1.68	1.60	1.00	2.18	1.93	0.98	1.15	1.53	0.76
32	0.56	0.80	0.92	0.92	0.69	0.89	1.33	1.74	0.92	0.86	1.01	0.7
34	0.93	1.32	0.41	0.35	0.40	0.30	2.10	0.89	2.68	0.36	1.04	1.75
Overall error	1.12	1.42	0.96	1.14	1.13	1.09	1.46	1.08	1.04	0.91	**1.21**	**0.28**

Table 19: Mean Euclidean distance between the corresponding landmarks for each facial expression (mm).

Landmark number	Landmarks		Lateral mandible shift	Cheek puff	Forward mandible shift	Smile	Lip purse	Mean (mm)	SD (mm)
	Abbr.	Name	Mean	Mean	Mean	Mean	Mean		
1	EBR	Eyebrows-R	1.87	1.10	1.25	1.62	1.07	1.38	0.35
2	Gla	Glabella	1.08	0.58	1.01	0.97	0.50	0.83	0.27
3	EBL	Eyebrows-L	1.23	1.23	1.43	1.5	1.08	1.29	0.17
10	SbtrR 1/3	Subtragion-R (1/3)	1.09	1.65	0.82	1.85	1.11	1.30	0.43
11	Sbtr R2/3	Subtragion-R (2/3)	1.08	1.95	0.78	1.63	1.10	1.31	0.47
12	Ala-R	Alar curvature-R	0.96	1.76	0.98	1.02	1.35	1.21	0.35
16	Ala-L	Alar curvature-L	0.99	1.67	0.66	0.93	1.44	1.14	0.41
17	Sbtr L1/3	Subtragion-L (1/3)	0.83	2.03	0.88	1.60	1.04	1.28	0.52
18	Sbtr L2/3	Subtragion-L (2/3)	0.94	1.62	0.80	1.81	1.01	1.24	0.45
20	GoR	Gonion-R	1.40	1.58	2.49	2.51	1.27	1.85	0.60
21	GoR 1/3	Gonion-R 1/3	1.31	1.76	0.97	1.80	1.62	1.49	0.35
22	GoR 2/3	Gonion-R 2/3	0.70	0.84	0.77	0.97	0.87	0.83	0.10
24	PhLR	Philtrum crest-R	0.69	1.03	0.72	1.16	0.87	0.89	0.20
26	PhLL	Philtrum crest-L	0.53	0.90	0.66	1.11	0.83	0.81	0.23
28	GoL 2/3	Gonion-L 1/3	0.78	1.25	1.07	1.30	1.08	1.10	0.20
29	Go L1/3	Gonion-L 2/3	0.99	1.65	1.38	2.11	1.53	1.53	0.41
30	GoL	Gonion-L	1.51	1.41	1.35	2.15	1.23	1.53	0.36
32	Li	Labial inferius	1.39	0.68	1.16	0.61	1.19	1.01	0.34
34	Pog	Pogonion	0.74	0.76	1.89	0.99	0.82	1.04	0.48
Overall mean			1.06	1.34	1.11	1.46	1.11	1.21	
SD			0.33	0.45	0.46	0.51	0.27	0.28	

It would have been ideal to track every vertex on the conformed mesh to evaluate the accuracy of the conformation process. However, this was not possible to achieve. Instead, the positional changes of a set of pre-defined landmarks that were digitized on the pre-conformed surface mesh were tracked to detect any shift from their original anatomical position as a result of the conformation process. Although this was not a comprehensive surface analysis, its robustness was maximised by carefully selecting the set of landmarks to represent various anatomical regions of the face. We have also considered two methods of measuring the disparities between the two surface meshes, the absolute distances and the Euclidean ones. The first method takes in consideration the discrepancies between the two meshes in both directions and produces positive and negative values. Despite the fact that these measurements are descriptive to the magnitude and the direction of the conformation errors, the mean value of these measurements would be small as the positive and the negative measurements would cancel each other. On the other hand the Euclidean distances which measure the shortest distances between corresponding points of the two surface meshes, do not consider the directionality of the mismatch between the two surface meshes, therefore, the average arithmetic value of this distances is more meaningful. The combination of the two methods of measurements considered in this study provides the most comprehensive analysis for the assessment of the accuracy of the conformation process which is novel.

Stereophotogrammetry was the chosen facial capture method, in this study, to avoid exposing the volunteers to harmful radiation. At the same time, the method produced a three dimensional surface image of the face that contained the texture information which facilitated landmark identification.

In order to simulate the variation associated with facial expression, five facial expressions were captured for each participant in addition to the baseline relaxed posture. The participants were asked to slide the bottom jaw forward to resemble prognathic mandible, slide the mandible to the left to resemble mandibular asymmetry, cheek puff, lip purse, and smile postures to test the

accuracy of the conformation on variable facial features and with various expressions.

This approach also allowed a comprehensive analysis of landmarking error which impacts on the reliability of the conformation process. To reduce the effect of landmarking errors rounded 2mm landmarks markers were placed on the positions of the 34 anatomical landmarks on each participant face. The presence of these markers significantly reduced the landmarking error and allowed the conformation process to be analysed comprehensively by adding a reliable landmarks on the peripheries of the face (245). The rounded shape of the landmark indicators facilitated the accurate in landmarks digitization, (0.23mm±0.11mm).

Image registration was not necessary in this project. The initial step of the conformation process involved the translation of the corresponding landmarks to match their positions of the target image followed by the elastic deformation to minimize bending energy (thin plate spline). This process included both shape and positional change. The six facial postures were captured at the same session. This provided a relatively close starting point for the conformation process.

Despite the fact that only 10 volunteers participated in this study, each of the facial postures was considered an individual case, therefore; the total number of the images involved in the study was 50. A total of 15 landmarks were used to execute the conformation procedure. To eliminate bias, these landmarks were excluded from the analysis of the accuracy of the conformation procedure.

The results of this study confirmed that landmarks around the lips and nose were associated with lower level of conformation error of facial surface meshes compared to those around the borders of the image such as cheeks, gonial angle regions. This might be due to the lack of distinguished surface topography upon which the elastic deformation relied. However, these areas are of our least concern as the regions around the lips, nose, and chin are the focus of facial

analysis following orthognathic surgery and they showed a higher level of accuracy.

Despite the minimal conformation error detected in both methods of analysis, the results confirmed our assumption that there is a higher level of error in mesh conformation that could not be detected using traditional closest surface distance measurement which produced elusive high conformation accuracy. Two main factors might attribute in the errors in the conformation process; first and most important is the accuracy and reproducibility of the operator's landmarks digitization used in the initial conformation stage, and second is the deficiency of the associated algorithm of conformation which can compensate for these errors especially in the peripheral areas of the facial mesh (244).

2.3.1.6 Conclusions

The conformation procedure has an acceptable level of accuracy and could be applied for the 3D dense correspondence analysis of facial morphology. This has broad clinical applications including facial analysis, evaluation of the impact of orthognathic surgery in changing facial morphology, and monitoring of facial growth. The conformation accuracy is higher toward the centre of the face than the peripheral regions.

2.4 Section D: Analysis of skeletal and soft tissue changes following orthognathic surgery.

This final section is aimed at relating the hard tissue changes of the maxilla and mandible with the overlying soft tissue change in three-dimensions. The previous described methods and validations have been used to determine the skeletal change and soft tissue changes.

To perform the analysis, three main steps were followed; these include; pre-analysis 3D image preparation, Analysis of skeletal surgical displacement, Analysis of soft tissue changes in response to surgery.

- The pre-analysis 3D image preparation includes; *DICOM image superimposition; soft and hard tissue models segmentation and Soft tissue image processing*.

- Analysis of skeletal surgical displacement include; *DICOM image orientation and creation of reference planes; DICOM slice landmarking and data analysis*.

- Analysis of soft tissue changes following surgery includes; *construction of generic mesh; conformation of the generic mesh to the full set of the pre- and post- surgical soft tissue models; soft tissue model averaging and generation of the dense correspondence analysis*.

2.4.1 Pre- analysis 3D image preparation

2.4.1.1 Volumetric image superimposition using voxel based registration

Previously the add-on module for Maxilim was used but an alternative software package, OnDemand3D (Cybermed, Seoul, South Korea) was used for this purpose. The accuracy of the voxel based registration of this software has been previously validated by Lee *et al.*, 2012 (67). The process was however the

same. For each patient both the pre- and post-operative images were loaded into the software using the "fusion" module. The user interface of this module showed three orthogonal slices of each image; the primary image "pre-operative", the secondary image "post-operative" in addition to a combined view, (figure 36). The secondary image was the movable one or source whereas the primary image was the target.

Four steps were involved in the registration procedure. Firstly using manual registration, the post-operative image was moved manually in three dimensions by translating and rotating the images to align it as close as possible to the target pre-operative image. Secondly the region of interest on which the automated voxel based registration was to be performed was selected. The region of interest was selected as a 3D box occupying the anterior cranial base and extended to involve the forehead. Thirdly the automated registration was completed. The combined view orthogonal slices window allowed visually checking of the alignment between the two images. Fourthly the software provided a re-slicing function by which the registered DICOM image could be saved in the new position for further analysis. This procedure was applied to the 100 patient's data sets.

2.4.1.2 Hard and soft tissue segmentation

Following voxel based registration and in order to perform the soft tissue analysis, the 3D soft and hard tissue models of the superimposed pre- and post-operative images were segmented or extracted from the DICOM images. This was achieved using Maxilim software as previously described and involved segmenting the images at HU=276 and -967 for the hard and soft tissue models respectively, (figure 37).

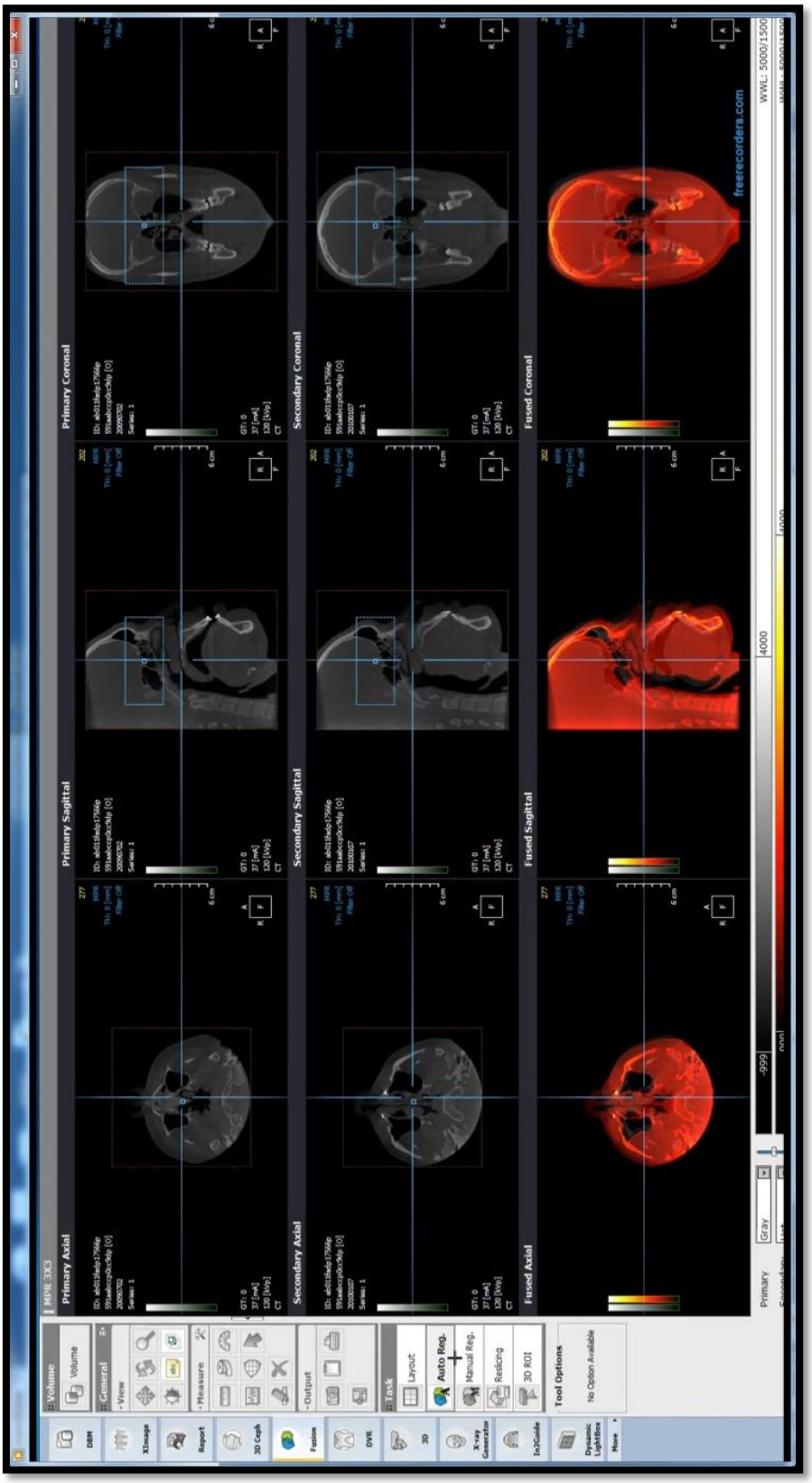

Figure 36: Voxel based registration: showing the pre-operative(top row), post-operative (middle row) and combined view (bottom row). The volume of interest was highlighted with a blue dotted box.

2.4.1.3 Soft tissue model processing

Since the soft tissue models were segmented from CBCT scans, all the connected tissue surface that shared the same HU value were segmented as one model. For the soft tissue model, the facial surface was successfully segmented. However the oro-nasal and pharyngeal soft tissue surfaces were also segmented as one continuous model attached to the facial soft tissue. The presence of the internal nasal soft tissue affected the accuracy of the generic mesh conformation and had to be removed and holes in the facial mesh were successfully filled using VRMesh. The process was accomplished by isolation of the undesirable tissue surface mesh from the main facial surface mesh and deleting the unwanted part using the function "delete floating models". The holes in the mesh such as the mouth opining and nostrils were mended using the function "Mend gaps" in VRMesh software.

For future soft tissue analysis in the in-house developed software, the STL models were converted to Virtual Reality Modelling Language (VRML) (.WRL) file format using VRMesh software. The image coordinates and units were preserved during the conversion process.

2.4.2 Measurement of hard tissue displacement following surgery

2.4.2.1.1 Image orientation and creation of reference planes

Maxilim software was used to segment the pre-operative hard tissue and a horizontal (axial) reference plane was created by identifying the left and right orbitale and left porion landmarks.

To establish the median (sagittal) reference planes, hard tissue nasion and sella were identified. The median plane was oriented perpendicular to the horizontal plane and passed through these nasion and sella. The vertical (coronal) was automatically generated perpendicular to both planes passing through the sella point, (figure 38).

Table 20: Landmarks definitions used for the measurements of skeletal displacement

	Landmark's name	Code	Definition
1	Incisive foramen	IF	The most posterior point of the incisive canal opining on the first axial slice showing the full form of the canal when scrolling coudo-cranially through DICOM slices.
2	Greater palatine foramen/Right	GPR	The most posterior point of the right greater palatine foramen on the first axial slice showing the full form of the foramen when scrolling coudo-cranially through DICOM slices.
3	Greater palatine foramen/Left	GPL	The most posterior point of the right greater palatine foramen on the first axial slice showing the full form of the foramen when scrolling coudo-cranially through DICOM slices.
4	Lingual foramen/Right	LR	The lowest point of the right lingual foramen on the first coronal slice that shows the full form of the foramen when scrolling antero-posteriorly through DICOM slices.
5	Lingual foramen/Left	LL	The lowest point of the left lingual foramen on the first coronal slice that shows the full form of the foramen when scrolling antero-posteriorly through DICOM slices.
6	Mental foramen/Right	MR	The outermost point of the right mental foramen on the first axial slice that shows the full form of the foramen when scrolling cranio-coudaly through DICOM slices.
7	Mental foramen/Left	ML	The outermost point of the left mental foramen on the first axial slice that shows the full form of the foramen when scrolling cranio-coudaly through DICOM slices.
8	Lingual tubercle	Ling	The tip of the lingual tubercle on the first coronal slice that showed the most posterior point on the lingual tubercle when scrolling postero-anteriorly.
9	Pogonion*	Pog	The most anterior point of the chin on the first slice that showed the first bony chin when scrolling antero-posteriorly.
10	Menton*	Me	The lowest point of the chin on any coronal slice
11	Genioplasty Plate*	Pt	The most anterior point of the Genioplasty plate on the coronal slice when scrolling antero-posteriorly.

*** Landmarks used with genioplasty cases only**

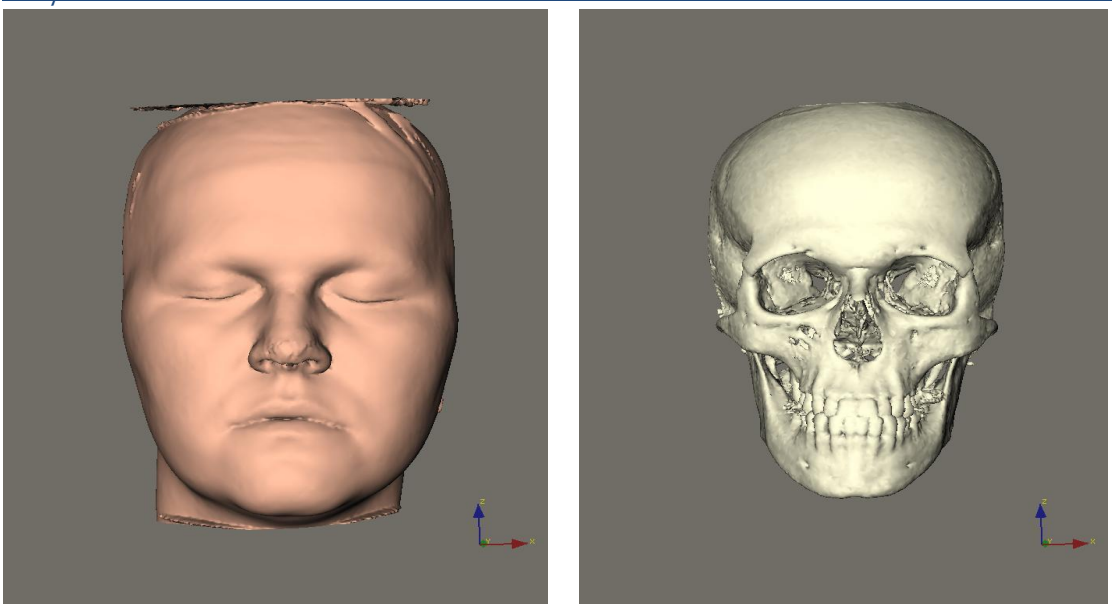

Figure 37: Segmented 3D models from the DICOM image using Maxilim software skeletal (right) and soft tissue (left).

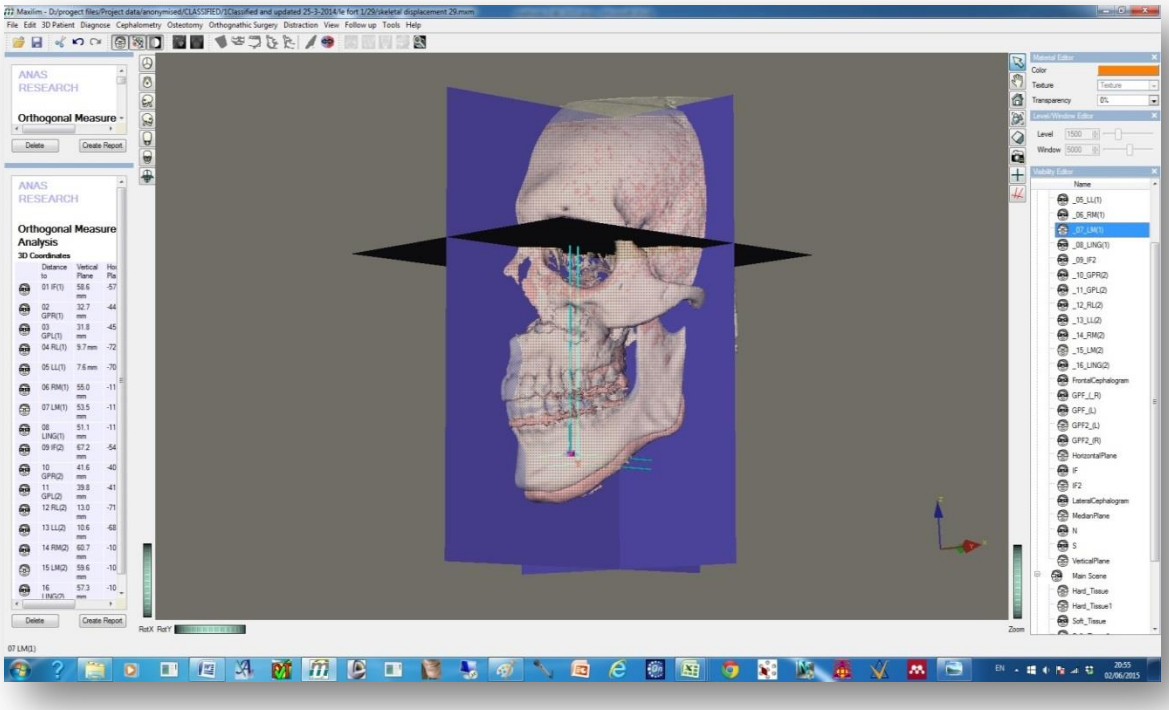

Figure 38: Reference planes: Showing the superimposed post-operative and the pre-operative models. The reference planes were created and one couple of corresponding landmarks were placed on the left mental foramen and were highlighted to show their orthogonal distances measurements to the reference planes. the full set of measurements was displayed on the left hand side of the screen

2.4.2.2 Landmarking pre- and post-operative images

The skeletal changes achieved by orthognathic surgery were measured using the newly developed method of directly landmarking the DICOM image slices. Detailed descriptions of the measuring technique and validation process were provided in section (2.2.2) the results of the validation study has been published in peer reviewed scientific journal (246). For the current study, the same technique was used. In summary, the technique measured the orthogonal distance from selected anatomical landmarks placed on the DICOM slices, following voxel based registration, of both the pre- and post-operative images to common reference planes. The definition of each anatomical landmark was given in table (20). The difference between the two measurements was a measure of the surgical change of the maxilla or mandible.

Using a custom cephalometric analysis in Maxilim software, eleven landmarks were identified on each of the pre- and post-operative CBCT images slice, (table (20). The custom cephalometric analysis was based on the orthogonal distances of 11 landmarks from each of the three reference planes. The measurements were then exported into a cephalometric report and saved as an EXCEL file for further analysis, (figure 38).

2.4.2.3 Data processing and analysis

Data analysis was accomplished using EXCEL software. Two sets of orthogonal landmark distances relative to the reference planes were listed for each case (one pre-operative and one post-operative). In the A-P dimension, since all the landmarks were located anterior to the coronal plane, a positive measurement meant anterior displacement of the landmark (away from the plane) while negative means a posterior displacement. In the vertical dimension, since all the landmarks are below the horizontal plane, negative sign measurement indicated a downward displacement of the landmark (away from the plane) and positive measurement meant upward displacement. In the x (medio-lateral) dimension, since the landmark may be located on either side of the plane, calculations are different. When both the pre- and post-operative landmarks had the same sign,

the calculations follow the same patterns of the above calculations with the same sign. In a few cases the pre- and post-operative landmarks carried different signs. In this case, the displacement equals the sum of the two measurements and in the direction of the post-operative measurement.

In this study, the main aim was to investigate the effect of skeletal movement on the soft tissue; therefore the movement of the maxilla and mandible were calculated considering the landmarks which were close to the soft tissue in the direction of movements. For maxilla, the incisive foramen (IF) landmark was used for A-P and lateral movements while in the vertical movement, the average of the right and left greater palatine foramen (GPR and GPL) were considered in addition to the measurements at the IF landmark. To assess mandibular movement, the mean displacement of the left and right mental foramen (LM and RM) and genial tubercle (Ling) were used. For cases with genioplasty, additional measurements were made in the region of the chin. Menton (Me), Pogonion (Pog) and Plate (Pt) were considered for the vertical and AP displacement, please refer to table(20) for landmark definitions. Unfortunately, no reliable landmark could be found to assess the lateral chin displacement.

2.4.2.4 Hard tissue landmarking error study

A landmarking error study was carried out on 30% of the total study sample. The error study sample was selected using a systematic sampling technique where the first one third of each group (Le Fort I, bimaxillary and BSSO) was selected. A total of 30 cases were included in the study.

The full set of landmarks used in the main study was re-digitized by the same researcher following a two week interval and the x, y and z coordinates were recorded. The orthogonal distance in each dimension (the distance from each landmark perpendicular to each of the three dimensional planes) was calculated and a mean distance at each dimension was computed using EXCEL software. The significance of the positional differences of the repeated landmark digitization were analysed in the three dimensions (x, y and z) using a paired sample *t*-test. Euclidian distances of the repeated measurements were

calculated in Excel using the 3D Pythagoras equation (Equation 2) and the mean error was calculated.

Table 21: Landmarks used for generic mesh conformation.

	Abbr.	Landmarks	Definition
1	Exc-R	Exocanthion-R	Outer commissure of the eye fissure
2	End-R	Endocanthion-R	Inner commissure of the eye fissure
3	Na	Nasion	Mid-point on the nasal bridge.
4	Exc-L	Exocanthion-L	Outer commissure of the eye fissure
5	End-L	Endocanthion-L	Inner commissure of the eye fissure
6	Ab-R	Alar base-R	Junction between the right nostril and upper lip
7	Prn	Pronasale	Most protruded point of the apex nasi (tip of the nose)
8	Ab-L	Alar base-L	Junction between the right nostril and upper lip
9	Ch-R	Cheilion-L	Point located at lateral labial commissure
10	FL-R	Philtrum crest-R	Tip of the right philtral ridge at the upper lip vermilion border
11	Ls	Labial superius	Midpoint of the upper vermilion line
12	FL-L	philtrum crest-L	Tip of the right philtral ridge at the upper lip vermilion border
13	Ch-L	Cheilion-L	Point located at lateral labial commissure
14	Li	Labial inferius	Mid-point of the lower vermilion line
15	UM-R	Upper lip Mid distance-R	Mid-point on the upper lip vermilion border between Ch-R and FL-R
16	UM-L	Upper lip Mid distance-L	Mid-point on the upper lip vermilion border between Ch-L and FL-L
17	LM-R	Upper lip Mid distance-R	Mid-point on the lower lip vermilion border between Ch-R and Li
18	LM-L	Upper lip Mid distance-L	Mid-point on the lower lip vermilion border between Ch-L and Li
19	Lm	Labio-Mental fold	Deepest median point on the curve between the lower lip and chin
20	Pog	Pogonion	Most prominent Median point of the chin

2.4.3 Analysis of soft tissue changes following surgery

A dense correspondence analysis was used for the soft tissue analysis. In addition to the Euclidean distance analysis, the positional changes of facial mesh nodes were analysed in x, y and z dimensions individually. The analysis relied on the pre-and post-operative conformed generic meshes to create the dense correspondence. These meshes contain the same number of vertices and triangles which helped in identifying the corresponding vertices of the compared meshes. Based on this correlation, the translation of each vertex from the pre-operative to the post-operative mesh was measured both as a Euclidian distance and orthogonal (x, y and z) dimensions separately.

The full data sample of 100 patients was grouped according to surgical procedure into six groups. These were; Le Fort I maxillary advancement; Le Fort I maxillary advancement with genioplasty; BSSO mandibular advancement; BSSO mandibular advancement with genioplasty; bimaxillary advancement; bimaxillary advancement with genioplasty. Only three groups were successful in producing a satisfactory sample size (more than 10 samples). These were Le Fort I maxillary advancement (33 samples); BSSO mandibular advancement (12 samples); and bimaxillary advancement groups (12 samples). The soft tissue analysis was limited to these three groups.

For each of the selected groups, soft tissue model averaging was carried out. This procedure produced pre-operative and post-operative average soft tissue models which were used for analysing soft tissue changes following orthognathic surgery within the group.

2.4.3.1 Construction of the generic mesh

The generic mesh used in this project was created by our research group in the University of Glasgow. The facial polygonal mesh composed of approximately 1000 vertices distributed in almost equal distances from each other. Using VRMesh further modifications of the original mesh were carried out; any holes in

the mesh were filled i.e. nostrils, eyes and mouth and removal of any unwanted areas of the mesh i.e. back of the head.

This created a generic mesh with uniform 2 - 3 mm sized triangles free from defects extending from the upper hairline to the submental area vertically and to the tragus of the ears bilaterally. The generic mesh carried no texture information and was saved as a VRML (.wrl) file to be used later for the conformation procedure.

Using VRMesh software the mesh was duplicated and segmented into 9 anatomical regions; forehead, nose, left and right paranasal areas, left and right cheek areas, upper lip, lower lip and chin. The 9 regions were segmented but remained at the same coordinates to preserve the generic mesh vertices index, (figure 39).

2.4.3.2 Generic mesh conformation

The in-house developed software was used to perform the conformation (elastic deformation) as previously described (Section 2.3.1.3.6.2). The same generic mesh was conformed to the pre- and post-operative soft tissue models of the 100 patients included in the sample.

Either the pre- or the post-operative 3D models (one at a time), was loaded into the software in the “scan” panel, (figure 40). The generic mesh was loaded to the software in the “generic mesh” panel. A set of landmarks, (table 21) were identified on both models. The sequence of landmarking was crucial for a successful conformation since it represents the corresponding points “anchor points” between the generic mesh and the facial 3D model mesh.

No superimposition (rigid registration) was required since the elastic deformation process moved the generic mesh into the position of the facial model mesh. The initial step was semi-automated and was guided by the corresponding landmarks on both images combined with elastic deformation of

the entire mesh based on bending energy reduction (thin plate spline). The next step was fully automated performing refinement of the generic mesh surface with elastic deformation based on localised geometrical feature matching.

The conformed mesh was then exported as a (.wrl) file. The x, y and z coordinate of the conformed mesh were also exported. At the end of this process, 200 conformed meshes (pre and post-operative meshes for each of the 100 patient) were saved with their respective coordinate data for further analysis.

The complete generic mesh was used for the purpose of conformation (elastic registration) of the per- and post-operative models and soft tissue analysis. While the segmented mesh was used for the analysis of the final prediction accuracy.

2.4.3.3 Facial Soft tissue model averaging

Following the conformation of the generic mesh onto the soft tissue models of both the pre-operative and the post-operative scans. An average face for each group, pre-operative and post-operative, was created. The face averaging procedure was based on the conformed generic meshes. Since the correspondence was already established using the generic mesh index, partial Procrustes Analysis (PPA) was performed on each of the groups where translation and rotation was performed and the average position for each vertex was calculated based on the generic mesh correspondence. The result of this procedure was an average pre-operative and post-operative facial model. The average face carried the same number and index of vertices as the original generic mesh. The procedure of facial averaging was performed for the analysis of the facial changes following Le Fort I advancement, BSSO advancement and bimaxillary advancement surgeries.

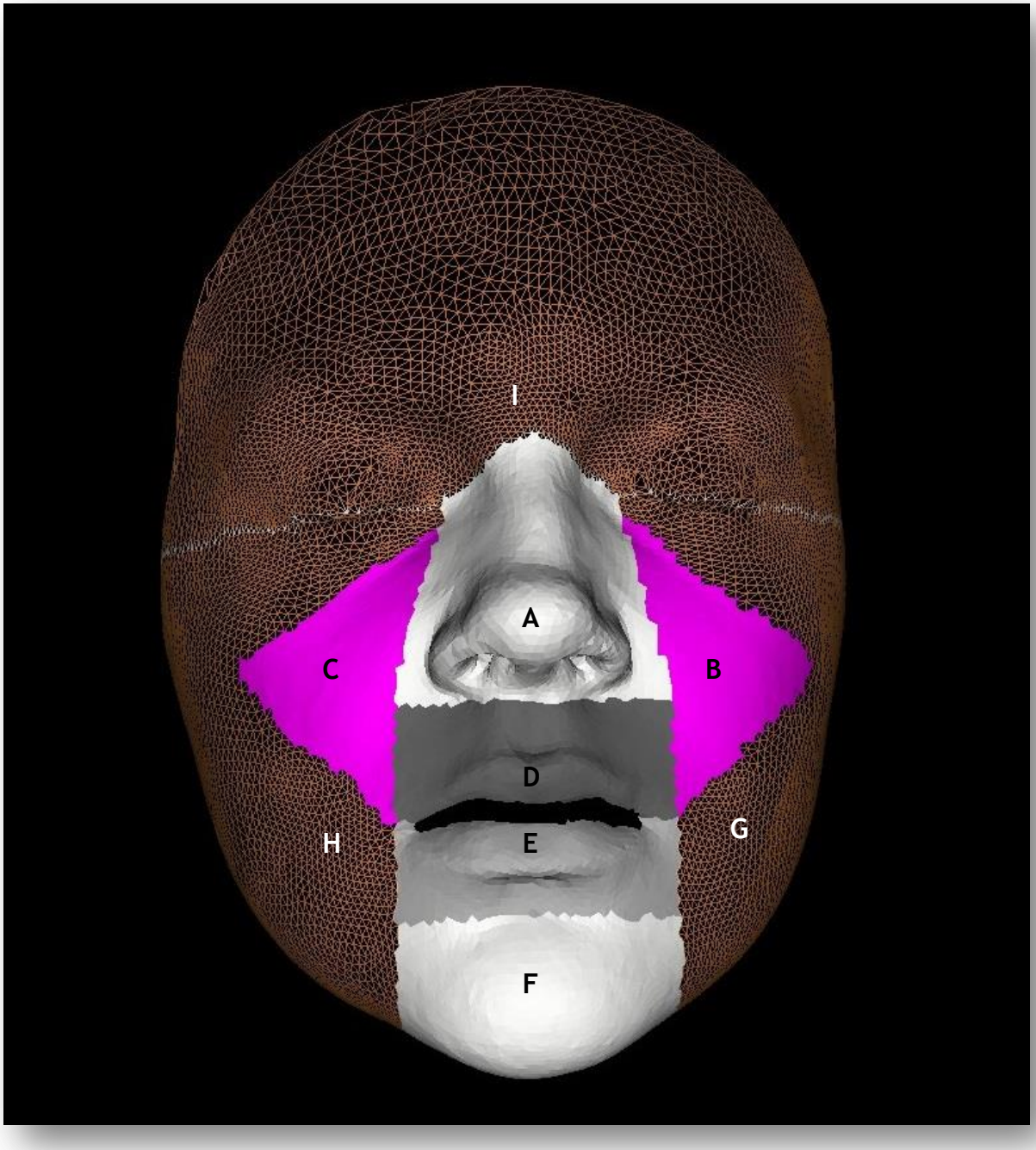

Figure 39: The generic mesh. Nine segments were detached (preserve the same 3D coordinate). The nose (B), the right and left Paranasal areas (B,C), the upper lip (D), the lower lip €, the chin (F), the right and left cheeks (G,H), and the forehead (A), the cheeks and forehead areas were not involve in the analysis.

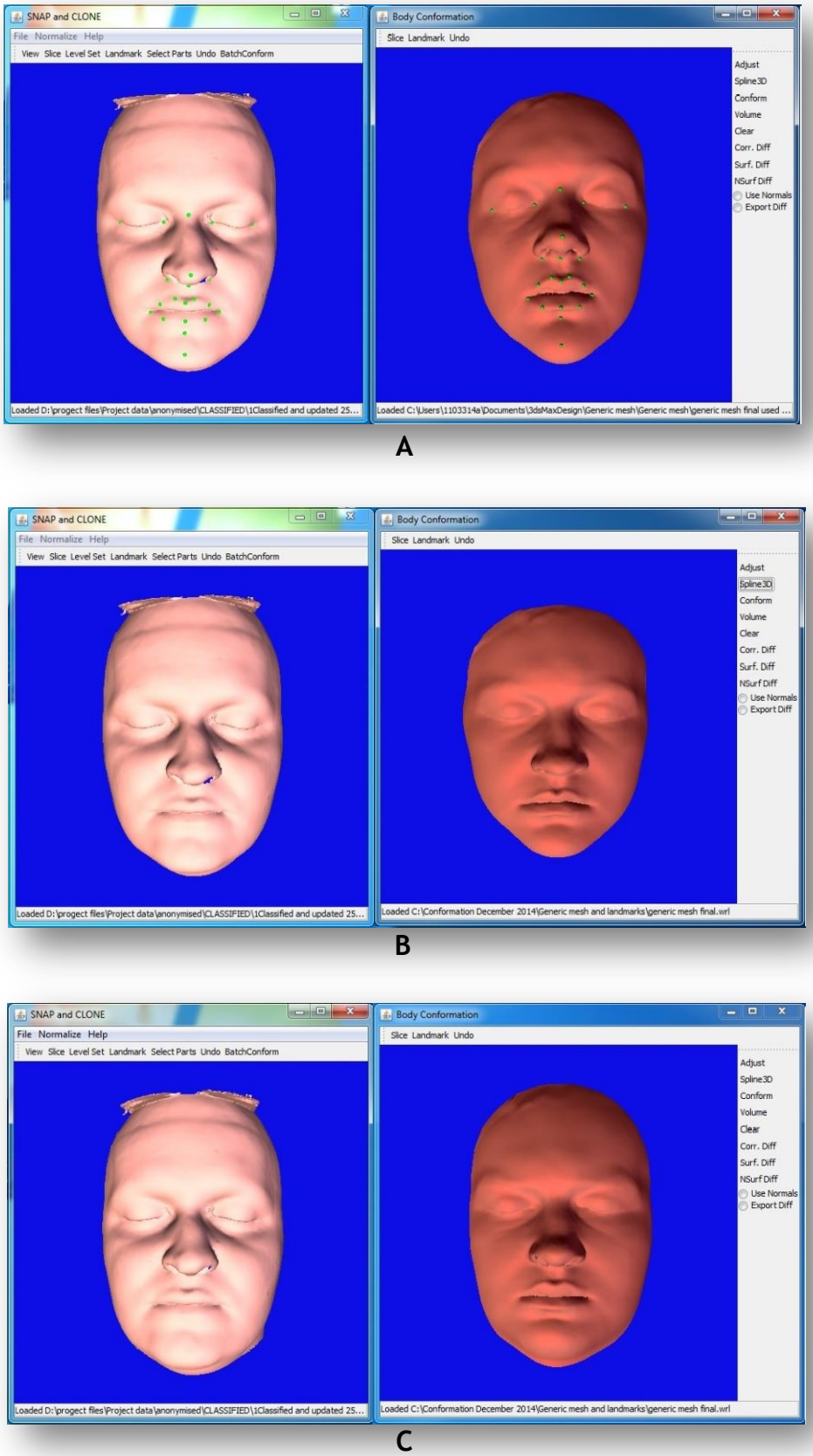

Figure 40: Steps of generic mesh conformation: Landmarks placement (A), initial elastic deformation (B), final elastic deformation(c)

2.4.3.4 Anatomical dense correspondence analysis

Following facial averaging, the average pre-operative and post-operative faces were superimposed on the eyes-nasal bridge region using surface rigid registration. The process was accomplished using VRMesh software. An interim template for registration was created as a copy of the preoperative model cropped to the region of the eyes and nasal bridge regions only without changing the 3D original position. The post-operative model was then registered on the template using PPA followed by ICP surface rigid registration. The template was then discarded. Since the template and the preoperative model have the same 3D position, the post-operative model is now registered to the pre-operative model. The generic mesh index was applied to create the correspondence between the superimposed average faces and the changes at the surgical sites were analyzed using in-house software. The distance between the corresponding vertices was displayed as a colour scale in millimeters ranging from red colour (outward located vertices) to blue (inward located vertices) whereas green colour represented no change. The intensity of the colour, on both sides of the scale, represents the distance from zero location.

The differences in the corresponding vertices position were analyzed in the individual dimension of space (x, y and z) using in-house software. The difference in each dimension was displayed as a colour coded distance map, (figure 41). Since a directional element was involved. A right hand coordinate system was constantly adopted in the analysis. The colour map was specific for each directional change. For the horizontal (medio-lateral) changes the points which were displaced to the left of the face were shown in red whereas points displaced to the right of the face were shown in blue. Non displaced points were shown in green colour. The intensity of the colour represented the amount of the displacement. The upper and lower limits of the colour scale were set at the mean skeletal displacement in each of the analyzed surgical groups. The same was applied to the rest of the directions with specific directional indicators, i.e. in the y-dimension points which moved up were shown in red while those which moved down in blue. In the z-dimension points which moved towards the observer were shown in red while those away from the observer in blue.

2.4.4 Simulation of soft tissue following orthognathic surgery

2.4.4.1 Prediction of soft tissue changes following orthognathic surgery

The correlation between the soft and hard tissue displacements for Le Fort I advancement surgery were analyzed. Only Le Fort I osteotomy cases (with no genioplasty) were considered in this part of the study, with 30 pairs of pre-and post-operative conformed generic meshes. The facial shapes were divided into the regions of forehead, nose, left and right paranasal, upper lip, low lip and chin regions. The displacements of soft tissues at these regions were calculated from the post and pre-operative conformed generic meshes. Principal component analysis (PCA) was used to analyze these displacements. The first 22 principal components (which represent 95% of variations of the displacements) were used to reconstruct the displacements of an individual case. With pairs data – loadings of 22 principal components versus the displacements of hard tissues, the relationship between the loadings of the first 22 principal components of the displacements of soft tissues and the displacements of hard tissues were calculated. With the relationship established, the displacements of hard tissues are now used to predict the 22 loadings of the principal components; further the soft tissue changes are calculated from the predicted loadings.

2.4.4.2 Validation of prediction accuracy.

Leave-one-out cross validation was applied to validate the approach of prediction of soft tissue changes. In this validation, 29 of the 30 cases were used as a training set to establish the relationship between the loadings of the first 22 principal components of the displacements of soft tissues and the displacements of hard tissues, while the remaining one case was used for validation. It is an iterative procedure so the next layer of analysis is to choose a different case for the sample

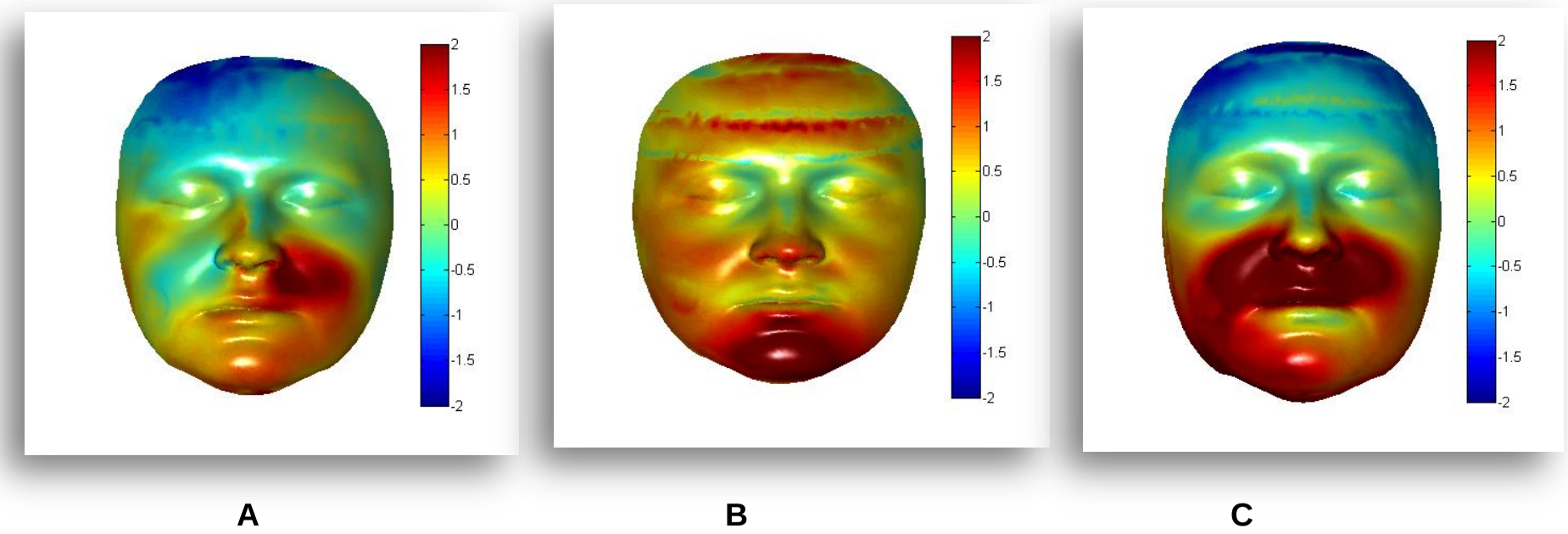

Figure 41: soft tissue changes in the three dimensions: (x) A, (y) B and (z) C.

Note the colour scale is different from the normal colour code used with closest surface distance measurement. In figure A (horizontal changes) the blue side of the scale highlights the regions displaced to the left side while the red side of the scale highlights the region that was displaced to the right side. In figure B (vertical changes) red highlight were given to region displaced upward while blue highlights were given to the regions displaced downward. In figure C (Anteroposterior changes) the red colour highlights the advancing regions while the blue colour highlights the setback regions of the facial soft tissue surface.

as a leave out case and use the rest as training set. The results were 30 trials providing the mean and standard deviation of the surface distance between the predicted displacements and the actual displacements of the validation case at each of the examined region. This procedure was applied to the regions of the upper lip, lower lip, chin, nose, and the right/left paranasal areas.

The mean and standard deviation of the differences between the predicted and the actual displacements of each region were calculated and a boxplot was used to display the results. Colour coded maps showing the mean difference between the predicted and the actual post-operative facial changes in the x, y, and z dimensions were also displayed.

3 Results

Contents

Introduction

A total of 137 pre-surgical and post-surgical CBCT scans were successfully retrieved from the database at the radiography department at the dental hospital. 37 cases were excluded from the sample for various reasons according to our exclusion criteria, (Section 2.1.1). Image quality and ethnic background were the two main reasons for exclusion. The remaining 100 cases were successfully processed according to the research protocol.

3.1 Error study

Landmarking a CBCT derived soft tissue image has always been challenging due to the relatively smooth surface and the lack of facial texture information. Therefore intra observer landmarking error was investigated. Table (22) shows the measured orthogonal distances between the coordinates of the corresponding 20 landmarks. The digitization was repeated two weeks later. These were the same landmarks employed for the conformation of the generic mesh of 30 cases randomly selected from the study sample.

In the x dimension (medio-lateral), the landmarking error ranged from (0.27 mm ± 0.37 mm) to (0.72 mm ± 0.89 mm). The mean error of the repeated digitization of the 20 landmarks was (0.45 mm ± 0.13 mm). In the z dimension (the depth), landmarking error ranged from (0.12 mm ± 0.18mm) to (0.42 mm ± 0.5 mm), the mean error of the repeated digitization of the 20 landmarks was (0.23 mm ± 0.17 mm). In the y dimension (Vertical), the landmarking cases ranged from (-0.37 mm ± 0.25 mm) to (0.87 mm ± 1.15 mm), the mean error of the repeated digitization of the 20 landmarks was (0.13 mm ± 0.19 mm). The only landmark that showed a statistically significant difference in the coordinates between repeated digitization which was limited to the x dimension was the Inner canthus-Right (0.44 mm ± 0.63 mm, p=0.01). Paired sample correlation test confirmed a high correlation between the repeated measurements for all the landmarks.

Table 22: Landmarking error (orthogonal distance) between the repeated digitization of landmarks used for generic mesh conformation.

No:	Mean x	SD	P value	Corr.	Mean z	SD	P value	Corr.	Mean y	SD	P value	Corr.
1	0.27	0.37	0.89	0.997	0.27	0.53	0.16	0.997	0.13	0.2	0.87	1.000
2	0.32	0.76	0.10	0.990	0.17	0.3	0.21	0.999	0.13	0.19	0.06	1.000
3	0.45	0.64	0.21	0.994	0.16	0.23	0.27	0.999	0.55	0.75	0.78	0.999
4	0.44	0.63	0.01	0.992	0.12	0.18	0.93	1.000	0.19	0.28	0.15	1.000
5	0.34	0.55	0.2	0.994	0.4	0.56	0.57	0.997	0.21	0.3	0.20	1.000
6	0.28	0.38	0.41	0.996	0.26	0.38	0.12	0.999	0.19	0.26	0.29	1.000
7	0.42	0.61	0.98	0.994	0.22	0.65	0.34	0.996	0.62	0.85	0.75	0.998
8	0.35	0.58	0.28	0.993	0.33	0.57	0.85	0.997	0.22	0.31	0.10	1.000
9	0.33	0.53	0.74	0.994	0.13	0.2	0.68	1.000	0.16	0.22	0.86	1.000
10	0.51	0.59	0.11	0.991	0.16	0.22	0.16	1.000	0.36	0.46	0.30	0.999
11	0.42	0.55	0.81	0.993	0.12	0.21	0.84	1.000	0.34	0.46	0.40	0.999
12	0.44	0.58	0.74	0.993	0.2	0.28	0.26	0.999	0.29	0.38	0.45	0.999
13	0.50	0.77	0.88	0.986	0.18	0.27	0.72	0.999	0.23	0.36	0.93	0.999
14	0.53	0.62	0.07	0.991	0.12	0.17	0.43	1.000	0.61	0.78	0.53	0.998
15	0.68	0.87	0.95	0.984	0.42	0.5	0.67	0.998	0.47	0.58	0.58	0.998
16	0.51	0.65	0.79	0.991	0.33	0.43	0.78	0.999	0.48	0.6	0.32	0.998
17	0.48	0.61	0.33	0.993	0.39	0.53	0.75	0.997	0.48	0.61	0.65	0.998
18	0.49	0.65	0.71	0.991	0.39	0.49	0.97	0.998	0.48	0.63	0.53	0.998
19	0.58	0.75	0.45	0.987	0.08	0.12	0.54	1.000	0.42	0.59	0.16	0.999
20	0.72	0.89	0.88	0.983	0.12	0.18	0.67	1.000	0.87	1.15	0.54	0.995
Mean			0.45			0.23				0.37		
SD			0.13			0.17				0.25		

The Euclidean distance landmarking errors were calculated. Table (23) shows the mean and standard deviation of the repeated measurements at each of the 20 landmarks. The error ranged from (0.45 mm ± 0.53 mm) to (1.26 mm ± 0.71 mm) with a mean of (0.72 mm ± 0.22 mm).

Table 23: Landmarking error (Euclidean distance) between the repeated digitisations of landmarks used for generic mesh conformation.

	Exc-R	End-R	Na	End-L	Exc-L	Ab-R	Prn	Ab-L	Ch-R	FL-R	Ls	FL-L	Ch-L	Li	UM-R	UM-L	LM-R	LM-L	Lm	Pog
1	1.98	0.81	2.21	1.96	0.81	0.79	1.19	0.46	0.52	0.18	0.77	0.47	0.34	0.86	1.03	1.80	0.44	0.24	0.60	1.12
2	0.22	0.12	1.20	0.62	0.03	1.51	0.08	0.42	0.26	0.75	0.52	0.67	0.55	1.05	1.06	0.60	0.35	1.59	1.74	2.59
3	0.23	0.22	0.36	0.39	0.61	1.48	0.69	0.05	0.21	0.21	1.73	0.65	0.65	1.05	0.82	1.14	0.87	0.39	0.22	2.33
4	0.52	0.19	0.71	0.33	0.71	0.43	1	0.73	0.55	1.24	0.51	1.71	0.12	0.89	0.64	0.74	1.00	0.57	0.71	0.25
5	0.30	1.33	0.58	0.8	0.07	0.21	1.69	0.28	0.69	0.68	1.68	0.91	0.27	1.20	1.31	1.02	1.98	1.97	0.50	1.88
6	0.26	0.23	0.52	0.39	1.23	0.27	0.92	1.05	2.01	0.34	0.56	0.58	0.72	0.58	0.59	1.39	0.51	0.24	0.16	1.44
7	0.34	0.07	1.56	0.64	0.12	0.78	0.48	0.4	0.12	0.94	0.22	0.58	0.38	1.27	0.25	1.68	1.15	1.13	0.10	0.86
8	0.51	0.19	1.21	0.31	0.75	0.22	1.26	0.16	0.34	0.38	0.65	0.71	0.06	1.03	0.42	0.61	0.65	0.57	0.52	1.27
9	0.18	0.12	1.26	0.80	0.30	1.02	1.27	0.97	0.19	0.48	0.13	0.41	0.64	0.65	2.30	0.81	0.42	0.39	0.28	2.89
0	2.42	0.25	1.06	2.57	1.45	0.14	2.17	2.18	0.04	0.09	0.43	0.34	0.04	1.13	0.68	0.90	0.34	2.24	0.40	2.23
11	0.17	4.15	2.40	0.7	0.36	0.94	0.60	0.35	0.64	1.06	0.32	0.35	0.72	0.81	1.22	0.48	0.92	0.54	0.79	2.19
12	0.57	0.15	1.14	0.08	0.11	0.28	4.14	0.05	0.15	0.71	0.82	0.63	0.93	1.61	0.37	1.37	0.28	1.90	0.20	1.80
13	1.05	0.08	1.19	0.15	0.45	0.25	0.63	0.14	1.27	1.19	0.29	0.14	2.03	0.41	2.16	0.82	0.33	0.98	0.16	1.48
14	0.79	0.28	1.11	0.83	0.45	0.43	0.59	0.64	0.56	0.91	0.11	0.60	1.53	0.12	1.15	0.55	0.52	0.97	0.49	0.76
15	0.02	0.37	0.66	0.17	0.08	0.15	1.63	0.13	0.67	0.14	0.71	0.73	0.17	0.76	1.73	0.78	0.41	0.36	0.64	0.85
16	0.58	0.89	1.00	1.14	1.15	0.27	2.00	0.37	0.00	0.91	0.61	0.20	0.27	0.84	1.30	1.14	0.40	0.36	0.55	1.21
17	0.16	0.76	0.4	0.83	0.58	0.36	0.21	0.35	0.13	0.57	0.23	0.58	0.29	0.39	0.49	0.38	0.69	0.08	1.36	0.84
18	0.28	0.28	0.46	0.33	0.22	0.17	0.42	3.18	0.6	0.85	0.93	0.30	0.33	2.14	0.89	0.51	1.12	0.75	1.09	0.65
19	0.12	0.28	0.24	0.03	0.40	0.51	0.27	0.44	0.08	0.48	0.26	0.38	0.41	0.45	0.74	0.86	0.52	1.46	0.99	0.11

Continue

	Exc-R	End-R	Na	End-L	Exc-L	Ab-R	Prn	Ab-L	Ch-R	FL-R	Ls	FL-L	Ch-L	Li	UM-R	UM-L	LM-R	LM-L	Lm	Pog
20	0.27	0.15	0.60	0.23	0.17	0.17	0.18	0.21	0.16	0.94	0.9	0.42	0.12	0.78	0.17	1.50	1.23	0.78	0.76	0.50
21	0.36	0.06	0.63	0.24	2.9	0.55	0.30	0.35	0.37	0.69	0.50	0.55	0.45	0.84	0.65	0.12	0.69	0.47	0.97	0.62
22	0.30	0.16	0.33	1.04	0.39	0.23	0.79	0.32	0.08	1.21	1.30	0.56	0.22	0.18	0.95	0.33	0.64	1.16	1.16	1.38
23	0.38	0.45	0.85	0.09	0.14	0.67	0.65	1.56	0.24	1.21	0.80	0.51	0.19	0.28	0.78	1.19	0.58	0.49	2.05	1.39
24	0.30	0.05	0.23	0.24	0.34	0.05	0.28	0.58	0.14	0.91	0.29	0.19	1.93	1.85	0.36	0.18	0.80	1.42	1.64	1.36
25	0.12	0.34	0.22	0.18	0.50	0.77	0.07	0.34	0.52	1.34	0.95	1.21	0.16	0.75	1.86	0.05	1.57	0.54	1.94	1.95
26	0.22	0.27	0.43	0.16	0.57	0.16	0.75	0.58	0.38	0.48	0.39	0.35	1.75	1.48	1.02	0.93	1.12	1.27	1.65	1.28
27	0.07	0.08	1.54	0.45	0.98	0.27	0.80	0.13	1.00	0.30	0.39	1.63	0.61	0.91	0.71	1.20	1.91	0.94	0.37	0.22
28	0.04	0.06	0.18	0.12	1.58	0.46	1.33	0.12	0.53	0.63	1.02	0.33	0.20	0.57	2.17	0.75	0.71	0.33	0.60	0.80
29	0.26	0.38	0.22	0.15	0.24	0.30	0.70	0.39	0.35	1.09	0.32	1.00	2.20	1.69	0.97	0.75	1.52	0.77	0.95	0.83
30	0.43	0.17	0.11	0.09	0.45	0.08	0.14	0.33	0.13	0.42	0.26	1.27	0.50	0.52	1.01	1.45	2.10	0.86	0.23	0.83
mean	0.45	0.43	0.82	0.54	0.60	0.46	0.91	0.58	0.43	0.71	0.62	0.63	0.63	0.90	0.99	0.87	0.86	0.86	0.79	1.26
SD	0.53	0.76	0.58	0.57	0.60	0.38	0.83	0.67	0.42	0.36	0.42	0.39	0.62	0.49	0.57	0.45	0.52	0.56	0.56	0.71
Overall Mean			0.72																	
Overall SD			0.22																	

3.2 Analysis of skeletal surgical movements

Table (24) shows the mean displacement of the maxilla and mandible in 3D following orthognathic surgery. Three groups were analysed; Le Fort I maxillary advancement, Bilateral sagittal split osteotomy (BSSO) mandibular advancement and Bimaxillary advancement groups. The measurements were based on landmarks at specific anatomical locations and recorded in the x, y and z dimensions (Section 2.4.1.2).

Le Fort I group expressed mainly a forward maxillary displacement of 5.95 mm. This was combined with minimal lateral maxillary displacement of 0.05 mm, anterior and posterior upward maxillary impaction of 0.14 mm and 0.6 mm respectively. The effect of Maxillary advancement extended to involve the mandible where 2.79 mm advancement and 2.13 mm upward displacement were recorded at the mandibular symphysis.

In the mandibular advancement group, forward and downward displacements of the mandible of 3.51 mm and -2.12 mm with minimal lateral displacement of -0.09mm were recorded at the mandibular symphysis.

In the bimaxillary advancement group, both the maxilla and mandible were displaced anteriorly by 5.51mm and 4.58mm respectively. The mandible was displaced 5mm upward at the symphysis while the maxilla was simultaneously impacted anteriorly and posteriorly by 2.74 mm and 2.36 mm respectively. Minimal lateral displacement was detected in both jaws at 0.19 mm and 0.4 mm at the maxilla and mandible respectively.

Table 24: Measurements (mm) of skeletal displacement following orthognathic surgery

Skeletal displacement	Le Fort I		BSSO		Bimax	
	Mean	SD	Mean	SD	Mean	STDV
Anterior maxillary displacement	5.95	1.79	------	------	5.51	2.79
Anterior mandibular displacement	2.79	2.09	3.51	2.64	4.58	3.28
Lateral maxillary displacement	0.05	0.95	------	------	0.19	1.50
Lateral mandibular displacement	0.21	0.97	-0.09	1.24	0.47	3.18
Vertical maxillary displacement anteriorly	0.14	1.72	------	------	2.74	2.59
Vertical maxillary displacement posteriorly	0.6	1.48	------	------	2.36	1.38
Vertical mandibular displacement	2.13	1.86	-2.12	2.71	5.00	3.68

3.3 Analysis of soft tissue changes following surgery

3.3.1 Soft tissue response to Le Fort I maxillary advancement.

3.3.1.1 Euclidean distance measurements

The average face models of the preoperative and post-operative facial meshes were superimposed on the eye region and the corresponding distances between the vertices on both models were presented in a colour coded map. The colour pattern represented the net Euclidian distance between the corresponding vertices, (figure 42). Considering the geometric centre of the facial mesh, the mesh vertices which were displaced in an outward direction due to Le Fort I surgery were highlighted in red whereas these displaced in an inward direction due to Le Fort I surgery were highlighted in blue . The colour spectrum ranging from red (maximum outward) to blue (maximum inward) assigned to each vertex of the mesh represented the variation in positional change of each vertex. The green colour represents the zero change and located at the centre of the spectral colour scale. The colour scale was displayed on the side of the image with the displacement values been assigned to each colour segment. The results are subcategorised into the following anatomical regions:

1. ***The nose***: The nasal bridge area showed no changes due to surgery, whereas the difference gradually increased toward the nasal cartilage and the tip of the nose. The most obvious changes in response to surgery were observed at the alar cartilage which was highlighted in red, the intensity of the red colour increased close to the nasolabial groove. This indicates widening of the nostrils following Le Fort I surgery. The region at the columella and the lower part of the nasal tip was highlighted in blue which indicates an inward movement toward the geometric centre of the face. This combined with the faint orange patches on the nasal tip indicates an minimal upward displacement of the nasal tip increases posteriorly at the columella secondary to Le Fort I osteotomy.
2. ***The upper lip***: The upper lip region is bounded by the nasolabial junction superiorly, extends to the inferior end of the vermillion border and to the oral commissures bilaterally. The majority of the region showed a uniform dark red highlight which indicates a marked anterior displacement in the

upper lip region in response to surgery. A change in colour to light green at the commissures was observed which indicated the limited effect of the maxillary advancement on this region.

3. ***The lower lip***: the region of the lower lip is anatomically bounded by the upper border of the lower lip vermilion border superiorly, extends to the labiomental fold inferiorly and to the oral commissures laterally. The majority of this region displayed a light red highlight due to the slight forward displacement at the lower lip. A colour change into a light blue at the area below the vermilion border extending to the labiomental fold downward and about 50% of the lip width was observed which indicates a backward and upward displacement of the lower lip at this region.
4. ***The chin***: The chin area extends from the labiomental fold to the lower border of the face and extends laterally to the area marked by an imaginary vertical lines descending from the oral commissures. The majority of the area was highlighted in red which appeared darker centrally at the pogonion region. A blue strip at the lower border of the chin was also observed, (figure 2,A). This together with the red colour at 'pogonion' point indicates a minor combined upward and forward change at chin region.
5. ***Paranasal regions***: The red colour display extended bilaterally to the nose and limited laterally to a vertical line from the outer canthi. Superiorly, there was a display of the red colour immediately below the malar eminence which extended down to the level of the oral commissures.
6. **The cheeks**: The light red colour highlight in this area indicates a minor change in response to maxillary surgery. A change to the blue colour at the lower border was noted. This was continuous with the strip of blue colour below the chin area. These findings indicated a minor upward movement of the soft tissue at the lower border of the mandible associated with the shortening of the lower facial height.

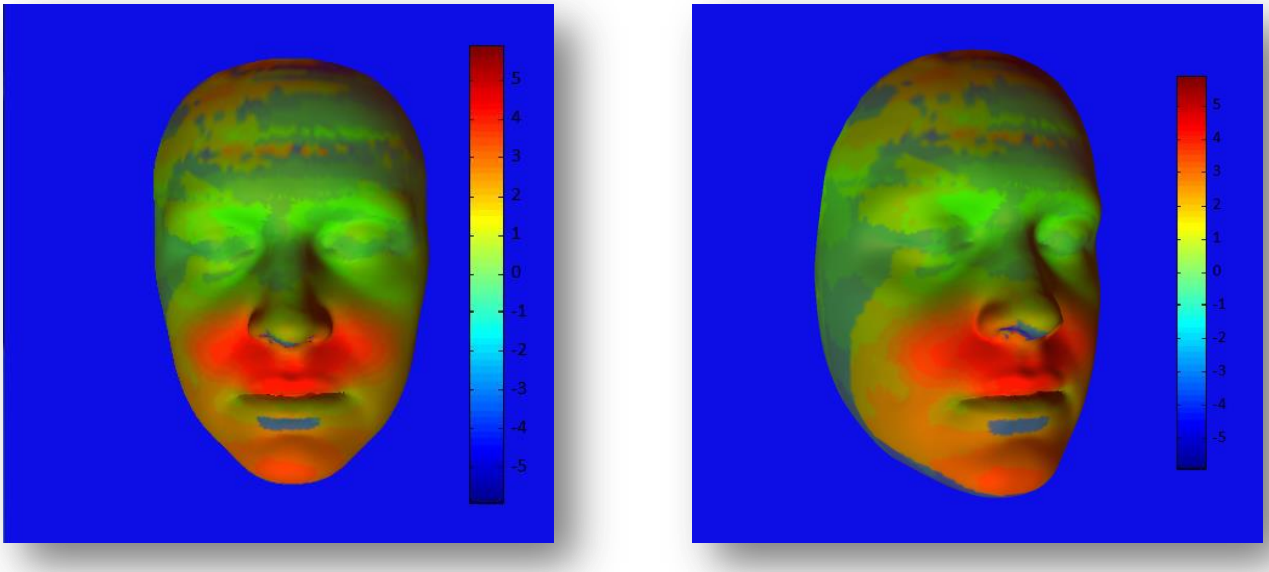

A B

Figure 42: Dense anatomical correspondence (Euclidean) showing soft tissue changes following Le Fort I advancement surgery in Front view (A) and 45° view (B)

In summary, the results shows generalised forward movements at the mid and lower face regions associated with widening of the nostrils and a limited shortening of the lower facial height.

3.3.1.2 Directional soft tissue changes

The soft tissue changes following Le Fort I osteotomy were analysed for each of the x, y and z dimensions separately. Therefore, different colour spectrum was assigned for this part of the analysis. The change at surface vertices due to surgery to the right or the top sides of the screen, or toward the observer, was considered a positive change and highlighted in red. While the change to the left or to the bottom of the screen or away from the observer was considered negative and were highlighted in blue. Green colour was for the regions where no changes were detected. The intensity of the colour indicated the magnitude of the change at the examined area.

The colour scale was displayed on the left side of the face, (figure 43). The higher and lower extremes of the spectral colour scale were limited to 5.5mm which was recorded as the mean A-P skeletal displacement in Le Fort I maxillary advancement group.

3.3.1.2.1 Soft tissue changes in x dimension (medio-Lateral).

Figure (43,A) shows the soft tissue surface changes in x dimension only. Minimal changes were noted around the eye regions and the nasal bridge was highlighted mostly in green which indicates a minimal change in the transverse direction as a result of surgery. The colour changed to yellow toward the nasal tip. A yellow colour patch on the right side at the lower part of the dorsum of the nose and a blue colour patch on the right side indicated a minor narrowing of the nose at this area. The opposite was observed at the alar region, the right ala of the nose displayed a blue colour while the left ala of the nose displayed a red colour which is an indication of widening of the nostrils.

Most of the soft tissue changes in response to Le Fort I osteotomy were in the reign of the upper lip and paranasal area. This was demonstrated by the well-defined distribution of the orange colour on the left side and the blue colour on the right side of these two regions which indicates a tendency toward a lateral expansion along these anatomical regions. The changes were limited to the anatomical boundaries of the paranasal region and upper lip. The changes at the commissures at the corners of the mouth, the lower lip and the chin were minimal.

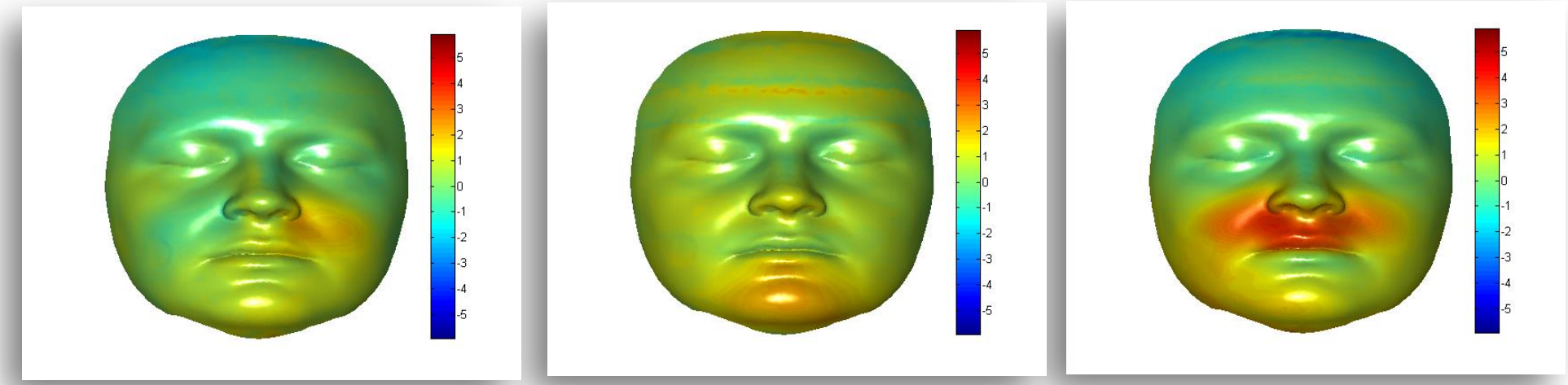

A B C

Figure 43: corresponding (directional) soft tissue changes in: X (Medio-lateral) dimension (A); Y (vertical) dimension and Z(antero-posterior) dimension following Le Fort I advancement surgery.

3.3.1.2.2 Soft tissue changes in y dimension (Vertical change)

Figure (43,B) shows the vertical component of soft tissue changes only in y dimension in response to Le Fort I osteotomy.

Most of the region around the eyes and the nasal bridge displayed green colour which confirms the trivial vertical changes of these areas. The dorsum of the nose showed minimal changes and displayed a green strip which extended toward the tip of the nose. The tip of the nose, the right and left alar curvatures and the columella showed a mild upward movement which was displayed as a yellowish orange colour.

The paranasal area showed a homogenous but mild upward movement coinciding with the adjacent cheek areas which displayed predominantly in a yellowish green colour. The upper lip displayed mostly green colour with yellow/green patches closer to the nostrils. This indicates there was a minimal vertical displacement of the upper lip following Le Fort I maxillary advancement.

Vertically, the lower lip showed two types of response to Le Fort I maxillary advancement separated by the vermillion border. The region above the vermilion border showed minimal vertical changes highlighted in green yellow, the region below the vermillion border showed a clear vertical change displayed in orange manly at the central region. This indicated an upward movement in this region and perhaps a minimal shortening of the lower lip length. The chin area on the other hand showed a predominant orange colour with the highest intensity centrally then decreased posteriorly toward the cheek areas on both sides. This was an indication of an upward movement of the chin area.

3.3.1.2.3 Soft tissue changes in z dimension (Antero-posterior changes)

Figure (43,C) shows the depth component (A-P) of the corresponding soft tissue changes in response to surgery. The region around the eyes and the nasal bridge showed a minimal change which was displayed as generalised green colour. The green colour continued on the dorsum of the nose toward the nasal tip with no

marked change in colour. The columella together with the right and left alae of the nose showed orange colour indicating a marked forward movement of this region.

A well-defined dark red region covered the upper lip and the paranasal Regions which indicates a marked forward displacement. The colour was confined to the anatomical boundaries of these two regions. The effect of surgery on the commeasures at the corner of the mouth was minimal, displayed as a yellowish green colour. Green colour was displayed on the lower lip. The chin showed a relatively homogenous mostly orange colour which indicates a moderate forward displacement secondary to surgery. Similar changes were evident on the lower part of the cheeks where the colour intensity reduced posteriorly.

Summary

In summary, there were distinctive forward soft tissue movements combined with a marked lateral expansion at the upper lip and paranasal regions, these changes were limited by the anatomical boundaries of these regions. The commeasures at the corners of the mouth showed minor changes in all directions. The effect extended to the chin area where a marked vertical and to a lesser extent forward displacement were evident. The lower lip showed minimal changes in all dimensions except a marked vertical movement at the region between the vermilion border and the labiomental fold. The effect on the nose was limited to the widening and advancement of the nostrils and the same was noted at the base of the nose (Subnasale and alar base) region with a minimal forward change at the nasal tip. The changes at the cheeks were to a lesser extent with minimal but consistent upward and forward displacement of the soft tissue in response to Le Fort I advancement osteotomy.

3.3.2 Soft tissue response to BSSO mandibular advancement.

3.3.2.1 Euclidean distance measurements

The pre and post-operative average facial models were superimposed and dense anatomical correspondence was created following the same protocol (Section 3.2.1). The results were displayed as a colour coded map, (figure 44).

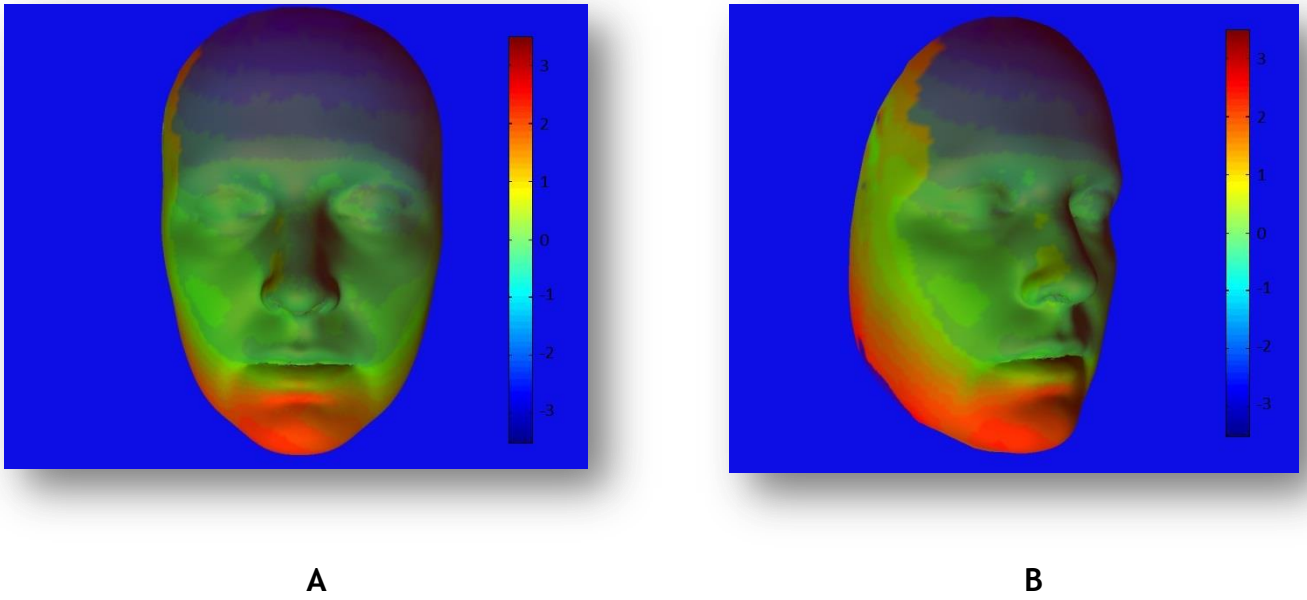

Figure 44: Dense anatomical correspondence (Euclidean) showing soft tissue changes following BSSO advancement surgery in Front view (A) and 45º view (B)

Unlike Le Fort I osteotomy, the soft tissue changes were confined to the lower third of the face corresponding to mandibular advancement. No marked changes were observed on the nose, paranasal areas, and upper lip regions where green colour was predominant. The lower lip showed a mild change at the vermilion border near the midline demonstrating the roll-in effect of the surgery on the lower lip. The marked colour change started to show just below the vermilion border and increase in intensity towards the chin region. The red colour continued backward along the mandibular border towards the gonial angle.

3.3.2.2 Directional changes measurements

In order to investigate the changes in more details, soft tissue analysis was segmented into the x, y, and z dimensions where changes at each of the three dimensions were analysed independently.

3.3.2.2.1 Soft tissue changes in x dimension (medio-Lateral)

Figure (45,A) shows the soft tissue surface changes in x dimension only. The changes around the eye regions and the nose were minimal, displayed mostly in green colour. The changes around the midface region were observed as a mild to moderate narrowing of the upper lip mainly at the sides near the commeasures of the mouth displayed as a yellow/orange colour on the right side and light blue on the left side of the face, whereas the commissures of the mouth expressed a minimal changes which displayed in green colour. Lateral to the Upper lip the same colour pattern extended slightly both sides. The lower lip demonstrated a tendency toward minimal to mild lateral expansion marked by an orange colour on the left side and central regions combined with a bluish green colour on the right side of the lip. The results also highlighted a mild shift of the chin to the left side which coincided with the recorded skeletal lateral shifting of the mandible.

3.3.2.2.2 Soft tissue changes in y dimension (vertical change)

Figure (45,B) shows the vertical component of soft tissue changes only in y dimension in response to BSSO mandibular advancement surgery.

Most of the regions around the eyes, nose and paranasal region displayed green colour which confirms the trivial vertical changes. The upper lip demonstrated a tendency toward downward movement which is displayed in blue colour, this diminished laterally to a minimal change at the commeasures of the mouth. The blue colour on the upper lip combined with the minimal change at the nose highlighted a mild tendency toward lengthening of the upper lip.

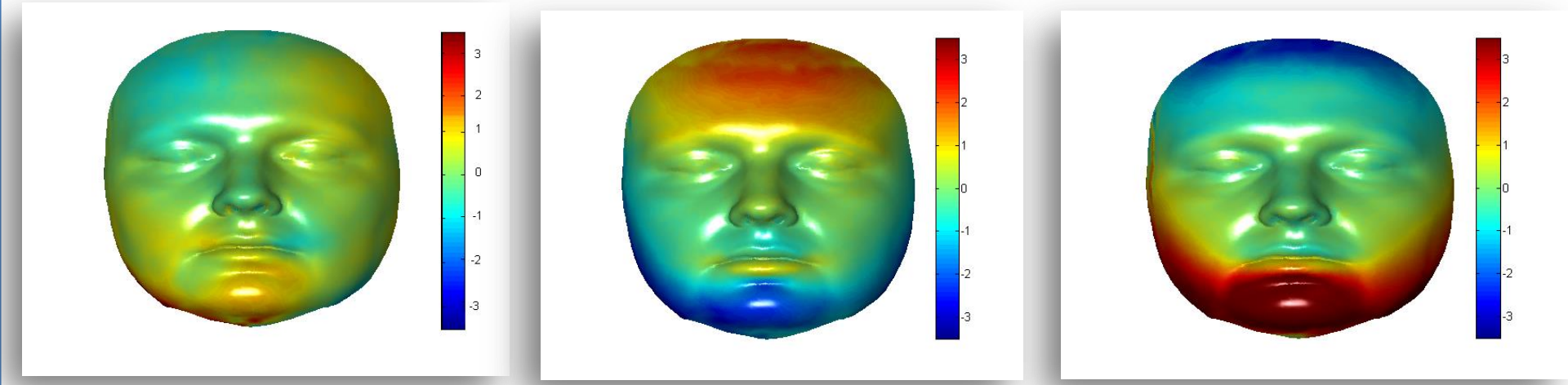

A **B** **C**

Figure 45: Corresponding (directional) soft tissue changes in: X (Medio-lateral) dimension (A); Y (vertical) dimension and Z(antero-posterior) dimension following Mandibular advancement surgery.

The vermilion border of the lower lip showed upward movement displayed as a yellow/orange patches mainly at the centre and diminished laterally toward the commeasures of the mouth. This change highlighted the inward and upward rolling of the lower lip as it moved forward and freed from the classical lip trap under the palatal surface of upper incisors associated with mandibular deficiency. Downward movement was noted at the region below the vermilion border of the lower lip, the chin and laterally extended to the cheeks region.

3.3.2.2.3 Soft tissue changes in z dimension (antero-posterior changes)

Figure (45,C) shows the depth component of the corresponding soft tissue changes in z dimension.

The region around the eyes, nose, paranasal regions and major part of the upper lip showed a minimal change which was displayed as a generalised green colour. The main changes were evident at the lower face and lateral cheeks region. A generalized and homogenous red colour covering these regions indicates a marked forward movement. The vermilion border of the lower lip showed a minimal change in the A-P dimension following BSSO advancement surgery. The same was noted at the commeasures of the mouth indicating a minimal change due to surgery. The vermilion region of the upper lip showed a mild backward movement displayed as a blue colour and extends laterally where the colour changed to green indicating minimal changes at the commissures.

Summary

There was a marked forward movement of the chin and lower lip regions extended posteriorly toward the gonial angle. A marked narrowing of the upper lip and widening of the lower lip were also observed. There was a generalised downward movement of the chin, lower lip and extended posteriorly toward the cheeks.

3.3.3 Soft tissue changes following bimaxillary advancement.

3.3.3.1 Euclidean distance measurements

The pre and post-operative average facial models were superimposed and dense anatomical correspondence was created. The results were displayed as a colours coded distance map, (figure 46).

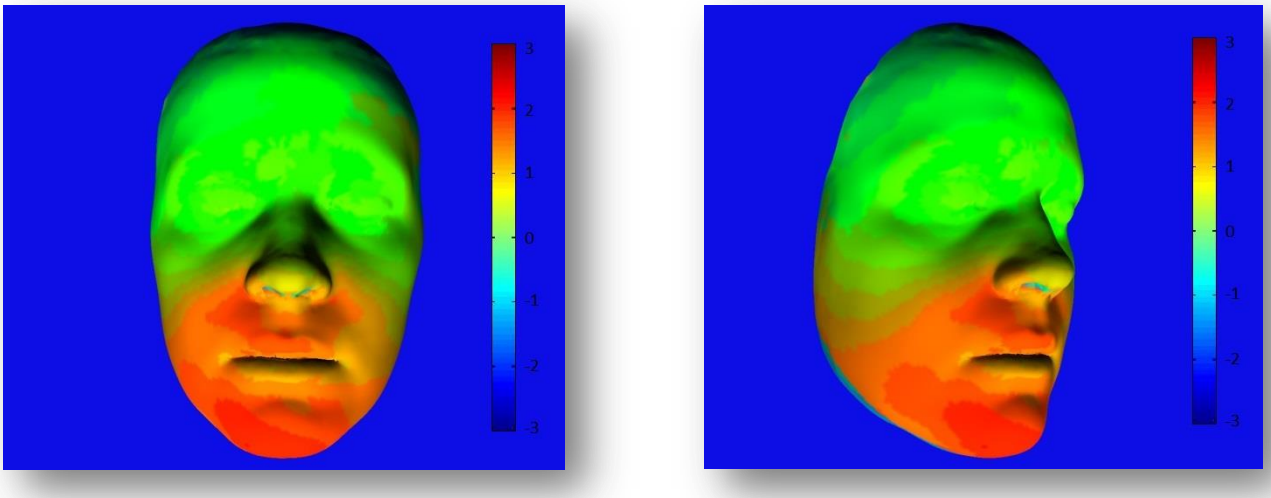

A B

Figure 46: Dense anatomical correspondence (Euclidean) showing soft tissue changes following Bimaxillary advancement surgery in Front view (A) and 45° view (B).

Soft tissue changes resembled to some extent the combined effect of advancement Le Fort I osteotomy and BSSO osteotomy. Changes at the eyes level and nasal bridge were minimal indicating good registration accuracy. The yellow colour at the tip of the nose was due to a mild forward and upward movement. The columella showed a mild upward displacement marked in light blue while the alar cartilages flared laterally and were displayed in orange. The upper lip and paranasal regions showed the major changes at the midface marked by a darker red colour in a relatively similar fashion to cases which had had a Le Fort I osteotomy only, (Section 3.2.1). However, in bimaxillary

advancement the red colour extended to cross the boundaries of the upper lip and paranasal regions laterally and inferiorly as it merged with the changes associated with the lower face as a result of the associated mandibular advancement. A moderate changes were observed at the oral commissures and lower lip vermilion. The changes started to increase toward the chin area marked by a darker red colour. Major changes were only observed at the chin area where the red colour started to fade into lighter shades laterally towards the gonial angles.

3.3.3.2 Directional changes measurements

In order to investigate the changes in more details, soft tissue analysis was separated into the x, y, and z dimensions where changes at each of the three dimensions were analysed independently.

3.3.3.2.1 Soft tissue changes in x dimension (medio-Lateral)

Figure (47,A) shows the soft tissue surface changes in x dimension only. Minimal changes were noted around the eye regions and the nasal bridge which were highlighted in green. The changes around the midface region are close to the changes observed following Le Fort I maxillary advancement, (section 3.2.1.2.1). The region around the nasal bridge and nasal tip demonstrated a green colour which indicates minimal changes at these regions. The right ala of the nose displayed a blue colour while the left ala of the nose displayed a yellowish-red colour, an indication of widening of the nostrils.

The upper lip and paranasal area showed a clear tendency toward lateral expansion demonstrated as a yellow/red colour on the left side of the face and the blue colour on the right side of these two regions. The changes were limited to the anatomical boundaries of the paranasal region and upper lip and was less than that observed with Le Fort I maxillary advancement cases (Section 3.2.1.2.1). The commissures at the corners of the mouth showed minimal tendency toward narrowing as demonstrated by a blue colour on the left commissure and yellow colour on the right side. The lower lip showed a similar

tendency toward narrowing as demonstrated by a blue colour on the left side and yellow colour on the right side of the lip. The chin region showed minimal change displayed in green colour.

3.3.3.2.2 Soft tissue changes in y dimension (vertical change)

Figure (47,B) shows the vertical component of soft tissue changes in response to Bi-maxillary advancement surgery.

Most of the region around the eyes and the nasal bridge displayed green colour which confirms the trivial vertical changes of the soft tissue of this region to bi-maxillary osteotomy. The dorsum of the nose showed minimal changes and was displayed in green/yellow colour. The tip of the nose, the right and left alar curvatures and the columella showed a marked upward movement which was displayed in orange/ red colour.

The paranasal area showed a homogenous but mild upward movement. The upper lip displayed yellowish green colour with patches of orange colours. This indicates there was a minimal vertical displacement of the upper lip following Bi-maxillary advancement surgery in the vertical dimension. The lower lip showed a compound response to surgery. The vermillion border showed minimal vertical changes highlighted in green, the region below the vermillion border demonstrated more vertical change displayed in red/orange colour with a central dark red colour patch. This indicated an upward movement in this region and perhaps a minimal shortening of the lower lip length. An upward movement was observed at the chin area which was marked by a well-defined red patch at the chin region.

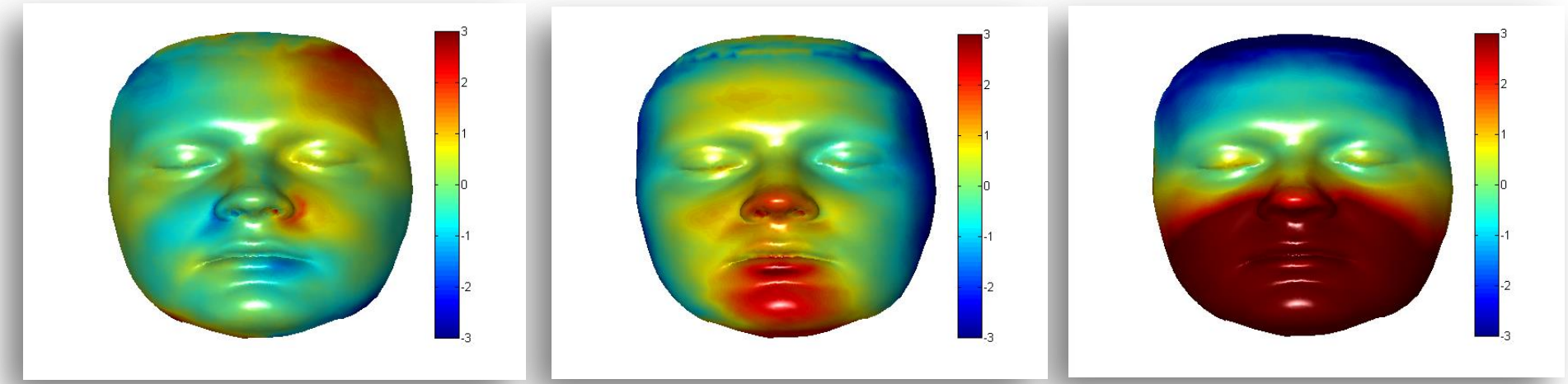

Figure 47: Corresponding (directional) soft tissue changes in: X (Medio-lateral) dimension (A); Y (vertical) dimension and Z(antero-posterior) dimension following Bimaxillary advancement surgery

3.3.3.2.3 Soft tissue changes in z dimension (antero-posterior changes)

Figure (47,C) shows the depth component of the corresponding soft tissue changes in z dimension.

The region around the eyes and the nasal bridge showed a minimal change which was displayed as a generalised green colour. The green colour on the dorsum of the nose extended toward the nasal tip with no marked change in colour. A change to red colour was evident at the nasal tip. The columella together with the right and left alas of the nose showed a well-defined dark red colour indicating a marked forward movement of this region. The forward displacement at this region coincided with a generalised forward displacement of most of the mid and lower face regions including the paranasal region, the upper lip and oral commeasures, the lower lip, the chin and extended posteriorly to involve most of the cheeks regions which were marked with a uniform dark red colour.

Summary

There was distinctive forward soft tissue movements in the mid and lower face combined with a marked lateral expansion at the nostrils, upper lip and paranasal regions. The expansion was limited by the anatomical boundaries of these three regions whereas a milled narrowing of the oral commissures and lower lip was observed. Marked vertical upward changes were evident at the tip of the nose, part of the lower lip and the chin regions. A relatively mild upward movement was observed at the upper lip and paranasal regions.

3.4 Prediction of facial soft tissue changes following Le Fort I advancement surgery.

The correlation between the soft and hard tissue was calculated for each of the facial anatomical regions, these included: The upper lip, lower lip, chin, nose, right paranasal and left paranasal regions. Soft tissue prediction and validation has been carried out using the statistical test "Leave-One-Out-Cross-Validation". Details about this test have been provided in the related methodology section. Thirty cases were included in the process, 29 of them were used as a training group and the resultant simulation was tested by applying the simulation algorithm on the preoperative image of the remaining one case. The difference between the actual post-operative change and the prediction was calculated. The process was then repeated 30 times to predict a case by case.

The results are visually displayed with a colour coded map showing the differences (errors of prediction) in the three dimensions between the predicted and the actual post-operative changes for each of the anatomical regions. The mean shape difference of the 30 trials is presented in each of the three dimensions (x, y and z). A Box-and-whisker plot was produced showing the median and the range of the 30 trials and the 25 percentile for each of the individual facial regions also in x, y, and z dimensions separately.

The mean values ranged from as low as (0.01 mm ± 0.582 mm) at the nose region to (-0.03 mm ± 2.1996 mm) at the chin region. Although the mean values were relatively small, there was a general tendency of over estimation of the predicted change of soft tissue in response to Le Fort I advancement osteotomy in the x dimension (medio-lateral) and y dimension (depth) while an underestimation of the vertical changes was noted. This was demonstrated on the colour coded map.

3.4.1 Upper lip

The results of the upper lip prediction are shown in figures (48 and 49). The difference between the predicted and the actual post-operative changes were individually analysed in the three dimensions.

The x dimension (Medio-lateral) showed the lowest mean ± standard deviation among other dimensions (-0.02 mm ± 1.04 mm) followed by the z dimension (the depth) and the y dimension (vertical) dimension with a mean value of (0.12 mm ± 0.96 mm) and (-0.07 mm ± 1.08 mm) respectively. In general, the total mean ± standard deviation in all dimensions was lower than 1.2 mm.

Figure (48) shows the difference in the three dimensions (x, y, and z) Box plot. The results showed that 50% of the trials showed less than 0.5 mm prediction errors. The size of the boxes showed a relatively low variation among the trials which was comparable in the three dimensions and equally distributed around the zero point. The range of the data represented by the whiskers showed a relatively lower level of variations in z dimension.

Figure (49) shows the colour map of the differences between the predicted and the actual post-operative soft tissue changes. There was a general tendency toward an overestimation (over prediction) of the changes at the upper lip region of around in the z (depth) dimensions. Whereas an under estimation of the same values were expressed in the y (vertical) dimensions as displayed on the associated colour scale.

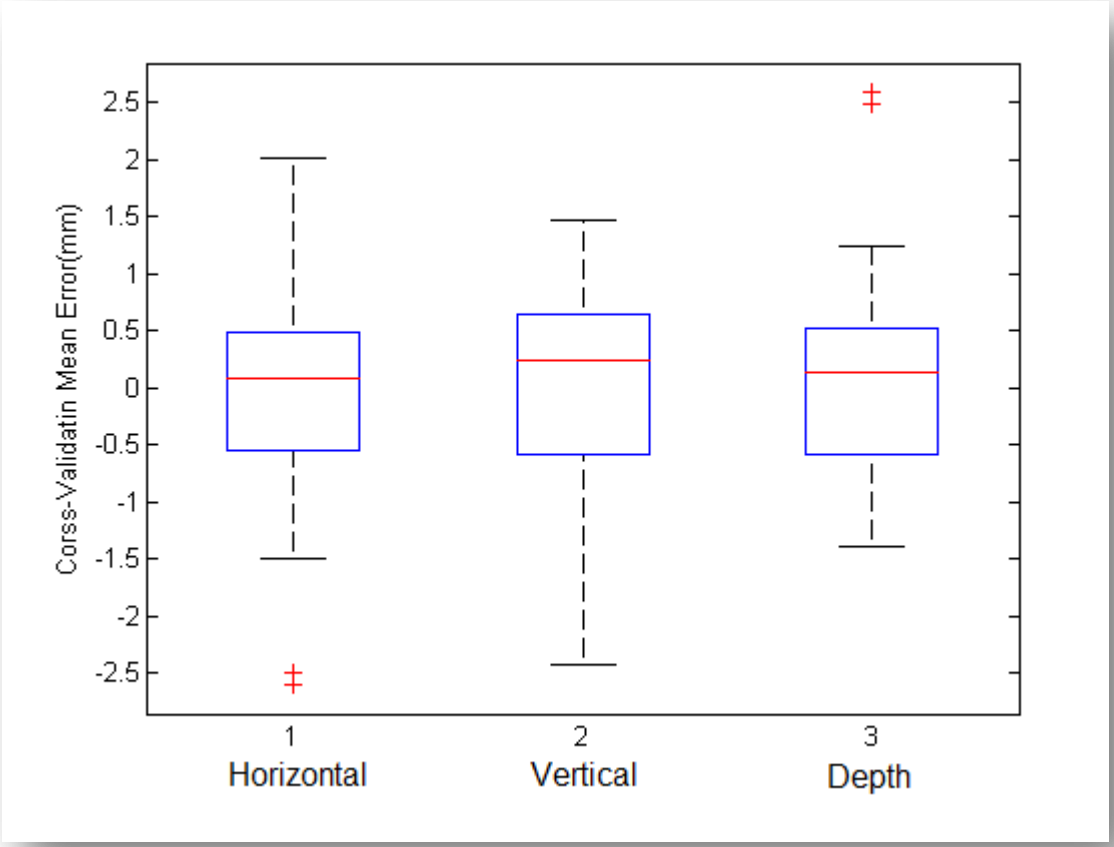

Figure 48: Accuracy of prediction at the upper lip region. Illustrates the median, the three quartiles and the whiskers of the errors associated with the prediction of soft tissue change following Le Fort I maxillary advancement at the Upper lip region in the three dimensions.

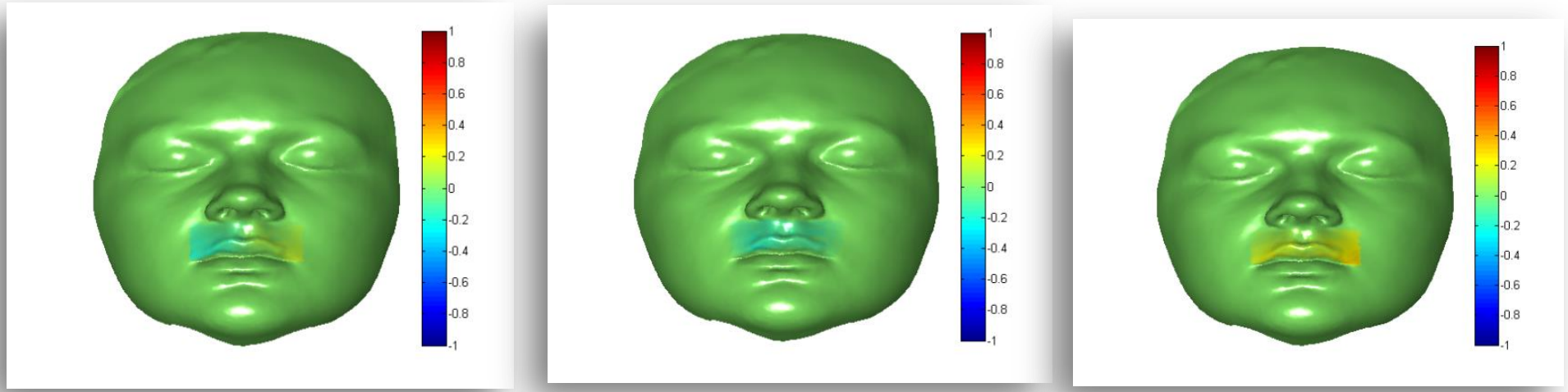

A B C

Figure 49: Accuracy of the prediction at the upper lip region. Colour map showing the (directional) mean error magnitude between the predicted Upper lip region and the real post-operative changes in the three dimensions: X (Medio-lateral) dimension (A); Y (vertical) dimension and Z(antero-posterior) dimension.

3.4.2 Lower lip

The results of the Lower lip prediction are shown in figures (50 and 51). The difference between the predicted and the actual post-operative changes were individually analysed in the three dimensions.

The x dimension (medio-lateral) showed the lowest mean ± standard deviation among other dimensions (-0.02 mm ± 1.09 mm) followed by the y dimension (vertical) dimension and the z dimension (the depth) with a mean value of (-0.07 mm ± 1.81 mm) and (-0.16 mm ± 1.27 mm) respectively. In general, the total mean ± standard deviation in all dimensions was lower than 1.44 mm.

Figure (50) shows the difference in the three dimensions (x, y and z) Box plot. The results showed that 50% of the trials showed less than 1 mm of error in prediction. The size of the boxes showed a relatively low variation among the trials which was higher in the y dimension than the other dimensions. All of the boxed were equally distributed around the zero point. The range of the data represented by the whiskers showed a higher level of variations in y dimension.

Figure (51) shows the colour map of the differences between the predicted and the actual post-operative soft tissue changes. There was a general tendency toward an overestimation (over prediction) of the changes at the lower lip region in the z (depth) dimension. Whereas an under estimation were expressed in the y (vertical) dimension as displayed on the associated colour scale.

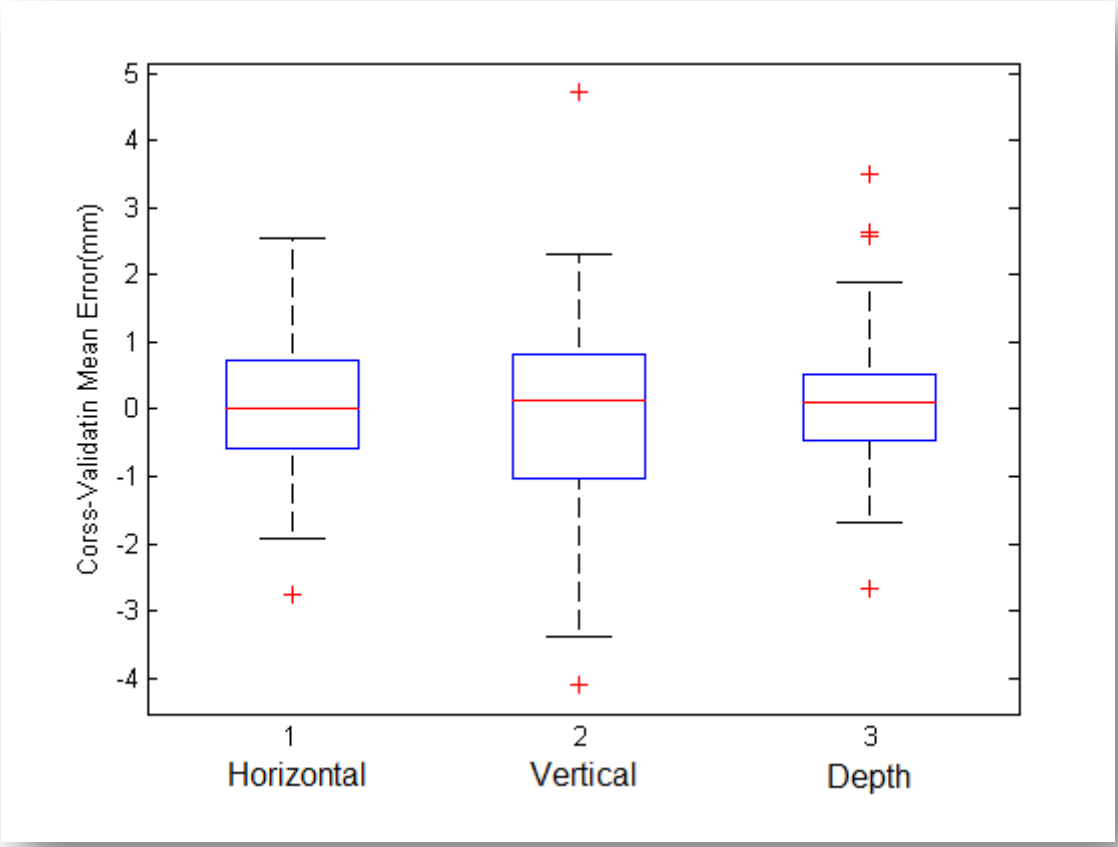

Figure 50: Accuracy of the prediction at the lower lip region. Illustrates the median, the three quartiles and the whiskers of the errors associated with the prediction of soft tissue change following Le Fort I maxillary advancement at the Lower lip region in the three dimensions.

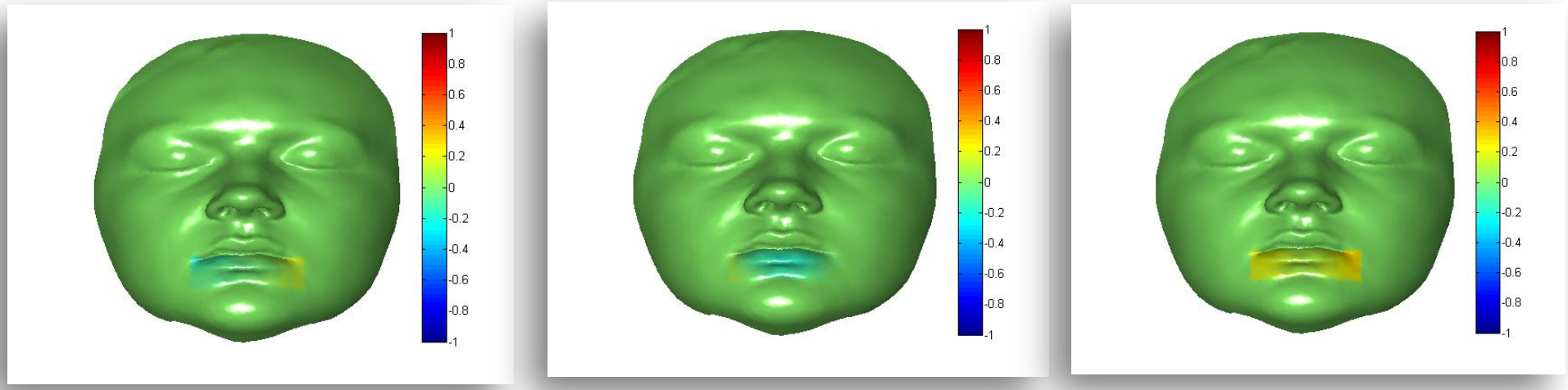

Figure 51: Accuracy of the prediction at the lower lip region. Colour map showing the mean (directional) error magnitude between the predicted Lower lip region and the real post-operative changes in the three dimensions; X (Medio-lateral) dimension (A); Y (vertical) dimension and Z(antero-posterior) dimension.

3.4.3 Chin

The results of the chin prediction are shown in figures (52 and 53). The difference between the predicted and the actual post-operative changes were individually analysed in the three dimensions.

The z dimension (the depth) showed the lowest mean and standard deviation among other dimensions (-0.12 mm ± 1.16 mm) followed by the x dimension (Medio-lateral) and the y dimension (vertical) dimension with a mean value of (0.07 mm ± 1.76 mm) and (-0.03 mm ± 2.19 mm) respectively. In general, the total mean ± standard deviation in all dimensions was lower than 2.24mm.

Figure (52) shows the difference in the three dimensions (x, y, and z) box plot. The results showed that 50% of the trials showed less than 1 mm of error in prediction. The size of the boxes showed a relatively low variation among the trials which was higher in the y dimension than the other dimensions. All of the boxed were equally distributed around the zero point. The range of the data represented by the whiskers showed a higher level of variations in y dimension.

Figure (53) shows the colour map of the differences between the predicted and the actual post-operative soft tissue changes. There was a general tendency toward an overestimation (over prediction) of the changes in all dimensions. However, a mixed blue and yellow colour patches were noticed over the chin region as displayed on the associated colour scale.

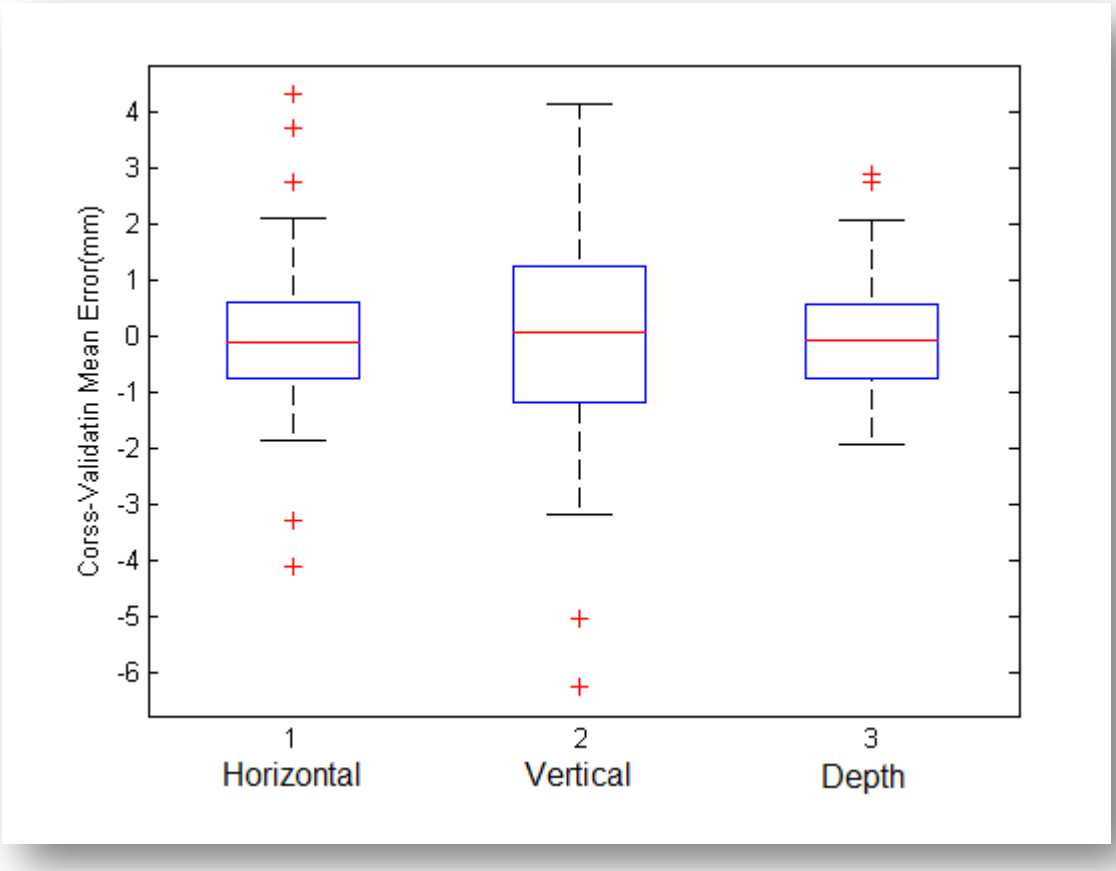

Figure 52: Accuracy of the prediction at the chin region. Illustrates the median, the three quartiles and the whiskers of the errors associated with the prediction of soft tissue change following Le Fort I maxillary advancement at the Chin region in the three dimensions.

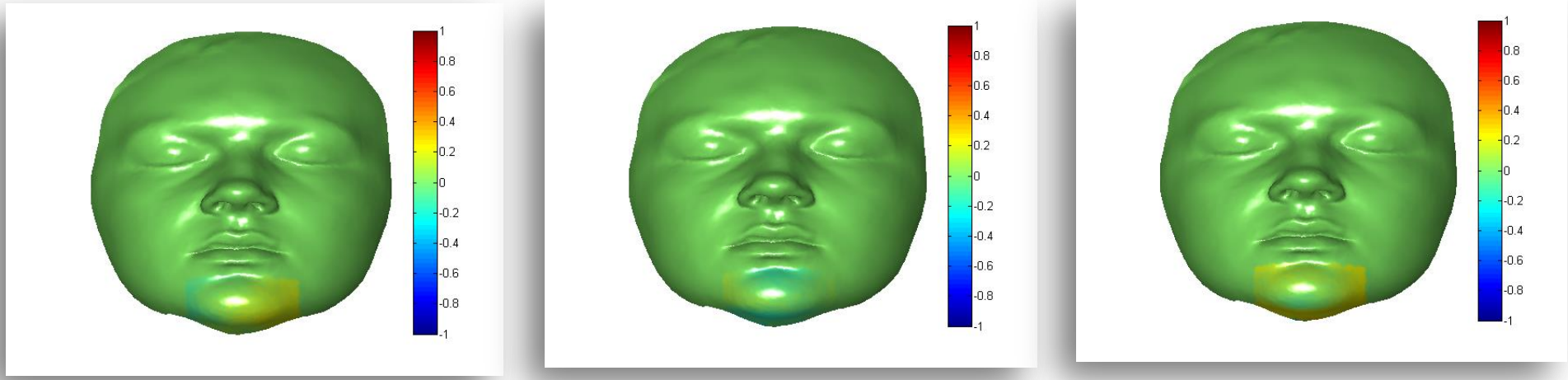

Figure 53: Accuracy of the prediction at the chin region. Colour map showing the mean (directional) error magnitude between the predicted Chin region and the real post-operative changes in the three dimensions; x (Medio-lateral) dimension (A); Y (vertical) dimension and Z(antero-posterior) dimension.

3.4.4 Nose

The results of the nose prediction are shown in figures (54 and 55). The difference between the predicted and the actual post-operative changes were individually analysed in the three dimensions.

The x dimension (medio-lateral) showed the lowest mean ± standard deviation among other dimensions (0.00 mm ± 0.58 mm) followed by the y dimension (vertical) dimension and the z dimension (the depth) with a mean value of (-0.04 mm ± 0.69 mm) and (-0.02 mm ± 0.75 mm) respectively. In general, the total mean ± standard deviation in all dimensions was lower than 0.79 mm.

Figure (54) shows the difference in the three dimensions (x, y, and z) box plot. The results showed that 50% of the trials showed less than 0.5 mm of error in prediction. The size of the boxes showed a relatively low variation among the trials which was higher in the z dimension than the other dimensions. All of the boxed were reasonably distributed around the zero point. The range of the data represented by the whiskers showed a lower level of variations in z dimension.

Figure (55) shows the colour map of the differences between the predicted and the actual post-operative soft tissue changes. Although marginal differences were recorded, there was a general tendency toward an underestimation (under prediction) at different regions and dimensions including the flaring of the nostrils region in the x dimension (medeo-lateral) and the nasal tip displacement was also underestimated in both the Y (vertical) and z (depth) dimensions as displayed on the associated colour scale.

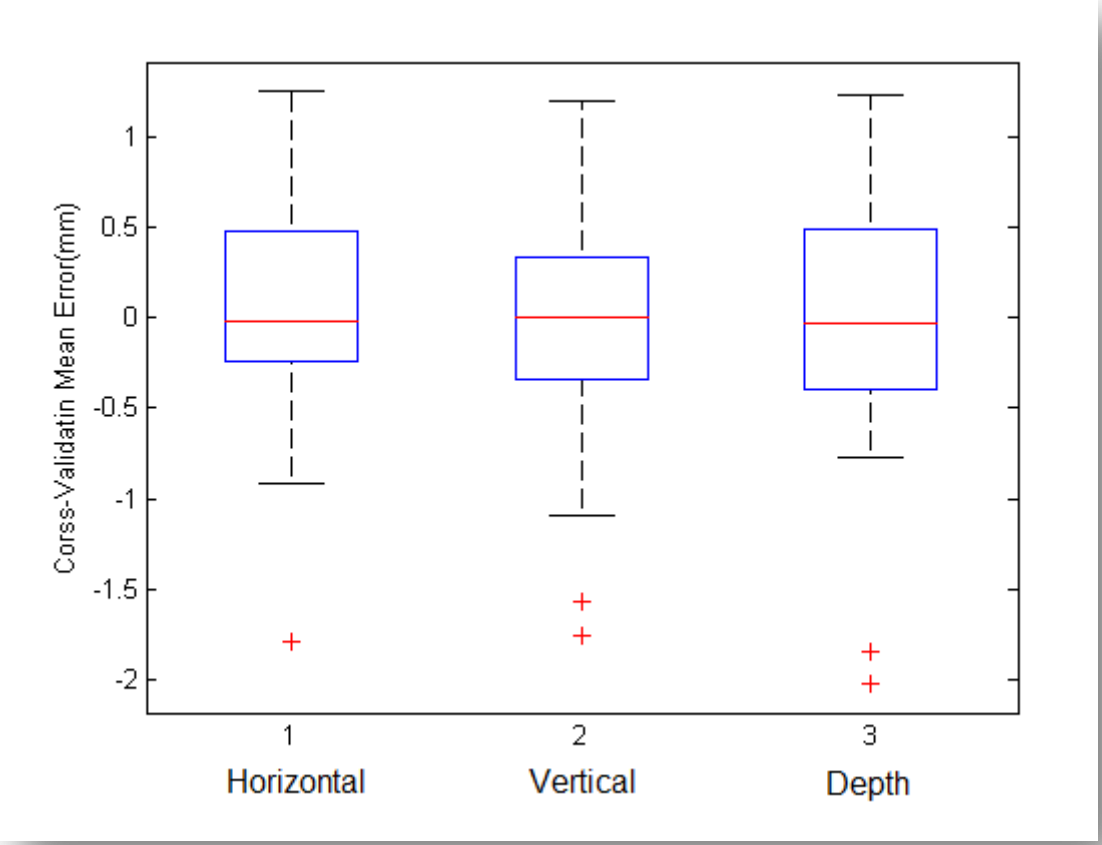

Figure 54: Accuracy of the prediction at the nose region. Illustrates the median, the three quartiles and the whiskers of the errors associated with the prediction of soft tissue change following Le Fort I maxillary advancement at the Nose region in the three dimensions.

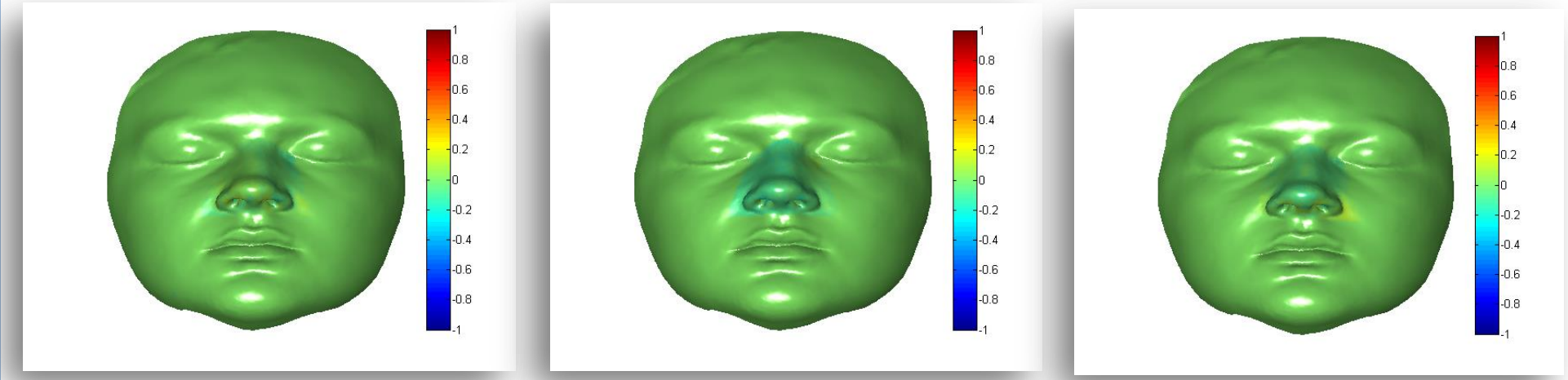

A B C

Figure 55: Accuracy pf the prediction at the nose region. Colour map showing the mean (directional) error magnitude between the predicted Nose region and the real post-operative changes in the three dimensions; X (Medio-lateral) dimension (A); Y (vertical) dimension and Z(antero-posterior) dimension.

3.4.5 Paranasal Left

The results of the left paranasal region prediction are shown in figures (56 and 57). The difference between the predicted and the actual post-operative changes were individually analysed in the three dimensions.

The z dimension (the depth) showed the lowest mean and standard deviation among other dimensions (0.09 mm ± 1.00 mm) followed by the y dimension (vertical) dimension and the x dimension (Medio-lateral) with a mean value of (0.02mm ± 1.08 mm) and (0.08 mm ± 1.19 mm) respectively. In general, the total mean ± standard deviation in all dimensions was lower than 1.26 mm.

Figure (56) shows the difference in the three dimensions (x, y, and z) box plot. The results showed that 50% of the trials showed less than 1 mm of error in prediction. The size of the boxes showed a relatively low variation among the trials which was comparable in all dimensions. All of the boxed were equally distributed around the zero point. The range of the data represented by the whiskers showed a comparatively higher level of variations in x dimension.

Figure (57) shows the colour map of the differences between the predicted and the actual post-operative soft tissue changes. There was a general tendency toward an overestimation (over prediction) of the changes in all dimensions as displayed on the associated colour scale.

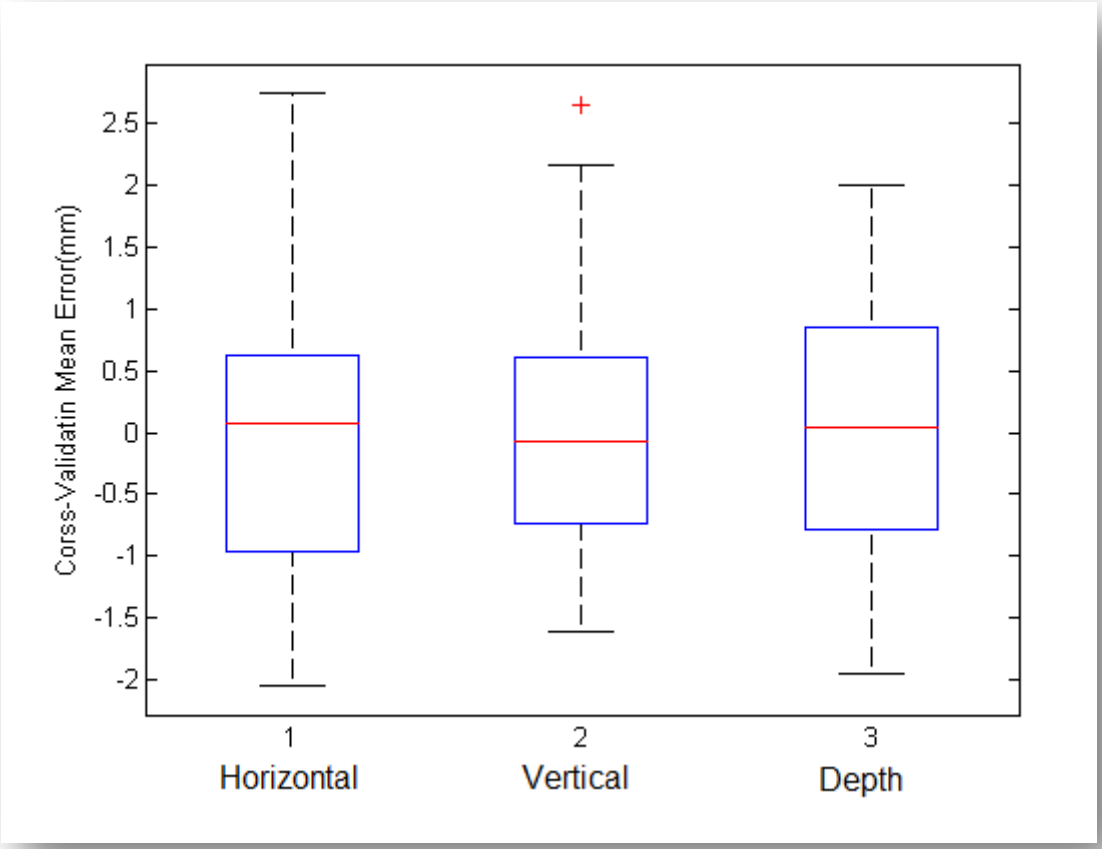

Figure 56: Accuracy pf the prediction at the left paranasal region. Illustrates the median, the three quartiles and the whiskers of the errors associated with the prediction of soft tissue change following Le Fort I maxillary advancement at the Paranasal Left region in the three dimensions.

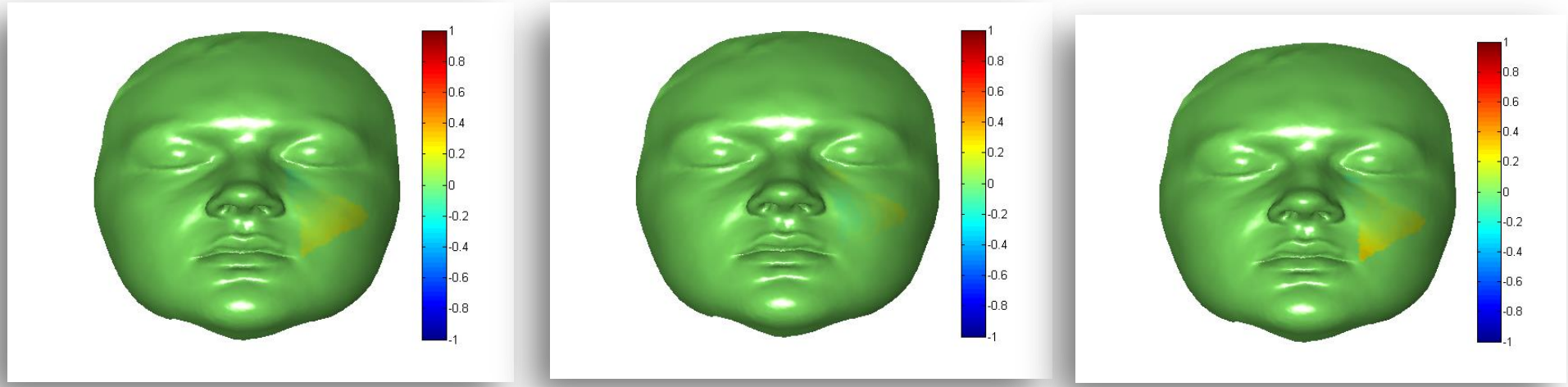

Figure 57: Accuracy of the prediction at the left paranasal region. Colour map showing the mean (directional) error magnitude between the predicted Left Paranasal region and the real post-operative changes in the three dimensions; X (Medio-lateral) dimension (A); Y (vertical) dimension and Z(antero-posterior) dimension.

3.4.6 Paranasal Right

The results of the right paranasal region prediction are shown in figures (58 and 59). The difference between the predicted and the actual post-operative changes were individually analysed in the three dimensions.

The z dimension (the depth) showed the lowest mean and standard deviation among other dimensions (0.019 mm ± 0.69 mm) followed by the x dimension (medio-lateral) and the y dimension (vertical dimension) with a mean value of (-0.05 mm ± 0.99 mm) and (-0.02 mm ± 1.1832 mm) respectively. In general, the total mean ± standard deviation in all dimensions was lower than 2.2 mm.

Figure (58) shows the difference in the three dimensions (x, y, and z) Box plot. The results showed that 50% of the trials showed less than 1 mm of error in prediction. The size of the boxes showed a relatively low variation among the trials which was comparable in all dimensions. All of the boxed were relatively equally distributed around the zero point. The range of the data represented by the whiskers showed a higher level of variations in y dimension and a lower variation in the z dimension.

Figure (59) shows the colour map of the differences between the predicted and the actual post-operative soft tissue changes. There was a general tendency toward an underestimation (under prediction) of the changes in the y and z dimensions but over estimation in x dimension. However, a mixed blue and yellow colour patches were noticed over the right paranasal region close to the corner of the mouth as displayed on the associated colour scale.

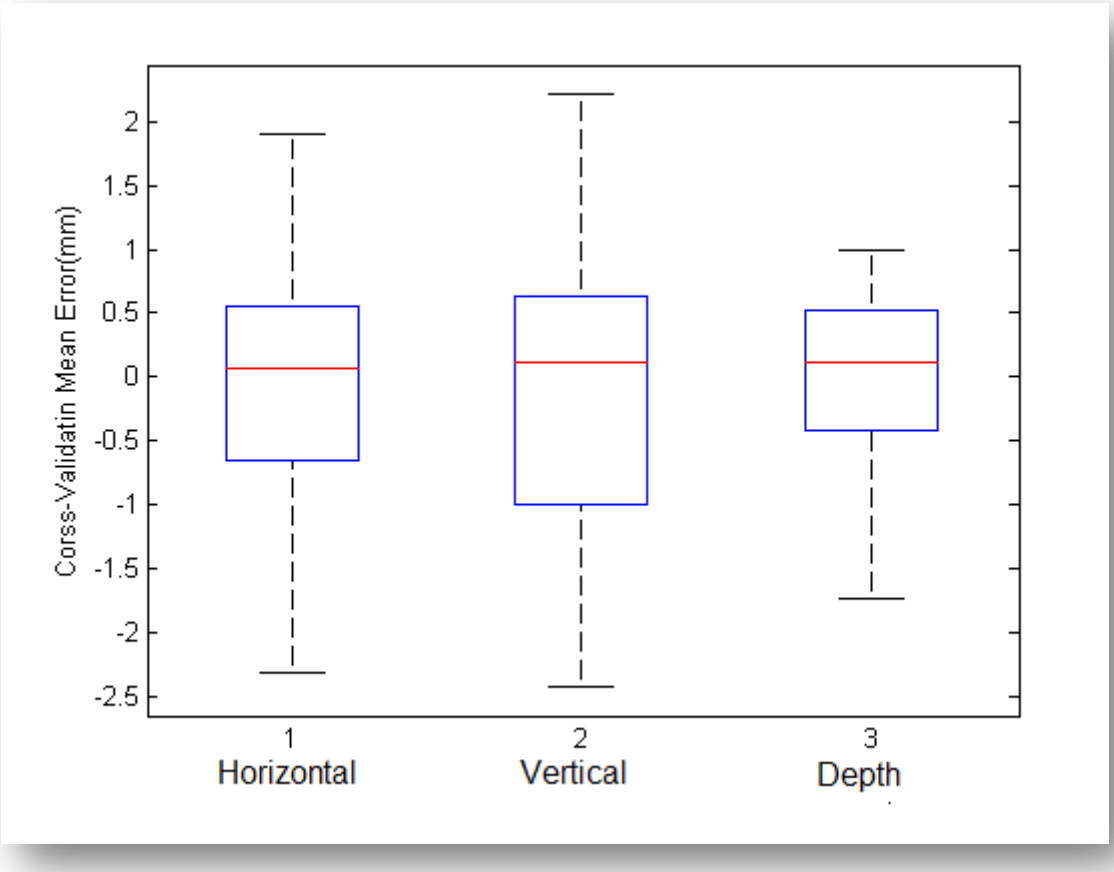

Figure 58: Accuracy of the prediction at the right paranasal region. Illustrates the median, the three quartiles and the whiskers of the errors associated with the prediction of soft tissue change following Le Fort I maxillary advancement at the Paranasal Right region in the three dimensions.

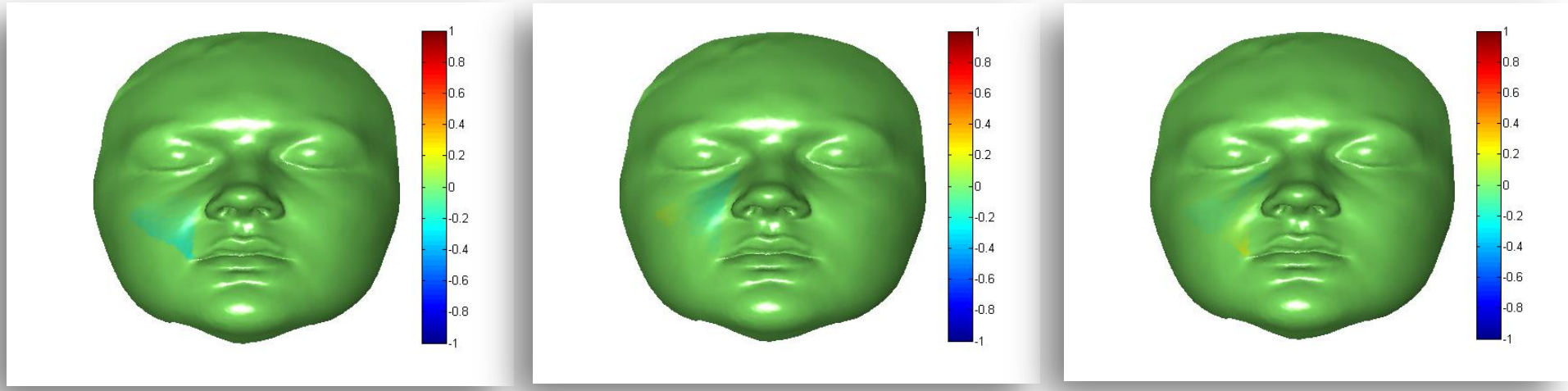

A B C

Figure 59: Accuracy of prediction at the right paranasal region. Colour map showing the mean (directional) error magnitude between the predicted Right Paranasal and the real post-operative changes in the three dimensions; X (Medio-lateral) dimension (A); Y (vertical) dimension and Z(antero-posterior) dimension.

Summary

The differences between the predicted and the actual results were minimal. Relatively large variation in the prediction were observed at the vertical dimension represented by a higher than average standard deviations in addition to wider range (whiskers) in most of the compared boxplots. There is no specific pattern of under and over estimation of the predicted results as the means were divided equally between underestimation and overestimation of the changes distributed among different regions and dimensions.

4 Discussion

Contents

4.1 Study Sample

The analysis of pre- and post-operative records to investigate surgical changes following orthognathic surgery has been previously reported (107). Superimposition of the pre-operative and post-operative images provide valuable information to quantify the magnitude of surgical movements and the overlying soft tissue response (247). Three main reasons justified the choice of CBCT imaging as the main source of data for this study. Firstly, the 3D surface analysis applied in this research necessitates 3D image of the skeletal and soft tissue facial structures. 3D data cannot be obtained from a lateral cephalogram alone and therefore the choice was between CT and CBCT. Cone beam computerized tomography (CBCT) images provide three-dimensional volumetric data with a lower exposure to radiation compared to conventional CT but more than a plain film (248,44,45) more details were provided in the literature review chapter. CBCT facial scans were validated for their accuracy in capturing facial images (248–253). Farman *et al.,* 2006 reported that the soft tissue definition of the CBCT was sufficient to determine air/soft boundaries (252). Moerenhout *et al.,* 2009 used mannequin head to determine the 3D surface accuracy of soft tissue acquired from a CBCT scan. They found that the 3D surface of the facial soft tissues segmented from a CBCT scan were accurate and comparable to laser surface scan (253). Kau *et al.,* 2005 stated that "The CBCT is excellent for imaging hard tissues structures and most soft tissue components" (248).

Secondly, the aim of this research was to investigate the surface changes of the soft tissue following orthognathic surgery. A CBCT scan captures the hard and soft tissues simultaneously and preserves the relation between them. Finally, the availability of the pre-surgical and post-surgical CBCT scans routinely captured for orthognathic patients.

Ethical approval was obtained from the West of Scotland Research Ethics Service on 24th May 2012 (Rec Reference 12/WS/0133). The approval limited the study to a retrospective analysis of the pre-existing data, hence there was limited control with respect to the technical parameters of the CBCT scans, as the radiography technicians standardised the method of CBCT scans for orthognathic surgery patients (Section 2.1.2). Ethical approval allowed the analysis of other types of images such as facial stereophotogrammetry, to validate the methodology.

A total of 137 pre-surgical and post-surgical CBCT scans were successfully retrieved from the database in the radiography department of the Glasgow Dental Hospital; 37 cases were excluded from the final sample as they failed to meet the inclusion criteria. Image quality and ethnic background were the two main reasons for exclusion. The remaining 100 cases were successfully processed according to the research protocol mentioned earlier, (Section 2.4.1).

The sample size was based on previous studies which investigated the accuracy of orthognathic surgical simulation and prediction planning (table 25). The range of the sample size of previous studies varied from 1 to 100 patients. The cases in most of the studies were mixtures of maxillary and mandibular surgical procedures.

Table 25: Sample size reported in previous studies.

Author	Year	Type of simulation	Sample size
Marchetti *et. al.*, (170)	2011	Mathematical modelling and numerical simulation	10
Marchetti *et. al.*, (255)	2006	Mathematical modelling and numerical simulation	25
Tucker *et. al.*, (256)	2010	Mathematical modelling and numerical simulation	20
Rihan Ullah (236)	2012	Mass spring model	13
Shafi *et. al.*, (158)	2013	Mass tensor model	13
Lieberegts et al., (312)	2015	Mass tensor model	100
Beldie *et. al.*, (257)	2010	Finite element analysis	1
Meehan *et. al.*, (234)	2003	mass spring model	1
Deuflhard *et. al.*,(258)	2006	Mathematical modelling and numerical simulation	4

The need for homogeneous samples when studying soft- and hard-tissue behaviour following orthognathic surgery is essential. Soft tissue behaviour following orthognathic surgery proved to be variable in the various regions of the face (223,254). Therefore the study sample was sub-grouped according to the type of surgical intervention, i.e. cases which had maxillary surgery only (52 patients), cases which had mandibular surgery only (20 patients) and cases which had bimaxillary surgery (28 patients).

Several factors can be attributed to the predominance of maxillary surgery in the current sample, as compared to other studies conducted in the UK(259). These include the prevalence of Class III deformities in the West of Scotland which is greater than other regions in the United Kingdom (260); In addition, the prevalent attitude is to postpone the treatment of mild to moderate skeletal Class III jaw deformities until the completion of growth for a number of reasons, including the limited application of mid-face protraction and growth modification (261,262).

Variation in facial soft tissue characteristics among different ethnic groups has been documented (167,188,215,221). Soft tissue thickness, consistency and facial features were the most common ethnic variations that may affect orthognathic surgery planning (215,221). To establish a reasonable homogeneity, the study sample was confined to Caucasian subjects.

Patients who had a history of previous operations in the orofacial region were excluded to avoid the effect of previous facial scaring on soft tissue response to orthognathic surgery (185,220); this includes cleft lip and palate, facial trauma and surgical treatment of facial pathologies.

No age restrictions were applied; however, the lowest age included was 17 years and 8 months. This excluded any significant growth related facial changes during the treatment period.

The timing for CBCT scan capture was a purely clinical decision. However, patients who had their scans captured within a month prior to surgery (pre-operative) and between 6-12 months after surgery (post-operative) were included in the study. This pre-operative time limit was set to avoid non-surgical soft tissue changes that might occur preoperatively. The post-operative scan limits were implemented to avoid the short-term effect of maxillofacial surgery on postoperative swelling (oedema from retraction, irritations, and inflammation), which has been well documented (186). It has been reported that facial morphology recovers to approximately 90% within 3 months after bimaxillary surgery (263). Dolce *et al.*, 2003 (264) showed that the swelling caused by BSSO for mandibular advancement began to resolve by 8 weeks and

was fully resolved by 6 months. Although the post-surgical relapse rate is multifactorial (including the technique and extent of the performed surgery), most studies evaluating surgical relapse suggested one year as a cut-off point for the collection of follow-up records. It was suggested that the majority of surgical relapse was evident during the first few months after surgery, following bone fragment consolidation, and the relapse rate was fairly minimal after one year (265–269). Therefore, in this study, the post-operative CBCT scans included the combined effect of orthognathic surgery and early relapse without affecting the robustness of the methodology. The exact bony movements were extracted by superimposing post-operative radiographs on the pre-operative CBCT scans and the changes of the soft tissue where related to the calculated skeletal movement.

Despite the noticeable technological advancement, CBCT scan is still a time consuming procedure. A full head 22 cm extended field of view (EFOV) scan takes from 17.5 to 36 seconds (248,270). The (i-Cat) CBCT scanner at the Glasgow Dental Hospital takes 20 seconds for facial capture with the radiation gantry rotating twice around the head. Patients were asked to remain still throughout the procedure, but minor movements during the scan are sometimes unavoidable. Depending on the extent of these movements, the distortion of the captured image may range from blurred image to a clear stepwise regional shift in the image. The retrospective nature of the research sample and the policy of the Glasgow Dental Hospital regarding CBCT scans made it impossible to repeat the scan for these cases. Errors associated with image capture were the main source of exclusion of cases in this study.

The surgical technique was another important exclusion criterion. The majority of the cases had Le Fort I maxillary osteotomy, bilateral sagittal split mandibular osteotomy or a combination of both. However, few cases were treated with different surgical techniques including total body otectomy, vertical sub sigmoid osteotomy and multi-piece segmental Le Fort I maxillary osteotomy. These few cases were excluded to preserve the homogeneity of the study sample.

4.2 DICOM image processing and analysis

4.2.1 Image superimposition

Image superimposition on a relatively stable region which was unaffected by the procedure was the classical approach for assessment of the outcome of orthognathic surgery. A variety of superimposition techniques were applied (Section 1.2.2). The choice for voxel based registration in this project was evidence based. A published study by our group (70) compared two common types of automated 3D image superimposition techniques (surface based registration and voxel based registration). The results revealed that there was no statistically significant difference between the accuracy of the two techniques in terms of the mean distance of the superimposed meshes. However the results also showed that the correlation between the soft and hard tissue models has been lost in the surface based registration group since each model was superimposed separately. This was not the case with the voxel based registration where the two tissues (soft and hard tissue) were registered simultaneously. The conclusions suggested that studies which aim to investigate the soft to hard tissue correlation should use the voxel based registration whenever it is applicable.

Around 40% of image superimpositions were carried out using the superimposition module of the Maxilim software package. This module was offered from the manufacturing company for a limited time to help with part of this study. The rest of the images were superimposed using another software package (OnDemand3D), which provided the same quality of 3D image superimposition. This software have been validated for its image registration accuracy (67) and hence was used for the rest of the sample in this study.

Only one DICOM image registration was carried out for each patient at the start of the analyses. Both soft and skeletal tissue analyses were carried out on the same image superimposition. This eliminated potential error of the repeated registration process.

Upon successful superimposition, both soft and hard tissues were segmented from each of the preoperative and postoperative DICOM images using Maxilim

software. This software applies the marching cube algorithm (61) to segment each tissue boundary according to its associated Hounsfield unit (HU) value. The optimal HU value for each tissue varied between patients. However it was not possible to estimate the exact value for each patient; this might have introduced another variable that could have affected the credibility of the analysis. For that reason, a standard HU value of (276) for skeletal tissue and (-976) for soft tissue segmentation were adopted for all cases. These were the default values built into Maxilim software.

When analysing the superimposed models, the skeletal tissue appears to align to a clinically acceptable level on the anterior cranial base, which is the region of registration, whereas the soft tissue models seem to have some inaccuracy on the forehead. Details of these inaccuracies were previously discussed (Section 2.2.1). This could be explained by the fact that voxel based registration relies on the grey scale values of the voxels of the selected region of interest and not on the surface of each tissue. Minor changes in soft tissue related to different facial expression during scan or weight gain or loss does not affect the registration since the surface has a limited effect on this variable. This, on the other hand, provided an accurate description of the real change and preserved the relation between the hard and soft tissue models rather than losing this relation to produce a better soft tissue superimposition which was achieved by surface based registration.

To address the aim of the project, that of finding the correlation between soft and hard tissue changes, three distinct steps of the analysis had to be followed; firstly to analyse the skeletal displacement; secondly to analyse soft tissue deformation and finally to find the correlation between the two changes.

4.3 Measurement of Skeletal Displacement

The measurement implemented to assess skeletal displacement was a novel approach developed and validated within this PhD project. The method was simple, reproducible and yet highly accurate in analysing the skeletal displacement in three dimensions of space. Previous methods to analyse skeletal displacement were less successful in achieving these goals without a higher magnitude of errors (75,100,210). Despite the problems with 2D lateral

cephalometric analysis with regard to its landmarking errors, with lack of recording of bilateral structures and with magnification issues (75,100,271–273), it is still considered by other researchers (274,275). The reason for this might have been the unavailability of the 3D CBCT scans. This project benefited from the availability of the CBCT scans in the data base to carry out the 3D analysis presented in this study.

A variety of 3D image analyses have been considered for the evaluation of soft and hard tissue changes following surgery. The most commonly used are the anatomical landmarking (3D cephalometry), Euclidean surface distance (mean distance on a surface patch or distance at specific points), and, less frequently volumetric analysis (110). Nevertheless, each of these methods has its drawbacks which affect its credibility on certain aspects. Details of shortcomings of each method have been explained earlier in the literature review.

The method applied in this study was based on creating an anatomically based local 3D axis (three orthogonal planes) to track the differential change of the jaw bones at different areas where the linear (distances) and the angular (pitch, role, and yaw) displacements could be measured. Each plain required at least three points to be established. The challenge was in finding valid and reproducible landmarks on the smooth bony surface of the jaw bones, especially the maxilla, to establish this plane. The three foramina on the hard palate surface (incisive foramen and bilateral greater palatine foramina) and five anatomical locations at the mandible (bilateral lingual foramina, bilateral mental foramina and lingual tubercle) were used. Although their boundaries were clearly visible on the DICOM slices, the relatively thin bony plate surrounding the foramina were not accurately segmented into the 3D model and in the majority of the cases there were noticeable differences in size and shape between the pre and post-operative images especially around the greater palatine foramina, (figure 60). This was in addition to the fact that digitizing landmarks on DICOM image slices were more accurate and reproducible than identifying them on the three dimensional model surface (96). Maxilim software provides the ability for DICOM slices landmarking; therefore, the decision was taken to place the landmarks on the shadow of the foramen boundary on the DICOM slices with a distinctive anatomical definition of each landmark.

Validation of the protocol of this method has been established by our research group (246)

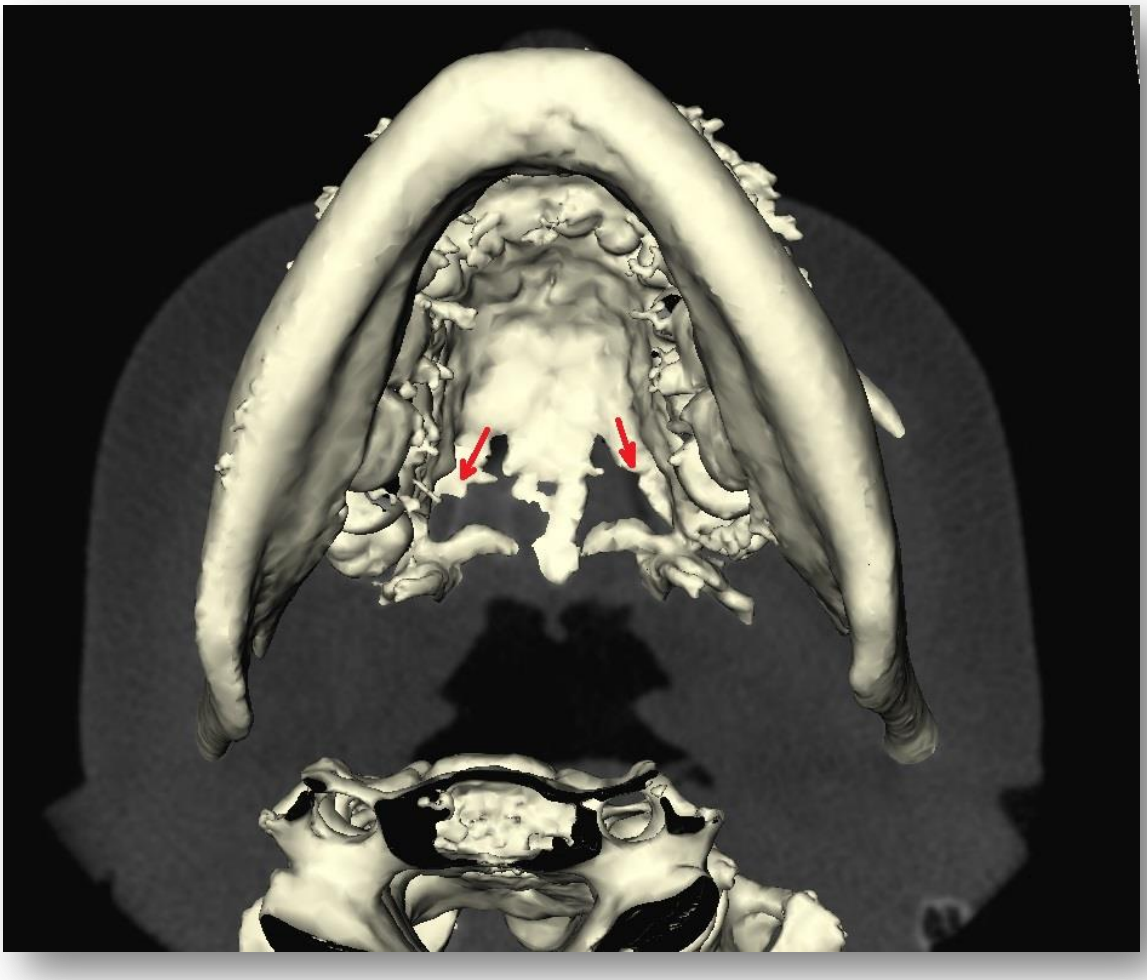

Figure 60: Difference between the 3D model and the radiographic shadow in representing the contour of the greater palatine foramina.

Only the linear measurements were considered in this project. Angular measurements were excluded from the study. The newly developed PCA simulation algorithm has not reached the level to allow incorporation of the rotational elements (pitch, role and yaw) and yet these were thought to be a source of noise to the statistical soft tissue analysis and it was believed to have a limited effect on the overlying soft tissue behaviour compared to the linear measurements. Future studies may enhance the overall result of the prediction planning by the addition of the rotational element.

The measurements in this study were established as the orthogonal distance from the selected landmarks to three orthogonal reference planes. A detailed

description of the measurements was previously provided (Section 2.2.2). The orthogonal distance from the same reference planes to each landmark on the pre- and post-operative images were measured following voxel based registration. This eliminates errors that could have developed as a result of the establishment of reference planes for the pre- and post-operative images separately.

4.4 Measurement of soft tissue changes in response to orthognathic surgery.

Soft tissue analysis was based on the concept of dense correspondence between the pre- and the post-operative images. Previous studies reported other methods for soft tissue analysis, including anatomical landmarking (cephalometric analysis), colour coded surface distance and volumetric analysis (110,147,276). Each of these methods has its own shortcomings and could not be used to address the aim of our research (details were provided in Section 1.3.2).

The application of the corresponding surface analysis is relatively new to the field of orthognathic surgery. Mao *et al.,* 2006 (244)published their work on a similar concept which they named "Anatomical dense correspondence analysis" and showed that it could be applied to study human faces. Since then, limited studies have been carried out on this method. Claes *et al.,* 2011-2012 and Walters *et al.,* 2013 (152,175,277) described the use of an "the anthropometric facial mask ", which followed the same concept. The aim of their studies was to describe the soft tissue changes due to growth and after correction of asymmetric faces by orthognathic surgery. However, their analysis did not progress further and the two studies were concluded as a visual description of the vectors connecting the corresponding vertices on the pre and post-operative facial meshes or at two time intervals. A number of reasons might have contributed to the limited number of publications including the complicated procedure associated with generic mesh construction and conformation; limited software packages providing this type of analysis (usually coded specifically for this purpose within the research group) and lastly the lack of evidence to support any superiority of the method.

The advantage of this method over other surface or landmarks based analyses, is in the preservation of the anatomical correspondence while a comprehensive facial surface analysis is carried out. The technique however, is sensitive and a high level of accuracy is required in all the stages of the analysis, including image capture, generic mesh construction, landmark digitization and conformation procedure.

In this project, an investigation was carried out to ensure the highest possible accuracy of all stages of the analysis. The results showed an acceptable level of accuracy and formed a solid base for a comprehensive analysis, (Section 2.3.1).

Although the magnitude of surgical displacement was variable among the cases, the surgical technique and the direction of movement were standardised to reduce the variability within each group. This variation might have a negative effect on the analysis. However, the clear correlation between the results of the analysis and the clinical observation support its validity. A larger sample size is recommended for future studies to reduce this margin of error.

Dense correspondence was the selected method of the analysis in this project for two main reasons: Firstly, it provided surface information data hence it overcame the shortcomings associated with the landmarks based analysis. Secondly, it provided an anatomical correspondence between the pre- and post-operative facial meshes, thus, it avoids the limitations associated with the traditional closest distance and coloured coded map. The availability of the database and the in house developed software packages allowed the application and validation of the method.

In order to apply the concept of dense correspondence, a facial generic mesh conformation was used. The original generic mesh was previously generated by our research group for a similar purpose. VRMesh software was employed to reduce the number of surface mesh triangles to 1000, closing mesh holes and removing duplicate triangles. The resultant generic mesh has a uniformly distributed approximately 3mm apart nodes with around 1000 triangles.

The process of conformation (elastic deformation) of the generic mesh to the pre- and post-operative soft tissue models was carried out using in house

developed software (Section 2.3.1). Validation study was carried out to confirm the software package accuracy and to test the accuracy of the conformation process. Errors, including mesh sliding and poor elastic deformation, were examined. The results showed high accuracy of the conformation with a mean error of 1.12±0.23 mm.

The procedure of conformation was previously described, following the placement of 20 anatomical landmarks, the conformation performed in two steps: firstly was the "spline" step which is the application of the 'thin plate spline' algorithm; secondly was the "conformation" which is a localised automated elastic deformation algorithm. The first step relied on 20 landmarks manually placed on both the generic mesh and the target mesh (pre- or post-operative images). The CBCT scan produces one of the most challenging landmarking placement soft tissue images due to the smooth and texture-less surface (248). Landmarking error study was carried out and results showed a reasonable level of accuracy for clinical application and soft tissue analysis. Although the landmarking error was below the clinical significance level, two additional measures were carried out to reduce the range of errors: Firstly the generic mesh was landmarked only once for the purpose of conformation on all cases; This reduced the landmarking errors to 50% by excluding the potential errors associated with repeated generic mesh landmarking for each case. Secondly, the pre- and post-operative meshes were landmarked simultaneously on a multi view window on the same screen which facilitated and improved the accuracy of landmark identification. Digitizing the landmarks on the exact position on both images was the key for successful facial dense correspondence analysis.

4.4.1 The generation of the "average face"

The use of the "average face" to study human facial features has been previously reported (162). This method provided a possible solution to process a large data set of facial meshes by averaging facial shapes into a single mesh. A single visual outcome of the facial analysis was achieved for the entire sample; this could not have been possible through individual case analysis. However, the accuracy of this type of analysis is highly dependent on the magnitude of case variations and the sample size to generate the "average face". In this study, the

variations were reduced through strict case selection criteria, excluding cases with additional genioplasty procedures and subdividing the study sample into five groups (Le Fort I advancement, BSSO advancement, BSSO setback, bimaxillary (Maxillary advancement-Mandibular setback) and bimaxillary advancement. Despite the large number of collected sample (100 cases), only three of the five groups achieved a sufficient sample size to be considered in the analysis. These were Le Fort I advancement (33 cases); BSSO advancement (12 cases) and Bimaxillary advancement (12 cases).

The method applied for facial averaging was relatively new to the field of facial analysis. Limited work has been published on this topic, (Hutton *et al.*, 2003 and Hammond *et al.*, 2004). Both studies applied the average facial meshes to study facial morphology. Their methods were based on a similar concept of establishing a closest point dense correspondence between the two averaged meshes. The selection of the initial facial mesh was critical in their study, as it has a direct effect on the generation of an average mesh which was the result of subsequent superimposition and averaging of all individual meshes of the study sample. The starting mesh (template), therefore, should be selected at the middle of the shape variation across the sample. This was achieved by landmarking the entire study sample with a minimal set of facial points, followed by the application of full Procrustes analysis. Principal component analysis was then used to extract the facial averaging template (initial mesh).

The closest point correspondence has been used by many researchers to assess facial changes and was found to be more accurate than other methods (177), however, it still carries a considerable amount of error, especially at the peripheral regions of the mesh.

The method of facial averaging used in our project is more accurate, and yet considerably less complicated. A detailed description has been previously provided (Section 2.4.1.1.7). The averaging procedure was based on using the conformed generic meshes utilizing the common 3D index of the generic mesh vertices to establish the dense correspondence among the facial meshes of the whole study sample. Facial average was generated by applying partial Procrustes analysis (PPA) on the entire sample. Each vertex was considered as a landmark and participated in the (translation and rotation) procedure of the PPA based on

the generic index. The mean position of each vertex across the full sample was considered as the average position of all vertices that carries the same index. The resultant face was an average facial mesh at the centre of the facial variations across the study sample.

This method appeared to be more reliable than the previously published data (278). Increasing the study sample would be highly advantageous for future studies.

4.4.2 The corresponding 3D facial soft tissue changes in response to Le Fort I maxillary advancement.

4.4.2.1 Euclidean distance measurements

The average pre-operative and post-operative faces were superimposed on the eye and nasal bridge regions. The forehead region was not used in this analysis because it was deficient in some of the averaged facial meshes which affected the position of the forehead in the average face. Figure (42) showed good accuracy of superimposition by expressing a predominant green colour on the region of the superimposition and the surrounding areas. Since the average face was constructed by averaging conformed facial meshes which belong to the same generic mesh, the vertices indexing were still valid and the two meshes had an identical number of triangles. The colour assignment was generated by cross-matching the vertices indices of the two images creating a corresponding distance colour map. Some of the areas on the mesh surface were assigned with the colour red which indicated a significant movement, even though they were extremely close to the corresponding mesh surface. This was due to the detection of mesh sliding movement which was completely overlooked in the classical colour surface analysis. Figure (61) shows the difference between the two analyses, the closest point correspondence and the anatomical dense correspondence, of cases which had had a Le Fort I advancement osteotomy. It is clear that a major area around the cheeks, nose and chin were overlooked or misinterpreted when the closest surface distance, (figure 61 A) was applied. Figure (61 B) shows the corresponding distance which reveals an area of additional changes involving chin, cheeks and nose region. However the classical inner and outer surface colour scale assignment (inner blue, outer red) was still considered. Using the Euclidean distances obscured the directionality of the

change, the red colour at the chin may be due to an upward, downward, right or left movement of soft tissue following surgery. To solve this problem, a separate analysis of each dimension was developed.

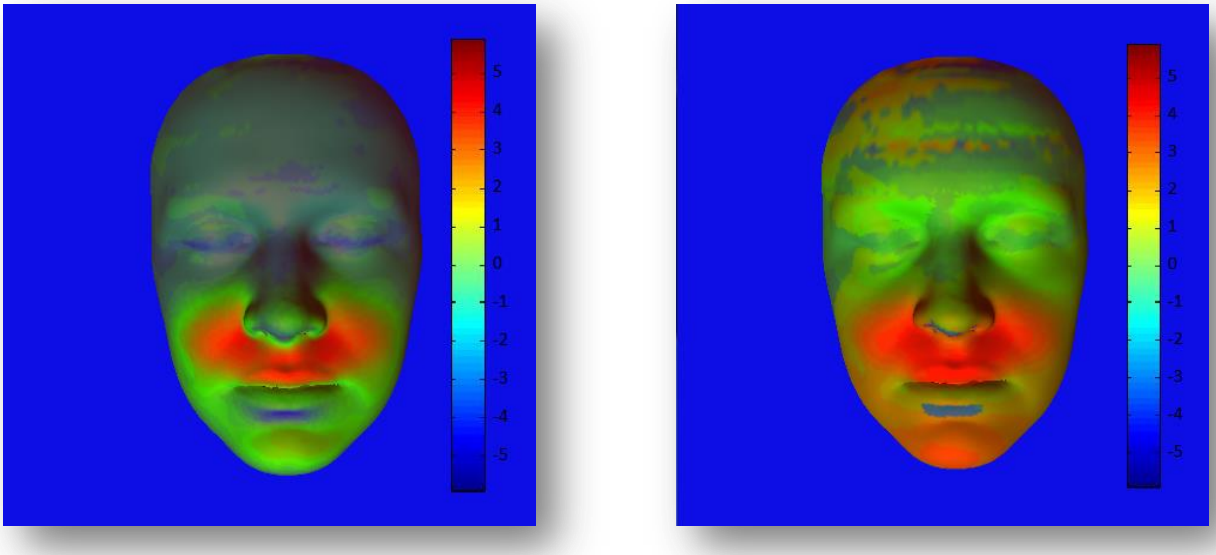

A B

Figure 61: Comparison between classical colour map A, and the corresponding analysis B.

4.4.2.2 Directional changes measurements

Surface distance, in a form of a colour map, is commonly applied for a descriptive analysis of surface changes (276), however, it lacks the directionality of the change. The classic landmark based analysis provided some information regarding the direction of the displacement at selected regions (17–20). Verdenik *et al.*, 2014 modified this approach to overcome this issue, four horizontal and two vertical planes were established anatomically to segment the facial surface into ten regions. The method provided additional regional information without the need for measuring the change at certain landmark. However, the segmentation procedure was not representative of the anatomical regions, especially in the paranasal region. It was also assumed that most of the changes were in the A-P direction. The authors commented that the changes around the lower lip and chin areas showed minimal change. However, they also noted significant change in the submandibular region in an upward direction. This contradiction was due to the fact that the method used for the analysis (closest surface distance) did not detect the upward sliding of the facial soft tissue mesh that occurred at the lower lip and chin area, unlike the submandibular region

where the upward surgical movement set the two surfaces apart, therefore, the changes were detected only in the submandibular region. With our approach, anatomical correspondence (dense correspondence analysis) has the ability to detect mesh sliding and to produce an accurate analysis of the changes at this region.

In this study, the application of the dense correspondence analysis combined the advantage of anatomical landmarking and the comprehensive surface analysis which is desirable and innovative.

The results presented by the corresponding colour map in the x (medio-lateral) dimension were novel, (figure 43). Most of previous studies focused on the A-P changes of facial morphology at the mid-facial region following Le Fort I osteotomy (147,187,201,281–284); other directional changes were largely overlooked. In addition to the well-defined forward displacement of the mid face soft tissue, the four striking features observed in this analysis were the lateral stretching of the upper lip and paranasal areas; the limited effect of surgery on the lower lip vermilion and oral commeasures; the vertical and forward chin movement and lastly the shortening of the nostril height associated with flaring of the alar cartilages.

The detected changes In the x (medio-lateral) dimension (figure 43 A) on the nose including widening of the nostrils, were in agreement with the vast majority of previous published studies (147,161,259,285). However, this effect was evident at the alar curvature more than the alar base. This may be due to the fact that the cases in this study had a nasal cinching stitch which might have reduced the alar base width. This observation was in agreement with Metzler *et al.*, 2014 (282). However, their measurements were based on linear distances between anatomical landmarks whereas in this study the total alar base region and alar curvature surfaces were analysed more comprehensively.

Keep in mind that Le Fort I maxillary osteotomy is performed to address the underlying maxillary hypoplasia with its characteristic soft tissue facial configuration. One of these soft tissue characteristics is the narrow alar base. Therefore, it is not unusual to allow some widening of the alar base to occur following surgery to restore normal facial appearance. It is difficult, however, to

report on the effect of cinching stitch on the width of the nostrils and whether this effect was intended.

The main detected effect of the Le Fort I osteotomy on the mid face region was the lateral widening of the upper lip and the paranasal areas. To date, no previous studies have reported on similar findings. Metzler *et al.,* 2014(282) reported on an increase in the upper lip philtrum width following Le Fort I osteotomy. On the other hand they showed a limited change of the upper labial width. This was not in agreement with our study. This disagreement was due to the fact that the labial width was measured as the linear distance between the two oral commeasures. We demonstrated that the expansion of the upper lip was evident at a higher level outlining the oral commissures as anatomical boundaries of that expansion. van Loon *et al.,* 2015 (286) reported an increase in the upper lip volume following Le Fort I advancement. Our conclusion was that the widening of the upper lip and paranasal regions were a result of an increase in fullness in these regions secondary to surgery and the changes were limited to their anatomical boundaries.

Vertical skeletal maxillary displacement was minimal in the study sample. Soft tissue vertical displacement was only observed at the nostrils and chin (figure 43 B). No marked vertical changes were observed at the upper lip region (0mm-0.5mm). This was combined with a relatively higher upward displacement observed at the naso-labial junction and sub-alar area. This led to the conclusion of an increase in lip length following Le Fort I advancement surgery. This result was in agreement with previous studies(281). The lower lip on the other hand showed a generalised upward displacement in response to the Le Fort I osteotomy. However, the lower lip vermilion border was relatively stable within (0mm-0.5mm) of the pre-operative position; this observation led to the assumption that the lower lip had shortened vertically secondary to Le Fort I osteotomy. At the chin area, major upward displacement had occurred which was relatively confined to the chin region and faded away laterally. Although the mean vertical maxillary displacement was minimal, the changes were observed at the chin secondary to the mandibular autorotation as a result of posterior maxillary impaction.

The red colour at the nostrils and nasal tip suggested an upward movement of this region secondary to Le Fort I advancement osteotomy. This result was in agreement with previous studies (281,285).

In the antero-posterior z dimension (figure 43 C), there was an obvious forward movement of the mid face region at the upper lip, paranasal areas and nostrils with a less extent at the chin region. These results were predictable with advancement of the maxilla at Le Fort I level and were in agreement with the previous studies (161,259).

Interestingly, the tip of the nose did not show significant change in the A-P direction; this was associated with a significant forward displacement of the alar cartilages and columella of the nose. The combined effect in x, y and z dimension could be described as compression of the nostrils in the A-P dimension which were expressed as shortening of the columella and widening of the alar cartilage curvature. This result was in partial agreement with previous studies which suggested shortening of the nostrils and increase of the alar width(281,287). However, the majority of these studies reported a significant nasal tip protrusion following Le Fort I osteotomy(281,285,287). The reason behind this disagreement might have been the minimal maxillary impaction in our study, the removal of the anterior nasal spine and the reduction in the inferior borders of the pyriform aperture during Le Fort I osteotomy.

The relationship between the soft tissue surface changes and the underlying anatomical structures was clear. The orientation of the muscles and their attachments played a marked role in the expression of the overlying soft tissue changes, (figure 62). The bilateral group of muscles of facial expression which originated from the side of the bridge of the nose including the *levator labii superioris alaeque nasi* and from the zygomatic bone including *zygomatico major*, *zygomatico minor* and *levator labi superioris* muscles which are inserted in the facia of the upper lip and the muscle fibre of *orbicularis oris* muscle. This group of muscles were stretched by the advancement of the maxilla, which contributed to the augmentation of the relatively depressed area at the paranasal region. These effects were limited superiorly by the origin of these muscles and laterally by the anterior superficial fibres of masseter muscle which were not affected by the surgery. This was in agreement with previous

studies which proposed similar boundaries of the soft tissue changes at these regions of the face(279).

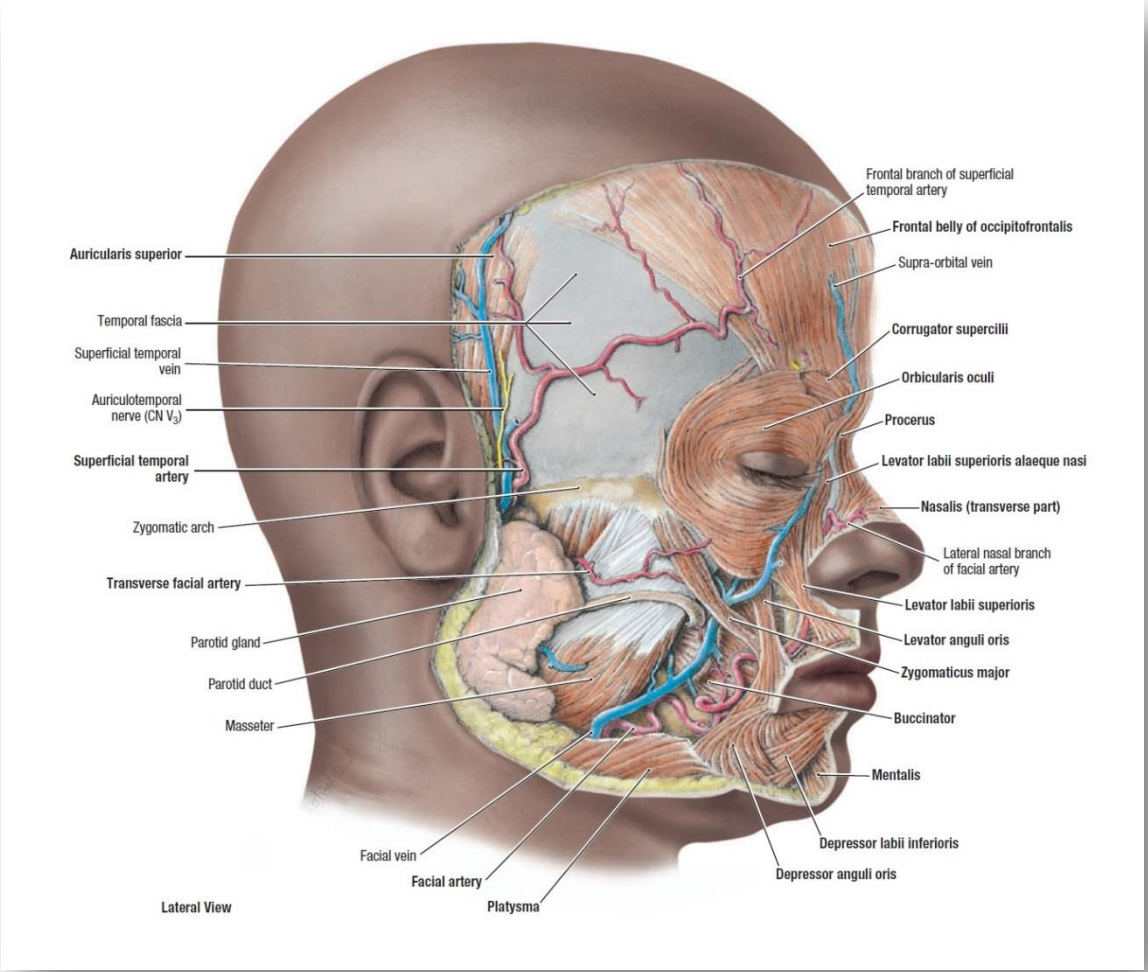

Figure 62: Anatomy of mid-face muscle) quoted from Grant's atlas of anatomy)

4.4.3 The corresponding 3D facial soft tissue changes in response to BSSO mandibular advancement.

4.4.3.1 Euclidean distance measurements

Figure (63) shows the difference between two methods of analyses of the BSSO mandibular advancement group, the closest point correspondence and the anatomical dense correspondence analysis. It is clear that changes around the cheeks, nose and chin were completely overlooked or underestimated when the closest surface distance, figure (63-A), was applied. Figure (63-B) showed the corresponding distance which revealed more extensive but homogenous pattern

of changes involving the chin, lower lip and extended back to the cheeks and gonial angle regions. Colour coded analysis obscures the directionality of the change. This means the red noted colour at the chin may be an upward, downward, right or left direction. To solve this problem, a separate analysis of each dimension was again used.

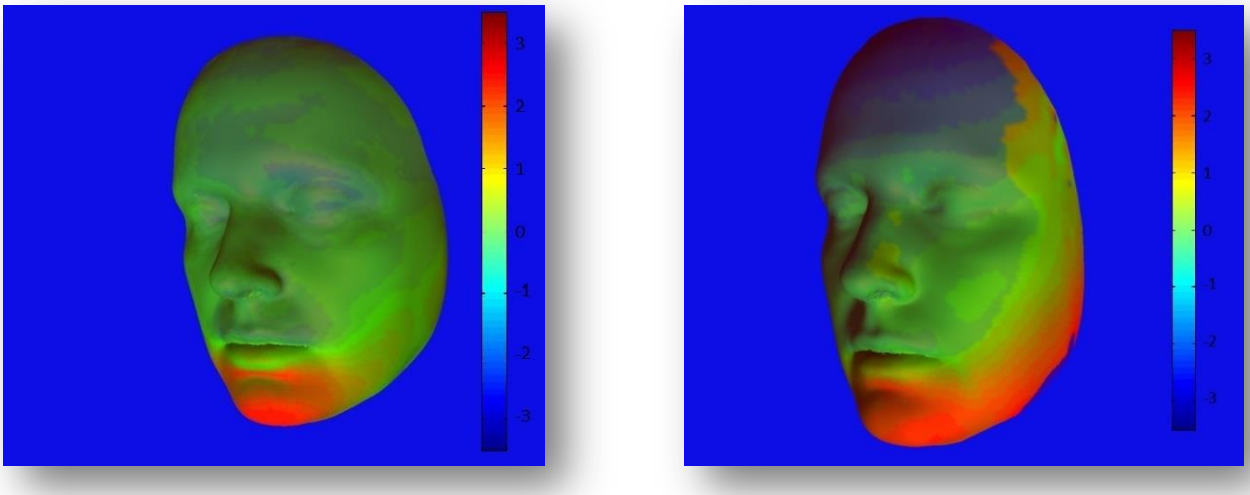

A B

Figure 63: Comparison between classical colour map A, and the corresponding analysis B.

4.4.3.2 Directional changes measurements

The current study attempts to clarify the three dimensional changes of the soft tissue following mandibular advancement surgery in a comprehensive and anatomically guided surface analysis. Every effort has been made to standardise the multi stage method of assessment. The small sample size (12 cases) was due to the strict exclusion criteria. BSSO mandibular advancement with minimal lateral shift surgery with rigid fixation was selected and cases with adjunctive genioplasty were excluded.

The colour map was stratified to reveal the directional changes in each of the three dimensions. This helped in providing a comprehensive 3D description of the soft tissue changes following mandibular advancement. The results of this study clarified the areas of controversy and introduced further details of the soft tissue changes following BSSO mandibular advancement surgery.

Facial soft tissue changes following BSSO mandibular advancement has been investigated previously either by profile assessment using 2D cephalometric analysis (288–290) or by the 3D soft tissue analysis (159,288).

Apart from the frequently reported direct forward movement of the chin soft tissue, the lower lip showed less forward movement, this displayed as a lower intensity of the colour red when compared to the chin region, while the upper lip showed a backward movement marked by a light blue colour, (figure 45). This was in agreement with most of the published studies, (223). In addition, a wider lower lip and narrower upper lip were also demonstrated, (figure 45), as a result of mandibular advancement.

Mobarak *et al.,* 2001 (222) showed that the lip thickness decreased as the mandible moved forward. This could be logically clarified by the tendency of the soft tissue, on both sides of the lip, to move laterally, stretching the lip and reducing its thickness, (figure 45). Stretching the lower lip laterally gave the mandible a broader aspect, which was in agreement with previous studies(291).

Reduction of lower lip eversion following mandibular advancement was reported (289,291). This in agreement of our findings and was clearly demonstrated by the minimal change in both the vertical and A-P position of the vermilion part of the lower lip when compared to the marked forward and downward displacement of the cutaneous part (figure 45).

Minimal vertical change in the vermilion part, combined with a marked downward displacement of the cutaneous part of the lip was observed (figure 45). This was in agreement with Raschke *et al.,* 2013 (291), who showed a marked Lengthening of the lower lip.

In general, the change of the facial soft tissue in response to mandibular advancement surgery was confined to the anatomical borders of the underlying skeletal structures. Muscle orientation and attachments played a marked role in controlling the expression of the overlying soft tissue changes as shown in figure (64). The firm control of the supra labial muscle group kept the changes at the commissures of the mouth to a minimum and the sharp colour change on the cheeks in both A-P and vertical dimensions appeared to be limited superiorly to

the position of the teeth. Stretching of the platysma muscle in the A-P dimension, in addition to the change in the orientation of the masseter muscle following mandibular advancement, (292) was clearly responsible for the well-defined expression of the displacement of the overlying soft tissue especially at the cheeks regions.

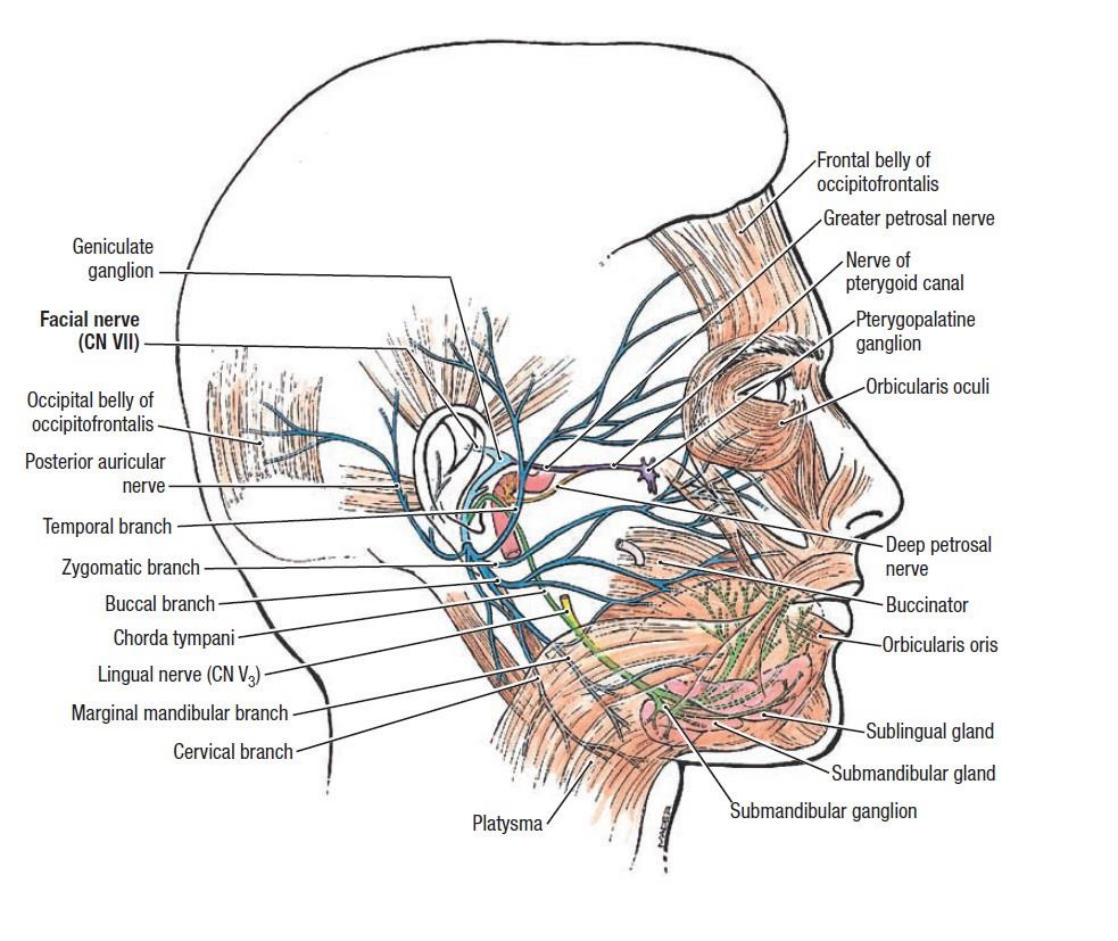

Figure 64: Anatomy of mandibular muscles (quoted from Grant's atlas of anatomy)

4.4.4 The corresponding 3D facial soft tissue changes in response to bimaxillary advancement.

4.4.4.1 Euclidean distance measurements

Figure (65) shows the difference between the two analyses, the closest point correspondence and the anatomical dense correspondence analysis, of the bimaxillary advancement group. It is clear that major areas around the cheeks,

nose, mandibular borders and chin were completely overlooked or misinterpreted when the closest surface distance, (figure 65,A), was applied. Figure (65-B) shows the corresponding distance analysis which revealed a more extensive displacement which extended back to the cheeks and gonial angle regions. A separate analysis of each of the three dimensions (x, y and z) was carried out to investigate the changes in detail.

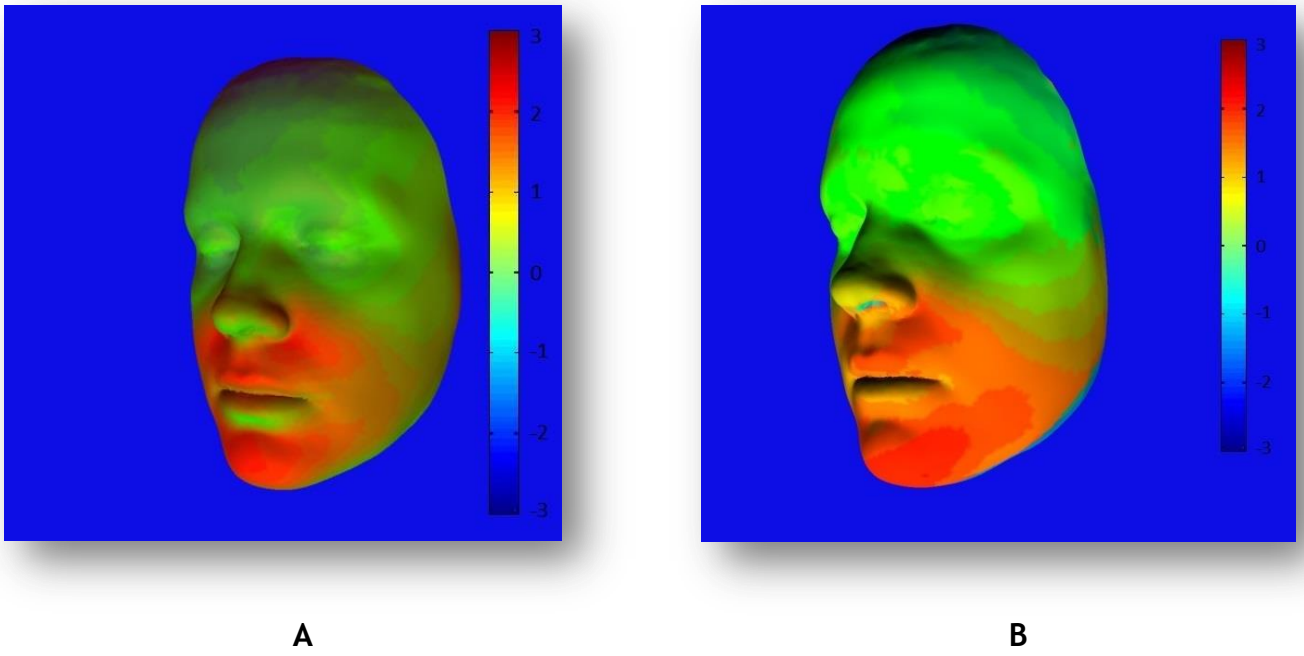

A B

Figure 65: Comparison between classical colour map A, and the corresponding analysis B.

4.4.4.2 Directional changes measurements

The method used in this study for the analysis of soft tissue changes is unique, which enabled a comprehensive 3D description of the soft tissue changes following bi-maxillary advancement surgery. Limited publications were found focusing on soft tissue changes following bimaxillary advancement surgery; this might be due to the fact that the surgical procedure was applied mainly for treatment of obstructive sleep apnoea cases with most of the publication focussed on its effect on the pharyngeal airspace rather than facial soft tissue changes. However, bi-maxillary advancement surgery has been used for the correction of high angle class II cases (274).

The earlier 2D and 3D landmark based analysis helped in identifying the direction of the displacement at selected anatomical sites on the mid and lower face regions following maxillo-mandibular advancement surgery (134,274,293) but the extent of these changes were not examined. Surface distance, in a form of colour coded map, was commonly applied as a descriptive analysis (276). However, the lack of anatomical correspondence was its main limitations.

In this study, the application of the anatomical dense correspondence analysis combined the advantages of the anatomical landmarking and the comprehensive surface analysis. Since the average pre and post-surgery facial surface meshes have the same number and index of the vertices, the correspondence between the two meshes was built on the anatomical bases and the displacement of each vertex from the pre-operative to the post-operative position was calculated. The results of the all measurements of all the vertices on the facial mesh were displayed as a colour coded map to simplify the analysis. A similar method was previously applied, (152,294), to monitor facial growth and to evaluate facial asymmetry correction where each point on the facial mesh was tracked to its displaced position, the displacement was displayed as a coloured line joining the two positions. However, in their analysis, it was not possible to determine the direction of change since the classical method of the outward-inward colour map configuration was applied. In our analysis, soft tissue changes in each the x, y and z dimensions were analysed separately with a unique colour coding display. This enabled the current analysis to investigate the changes in a more comprehensive manner and enabled the analysis of the extent of lateral expansion of the midface in response to maxillary advancement which was not previously reported.

The use of the average pre and post-surgical face mesh for soft tissue analysis was reported (295). Gerbino *et al.*, 2014 (295) reported on the use of average pre- and post-surgery facial meshes to analyse soft tissue changes following maxillo-mandibular advancement surgery for treatment of obstructive sleep apnoea (OSAS). The sample size was close to our study (10 cases) and the results were in partial agreement. They also reported minimal widening of alar curvatures. However, their study also showed widening at the commissure of the mouth which was in disagreement with our study. The reason behind the disagreement might be due to the fact that their measurements were based on

the linear distance between the right and left chilion points passing through subnasali and pogonion points (Chil r- Sn- Chil l). Their measurements indicated an increase in fullness of the upper lip but not necessarily widening of the inter-commissural distance. Our findings suggested widening of the upper lip at a higher level whereas the inter-commissural distance remained constant.

The colour distribution on the lower lip showed narrowing of the sub commissural regions. The surgical movements involved advancement of the mandible with an element of vertical movement, especially in open bite cases, which might have contributed to the noted soft tissue behaviour of the lower lip. The response of the lower lip to these skeletal movements is complex. Three factors might have contributed to the noted soft tissue response to surgery: The vertical element of mandibular and/or maxillary surgical displacement; the magnitude of maxilla-mandibular advancement and the achievement of lip seal following bimaxillary advancement surgery.

The extents of the soft tissue changes were confined to the anatomical boundaries of the affected regions. The medio-lateral changes at the upper lip and paranasal regions were limited to the muscular attachments around the osteotomy site where as the effect of the BSSO advancement was localized to the lower lip and commissures of the mouth, which are the most affected regions by surgery. It is difficult to separate the effect of the two osteotomies since the soft tissue acts as a single unit and changes in one region may be affected by changes in other regions. This contributed to the reason for the difference in the response of the lower lip noted in Mandibular advancement cases in the x dimension and not seen with a combined maxilla-mandibular advancement.

In the A-P dimension, the effect of the bi-maxillary advancement on the midface extended posteriorly more than what was observed with a Le Fort I maxillary advancement alone. The reason might be the loss of the posterior boundaries of this region as a result of the change of the masseter muscle orientation following BSSO mandibular advancement (292).

The vertical changes were less obvious than those in the other dimensions. This was in agreement with previous studies (293) Vertically, shortening of the lower

lip was observed as a combined display of a red colour at the cutaneous part of the lower lip down to point B and yellowish green colour at the vermillion part, whereas minimal lengthening of the upper lip was observed with green colour on the upper lip and orange colour in the naso-labial junction and supra commissures regions. These two observations were in agreement with the previous studies of Gerbino *et al.*, 2014 (295) and Conley and Boyd 2007 (293).

4.5 Soft tissue prediction

The relationship between hard and soft tissue changes has been extensively investigated over the past decades using 3D imaging tools (170,235,296,297). Novel approaches were applied for prediction of soft tissue changes following orthognathic surgery, which included three main approaches; Mass Spring model (MSM); Linear/Non Linear Finite Element Model (FEM) and Mass Tensor Models (MTM). In general, the volume tissue in-between the skin surface and the bone surface is occupied by mathematical dense tetrahedron prisms or individual connectors (298,299). Each prism or connector has a fixed side at the bone surface and a free side at the skin side. Movement of the jaw bones introduces a stress on the overlying soft tissue volume, which in turn results in an internal strain. The associated algorithm reacts to this by minimizing the energy through displacing the soft tissue side to re-establish equilibrium state (227). The magnitude of skin surface displacement is directly dependent on the function built into the algorithm that defines the stiffness at each connection site. Some of these methods were found to be more accurate and more reliable than the others but there was an agreement on the need for improved soft tissue prediction following orthognathic surgery.

The approach in this study is unique, with no reliance on the inter-surface connectors or on the stress strain correlation. Instead, a statistical model was built on the actual soft tissue surface changes associated with the skeletal tissue displacement.

4.5.1 Mass spring model (MSM)

Spring mass model (MSM) originated in the computer animation world (Keeve *et al.*, 1998, Teschner 2001). The application of this method for prediction of facial soft tissue changes in response to orthognathic surgery was based on quoting constants from pure engineering contexts of materials addressing stress-strain properties and applying them for the prediction of soft tissue changes. The prediction algorithm of this approach relies on a dense mesh of connectors between each vertex on the soft tissue surface mesh and the nearest point on the hard tissue surface. These connections were described as springs and each

three springs at the corner of a mesh triangle formed a tetrahedral prism. The stiffness of these springs is determined by a constant representing the stress-strain (stiffness) value which is only an approximation to the soft tissue stiffness and has no biomechanical characteristics.

The weakness in this approach is two folds; first is the assumption of the similarity of the behaviour of soft tissue to that of artificial material, and second is the assumption of a linear stress-strain relationship. It is well known from previous literature that biological tissue is anisotropic, inhomogeneous and has a non-linear stress-strain relationship (300). Human soft tissue is composed of a multi layered volume of tissues which contains variable percentages of various tissues types, including muscle fascia and fat, each of these had its own stress strain curve which is not necessary a linear correlation. There is no way to really control the volume conservation to resemble biological tissue behaviour during simulation, even when the model is extended with extra 'volume spring' as described by Molleman *et al.,* 2003 (227).

Keeve *et al.,* 1998 (230) proposed an approach to solving these problems by introducing a multi layered spring with different stiffness values in addition to a non-linear stress-strain relationship. The total spring stiffness value is the summation of its layers. This improves the quality of the prediction of soft tissue changes due to surgery. However, the choice of the value was still based on pure physical, non-biological material properties. The results of the experiment showed lower accuracy compared to the finite element analysis. However, a considerable gain in computational time was achieved with this method (230). 3dMD vultus software is one of the surgical prediction planning software packages that used this algorithm.

4.5.2 Finite element model (FEM)

The analysis of facial soft tissue changes using finite element analysis is based on a similar concept to MSM in terms of correlating each vertex on the soft tissue mesh to a single point on the skeletal surface. However, the connections in this method are treated individually rather than the tetrahedral prisms structure of

the MSM and their stiffness is a function of stress-strain values based on biological tissue properties. These values were obtained mainly from the online source "Diffpack" (301). For a linear FEM, the assumption of the linearity of facial biomechanical behaviour was based on the work of Gladilin *et al.*, 2001 (302) who described the biomechanical behaviour of soft biological tissue as an isotropic, homogenous and linear elastic continuum. However, it is well known from previous studies that biological tissue is anisotropic, inhomogeneous and has a non-linear stress-strain relationship (300). The stiffness values of FEM are obtained from different tissues, mainly thigh muscles and forehead tissues. The results showed better prediction accuracy when compared to the MSM approach (299). However, the assumption of a linear stress-strain correlation was a major source of deficiency of this method in addition to the inability to separate each connection into layers as in the MSM approach, rendered it short of an accurate soft tissue prediction. Moreover, the high computational power and long computational time (up to 10 minutes) made it difficult to use in a regular clinical settings (299).

Ulusoy *et al.*, 2010 (303) proposed a solution to the computational demand and the high processing time named "Dynamic volume spline". This approach was based on condensing the analysis into number of selected vertices scattered on the facial mesh surface then joining them with a continuous spline (303). This approach reduced the processing time but introduced another source of error in the areas between the selected points.

In an attempt to improve the prediction accuracy of the soft tissue changes following orthognathic surgery, Delingette *et al.*, 1998 (304) applied a biomechanical FEM that has non-linear stress-strain correlation. This was found to be more accurate in predicting facial changes (304). However the difference between the two models was non-significant.

In FEA, the tetrahedron prisms of the FEM are not segmented into layers as with the MSM. To overcome this shortcoming, Delingette *et al.*, 1998 and Chabanas *et al.*, 2003 (231,304) structured the skull, muscle and skin in the patient's face with three to four connected 3D mesh layers to reconstruct patient's realistic

facial anatomy. The muscles of the face were individually modelled at their anatomical position with interconnected meshes allowing each mesh to deform individually under the stress generated by surgical skeletal displacement. This approach required a higher computational power; it is individualized to each patient and an operator input is necessary to model each muscle.

Although the FEM in its linear and non-linear types has a higher level of accuracy compared to the mathematical mass spring model (227,299), the marked higher computational time was a disadvantage. Molleman *et al.,* 2007 highlighted the fact that there is always a trade between the accuracy of prediction and the processing time (227).

VISU simulation model as a novel modification of the classic FEM was introduced by Sarti *et al.,* 1999 (232). The CT image was segmented in three components; skin surface, bone surface and the bulk of tissue in-between. The simulation algorithm applied the finite differences on the acquired CT grid directly and utilised the bulk of soft tissue volume rather than the bone and soft tissue surface meshes thereby reducing the computational cost without losing details of the anatomic structures. The algorithm utilized the modified linear elasticity equation system(305) based on the in vivo mechanical properties of skin and muscles described by Black and Hastings 1989, which assumed that soft tissue responded as a linear, elastic, isotropic material (306).

This algorithm was later incorporated in commercially available software (SurgiCaseCMF®). In a 10-patient series, Marchetti *et al.,* 2006 (255) reported 80% reliability and reproducibility for VISU. Bianchi *et al.,* 2010 (296) reported 0.94 mm ±0.9mm absolute error with an average 86.8% of the errors remaining below 2mm.

4.5.3 Mass tensor model (MTM)

This method could be seen as a combination of the MSM and the FEM. On one hand the model preserves the easy architecture of the MSM and on the other hand the model has the bio-mechanical relevance of FEM. The original MTM was

introduced by Cotin *et al.,* 1999 (235), modified by Schwartz *et al.,* 2005 and Molleman *et al.,* 2007 (300)(227) to be applied for soft tissue prediction. The algorithm has been incorporated in commonly used software packages including Maxilim prediction software. In MTM the modelled object is subdivided into tetrahedral mesh prisms. Inside every tetrahedron, the field is defined by a linear interpolation of the displacement vectors of the four vertices as defined by the finite element theory using biomechanical elastic constants.

During simulation of the surgical facial changes, the displacement at one side of the prism is fixed to represent the skeletal displacement. Vertices at the other side of the prism are then free to move affected by the vectors of the generated elastic forces. The new rest position of these free points is established when total elastic force in all dimensions is zero while the object is at rest.

Using this novel algorithm, Molleman *et al.,* 2007 (227) were able to predict soft tissue changes in response to orthognathic surgery at up to 0.6 mm accuracy, with 90% of the errors remained below 1.5 mm. However, the linear stress/strain model, on which this method is based, might be the cause of constant overcorrection of specific regions on the face including the upper lip (307).

All previous methods share the common concept of employing engineering oriented mathematical algorithms, which were originally applied to simulate mechanical behaviour of a stressed raw materials or alloys based on their pure physical properties, and modifying this to simulate the biomechanical behaviour of a biological tissue under stress. The methods could be divided into two main groups; the first group are those who appreciated the differences between biological tissue and raw material properties such as the non-linear FEM by Delingette *et al.,* 1998 (304) and the anatomy based FEM by Keeve *et al.,* 1996 (301), with their algorithms built on a non-linear stress-strain correlation. Those researchers were faced with individual tissue variations in addition to human differences, which rendered their analysis to be of a limited accuracy with a high need for computation power. These might be the reason that none of these methods had broad clinical applications.

The second group of prediction methods are those which ignored the difference between the biological tissues and the raw materials and built the analysis on linear stress- strain correlation hypotheses such as MTM (227), Linear FEM (299) and VISU prediction (232,255).The algorithm expressed relatively lower simulation accuracy (299). However, they showed a reduced need for computational power with a higher level of reproducibility (255).

All the methods were not fully successful in bridging the gap between the raw materials and biological tissue to develop a reliable prediction of soft tissue changes following orthognathic surgery. The algorithm that was developed in this study is based on decomposing the actual soft tissue changes following orthognathic surgery into its principal components of the three-dimensional shape variation and finding the correlation of each to the associated skeletal displacement. This was accomplished by applying the principal component analysis (PCA) to the CBCT scans of a homogenous cohort of cases to develop the prediction algorithm. The identified principal components would predict the facial shape changes in response to orthognathic surgery for future cases.

In this method, the principal components of the shape difference for soft tissue prediction were derived from the actual soft tissue changes which are biologically reliable. The simple statistical equation of PCA and the relatively low required computational power allowed an instant prediction. The segmentation of the face into 6 anatomical regions (nose, upper lip, lower lip, chin, right paranasal region and left paranasal region) facilitated region specific analysis and produced an anatomically guided prediction.

The estimation of the soft tissue changes is based on the pre analysed PCA values where the skeletal surgical movement is simply a one numerical value in each of the x, y and z dimensions. This enabled the algorithm to predict soft tissue changes without the need for the skeletal surface model similar to the FEM and MTM prediction methods. In other words, prediction of soft tissue changes could be applied to any facial soft tissue model such as stereophotogrammetry image or laser scanned image simply by providing the numerical three-dimensional skeletal surgical movements. The overall accuracy

of the prediction was comparable to previous methods. However, prediction of the changes at specific regions such as the upper and lower lip showed better results when compared individually. The method could be applied to a variety of facial deformities including cleft lip and palate, facial paralysis and facial reconstruction surgery without the need for CBCT scan. The prediction of various facial motions could also be achieved with the appropriate application of a 4D training set.

4.5.4 Measurement of prediction accuracy

The aims of the prediction algorithms are to simulate the surgical outcome of facial soft tissue changes which will help in patient education and, more importantly, in finalising a surgical treatment plan. Thus, the accuracy of prediction is crucial.

Three general criteria should be considered when establishing a method to evaluate the prediction accuracy. Firstly, the measurements should disclose errors at all the vertices of the 3D mesh rather than at a few selected points; secondly the measurements of prediction accuracy using 3D surface mesh should not be based on the mean value of the whole face as this will camouflage errors at specific facial regions; and lastly a reliable form of correspondence should exist to allow tracking of these vertices.

Most of the previously published studies which evaluated the accuracy of soft tissue prediction following orthognathic surgery were either based on surface analysis or evaluation of the changes at certain landmarks. Surface based analysis is the most common approach(158,170,227,296,303,308). The analysis is based on calculating the square root of the distances of all vertices on the predicted facial meshes to the nearest points on the real post-operative facial surface mesh. The main drawback of this method is the lack of a true correspondence between the two meshes and more important is the reliance in some studies (227,303)on the whole facial mesh for estimation of the mean value of the prediction accuracy. The inclusion of anatomical areas away from the surgical site, including the eye region which has a low error values, could

camouflage the relatively higher errors in specific regions of the face. Bianchi *et al.*, 2010 and Marchetti *et al.*, 2011 (170,296), tried to overcome this problem by including the lower and midface regions only in the analysis in addition to setting a threshold for the acceptable error and calculated the percentage of the vertices which lies below that level. Their method gave a better description of the prediction accuracy (86.8% of vertices lower than 2mm of error) using SurgiCase® software. However, this was not region specific, in addition to the classical lack of the anatomical surface correspondence. Further refinement of the analysis was carried out by Shafi *et al.*, 2012 (158) and Khambay *et al.*, 2014(309). Both studies added the segmentation of the facial meshes into various anatomical regions to measure the relative accuracy at each area using Maxilim and 3dMD Vultus software packages respectively. Although this method provided a more detailed analysis of regional error, it still suffers from the fundamental lack of anatomical correspondences in addition to the inevitable subjectivity in the segmentation of the facial regions. However, to avoid the latter problem, 90th percentile of the mesh surface was considered in the analysis.

On the other hand, landmark based analysis was applied to investigate the accuracy of soft tissue change prediction following orthognathic surgery. Hemelen *et al.*, 2015 (310) applied landmark based analysis to investigate the accuracy of 3D soft tissue prediction. This approach has the advantage of establishing anatomical correspondence between landmarks on the predicted and post-surgical facial meshes. However, using few landmarks on the face does not represent the surface changes comprehensively.

In an attempt to overcome the deficiencies associated with both methods (surface and landmarks based analyses), some studies were undertaken to incorporate the two methods in the analysis (237,311). The combined analysis benefited from the advantages of both of them but it also included their associated limitations. Neither the limited reliability of the closest point correspondence associated with the surface distance measurements, nor the deficient surface representation of the landmarks based analysis were addressed.

In this study, the accuracy measurement was based on the dense anatomical correspondence provided by the conformed generic mesh index. This approach combined the comprehensiveness of surface analysis with the reliability of anatomical correspondence.

"Leave-One-Out cross-validation" is a well-known statistical method which was applied in this study to overcome the problem of the relatively small sample size. The method considers one of the total 30 samples included in this study as a tester while the remaining 29 samples as training set for the PCA. The result of the training set is then applied to predict the surgical results of the tester case and compared against its postoperative image. The next step is to choose the next case in the 30 cases sample as a tester and follow the same root, and so on. This produced 30 measurements for the analysis of the accuracy prediction method of soft tissue changes to orthognathic surgery. The procedure was applied six times one for each of the segmented facial region.

The application of the dense correspondence analysis in facial anthropometry and specifically for orthognathic surgery, was first introduced by Mao *et al.*, 2006 (176). The approach not only combines the advantages of the landmarks based analysis and surface based analysis, but also addresses most of their deficiencies. The applied generic mesh in this study consisted of over 1000 vertices, the use of the generic mesh index made every single mesh vertex as an actual corresponding landmark between the analysed images. This addressed both issues of the lack of actual correspondence and lack of surface representation associated with the previous methods.

The main advantages of our analysis could be summarised in the following points:

1. The use of the generic mesh index provided a comprehensive and accurate method for analysis of the facial soft tissue changes in response to orthognathic surgery.

2. The adoption of the novel directional change analysis, based on the conformed generic mesh index enabled the analysis of errors in each of the x, y and z dimensions. This provided more detailed information on the prediction accuracy in 3D.

3. The segmentation of the face into anatomical regions of interest lends itself to a comprehensive and specific analysis of the errors of soft tissue prediction in response to orthognathic surgery.

4. The adoption of the true mean and standard deviation, rather than the absolute mean used in previous studies (158,309), augments the credibility of the results, as it shows the variation of the measurements around the mean. In addition, it enables the differentiation between over and under estimation of facial soft tissue changes in response to surgery which was not possible using the absolute mean distance measurements. However it is essential to consider the standard deviation for the interpretation of the mean values.

In general, the mean±SD of the difference between the predicted and actual changes of facial soft tissue in the A-P (y dimension) was equal or lower than the lowest previously recorded value of 2 mm (158,170,296,309) at the lower lip, nose and right and left paranasal regions. However, a slightly higher error was recorded for the upper lip (0.12 mm ± 0.95 mm) and chin (-0.03 mm ± 2.19 mm) regions.

A general tendency of overestimation at the upper lip change in response to Le Fort I osteotomy was observed. This was in agreement with Shafi *et at.,* (158) and Ullah *et al.,* 2014 (236), who recorded similar findings using the MTM and MSM algorithm respectively.

The prediction approach is a promising prospect. However, as with any other approach, some limitations do exist. Nevertheless, most of these are

manageable and could be addressed through further research. The main weaknesses can be summarised as follows:

1. The relatively high cumulative baseline errors associated with the preparatory stage up to the final prediction. Errors associated with generic conformation including landmarking accuracy which imposes a total of around 1.5mm baseline error. Further improvement of the landmarking accuracy and conformation algorithm could address most of these errors.

2. The low sample size used as training set for the prediction algorithm. Although the level of the prediction accuracy is close to the baseline error values, increasing the number of the training set samples will improve the accuracy of prediction.

3. Increase the homogeneity in terms of phenotype by sub phenotypes.

5 Conclusions & Suggestions

Contents

5.1 Conclusions

Voxel based registration and surface based registration are both valid methods of 3D images superimposition with a comparable registration accuracy level. Voxel based registration; however, has the advantage of preserving the link between the skeletal and soft tissue structures during the registration process.

Direct DICOM slice landmarking is clinically applicable measurement method with an acceptable level of accuracy in measuring skeletal tissue displacement following orthognathic surgery in 3D with low intra- and inter-examiner landmarking errors.

Generic mesh conformation has an acceptable level of accuracy. Variable range of errors at different areas of the face were recorded, peripherally more than centrally, which were all within an acceptable range for clinical application.

The introduced dense correspondence analysis (directional analysis) was novel. New range of information regarding soft tissue changes following orthognathic surgery.

The novel statistical algorithm for prediction of soft tissue changes following Le Fort I advancement surgery was proved to be applicable, practical and produced low prediction errors.

5.2 Suggestions for future studies

1. A larger sample size would be beneficial since more variation in surgical procedures could be specifically analysed. This could be achieved by establishing a substantial database, probably through multicentre collaboration.

2. The prediction algorithm in its current state predicts soft tissue changes following orthognathic surgery based on regional analysis. Further improvement on the prediction algorithm, including connection between facial regions to produce a full face prediction, will be the next step.

5.3 Possible applications

The promising approach of dense correspondence analysis opens the doors toward a simpler and yet more reliable tool of a multi-disciplinary applications including cleft lip and palate, facial paralysis, variable craniofacial reconstruction procedures and breast cancer reconstructive surgery. The novel approach of producing a reliable soft tissue prediction without the need for 3D radiography will be a significant addition to the current diagnoses and treatment planning protocol.

6 References

1. Moorrees CFA, Lebret LM. The mesh Diagram and Cephalometrics. Angle Orthodontics; 1962. p. 214–31.

2. Moorrees CFA, Venrooij ME van, Tandarts, Lebret LM 1., Carlton B. Glatky MA, Jr RK. New norms for the mesh diagram analysis. Am J Orthod. 1976;69(1):57–71.

3. Ferrario VF, Sforza C, Schmitz JH, Miani A. ORIGINAL ARTICLE A three-dimensional computerized mesh diagram analysis and its application in soft tissue facial morphometry. Am J Orthod Dentofac Orthop. 1998;114:404–13.

4. Lovesey EJ. The devet t of a 3-dimensional anthrop measuring technique. Appl Ergon. 1974;5(1):36–41.

5. Motoyoshi M, Arai HY, Ridge P. A three-dimensional measuring system for the human face using three-directional photography. Am J Orthod Dentofac Orthop. 1992;101:431–40.

6. Wu J, Tillett R, Mcfarlane N, Ju X, Siebert JP, Schofield P. Extracting the three-dimensional shape of live pigs using stereo photogrammetry. Comput Electron Agric. 2004;44:203–22.

7. Winder RJ, Darvann TA, Mcknight W, Magee JDM, Ramsay-baggs P. Technical validation of the Di3D stereophotogrammetry surface imaging system. Br J Oral Maxillofac Surg. 2008;46:33–7.

8. Burke P., Beard HF. Stereophotogranwnetry of the face. Am J Orthod. 1967;53(10):769–82.

9. Tzou C-HJ, Artner NM, Pona I, Hold A, Placheta E, Kropatsch WG. Comparison of three-dimensional surface-imaging systems. J Plast Reconstr Aesthet Surg. 2014;67(4):489–97.

10. Ras F, Habets LLMH, van Ginkel FC, Prahl-Andersen B. Quantification of facial morphology using stereophotogrammetry — demonstration of a new concept. J Dent. 1996;24(5):369–74.

11. Hajeer MY. Changes Psychosocial and Following Orthognathic Surgery Mohammad Younis Hajeer Thesis submitted to the University of Glasgow for the degree of PhD in Orthodontics Faculty. 2003.

12. Khambay B, Nairn N, Bell A, Miller J, Bowman A, Ayoub AF. Validation and reproducibility of a high-resolution three-dimensional facial imaging system. 2008;46:27–32.

13. Pfister A, West AM, Bronner S, Noah JA. Comparative abilities of Microsoft Kinect and Vicon 3D motion capture for gait analysis. J Med Eng Technol. 2014;38(5):274–80.

14. Macleod C a, Conway B a, Allan DB, Galen SS. Development and validation of a low-cost, portable and wireless gait assessment tool. Med Eng Phys. 2014;36(4):541–6.

15. Mishima K, Yamada T, Ohura A, Sugahara T. Production of a range image for facial motion analysis: a method for analyzing lip motion. Comput Med Imaging Graph. 2006;30(1):53–9.

16. Sjögreen L, Lohmander a, Kiliaridis S. Exploring quantitative methods for evaluation of lip function. J Oral Rehabil. 2011;38(6):410–22.

17. Al-Anezi T, Khambay B, Peng MJ, O'Leary E, Ju X, Ayoub a. A new method for automatic tracking of facial landmarks in 3D motion captured images (4D). Int J Oral Maxillofac Surg. 2013;42(1):9–18.

18. Ju X, O'Leary E, Peng M, Al-Anezi T, Ayoub A, Khambay B. Evaluation of the Reproducibility of Nonverbal Facial Expressions Using a 3D Motion Capture System. Cleft Palate Craniofac J. 2014 Dec 22. [Epub ahead of print] .

19. Shujaat S, Khambay BS, Ju X, Devine JC, McMahon JD, Wales C. The clinical application of three-dimensional motion capture (4D): a novel approach to quantify the dynamics of facial animations. Int J Oral Maxillofac Surg. 2014;43(7):907–16.

20. Popat H, Zhurov AI, Richmond S, Marshall D, Rosin PL. Determining normal and abnormal lip shapes during movement for use as a surgical outcome measure. J Oral Rehabil. 2013;40(5):348-57.

21. McCance A, Moss J, Wright W. A three-dimensional soft tissue analysis of 16 skeletal class III patients following bimaxillary surgery. Br J Oral Maxillofac Surg. 1992;30:221–32.

22. Moss JP, Mccance AM, Fright WR, Linney AD. A three-dimensional soft tissue analysis of fifteen patients with Class II , Division I malocclusions after bimaxillary surgery. Am J Orthod Dentofacial Orthop. 1994;105(5):430-7.

23. Kau, C.H., Zhurov, A.I., Knox, J., Chestnutt, I., Playle, R., Hartles, F.R., and Richmond, S. Reliability of measuring facial morphology. Am J Orthod Dentofacial Orthop 2005;128:(3)424-430.

24. Kau CH, Richmond S, Zhurov AI, Knox J, Chestnutt I, Hartles F. Reliability of measuring facial morphology with a 3-dimensional laser scanning system. Am J Orthod Dentofacial Orthop. 2005;128(4)424–30.

25. Ovsenik M, Perinetti G, Zhurov A, Richmond S, Primozic J. Three-dimensional assessment of facial asymmetry among pre-pubertal class III subjects: a controlled study. Eur J Orthod. 2014;36(4):431-5.

26. Perinetti G, Zhurov A, Richmond S, Ovsenik M. Assessment of facial asymmetry in growing subjects with a three- dimensional laser scanning system. Orthod Craniofac Res. 2012;15(4):237-44..

27. Zhurov A, Playle R, Richmond S. S Richmond A three-dimensional look for facial differences between males and females in a British-Caucasian sample aged 15½ years old. Orthod Craniofacial Res. 2008;11:180–5.

28. Stephen RMBCHK, Ovsenik NIHAZMUSMMO. Facial Morphology of Slovenian and Welsh White Populations Using 3-Dimensional Imaging. Angle Orthod. 2009;79:640–5.

29. Kau CH, Richmond S. Three-dimensional analysis of facial morphology surface changes in untreated children from 12 to 14 years of age. Am J Orthod Dentofac Orthop. 2008;134(6):751–60.

30. Guest E, Berry E, Morris D. Clinical paper : Orthognathic surgery Novel methods for quantifying soft tissue changes after orthognathic surgery. Int J Oral Maxillofac Surg. 2001;30:484–9.

31. Kau C, Richmond S. Three-dimensional surface acquisition systems for the study of facial morphology and their application to maxillofacial surgery. Int J Med Robot. 2007;3(2):97–110.

32. Tartaglia GM, Grandi G, Mian F, Sforza C, Ferrario VF. Non-Invasive 3D Facial Analysis And Surface Electromyography During Functional Pre-Orthodontic Treatment. J Appl Oral Sci. 2009;17(5):487–94.

33. Sforza C, Grandi G, De Menezes M, Tartaglia GM, Ferrario VF. Age- and sex-related changes in the normal human external nose. Forensic Sci Int. 2011;204(1-3):205.e1–9.

34. Sforza C, Peretta R, Grandi G, Ferronato G, Ferrario VF. Three-dimensional facial morphometry in skeletal Class III patients. A non-invasive study of soft-tissue changes before and after orthognathic surgery. Br J Oral Maxillofac Surg. 2007;45(2):138–44.

35. Kalender W a. X-ray computed tomography. Phys Med Biol. 2006;51(13):R29–43.

36. Guerrero ME, Jacobs R, Loubele M, Schutyser F, Suetens P, van Steenberghe D. State-of-the-art on cone beam CT imaging for preoperative planning of implant placement. Clin Oral Investig. 2006;10(1):1–7.

37. White SC, Pharoah MJ. The evolution and application of dental maxillofacial imaging modalities. Dent Clin North Am. 2008;52(4):689–705.

38. Mah JK, Danforth R a., Bumann A, Hatcher D. Radiation absorbed in maxillofacial imaging with a new dental computed tomography device. Oral Surgery, Oral Med Oral Pathol Oral Radiol Endodontology. 2003;96(4):508–13.

39. Park W, Kim K. Reduction of metal artifact in three-dimensional computed tomography (3D CT) with dental impression materials. Conf Proc IEEE Eng Med Biol Soc. 2007;2007:3496-9.

40. Nandini S, Velmurugan N, Kandaswamy D. Calcific healing of a crown root fracture of a maxillary central incisor evaluated with spiral computed tomography and hounsfield units: a case report. Dent Traumatol. 2008;24(6):e96–100.

41. Gray a. D, Marks JM, Stone EE, Butler MC, Skubic M, Sherman SL. Validation of the Microsoft Kinect as a Portable and Inexpensive Screening Tool for Identifying ACL Injury Risk. Orthop J Sport Med. 2014; 2(7)(suppl 2).

42. Sohmura T, Hojoh H. A novel method of removing artifacts because of metallic dental restorations in 3-D CT images of jaw bone. Clin oral Implant Res. 2005;16:728–35.

43. Nkenke E, Zachow S, Benz M, Maier T, Veit K, Kramer M. Fusion of computed tomography data and optical 3D images of the dentition for streak artefact correction in the simulation of orthognathic surgery. Dentomaxillofac Radiol. 2004;33(4):226–32.

44. Scarfe WC, Farman AG, Sukovic P. Clinical applications of cone-beam computed tomography in dental practice. J Can Dent Assoc. 2006;72(1):75–80.

45. Mah J, Hatcher D. Three-dimensional craniofacial imaging. Am J Orthod Dentofac Orthop. 2004;126(3):308–9.

46. Palomo JM, Kau CH, Palomo LB, Hans MG. Three-dimensional cone beam computerized tomography in dentistry. Dent Today. 2006;25(11):130, 132-5.

47. Swennen GRJ, Mollemans W, De Clercq C, Abeloos J, Lamoral P, Lippens F. A cone-beam computed tomography triple scan procedure to obtain a three-dimensional augmented virtual skull model appropriate for orthognathic surgery planning. J Craniofac Surg. 2009;20(2):297–307.

48. Lewis EL, Dolwick MF, Abramowicz S, Reeder SL. Contemporary imaging of the temporomandibular joint. Dent Clin North Am. 2008;52(4):875–90, viii.

49. Bearcroft PWP. Imaging modalities in the evaluation of soft tissue complaints. Best Pract Res Clin Rheumatol. 2007;21(2):245–59.

50. Strauss R a, Burgoyne CC. Diagnostic imaging and sleep medicine. Dent Clin North Am. 2008;52(4):891–915, viii.

51. Tasaki MM, Westeson P-L. Temporomandibular joint: diagnostic accuracy with sagittal and coronal MR imaging. Radiology. 1993;186:723–9.

52. Ayoub a F, Siebert P, Moos KF, Wray D, Urquhart C, Niblett TB. A vision-based three-dimensional capture system for maxillofacial assessment and surgical planning. Br J Oral Maxillofac Surg. 1998;36(5):353–7.

53. Eggers G, Rieker M, Kress B, Fiebach J, Dickhaus H, Hassfeld S. Artefacts in magnetic resonance imaging caused by dental material. MAGMA. 2005;18(2):103–11.

54. Hell B. 3D Sonography. Int J Oral Maxillofac Surg. 1995;24(1):84–9.

55. Nonnast-Daniel B, Martin RP, Lindert O, Mügge A, Schaeffer J, vd Lieth H, Söchtig E, Galanski M, Koch KM, Daniel WG. Colour doppler ultrasound assessment of arteriovenous haemodialysis fistulas Satisfactory function of the arteriovenous fistula. Lancet. 1992;339(8786):143-5.

56. Lomka PIJS, Andel JOM, Owney DOD, Enster AAF. Evaluation of voxel-based registration of 3-D power Doppler ultrasound and 3-D magnetic resonance angiographic images of carotid arteries. Ultrasound Med Biol. 2001;27(7):945–55.

57. Akizuki H, Yoshida H, Michi K. Ultrasonographic evaluation during reduction of zygomatic arch fractures. J Cranio-Maxillofacial Surg. 1990 ;18(6):263–6.

58. McCann P, Brocklebank L, Ayoub A. Assessment of zygomatico-orbital complex fractures using ultrasonography. Br J Oral Maxillofac Surg. 2000;38(5):525-9.

59. Khambay B, Nebel J, Bowman J, Walker F, Hadley D, Ayoub A. 3D stereophotogrammetric image superimposition onto 3D CT scan images the future of orthognathic surgery A pilot study. Int J Adult Orthodon Orthognath Surg. 2002;17(4):331–41.

60. Hajeer M, Ayoub A, Millett D, MitchumBock, Siebert P. Three-dimensional imaging in orthognathic surgery The clinical application of a new method. Int Adult Orthod Orthognath Surg. 2002;17(4):318–30.

61. Lorensen W, Cline H. Marching cubes: A high resolution 3D surface construction algorithm. ACM siggraph Comput Graph. 1987;21(4):163–9.

62. Udupa J. Interactive segmentation and boundary surface formation for 3-D digital images. Comput Graph Image Process. 1982;18(3):213–35.

63. Roth SD. Ray casting for modeling solids. Comput Graph Image Process. 1982;18(2):109–44.

64. Jayaratne YSN, Zwahlen R a, Lo J, Cheung LK. Three-dimensional color maps: a novel tool for assessing craniofacial changes. Surg Innov. 2010;17(3):198–205.

65. Hoefert CS, Bacher M, Herberts T, Krimmel M, Reinert S, Hoefert S, Göz G. Implementing a superimposition and measurement model for 3D sagittal analysis of therapy-induced changes in facial soft tissue: a pilot study. J Orofac Orthop. 2010;71(3):221–34.

66. Maal TJ, Verhamme LM, van Loon B, Plooij JM, Rangel FA, Kho A, Bronkhorst EM, Bergé SJ. Variation of the face in rest using 3D stereophotogrammetry. Int J Oral Maxillofac Surg. 2011;40(11):1252–7.

67. Lee J-H, Kim M-J, Kim S-M, Kwon O-H, Kim Y-K. The 3D CT superimposition method using image fusion based on the maximum mutual information algorithm for the assessment of oral and maxillofacial surgery treatment results. Oral Surg Oral Med Oral Pathol Oral Radiol. 2012;114(2):167–74.

68. Lee J, Kim M, Kim S, Kwon O, Kim Y. The 3D CT superimposition method using image fusion based on the maximum mutual information algorithm for the assessment of oral and maxillofacial surgery. Oral Surg Oral Med Oral Pathol Oral Radiol. 2012;114(2):167–74.

69. Nada RM, Maal TJJ, Breuning KH, Bergé SJ, Mostafa Y a, Kuijpers-Jagtman AM. Accuracy and reproducibility of voxel based superimposition of cone beam computed tomography models on the anterior cranial base and the zygomatic arches. PLoS One. 2011;6(2):e16520.

70. Almukhtar A, Ju X, Khambay B, McDonald J, Ayoub A. Comparison of the accuracy of voxel based registration and surface based registration for 3D assessment of surgical change following orthognathic surgery. PLoS One. 2014;9(4):e93402.

71. Vinchon M, Pellerin P, Pertuzon B, Fénart R, Dhellemmes P. Vestibular orientation for craniofacial surgery: application to the management of unicoronal synostosis. Childs Nerv Syst. 2007;23(12):1403–9.

72. Baumrind S, Frantz RC. The reliability of head film measurements: 1. Landmark identification. Am J Orthod. 1971;60(2):111–27.

73. Baumrind S, Frantz RC. The reliability of head Jilm measurements: 2. Conventional angular and linear measures. Am J Orthod. 1971;60(5):555–517.

74. Baumrind S, Miller D, Molthen R. The reliability of head film measurements: 3. Tracing superimposition. Am J Orthod. 1976;70(6):617–44.

75. Adams GL, Gansky S a., Miller AJ, Harrell WE, Hatcher DC. Comparison between traditional 2-dimensional cephalometry and a 3-dimensional approach on human dry skulls. Am J Orthod Dentofac Orthop. 2004;126(4):397–409.

76. Van Vlijmen OJC, Maal T, Bergé SJ, Bronkhorst EM, Katsaros C, Kuijpers-Jagtman a M. A comparison between 2D and 3D cephalometry on CBCT scans of human skulls. Int J Oral Maxillofac Surg. 2010;39(2):156–60.

77. William B. Downs. Analysis of facial profile. Angle Orthod. 1956;26(4):191–212.

78. Downs WB, Aurora Ill. Variations in Facial Relationships: Their Significance in Treatment and Prognosis. Angle Orthod. 1948;14(3):812–40.

79. Steiner CC. Cephalometrics for you and me. Am J Orthod. 1953;39(10):720–55.

80. Steiner CC. Cephalometrics in clinical practice. Angle Orthod. 1959;29(1):8–20.

81. Satrom KD, Sinclair PM, Wolford LM. The stability of double jaw surgery: a comparison of rigid versus wire fixation. Am J Orthod Dentofacial Orthop. 1991;99(6):550–63.

82. Burston CJ. The integumental profile. Am J Orthod. 1958;44(1):1–25.

83. Sassouni V. A classification of skeletal facial types. Am J Orthod. 1969;55(2):109–23.

84. Phillips JG. Photo-cephalometric analysis in treatment planning for surgical correction of facial disharmonies. J Maxillofac Surg. 1978;6(3):174–9.

85. Ricketts R. Cephalometric analysis and synthesis. Angle Orthod. 1961;31(3):141–56.

86. Hwang H-S, Kim W-S, McNamara J a. Ethnic differences in the soft tissue profile of Korean and European-American adults with normal occlusions and well-balanced faces. Angle Orthod. 2002;72(1):72–80.

87. Sutter R, Turley P. Soft tissue evaluation of contemporary Caucasian and African American female facial profiles. Angle Orthod. 1988;68(6):487–95.

88. Di Paolo RJ, Philip C, Maganzini a L, Hirce JD. The quadrilateral analysis: an individualized skeletal assessment. Am J Orthod. 1983;83(1):19–32.

89. Kurt Butow. A lateral photometric analysis for aesthetic-orthognathic treatmen. J Maxillofac Surg. 1984;12(5):201–7.

90. Swennen GRJ, Schutyser F, Barth E-L, De Groeve P, De Mey A. A new method of 3-D cephalometry Part I: the anatomic Cartesian 3-D reference system. J Craniofac Surg. 2006;17(2):314–25.

91. Fuhrmann RAW. Three-dimensional cephalometry and three-dimensional skull models in orthodontic/surgical diagnosis and treatment planning. Semin Orthod. 2002;8(1):17–22.

92. G.R.J. Swennen, F. Schutyser, E.-L. Barth, A. Lemaitre, C. Malevez, A. De Mey. Presentation and validation of a voxel-based three-dimensional (3-D) hard and soft tissue cephalometric analysis. Int J Oral Maxillofac Surg. 2005;34(sup1):72-86.

93. Olszewski R, Cosnard G, Macq B, Mahy P, Reychler H. 3D CT-based cephalometric analysis: 3D cephalometric theoretical concept and software. 2006;48(11):853–62.

94. Olszewski R, Zech F, Cosnard G, Nicolas V, Macq B, Reychler H. Three-dimensional computed tomography cephalometric craniofacial analysis: experimental validation in vitro. Int J Oral Maxillofac Surg. 2007;36(9):828-33.

95. Lee S-H, Kil T-J, Park K-R, Kim BC, Kim J-G, Piao Z, Corre P. Three-dimensional architectural and structural analysis--a transition in concept

and design from Delaire's cephalometric analysis. Int J Oral Maxillofac Surg. 2014;43(9):1154–60.

96. De Oliveira AEF, Cevidanes LHS, Phillips C, Motta A, Burke B, Tyndall D. Observer reliability of three-dimensional cephalometric landmark identification on cone-beam computerized tomography. Oral surg oral med oral pathol oral radiol Endod. 2009;107(2):256–65.

97. Lou L, Lagravere MO, Compton S, Major PW, Flores-Mir C. Accuracy of measurements and reliability of landmark identification with computed tomography (CT) techniques in the maxillofacial area: a systematic review. Oral Surg Oral Med Oral Pathol Oral Radiol Endod [Internet]. 2007 Sep [cited 2014 Apr 29];104(3):402–11. Available from: http://www.ncbi.nlm.nih.gov/pubmed/17709072

98. Damstra J, Fourie Z, Huddleston Slater JJR, Ren Y. Reliability and the smallest detectable difference of measurements on 3-dimensional cone-beam computed tomography images. Am j orthod Dentofac orthop. 2011;140(3):e107–14.

99. Lamichane M, Anderson NK, Rigali PH, Seldin EB, Will L a. Accuracy of reconstructed images from cone-beam computed tomography scans. Am J Orthod Dentofac Orthop. 2009;136(2):156.e1–156.e6.

100. Ludlow JB, Gubler M, Cevidanes L, Mol A. Precision of cephalometric landmark identification: cone-beam computed tomography vs conventional cephalometric views. Am J Orthod Dentofacial Orthop. 2009;136(3):312.e1–10; discussion 312–3.

101. Damstra J, Fourie Z, Ren Y. Comparison between two-dimensional and midsagittal three-dimensional cephalometric measurements of dry human skulls. Br J Oral Maxillofac Surg. 2011;49(5):392–5.

102. Katsumata A, Fujishita M, Maeda M, Ariji Y, Ariji E, Langlais RP. 3D-CT evaluation of facial asymmetry. Oral Surg Oral Med Oral Pathol Oral Radiol Endod. 2005;99(2):212–20.

103. Gaia BF, Pinheiro LR, Umetsubo OS, Santos O, Costa FF, Cavalcanti MGP. Accuracy and reliability of linear measurements using 3-dimensional computed tomographic imaging software for Le Fort I Osteotomy. Br J Oral Maxillofac Surg. 2014;52(3):258–63.

104. Rossini G, Cavallini C, Cassetta M, Ph D, Barbato E. 3D cephalometric analysis obtained from computed tomography. Review of the literature. Ann Stomatol (Roma). 2011;2(3-4):31–9.

105. Pittayapat P, Limchaichana-Bolstad N, Willems G, Jacobs R. Three-dimensional cephalometric analysis in orthodontics: a systematic review. Orthod Craniofac Res. 2014;17(2):69–91.

106. Almeida RC, Cevidanes LHS, Carvalho FAR, Motta AT, Almeida MAO, Styner M, T. Turveye, W.R. Proffitb, C. Phillipsb. Soft tissue response to

mandibular advancement using 3D CBCT scanning. Int J Oral Maxillofac Surg. 2011;40(4):353–9.

107. Cevidanes LHS, Bailey LJ, Tucker SF, Styner M a, Mol A, Phillips CL, William R. Proffit, and Timothy Turveyh. Three-dimensional cone-beam computed tomography for assessment of mandibular changes after orthognathic surgery. Am j orthod Dentofac orthop. 2007;131(1):44–50.

108. De Assis Ribeiro Carvalho F, Cevidanes LHS, da Motta ATS, de Oliveira Almeida MA, Phillips C. Three-dimensional assessment of mandibular advancement 1 year after surgery. Am J Orthod Dentofac Orthop. 2010;137(4):S53.e1–S53.e12.

109. Cevidanes LH, Franco AA, Gerig G, Proffit WR, Slice DE, Enlow DH, Yamashita HK, Kim YJ, Scanavini MA, Vigorito JW. Assessment of mandibular growth and response to orthopedic treatment with 3-dimensional magnetic resonance images. Am J Orthod Dentofac Orthop. 2005;128(1):16–26.

110. Maal TJJ, de Koning MJJ, Plooij JM, Verhamme LM, Rangel FA, Bergé SJ, W.A. Borstlap. One year postoperative hard and soft tissue volumetric changes after a BSSO mandibular advancement. Int J Oral Maxillofac Surg. 2012;41(9):1137–45.

111. Park K-R, Park H-S, Piao Z, Kim M-K, Yu H-S, Seo JK, Sang-Hwy Lee. Three-dimensional vector analysis of mandibular structural asymmetry. J cranio-maxillo-facial Surg. 2013;41(4):338–44.

112. Farkas LG, Bryson W, Klotz J. Is photogrammetry of the face reliable? Plast Reconstr Surg. Plastic and reconstructive surgery; 1980;66(3):346–55.

113. DiBernardo BE, Adams RL, Krause J, Fiorillo M a, Gheradini G. Photographic standards in plastic surgery. Plast Reconstr Surg. 1998;102(2):559–68.

114. Ettorre G, Weber M, Schaaf H, Lowry JC, Mommaerts MY, Howaldt H-P. Standards for digital photography in cranio-maxillo-facial surgery - Part I: Basic views and guidelines. J cranio-maxillo-facial Surg. 2006;34(2):65–73.

115. Schaaf H, Streckbein P, Ettorre G, Lowry JC, Mommaerts MY, Howaldt H-P. Standards for digital photography in cranio-maxillo-facial surgery – Part II: Additional picture sets and avoiding common mistakes. J Cranio-Maxillofacial Surg. 2006;34(7):444–55.

116. Proffit WR and Fields HW. Contemporary Orthodontics. St. Louis: Mosby-Year Book, Inc., 2003: P 233.

117. Farkas LG. Accuracy of anthropometric measurements: past, present, and future. Cleft palate-craniofacial J. 1996;33(1):10–8; discussion 19–22.

118. Driessen JP, Vuyk H, Borgstein J. New insights into facial anthropometry in digital photographs using iris dependent calibration. Int J Pediatr Otorhinolaryngol. 2011;75(4):579–84.

119. DiSaia JP, Ptak JJ, Achauer BM. Digital photography for the plastic surgeon. Plast Reconstr Surg. 2000;105(7):2636.

120. Farkas LG, Sohm P, Kolar JC, Katic MJ, Munro IR. Inclinations of the facial profile: Art versus Reality. Plast Reconstr Surg. 1985;75(4):509–19.

121. Hajeer MY, Millett DT, Ayoub a F, Siebert JP. Applications of 3D imaging in orthodontics: part II. J Orthod. 2004;31(2):154–62.

122. Hwang H-S, Yuan D, Jeong K-H, Uhm G-S, Cho J-H, Yoon S-J. Three-dimensional soft tissue analysis for the evaluation of facial asymmetry in normal occlusion individuals. Korean J Orthod. 2012;42(2):56–63.

123. Devlin MF, Ray A, Raine P, Bowman A, Ayoub AF. Facial symmetry in unilateral cleft lip and palate following alar base augmentation with bone graft: a three-dimensional assessment. Cleft palate-craniofacial J. 2007;44(4):391–5.

124. Woo J, Yeol J, Oh T, Man S, Joon S. Frontal soft tissue analysis using a 3 dimensional camera following two-jaw rotational orthognathic surgery in skeletal class III patients. J Cranio-Maxillofacial Surg. 2014;42(3):220–6.

125. Galantucci L, Percoco G, Gioia E Di. Photogrammetric 3D digitization of human faces based on landmarks. In: Proceedings of the International MultiConference of Engineering and computer science. 2009;1:978–88.

126. Honrado CP, Lee S, Bloomquist DS, Larrabee WF. Quantitative assessment of nasal changes after maxillomandibular surgery using a 3-dimensional digital imaging system. Arch Facial Plast Surg. 2014;8(1):26–35.

127. Menezes M De, Sforza C. Three-dimensional face morphometry. Dental Press J Orthod. 2010;15(1):13–5.

128. Sforza C, Peretta R, Grandi G, Ferronato G, Ferrario VF. Soft tissue facial volumes and shape in skeletal Class III patients before and after orthognathic surgery treatment. J Plast Reconstr aesthetic Surg. 2007;60(2):130–8.

129. Terajima M, Yanagita N, Ozeki K, Hoshino Y, Mori N, Goto TK, Tokumori K, Aoki Y, Nakasima A. Three-dimensional analysis system for orthognathic surgery patients with jaw deformities. Am J Orthod Dentofac Orthop. 2008;134(1):100–11.

130. Kim Y-I, Park S-B, Son W-S, Hwang D-S. Midfacial soft-tissue changes after advancement of maxilla with Le Fort I osteotomy and mandibular setback surgery: comparison of conventional and high Le Fort I osteotomies by superimposition of cone-beam computed tomography volumes. J oral Maxillofac Surg. 2011;69(6):e225–33.

131. Park S, Kim Y, Hwang D, Lee J. Midfacial soft-tissue changes after mandibular setback surgery with or without paranasal augmentation: Cone-beam computed tomography (CBCT) volume superimposition. J Cranio-Maxillofacial Surg. 2013;41(2):119–23.

132. Sforza C, Grandi G, Pisoni L, Diablo C, Gondolfini M, Ferrario V. Soft tissue facial morphometry in subjects with Moebius syndrome. Eur J Oral Sci. 2009;117:695–703.

133. Sforza C, Laino A, Grandi G, Pisoni L, Ferrario V. Three-dimensional facial asymmetry in attractive and normal people from childhood to young adulthood. Symmetry (Basel). 2010;2:1925–44.

134. Ryckman MS, Harrison S, Oliver D, Sander C, Boryor AA, Hohmann AA, Kilic F, Kim KB. Soft-tissue changes after maxillomandibular advancement surgery assessed with cone-beam computed tomography. Am J Orthod Dentofac Orthop. 2010;137(4 Suppl):S86–93.

135. Schwenzer-Zimmerer K. Systematic contact-free 3D topometry of the soft tissue profile in cleft lips. Cleft palate-craniofacial J. 2008;45(6):607–13.

136. Park S-B, Yoon J-K, Kim Y-I, Hwang D-S, Cho B-H, Son W-S. The evaluation of the nasal morphologic changes after bimaxillary surgery in skeletal class III maloccusion by using the superimposition of cone-beam computed tomography (CBCT) volumes. J cranio-maxillo-facial Surg. 2012;40(4):e87–92.

137. Terajima M, Furuichi Y, Aoki Y, Goto TK, Tokumori K, Nakasima A. A 3-dimensional method for analyzing facial soft-tissue morphology of patients with jaw deformities. Am J Orthod Dentofac Orthop. 2009;135(6):715–22.

138. Schimmel M, Christou P, Houstis O, Herrmann FR, Kiliaridis S, Müller F. Distances between facial landmarks can be measured accurately with a new digital 3-dimensional video system. Am J Orthod Dentofac Orthop. 2010;137(5):580.e1–580.e10; discussion 580–1.

139. Vezzetti E, Marcolin F. Geometry-based 3D face morphology analysis: soft-tissue landmark formalization. Multimed Tools Appl. 2014;68(3):895–929.

140. Fourie Z, Damstra J, Gerrits PO, Ren Y. Evaluation of anthropometric accuracy and reliability using different three-dimensional scanning systems. Forensic Sci Int. 2011;207:127–34.

141. Plooij J, Swennen G, Rangel F. Evaluation of reproducibility and reliability of 3D soft tissue analysis using 3D stereophotogrammetry. Int J Oral Maxillofac Surg. 2009;38(3):267–73.

142. Othman SA, Ahmad R, Jamaludin AFMM. Reproducibility of facial soft tissue landmarks on facial images captured on a 3D camera. Aust Orthod J. 2013;29(1):58–66.

143. Gwilliam JR, Cunningham SJ, Hutton T. Reproducibility of soft tissue landmarks on three-dimensional facial scans. Eur J Orthod. 2006;28(5):408–15.

144. Toma a M, Zhurov a, Playle R, Ong E, Richmond S. Reproducibility of facial soft tissue landmarks on 3D laser-scanned facial images. Orthod Craniofac Res. 2009;12(1):33–42.

145. Nakamura N, Okawachi T, Nozoe E, Nishihara K, Matsunaga K. Three-dimensional analyses of nasal forms after secondary treatment of bilateral cleft lip-nose deformity in comparison to those of healthy young adults. J oral Maxillofac Surg. 2011;69(11):e469–81.

146. Schwenzer-Zimmerer K, Chaitidis D, Boerner I, Kovacs L, Schwenzer NF, Holberg C, Zeilhofer HF. Systematic contact-free 3D topometry of the soft tissue profile in cleft lips. Cleft palate-craniofacial J. 2008;45(6):607–13.

147. Ubaya T, Sherriff a, Ayoub a, Khambay B. Soft tissue morphology of the naso-maxillary complex following surgical correction of maxillary hypoplasia. Int J Oral Maxillofac Surg. 2012;41(6):727–32.

148. Chen C, Lai S, Lee H, Chen K, Hsu K. Soft-tissue profile changes after orthognathic surgery of mandibular prognathism. Kaohsiung J Med Sci. 2012;28(4):216–9.

149. Verzé L, Nasi A, Quaranta F, Vasino V, Prini V, Ramieri G. Quantification of facial movements by surface laser scanning. J Craniofac Surg. 2011;22(1):60–5.

150. Popat H, Richmond S, Marshall D, Rosin PL. Three-dimensional assessment of functional change following Class 3 orthognathic correction--a preliminary report. J cranio-maxillo-facial Surg. 2012;40(1):36–42.

151. Amm C a., Denny AD. Correction of Sagittal Synostosis Using Foreshortening and Lateral Expansion of the Cranium Activated by Gravity: Surgical Technique and Postoperative Evolution. Plast Reconstr Surg. 2005;116(3):723–35.

152. Claes P, Walters M, Clement J. Improved facial outcome assessment using a 3D anthropometric mask. Int J Oral Maxillofac Surg. 2012;41(3):324–30.

153. Bugaighis I, O'Higgins P, Tiddeman B, Mattick C, Ben Ali O, Hobson R. Three-dimensional geometric morphometrics applied to the study of children with cleft lip and/or palate from the North East of England. Eur J Orthod. 2010;32(5):514–21.

154. Bookstein FL. Linear machinery for morphological distortion. Comput Biomed Res. 1978;11(5):435–58.

155. Paton NI, Yang Y, Sitoh Y-Y, Tha NO. Validation of three-dimensional laser scanning for the assessment of facial fat changes. HIV Med. 2007;8(8):498–503.

156. Luximon Y, Ball R, Justice L. The Chinese Face: A 3D Anthropometric Analysis. In: Proceedings of the TMCE, Anacona, Italy. 2010. pp. 1–11.

157. Toma AM, Zhurov AI, Playle R, Marshall D, Rosin PL, Richmond S. The assessment of facial variation in 4747 British school children. Eur J Orthod. 2012;34:655–64.

158. Shafi MI, Ayoub a, Ju X, Khambay B. The accuracy of three-dimensional prediction planning for the surgical correction of facial deformities using Maxilim. Int J Oral Maxillofac Surg. 2013;42(7):801–6.

159. Maal TJJ, Plooij JM, Verthamme LM, Rangel FA, Berge SJ, Borstlap WA. One year postoperative hard and soft tissue volumetric changes after a BSSO mandibular advancement. Int J Oral Maxillofac Surg. 2012;41:1137–45.

160. Djordjevic J, Lewis BM, Donaghy CE, Zhurov AI, Knox J, Hunter L, Richmond S. Facial shape and asymmetry in 5-year-old children with repaired unilateral cleft lip and/or palate: an exploratory study using laser scanning. Eur J Orthod. 2014;36(5).

161. Baik H-S, Kim S-Y. Facial soft-tissue changes in skeletal Class III orthognathic surgery patients analyzed with 3-dimensional laser scanning. Am J Orthod Dentofac Orthop. 2010;138(2):167–78.

162. Kau CH, Zhurov A, Richmond S, Cronin A, Savio C, Mallorie C. Facial templates: a new perspective in three dimensions. Orthod Craniofac Res. 2006;9(1):10–7.

163. How C, Richmond S, Savio C, Mallorie C. Measuring Adult Facial Morphology in Three Dimensions. Angle Orthod. 2006;76(5):773–8.

164. Kau CH, Kamel SG, Wilson J, Wong ME. New method for analysis of facial growth in a pediatric reconstructed mandible. Am J Orthod Dentofac Orthop. 2011;139(4):e285–90.

165. Maal TJJ, van Loon B, Plooij JM, Rangel F, Ettema AM, Borstlap WA, Bergé SJ. Registration of 3-dimensional facial photographs for clinical use. J oral Maxillofac Surg. 2010;68(10):2391–401.

166. Popat H, Richmond S, Playle R, Marshall D, Rosin P, Cosker D. Three-dimensional motion analysis – an exploratory study . Part 1: Assessment of facial movement. Orthod Craniofac Res. 2008;11(4):216–23.

167. Kau CH, Richmond S, Zhurov A, Ovsenik M, Tawfik W, Borbely P, English JD. Use of 3-dimensional surface acquisition to study facial morphology in 5 populations. Am J Orthod Dentofac Orthop. 2010;137(4suppl):S56.e1–9; discussion S56–7.

168. Nada R, Loon B Van, Maal T. Three-dimensional evaluation of soft tissue changes in the orofacial region after tooth-borne and bone-borne surgically assisted rapid maxillary expansion. Clin oral investig. 2013;17(9):2017–24.

169. Naudi KB, Benramadan R, Brocklebank L, Ju X, Khambay B, Ayoub A. The virtual human face: superimposing the simultaneously captured 3D photorealistic skin surface of the face on the untextured skin image of the CBCT scan. Int J Oral Maxillofac Surg. 2013;42(3):393–400.

170. Marchetti C, Bianchi a, Muyldermans L, Di Martino M, Lancellotti L, Sarti A. Validation of new soft tissue software in orthognathic surgery planning. Int J Oral Maxillofac Surg. 2011;40(1):26–32.

171. Verhoeven TJ, Coppen C, Barkhuysen R, Bronkhorst EM, Merkx MA, Bergé SJ, Maal TJ. Three dimensional evaluation of facial asymmetry after mandibular reconstruction: validation of a new method using stereophotogrammetry. Int J Oral Maxillofac Surg. 2013;42(1):19–25.

172. Maal TJJ, Verhamme LM, Loon B Van, Plooij JM, Rangel FA, Kho A. Variation of the face in rest using 3D stereophotogrammetry. Int J Oral Maxillofac Surg. 2011;40(11):1252–7.

173. Nada RM, van Loon B, Maal TJ, Bergé SJ, Mostafa YA, Kuijpers-Jagtman AM, Schols JG. Three-dimensional evaluation of soft tissue changes in the orofacial region after tooth-borne and bone-borne surgically assisted rapid maxillary expansion. Clin Oral Investig. 2013;17(9):2017–24.

174. Miller L, Morris DO, Berry E. Visualizing three-dimensional facial soft tissue changes following orthognathic surgery. Eur J Orthod. 2007;29(1):14–20.

175. Claes P, Walters M, Vandermeulen D, Clement JG. Spatially-dense 3D facial asymmetry assessment in both typical and disordered growth. J Anat. 2011;219(4):444–55.

176. Mao Z, Ju X, Siebert JP, Cockshott WP, Ayoub A. Constructing dense correspondences for the analysis of 3D facial morphology. Pattern Recognit Lett. 2006;27(6):597–608.

177. Kau CH, Richmond S. Three-dimensional imaging for orthodontics and orthognathic surgery. London. Wiely-Blackwell; 2010. pp 28-44.

178. Qureshi F. Constructing Anatomically Accurate Face Models using Computed Tomography and Cyberware data. 2000. p. 11, 47, 63. Available from: http://www.cs.ucla.edu/~dt/theses/qureshi-ms-thesis.pdf

179. Goodall C. Procrustes Methods in the Statistical Analysis of Shape. J R Stat Soc Ser B. 1991;53(2):285–339.

180. Al-Hiyali A, Ayoub A, Ju X, Almuzian M, Al-Anezi T. The Impact of Orthognathic Surgery on Facial Expressions. J oral Maxillofac Surg. 2015;In Press.

181. Higgins JE. Curve Extraction and Facial Analysis Using Statistical Techniques. PhD thesis submited to the University of Glasgow 2009. p. 100–3.

182. Chau H, Dasgupta R, Sauret V, Kenyon G. Use of an optical surface scanner in assessment of outcome following rhinoplasty surgery. J Laryngol Otol. 2008;122(9):972–7.

183. Sforza C, Grandi G, Pisoni L, Di Blasio C, Gandolfini M, Ferrario VF. Soft tissue facial morphometry in subjects with Moebius syndrome. Eur J Oral Sci. 2009;117(6):695–703.

184. Sforza C, Grandi G, Binelli M, Dolci C, Menezes M De, Ferrario VF. Age- and sex-related changes in three-dimensional lip morphology. Forensic Sci Int. 2010;200(1-3):182e1–183e7.

185. Bell A, Lo TW, Brown D, Bowman AW, Siebert JP, Simmons DR, Millett DT, Ayoub AF. Three-dimensional assessment of facial appearance following surgical repair of unilateral cleft lip and palate. Cleft palate-craniofacial J. 2014;51(4):462–71.

186. Joss CU, Joss-Vassalli IM, Bergé SJ, Kuijpers-Jagtman AM. Soft tissue profile changes after bilateral sagittal split osteotomy for mandibular setback: a systematic review. J oral Maxillofac Surg. 2010;68(11):2792–801.

187. Louis PJ, Austin RB, Waite PD, Mathews CS. Soft tissue changes of the upper lip associated with maxillary advancement in obstructive sleep apnea patients. J oral Maxillofac Surg. 2001;59(2):151–6.

188. Chew MT. Soft and Hard Tissue Changes after Bimaxillary Surgery in Chinese Class III Patients. Angle Orthod. 2005;75(6):1–5.

189. Sinthanayothin C. Computerized Cephalometric Line Tracing Technique on X-ray Images.In: 13th International Conference on Biomedical Engineering. Springer Berlin Heidelberg, 2009. ICBME proceedings. 2008. pp. 265–9.

190. Benson PE, Richmond S. A critical appraisal of measurement of the soft tissue outline using photographs and video. Eur J Orthod. 1997;19(4):397-409.

191. Sarver DM, Weissman SM. longterm soft tissue responce to maxillary superior reositioning. Angle Orthod. 1991;61(4):267–76.

192. Mansour S, Burstone C, Legan H. An evaluation of soft-tissue changes resulting from Le Fort I maxillary surgery. Am J Orthod. 1983;84(1):37–47.

193. Bell WH, Jacobs JD. Surgical-Orthodontic Correction of Maxillary Retrusion by Le Fort I Osteotorny and Proplast. J Maxillofac Surg. 1980;8(2):84–94.

194. Freihofer H. Changes in nasal profile after maxillary advancement in cleft and non-cleft patients. J Maxillofac Surg. 1977;5(1):20–7.

195. Wen-Ching Ko E, Figueroa AA, Polley JW. Soft tissue profile changes after maxillary advancement with distraction osteogenesis by use of a rigid external distraction device: a 1-year follow-up. J Oral Maxillofac Surg. 2000;58(9):959–69.

196. Stella JP, Streater MR, Epker BN, Sinn DP. Predictability of Upper Lip Soft Tissue Changes With Maxillary Advancement. J Oral Maxillofac Surg. 1989;47(7):697–703.

197. Schendel SA, Eisenfeld JH, Bell WH, Epker BN. Superior repositioning of the maxilla: Stability and soft tissue osseous relations. Am J Orthod. 1976;70(6):663–74.

198. Williams R. The diagnostic line. Am J Orthod. 1969;55(5):458–76.

199. Teuscher U, Sailer HF. Stability of Le Fort I Osteotomy in Class Ill Cases with Retropositioned Maxillae. J cranio-maxillo-facial Surg. 1982;10(2):80–3.

200. Engel GA, Quan RE, Chaconas SJ. Soft-tissue change as a result of maxillary surgery. A preliminary study. Am J Orthod. 1979 Mar;75(3):291-300.

201. Carlotti AE, Aschaffenburg PH, Schendel S A. Facial changes associated with surgical advancement of the lip and maxilla. J Oral Maxillofac Surg. 1986;44(8):593–6.

202. Freinhofer HPM. The Lip Profile after Correction of Retromaxillism in Cleft and Non-Cleft Patients. J Maxillofac Surg. 1976;4(3):136-41.

203. Hack G, Otterloo J Van, Nanda R. Long-term stability and prediction of soft tissue changes after Le Fort I surgery. Am J Orthod Dentofac Orthop. 1993;104(6):544–55.

204. Bergman RT. Cephalometric soft tissue facial analysis. Am J Orthod Dentofac Orthop. 1999;116(4):373–89.

205. Smith J, Thomas P, Proffit W. A comparison of current prediction imaging programs. Am J Orthod Dentofac Orthop. 2004;125(5):527–36.

206. Gallagher DM, Bell WH, Storum KA. Soft tissue changes associated with advancement genioplasty performed concomitantly with superior repositioning of the maxilla. J Oral Maxillofac Surg. 1984;42(4):238–42.

207. Donatsky O, Hillerup S. Computerized cephalometric orthognathic surgical simulation, prediction and postoperative evaluation of precision. Int J Oral Maxillofac Surg. 1992;21(4):199–203.

208. Clemente-Panichella D, Suzuki S, Cisneros G. Soft to hard tissue movement ratios: orthognathic surgery in a Hispanic population. Int J Adult Orthodon Orthognath Surg. 2000;15(4):255–64.

209. Bell WH, Dann JJ. Correction of dentofacial deformities by surgery in the anterior part of the Jaws. Am J Orthod. 1973;64(2):162–87.

210. Rosen HM. Lip-Nasal Aesthetics Following Le Fort I Osteotomy. Plast Reconstr Surg. 1988;81(2):171–9.

211. Dann J, Fonseca R, Bell W. Soft tissue changes associated with total maxillary advancement a preliminary study. J Oral Surg. 1976;34(1):19-23.

212. Burstone CJ. Lip posture and its significance in treatment planning. Am J Orthod. 1967;53(4):262-84.

213. Jakobsone G, Stenvik A, Espeland L. Importance of the vertical incisor relationship in the prediction of the soft tissue profile after Class III bimaxillary surgery. Angle Orthod. 2012;82(3):441-447.

214. Mobarak K, Krogstad O, Espeland L, Lyberg T. Factors influencing the predictability of soft tissue profile changes following mandibular setback surgery. Angle Orthod. 2001;71(3):216–27.

215. Aulsebrook WA, Becker PJ, Işcan MY. Facial soft-tissue thicknesses in the adult male Zulu. Forensic Sci Int. 1996;79(2):83–102.

216. Schweckendiek W. Nasal abnormalities in facial clefts. J Maxillofac Surg. 1976;4(3):141–9.

217. Hui E, Hägg E, Tideman H. Soft tissue changes following maxillary osteotomies in cleft lip and palate and non-cleft patients. J Cranio-Maxillofacial Surg. 1994;22(3):182–6.

218. Knowles C. Changes in the profile following surgical reduction of mandibular prognathism. Br J Plast Surg. 1965;18(4):432–4.

219. Aaronson S. A cephalometric investigation of the surgical correction of mandibular prognathism. Angle Orthod. 1967;37(4):251–60.

220. Lin S, Kerr W. Soft and hard tissue changes in Class III patients treated by bimaxillary surgery. Eur J Orthod. 1998;20(1):25–33.

221. Hu J, Wang D, Luo S, Chen Y. Differences in soft tissue profile changes following mandibular setback in Chinese men and women. J oral Maxillofac Surg. 1999;57(10):1182–6.

222. Mobarak KA, Espeland L, Krogstad O, Lyberg T. Soft tissue profile changes following mandibular advancement surgery: predictability and long-term outcome. Am J Orthod Dentofac Orthop. 2001;119(4):353–67.

223. Joss C, Joss IM, Kiliarids S, Kuijpers-Jagtman AM. Soft Tissue Profile After Bilateral Sagittal Split Osteotomy for Mandibular Advancement : A Systematic Review. J oral Maxillofac Surg. 2010;68(6):1260–9.

224. Jones RM, Khambay BS, McHugh S, Ayoub AF. The validity of a computer-assisted simulation system for orthognathic surgery (CASSOS) for planning the surgical correction of class III skeletal deformities: single-jaw versus bimaxillary surgery. Int J Oral Maxillofac Surg. 2007;36(10):900–8.

225. Cevidanes L, Tucker S, Styner M, Kim H, Chapuis J, Reyes M, Proffit W, Turvey T, Jaskolka M. Three-dimensional Surgical Simulation. Am J Orthod Dentofac Orthop. 2011;138(3):316–71.

226. Schendel S a., Lane C. 3D Orthognathic Surgery Simulation Using Image Fusion. Semin Orthod. 2009;15(1):48–56.

227. Mollemans W, Schutyser F, Nadjmi N, Maes F, Suetens P. Predicting soft tissue deformations for a maxillofacial surgery planning system: from

computational strategies to a complete clinical validation. Med Image Anal. 2007;11(3):282–301.

228. Schutyser F, Cleynenbreugel J Van, Ferrant M, Schoenaers J, Suetens P. Image-based 3D planning of maxillofacial distraction procedures including soft tissue implications. In: Medical Image Computing and Computer-Assisted Intervention – MICCAI 2000;104:999–1007.

229. Xia J, Samman N, Yeung RW, Shen SG, Wang D, Ip HH, Tideman H. Three-dimensional virtual reality surgical planning and simulation workbench for orthognathic surgery. Int J Adult Orthodon Orthognath Surg. 2000;15(4):265–82.

230. Keeve E, Girod S, Kikinis R, Girod B. Deformable modeling of facial tissue for craniofacial surgery simulation. Comput Aided Surg. 1998;3(5):228–38.

231. Chabanas M, Luboz V, Payan Y. Patient specific finite element model of the face soft tissues for computer-assisted maxillofacial surgery. Med Image Anal. 2003;7(2):131–51

232. Sarti A, Gori R, Lamberti C. A physically based model to simulate maxillo-facial surgery from 3D CT images. Futur Gener Comput Syst. 1999;15(2):217–21.

233. Teschner M, Girod S, Girod B. Direct Computation of Nonlinear Soft-Tissue Deformation. In: Vision, Modeling, and Visualization VMV'00. 2000.

234. Meehan M, Teschner M, Girod S. Three-dimensional simulation and prediction of craniofacial surgery. Orthod Craniofacial Res. 2003;6 (supl.1):102–7.

235. Cotin S, Delingette H, Ayache N. Real-Time Elastic Deformations of Soft Tissues for Surgery Simulation. IEEE Trans Vis Comput Graph. 1999;5(1):62–73.

236. Ullah R. The validity of 3dMD Vultus in predicting soft tissue morphology following orthognathic surgery. M.phil thesis submitted to the University of Birmingham. 2014. p. 96.

237. Schendel S a, Jacobson R, Khalessi S. Three-Dimensional Facial Simulation in Orthognathic Surgery: Is It Accurate? J oral Maxillofac Surg. 2013;71(8):1406–14.

238. Park S-B, Kim Y-I, Hwang D-S, Lee J-Y. Midfacial soft-tissue changes after mandibular setback surgery with or without paranasal augmentation: cone-beam computed tomography (CBCT) volume superimposition. J cranio-maxillo-facial Surg. 2013;41(2):119–23.

239. Cook J, Chandran V, Sridharan S, Fookes C. Face recognition from 3D data using Iterative Closest Point algorithm and Gaussian mixture models. in: 3D Data Processing, Visualization and Transmission(3DPVT) 2004. Proceedings of the 2nd International Symposium 2004. pp.502-509.

240. Vezzetti E, Marcolin F. 3D human face description: landmarks measures and geometrical features. Image Vis Comput. 2012;30(10):968–712.

241. De Assis Ribeiro Carvalho F, Cevidanes LHS, da Motta ATS, de Oliveira Almeida MA, Phillips C. Three-dimensional assessment of mandibular advancement 1 year after surgery. Am J Orthod Dentofac Orthop. 2010;137(4):S53.e1–S53.e12.

242. Heymann GC, Cevidanes L, Cornelis M, Clerck HJ De, Tulloch JFC. Three-dimensional analysis of maxillary protraction with intermaxillary elastics to miniplates. Am J Orthod Dentofac Orthop. 2010;137(2):274–84.

243. Khambay B, Ullah R. Current methods of assessing the accuracy of three-dimensional soft tissue facial predictions: technical and clinical considerations. Int J Oral Maxillofac Surg. 2015;44(1):132–8.

244. Zhili Mao, Xiangyang Ju, J. Paul Siebert, W. Paul Cockshott AA. Constructing dense correspondences for the analysis of 3D facial morphology. Pattern Recognit Lett. 2006;27(6):597–608.

245. Aynechi N, Larson BE, Leon-Salazar V, Beiraghi S. Accuracy and precision of a 3D anthropometric facial analysis with and without landmark labeling before image acquisition. Angle Orthod. 2011;81(2):245–52.

246. Almukhtar A, Khambay B, Ayoub A, Ju X, Al-Hiyali A, Macdonald J, Jabar N and Goto T. “Direct DICOM Slice Landmarking” A Novel Research Technique to Quantify Skeletal Changes in Orthognathic Surgery. PLoS One. 2015;10(8):e0131540.

247. Hajeer MY, Ayoub AF, Millett DT. Three-dimensional assessment of facial soft-tissue asymmetry before and after orthognathic surgery. Br J Oral Maxillofac Surg. 2004;42(5):396–404.

248. Kau CH, Richmond S, Palomo JM, Hans MG. Three-dimensional cone beam computerized tomography in orthodontics. J Orthod. 2005;32(4):282–93.

249. Kamburoğlu K, Kolsuz E, Kurt H, Kılıç C. Accuracy of CBCT measurements of a human skull. J Digit Imaging. 2011;24(5):787–93. Available from:

250. Brown A a, Scarfe WC, Scheetz JP, Silveira AM, Farman AG. Linear accuracy of cone beam CT derived 3D images. Angle Orthod. 2009;79(1):150–7.

251. Ghoneima A, Kula K. Accuracy and reliability of cone-beam computed tomography for airway volume analysis. Eur J Orthod. 2013;35(2):256–61.

252. Farman AG, Scarfe WC. Development of imaging selection criteria and procedures should precede cephalometric assessment with cone-beam computed tomography. Am J Orthod Dentofac Orthop. 2006;130(2):257–65.

253. Moerenhout B a MML, Gelaude F, Swennen GRJ, Casselman JW, Van Der Sloten J, Mommaerts MY. Accuracy and repeatability of cone-beam computed tomography (CBCT) measurements used in the determination of

facial indices in the laboratory setup. J cranio-maxillo-facial Surg. 2009;37(1):18–23.

254. Jokic D, Uglešic V, Macan D, Knezevic P. Soft tissue changes after mandibular setback and bimaxillary surgery in Class III patients. Angle Orthod. 2013;83(5):817–23.

255. Marchetti C, Bianchi A, Bassi M, Gori R, Lamberti C, Sarti A. Mathematical Modeling and Numerical Simulation in Maxillo-Facial Virtual Surgery (VISU). J Craniofac Surg. 2006;17(4):661–7.

256. Tucker S, Cevidanes LHS, Styner M, Kim H, Reyes M, Proffit W, Turvey T. Comparison of actual surgical outcomes and 3-dimensional surgical simulations. J oral Maxillofac Surg. 2010;68(10):2412–21.

257. Beldie L, Walker B, Lu Y, Richmond S, Middleton J. Finite element modelling of maxillofacial surgery and facial expressions—a preliminary study. Int J Med Robot Comput Assist Surg. 2010;6(4):422–30.

258. Deuflhard P, Weiser M, Zachow S. Mathematics in Facial Surgery. Notes AMS. 2006;53(9):1012–6.

259. Soncul M, Bamber MA. Evaluation of facial soft tissue changes with optical surface scan after surgical correction of Class III deformities. J Oral Maxillofac Surg. 2004;62(11):1331–40.

260. Luffingham J, Campbell H. The need for orthodontic treatment. A pilot survey of 14 year old school children in Paisley, Scotland. Trans Eur Orthod Soc. 1974;259–67.

261. Kim J, Viana MAG, Graber TM. The effectiveness of protraction face mask therapy: A meta-analysis. Am J Orthod Dentofac Orthop. 1999;115(6):675–85.

262. Proffit WR and Fields HW. Contemporary Orthodontics. St. Louis: Mosby-Year Book, Inc., 2013: 225-264.

263. Kau CH, Cronin a, Durning P, Zhurov a I, Sandham a, Richmond S. A new method for the 3D measurement of postoperative swelling following orthognathic surgery. Orthod Craniofac Res. 2006;9(1):31–7.

264. Dolce C, Hatch JP, Sickels JE Van, Rugh JD. Five-year outcome and predictability of soft tissue profiles when wire or rigid fixation is used in mandibular advancement surgery. Am J Orthod Dentofac Orthop. 2003;124(3):249–56.

265. Kor HS, Yang HJ, Hwang SJ. Relapse of skeletal class III with anterior open bite after bimaxillary orthognathic surgery depending on maxillary posterior impaction and mandibular counterclockwise rotation. J Cranio-Maxillofacial Surg. 2013;42(5):e230–8.

266. Kim Y-K, Kim Y-J, Yun P-Y, Kim J-W. Evaluation of skeletal and surgical factors related to relapse of mandibular setback surgery using the bioabsorbable plate. J cranio-maxillo-facial Surg. 2009;37(2):63–8.

267. Blomqvist JE, Ahlborg G, Isaksson S, Svartz K. A comparison of skeletal stability after mandibular advancement and use of two rigid internal fixation techniques. J oral Maxillofac Surg. 1997;55(6):568–74; discussion 574–5.

268. Ko EW-C, Lin SC, Chen YR, Huang CS. Skeletal and dental variables related to the stability of orthognathic surgery in skeletal Class III malocclusion with a surgery-first approach. J Oral Maxillofac Surg. 2013;71(5):e215–23.

269. Jung H-D, Jung Y-S, Kim SY, Kim DW, Park H-S. Postoperative stability following bilateral intraoral vertical ramus osteotomy based on amount of setback. Br J Oral Maxillofac Surg. 2013;51(8):822–6.

270. Liang X, Lambrichts I, Sun Y, Denis K, Hassan B, Li L. A comparative evaluation of Cone Beam Computed Tomography (CBCT) and Multi-Slice CT (MSCT). Part II: On 3D model accuracy. Eur J Radiol. 2010;75(2):270–4.

271. Olmez H, Gorgulu S, Akin E, Bengi AO, Tekdemir I, Ors F. Measurement accuracy of a computer-assisted three-dimensional analysis and a conventional two-dimensional method. Angle Orthod. 2011;81(3):375–82.

272. Chang Z-C, Hu F-C, Lai E, Yao C-C, Chen M-H, Chen Y-J. Landmark identification errors on cone-beam computed tomography-derived cephalograms and conventional digital cephalograms. Am J Orthod Dentofac Orthop. 2011;140(6):e289–97.

273. Gribel BF, Gribel MN, Frazäo DC, McNamara J a, Manzi FR. Accuracy and reliability of craniometric measurements on lateral cephalometry and 3D measurements on CBCT scans. Angle Orthod. 2011;81(1):26–35.

274. Aydil B, Özer N, Marşan G. Facial soft tissue changes after maxillary impaction and mandibular advancement in high angle class II cases. Int J Med Sci. 2012;9(4):316–21.

275. Ghang M-H, Kim H-M, You J-Y, Kim B-H, Choi J-P, Kim S-H, Choung PH.. Three-dimensional mandibular change after sagittal split ramus osteotomy with a semirigid sliding plate system for fixation of a mandibular setback surgery. Oral Surg Oral Med Oral Pathol Oral Radiol. 2013;115(2):157–66.

276. Kim B-R, Oh K-M, Cevidanes LHS, Park J-E, Sim H-S, Seo S-K, Reyes M, Kim YJ, Park YH. Analysis of 3D soft tissue changes after 1- and 2-jaw orthognathic surgery in mandibular prognathism patients. J oral Maxillofac Surg. 2013;71(1):151–61.

277. Walters M, Claes P, Kakulas E, Clement J. Robust and regional 3D facial asymmetry assessment in hemimandibular hyperplasia and hemimandibular elongation anomalies. Int J Oral Maxillofac Surg. International Association of Oral and Maxillofacial Surgery; 2013;42(1):36–42.

278. Mao Z, Siebert J, Cockshott WP, Ayoub A. Constructing dense correspondences to analyze 3d facial change. In :The 17th International Conference on Pattern Recognition (ICPR'04). Proceedings. 2004;3:1–5.

279. Oh K-M, Seo S-K, Park J-E, Sim H-S, Cevidanes LHS, Kim Y-JR, Park YH.. Post-operative soft tissue changes in patients with mandibular prognathism after bimaxillary surgery. J cranio-maxillo-facial Surg. 2013;41(3):204–11.

280. Nkenke E, Vairaktaris E, Kramer M, Schlegel A, Holst A, Hirschfelder U, Wiltfang J, Neukam FW, Stamminger M. Three-dimensional analysis of changes of the malar-midfacial region after Le Fort I osteotomy and maxillary advancement. Oral Maxillofac Surg. 2008;12(1):5–12.

281. Vasudavan S, Jayaratne Y, Padwa B. Nasolabial soft tissue changes after Le Fort I advancement. J Oral Maxillofac Surg. 2012;70(4):e270–7.

282. Metzler P, Geiger EJ, Chang CC, Sirisoontorn I, Steinbacher DM. Assessment of three-dimensional nasolabial response to Le Fort I advancement. J Plast Reconstr Aesthet Surg. 2014;67(6):756–63.

283. Ko EW-C, Figueroa A, Polley JW. Soft tissue profile changes after maxillary advancement with distraction osteogenesis by use of a rigid external distraction device: A 1-year follow-up. J Oral Maxillofac Surg. 2000;58(9):959–69.

284. Mansour S, Burstone C, Legan H. An evaluation of soft-tissue changes resulting from Le Fort I maxillary surgery. Am J Orthod. 1983;84(1):37–47.

285. Dantas WRM, da Silveira MMF, do Egito Vasconcelos BC, Porto GG. Evaluation of the nasal shape after orthognathic surgery. Braz J Otorhinolaryngol. 2015;81(1):19–23.

286. van Loon B, van Heerbeek N, Bierenbroodspot F, Verhamme L, Xi T, de Koning MJ, Ingels KJ, Bergé SJ, Maal TJ. Three-dimensional changes in nose and upper lip volume after orthognathic surgery. Int J Oral Maxillofac Surg. 2015;44(1):83–9.

287. Park S-B, Kim Y-I, Hwang D-S, Lee J-Y. Midfacial soft-tissue changes after mandibular setback surgery with or without paranasal augmentation: cone-beam computed tomography (CBCT) volume superimposition. J cranio-maxillo-facial Surg. 2013;41(2):119–23.

288. Almeida RC, Cevidanes LHS, Carvalho F a R, Motta a T, Almeida M a O, Styner M, Turvey T, Proffit WR, Phillips C. Soft tissue response to mandibular advancement using 3D CBCT scanning. Int J Oral Maxillofac Surg. 2011;40(4):353–9.

289. McCollum AGH, Gardener GJM, Evans WG, Becker PJ. Soft-Tissue Changes Related to Mandibular Advancement Surgery. Semin Orthod. 2009;15(3):161–71.

290. Iizuka T, Eggensperger N, Smolka W, Thüer U. Analysis of soft tissue profile changes after mandibular advancement surgery. Oral Surgery, Oral Med Oral Pathol Oral Radiol Endodontology. 2004;98(1):16–22.

291. Raschke GF, Rieger UM, Bader R. Soft tissue outcome after mandibular advancement — an anthropometric evaluation of 171 consecutive patients. Clin Oral Invest. 2013;17:1415–23.

292. Dicker GJ, Koolstra JH, Castelijns J a, Van Schijndel R a, Tuinzing DB. Positional changes of the masseter and medial pterygoid muscles after surgical mandibular advancement procedures: an MRI study. Int J Oral Maxillofac Surg. 2012;41(8):922–9.

293. Conley RS, Boyd SB. Facial soft tissue changes following maxillomandibular advancement for treatment of obstructive sleep apnea. J oral Maxillofac Surg. 2007;65(7):1332–40.

294. Claes P, Walters M, Vandermeulen D, Clement JG. Spatially-dense 3D facial asymmetry assessment in both typical and disordered growth. J Anat. 2011;219(4):444–55.

295. Gerbino G, Bianchi FA, Verzé L, Ramieri G. Soft tissue changes after maxillo-mandibular advancement in OSAS patients: a three-dimensional study. J cranio-maxillo-facial Surg. 2014;42(1):66–72.

296. Bianchi A, Muyldermans L, Di Martino M, Lancellotti L, Amadori S, Sarti A. Facial soft tissue esthetic predictions: validation in craniomaxillofacial surgery with cone beam computed tomography data. J oral Maxillofac Surg. 2010;68(7):1471–9.

297. Chabanas M, Payan Y. A 3D Finite Element model of the face for simulation in plastic and maxillo-facial surgery. In: The Medical Image Computing and Computer-Assisted Intervention – MICCAI. 2000. Proceedings of the Third International Conference Pittsburgh, PA, USA, October 11-14, 2000. pp. 1068–75.

298. Koch RM, Gross MH, Carls FR, Von BUren DF, Fankhauser G, Parish YIH. Simulating Facial Surgery Using Finite Element Models. In: SIGGRAPH '96. Proceedings of the 23rd annual conference on Computer graphics and interactive techniques, 1996. pp. 421-428.

299. Keeve E, Girod S, Girod B. Craniofacial Surgery Simulation. in: 4th International Conference, VBC '96, Hamburg, Germany, September 22 - 25, 1996. Proceedings of the Visualization in Biomedical Computing. 1996. pp. 541–6.

300. Zachow S, Gladiline E, Hege H, Deuflhard P. Finite-Element Simulation of Soft Tissue Deformation. In: Computer Assissted Radiology and Surgery (CARS). 2000. Proceedings of the 14th International Congress & Exhibition, San Francisco, USA. 2000. pp. 23–8.

301. Keeve E, Girod S, Pfeifle P, Girod B. Anatomy-Based Facial Tissue Modeling Using the Finite Element Method. At: The 7th Visualization Conference proceedings (VIS'96). 1996; pp. 21–8.

302. Gladilin, E.; Zachow, S.; Deuflhard, P.; Hege, H.-C. A biomechanical model for soft tissue simulation in craniofacial surgery. In: Medical Imaging and Augmented Reality, 2001. Proceedings. International Workshop. 2001. pp.137-141,

303. Ulusoy I, Akagunduz E, Sabuncuoglu F, Gorgulu S, Ucok O. Use of the dynamic volume spline method to predict facial soft tissue changes associated with orthognathic surgery. Oral Surg Oral Med Oral Pathol Oral Radiol Endod. 2010;110(5):e17–23.

304. Delingette H. Toward realistic soft-tissue modeling in medical simulation. in: Proceedings of the IEEE. 1998;86(3):512-523.

305. Platt JC, Barr AC. Constraint Methods for Flexible Models. Comput Graph (ACM). 1988;22(4):279–88.

306. Black J, Hasting G. Handbook of Biomedical properties. London: Chapman and Hall; 1998.PP 490-500

307. Jabar N, Robinson W, Goto TK, Khambay BS. The validity of using surface meshes for evaluation of three-dimensional maxillary and mandibular surgical changes. Int J Oral Maxillofac Surg. 2015;44(7):914–20.

308. Terzic A, Combescure C, Scolozzi P. Accuracy of computational soft tissue predictions in orthognathic surgery from three-dimensional photographs 6 months after completion of surgery: a preliminary study of 13 patients. Aesthetic Plast Surg. 2014;38(1):184–91.

309. Ullah R, Turner J, Khambay B. The Validity of 3dMD Vultus in Predicting Soft Tissue Morphology Following Orthognathic Surgery. Br J Oral Maxillofac Surg. 2014;52(8):e58.

310. Van Hemelen G, Van Genechten M, Renier L, Desmedt M, Verbruggen E, Nadjmi N. Three-dimensional virtual planning in orthognathic surgery enhances the accuracy of soft tissue prediction. J cranio-maxillo-facial Surg. 2015;43(6):918–25.

311. Liebregts J, Xi T, Timmermans M, De Koning M, Bergé S, Hoppenreijs T. Accuracy of three-dimensional soft tissue simulation in bimaxillary osteotomies. J cranio-maxillo-facial Surg. 2015;43(3):329–35.

312. Liebregts J, Timmermans M, De Koning M, Bergé S, Maal T. Three-dimensional facial simulation in bilateral sagittal split osteotomy: a validation study of 100 patients. J Oral Maxillofac Surg. 2015;73(5):961-70.

7 Appendices

Contents

7.1 Appendix 1 Presentations and awards

7.1.1 Verbal presentations

1. *"Internal DICOM slice landmarking" a novel method to quantify skeletal movement following orthognathic surgery.* 3D Bologna international conference in Italy 2014 (Bologna, Italy).

2. *Computer assisted surgical planning, current practice at the Glasgow dental hospital and school.* Collaboration visit to the University of (Lille, France), funded by the EuroCleft scientific Foundation 2014 (ESF).

3. *Comparison of the Accuracy of Voxel Based Registration and Surface Based Registration for 3D Assessment of Surgical Change following Orthognathic Surgery*. 3D User meeting 2013 (London, UK).

4. *Comparison between different 3D image registration methods used in the analysis orthognathic of facial changes following orthognathic surgery*. Graduate Research competition 2013 (Glasgow, UK).

5. *Computer assisted 3D planning in orthognathic surgery.* A four Hours of theory and Hands-On training course for Post Graduate students and staff members on 3D Planning in orthognathic surgery 2013-2015 (Glasgow, UK).

6. *Regular seminars presentation.* Ppost-Graduate seminars and journal club meetings 2011-2015 (Glasgow, UK).

7. *Effect of Le Fort I osteotomy on Alar base width.* Research audit Verbal presentation 2012 (Glasgow, UK).

7.1.2 Poster presentations

1. *State-of-the art analysis of soft tissue changes in response to Le Fort I maxillary advancement.* The First HCED Iraq initiative meeting 2015; London, UK.

2. *"Internal DICOM slice landmarking" a novel method to quantify skeletal movement following orthognathic surgery.* The annual International British Craniofacial society meeting 2014; Oxford, UK.

3. *Comparison between different 3D image registration methods used in the analysis orthognathic of facial changes following orthognathic surgery* The international Brand-Spasel Symposium 2014; Basel, Switzerland.

4. *"Internal DICOM slice landmarking" a novel method to quantify skeletal movement following orthognathic surgery.* The international Brand-Spasel Symposium 2014; Basel, Switzerland.

5. *Effects of Le Fort I Osteotomy on the Nasopharyngeal Airway—6-Month Follow-Up.* The annual BOS conference 2014; Edinburgh, UK.

7.1.3 Awards and recognitions

10th International Bernd-Spiessl-Symposium
for Innovative and Visionary Technologies in CMF-Surgery
Face and Identity I Systems Integration I The Whole and its Parts

June 19th – 21st 2014, University Hospital Basel, Switzerland
www.bernd-spiessl-symposium.com

Bernd-Spiessl
AWARD

The Winner of the Award
for the **Best Student Poster**
is:

Anas Mohammed Almukhtar

SGMKG
SSCOMF
SSOMFS

We congratulate the winner

On behalf of the Executive Committee

Scientific Endorsement by

EUROPEAN ASSOCIATION FOR CRANIO-MAXILLOFACIAL SURGERY
FOUNDED 1970

Prof. Dr. h.c. Dr. Dr. H.-F. Zeilhofer
Basle, June 21st 2014

View this email in your browser

PLOS | ONE

Anas Almukhtar
PLOS ONE Reviewer (2014)

May 2015

Dear Anas,

On behalf of PLOS and the *PLOS ONE* editorial team, I would like to thank you for participating in the peer review process this past year at *PLOS ONE*. We very much appreciate your valuable input in 2014. We know there are many claims on your time and expertise but with your help, we have continued to publish an influential, lively and highly accessed Open Access journal. Simply put, we could not do it without you and the thousands of other volunteers for *PLOS ONE* and the other PLOS journals who graciously contributed time reviewing manuscripts.

A public "Thank You" to our 2014 reviewers – including you – was published in February 2015.

> (2015) PLOS ONE 2014 Reviewer Thank You. PLoS ONE 10(2): e0121093. doi:10.1371/journal.pone.0121093

Your name is listed in the Supporting Information file associated with the article. I hope that you will be able to use this letter, along with the article citation, to claim the credit and recognition you deserve within your institution for supporting *PLOS ONE* and Open Access publishing.

If you would ever like to provide feedback on our processes, we would very much welcome that. Please send your feedback to us at plosone@plos.org.

With Gratitude,

Damian Pattinson
Editorial Director
PLOS ONE

P.S. If you'd like to receive news and information from PLOS, opt-in here.

7.2 Appendix 2 Publications

7.2.1 Published Journal articles

- Almukhtar A, Ju X, Khambay B, McDonald J, Ayoub A. *Comparison of the Accuracy of Voxel Based Registration and Surface Based Registration for 3D Assessment of Surgical Change following Orthognathic Surgery*. PLoS ONE. 2014; 9(4): e93402.

- Anas Almukhtar, Balvinder Khambay , Ashraf Ayoub, Xiangyang Ju , Ali Al-Hiyali, James McDonald, Norhayati Jabar, and Tazuko Goto. *"Direct DICOM slice landmarking" A novel research technique to quantify skeletal changes in orthognathic surgery*. PLoS One. 2015;10(8):e0131540.

- Mohammed Almuzian, Anas Almukhtar, Xiangyang Ju, Ali Al-Hiyali, Philip Benington, Ashraf Ayoub. *Effects of Le Fort I Osteotomy on the Nasopharyngeal Airway—6-Month Follow-Up*.J Oral Maxillofac Surg. 2016;74(2):380-91.

- Mohammed Almuzian, Anas Almukhtar, Michael O'Neil, Philip Benington, Thamer Al Anezi and Ashraf Ayoub. *Innovation in prediction planning for anterior open bite correction*. Aust Orthod J. 2015; 31: 78–86.

7.2.2 Accepted for publication

- Almukhtar A, Ju X, Khambay B, McDonald J, Ayoub A. *State-of-the art analysis of soft tissue changes in response to Le Fort I maxillary advancement*. Br J Oral Maxillofac Surg. 2016. XXXX.

- Almuzian M, Ju X, Almukhtar A, Ayoub A, Al-Muzian L, McDonald JP. *Does rapid maxillary expansion affect nasopharyngeal airway? A prospective Cone Beam Computerised Tomography (CBCT) based study*. Surgeon. 2016. XXXX.

- Khambay B, Cheungmy, Almukhtar A, Keeling A.J, tchsung, Ju X , McDonald JP, Ayoub A. *The accuracy of conformation of a generic surface mesh for the analysis of facial soft tissue changes*. PLoS ONE. 2016 XXXX.